

AD-A078 919

ROCKWELL INTENATIONAL CANOGA PARK CA ROCKETDYNE DIV
CHEMICALLY PUMPED IODINE LASER.(U)
SEP 79 S HURLOCK , H LAEGER , R WAGNER

F/6 20/5

UNCLASSIFIED

AFWL-TR-79-52

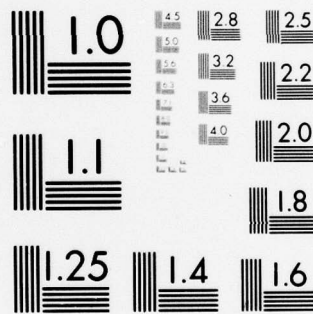
F29601-78-C-0023

NI

1 OF 3

AD
A078919





MICROCOPY RESOLUTION TEST CHART
NATIONAL BUREAU OF STANDARDS-1963-A

AD A078919

DDC FILE COPY

AFWL-TR-79-52

LEVEL 2

AD-E200 427

AFWL-TR
79-52

CHEMICALLY PUMPED IODINE LASER

S. Hurlock
H. Laeger
R. Wagner

Rocketdyne Division
Rockwell International
6633 Canoga Avenue
Canoga Park, CA 91304

September 1979

Final Report

Approved for public release; distribution unlimited.

AIR FORCE WEAPONS LABORATORY
Air Force Systems Command
Kirtland Air Force Base, NM 87117

79 11 05 102

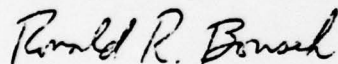
This final report was prepared by the Rocketdyne Division, Rockwell International, Canoga Park, California, under Contract F29601-78-C-0023, Job Order 33260311 with the Air Force Weapons Laboratory, Kirtland Air Force Base, New Mexico. Major Ronald R. Bousek (ALC) was the Laboratory Project Officer.

When US Government drawings, specifications, or other data are used for any purpose other than a definitely related Government procurement operation, the Government thereby incurs no responsibility nor any obligation whatsoever, and the fact that the Government may have formulated, furnished, or in any way supplied the said drawings, specifications, or other data, is not to be regarded by implication or otherwise, as in any manner licensing the holder or any other person or corporation, or conveying any rights or permission to manufacture, use, or sell any patented invention that may in any way be related thereto.

This report has been authored by a contractor of the United States Government. The United States Government retains a nonexclusive, royalty-free license to publish or reproduce the material contained herein, or allow others to do so, for the United States Government purposes.

This report has been reviewed by the Information Office and is releasable to the National Technical Information Service (NTIS). At NTIS, it will be available to the general public, including foreign nations.

This technical report has been reviewed and is approved for publication.

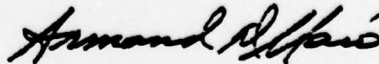


RONALD R. BOUSEK
Major, USAF
Project Officer



DAVID S. OLSON
Lt Colonel, USAF
Chief, Chemical Laser Branch

FOR THE DIRECTOR



ARMAND D. MAIO
Colonel, USAF
Chief, Advanced Laser Technology Div

UNCLASSIFIED

SECURITY CLASSIFICATION OF THIS PAGE (When Data Entered)

REPORT DOCUMENTATION PAGE		READ INSTRUCTIONS BEFORE COMPLETING FORM
1. REPORT NUMBER AFWL-TR-79-52	2. GOVT ACCESSION NO.	3. RECIPIENT'S CATALOG NUMBER
4. TITLE (and Subtitle) CHEMICALLY PUMPED IODINE LASER	5. TYPE OF REPORT & PERIOD COVERED Final Report	6. PERFORMING ORG. REPORT NUMBER
7. AUTHOR(s) S. Hurlock, H. Laeger, R. Wagner	8. CONTRACT OR GRANT NUMBER(s) F29601-78-C-0023	
9. PERFORMING ORGANIZATION NAME AND ADDRESS Rocketdyne Division, Rockwell International 6633 Canoga Avenue Canoga Park, CA 91304	10. PROGRAM ELEMENT, PROJECT, TASK AREA & WORK UNIT NUMBERS 62601F 33260311	
11. CONTROLLING OFFICE NAME AND ADDRESS Air Force Weapons Laboratory (ALC) Kirtland Air Force Base, NM 87117	12. REPORT DATE September 1979	13. NUMBER OF PAGES 224
14. MONITORING AGENCY NAME & ADDRESS (if different from Controlling Office) 16 3326 17 03	15. SECURITY CLASS. (of this report) Unclassified	15a. DECLASSIFICATION/DOWNGRADING SCHEDULE
16. DISTRIBUTION STATEMENT (of this Report) Approved for public release; distribution unlimited. 12 232		
17. DISTRIBUTION STATEMENT (of the abstract entered in Block 20, if different from Report) 18 AFWL, SBIE		
18. SUPPLEMENTARY NOTES 19 TR-79-52, AD-E244 427 O ₂ (1 Delta)		
19. KEY WORDS (Continue on reverse side if necessary and identify by block number) Singlet Molecular Oxygen Gas-liquid Reactions Chlorine Fluorosulfate ESR Spectroscopy Chlorine Hydrogen Peroxide Basic Hydrogen Peroxide Sodium Hydroxide		
20. ABSTRACT (Continue on reverse side if necessary and identify by block number) The production of O ₂ ⁿ (1Δ) by the reaction of chlorine fluorosulfate (CFS) vapor and chlorine gas with concentrated basic hydrogen peroxide solutions was studied under conditions of controlled contact area, contact time, and temperature. Variables were temperature, CFS and Cl ₂ flowrates, liquid flowrates, and liquid concentrations. Effluent flow, O ₂ ⁿ flow, and O ₂ ⁿ 1Δ/O ₂ were measured. O ₂ ⁿ (1Δ) yields with CFS were lower than with Cl ₂ due to quenching. O ₂ ⁿ production was about the same, governed primarily by contact time, liquid flow and temperature.		

DD FORM 1 JAN 73 1473

UNCLASSIFIED

SECURITY CLASSIFICATION OF THIS PAGE (When Data Entered)

390 199

O₂(1 Delta)/O₂

JUB

UNCLASSIFIED

SECURITY CLASSIFICATION OF THIS PAGE(When Data Entered)

20. ABSTRACT (Continued).

Qualitative quenching experiments identified serious quenchers present in the CFS system.

4

Accession For	
NTIS GFA&I	<input checked="checked" type="checkbox"/>
DDC TAB	<input type="checkbox"/>
Unannounced	<input type="checkbox"/>
Justification	
By _____	
Distribut _____	
Available _____	
Dist	Available for spec 1
A	

UNCLASSIFIED

SECURITY CLASSIFICATION OF THIS PAGE(When Data Entered)

SUMMARY

The base catalyzed reaction of chlorine fluorosulfate (CFS) with 90% hydrogen peroxide has been shown capable of producing clean streams of molecular oxygen with enough $O_2(^1\Delta)$ to produce an inversion in the population of the spin-orbit transition of atomic iodine at 1.31 μm (Ref. 1). The objective of the present study was to characterize further this reactive system, optimize the $O_2(^1\Delta)$ yield from it, and scale it for use with an iodine laser.

Experiments to characterize the first stage (CFS + excess 90% H_2O_2) of the reaction scheme used in Ref. 1 were carried out. CFS was reacted with 90% H_2O_2 and produced quantitative amounts of Cl_2 with no intermediate isolated. It was also shown subsequently that this reaction produces only ground state oxygen. Thus, it was decided to evaluate the CFS in a single-stage reactor in which CFS was reacted with basic hydrogen peroxide. A reactor was developed in which a rotating surface is wetted with the $H_2O_2/NaOH$ liquid, which is then carried past a gas nozzle for injection of CFS vapor. The surface rotates past a scraper for removal of unwanted byproducts. Cooling is provided for surface temperature control and shields provide a reasonably well-defined reaction zone. Reactant delivery systems for the CFS, H_2O_2 , and NaOH were developed so that reactant consumption and delivery could be monitored on a continuous basis. A downstream vacuum system (product delivery system) included various cryogenic traps. Diagnostics included pressure instrumentation, an optical monitor for $O_2(^1\Delta)$ detection, and an ESR spectrometer for detection of $O_2(^1\Delta)$ and $O_2(^3\Sigma)$. A μ -wave generator was available for producing $O_2(^1\Delta)$ for diagnostic calibration and for quenching studies.

Prior to operating this reactor, some baseline experiments were conducted using the reactor of Ref. 1. These experiments confirmed the general behavior but yielded significantly less $O_2(^1\Delta)$ than had been reported.

1. Pritt, A. T. et al., A Chemical Singlet Molecular Oxygen Generator, Final Report, Contract No. F29601-76-0070, Rockwell International Science Center, May 1978 (AFWL-TR-77-265).

Operation of the roller-drum reactor produced low yields of $O_2(^1\Delta)$ from CFS + $H_2O_2/NaOH$. Quenching of the excited oxygen was suspected and experiments confirmed that CFS, and its hydrolysis products $ClOSO_2F$ and H_2SO_4 , are very serious quenchers of $O_2(^1\Delta)$. It is suspected that the products $HOCl$ and HF are also bad, but this was not confirmed by direct experiment. Several modifications of the system were tried to improve the performance. Earlier removal of condensibles and temperature reduction led to significant improvement in the $O_2(^1\Delta)$ yield, but typical performance demonstrated that the best $O_2(^1\Delta)/O_2$ values of 0.12 to 0.16 were observed at low CFS flows, and dropped as the CFS flow was increased. Total oxygen production (O_2/CFS) was comparable with that observed using chlorine.

The roller-drum reactor was operated with $Cl_2 + H_2O_2/NaOH$ to characterize the reactor and to provide a basis for comparison of the CFS results. $O_2(^1\Delta)$ yields increased slightly with Cl_2 flow to maximum values in the 0.30 to 0.40 range. The lower values at low flows are associated with long residence times near the liquid surface. A reduction in the yield at higher flows was observed and is attributed to quenching by significant quantities of unreacted Cl_2 . Total oxygen production (O_2/Cl_2) was highest (0.40 to 0.70) at low Cl_2 flows (long residence times in the reactor) and dropped significantly (~ 0.20) at higher Cl_2 . This is attributed to insufficient residence time, indicating that the surface-to-volume ratio of this reactor design is apparently too small. Liquid flowrates and reactor temperature were observed to have significant effects on the O_2/Cl_2 performance.

PREFACE

This report contains results and conclusions from a study carried out by the Rocketdyne Division of Rockwell International under contract to the Air Force Weapons Laboratory. The primary objective of the two-phase, eight-task program was to demonstrate a 1 kW $I^*/O_2(^1\Delta)$ transfer laser operating with an $O_2(^1\Delta)$ generator utilizing the base-catalyzed reaction of chlorine fluorosulfate (CFS) with hydrogen peroxide.

The results of small-scale studies led to the conclusion that the CFS + $H_2O_2/NaOH/H_2O$ system was not viable for efficient $O_2(^1\Delta)$ production because of serious quenching of $O_2(^1\Delta)$ by CFS and its byproducts. The scope of the effort was then changed to eliminate generator scaleup and lasing demonstration. Significant data were provided for understanding chemistry and chemical engineering issues related to the two-phase reaction of $H_2O_2/NaOH/H_2O$ not only with CFS but also with Cl_2 , which was used in many of the experiments.

Several individuals contributed significantly to the progress of the program described in the report. The AFWL Project Officer was Major R. Bousek, who, along with Major W. McDermott and Captain N. Pchelkin, contributed through many discussions. At the Rockwell Science Center, Dr. I. Goldberg and Dr. A. T. Pritt contributed through discussions and technical support in the areas of chemical kinetics and diagnostics. Dr. D. Pilipovich served as Consultant in the areas of chemical mechanisms, kinetics, and experimental interpretation. At Rocketdyne, the Program Managers were Dr. J. Flannagan and Dr. L. Grant. Dr. J. Hon was Director of the Laser Technology organization in which the project was performed. Mr. M. Halloran directed the design and fabrication of hardware. Installation and testing was carried out with the able assistance of Mr. G. Storey, Mr. W. Musser, and Mr. R. C'Dealva. Theoretical analysis of reactor performance was carried out by Dr. G. Schindler, who is the author of Appendix A.

CONTENTS

<u>Section</u>	<u>Page</u>
I Introduction	11
II Basic Chemistry Experiments	13
III Small-Scale $O_2(^1\Delta)$ Generator	18
Reactant Delivery Systems	18
The Roller-Drum Reactor	42
Product Delivery System	56
Instrumentation and Diagnostics	79
IV $O_2(^1\Delta)$ Experiments	101
Testing and Data Summary	101
Roller-Drum Reactor Results With Chlorine	179
Roller-Drum Reactor Results With Chlorine Fluorosulfate.	187
$O_2(^1\Delta)$ Quenching Experiments	189
V Conclusions	191
References	192
<u>Appendix A</u>	
O_2 Concentration in Iodine Laser Reactor	195

ILLUSTRATIONS

1. Experimental Apparatus for Basic Chemistry Experiments	14
2. Tasks 1 and 2 Versatile Experimental Setup Schematic	19
3. Liquid Reactants Delivery System and Vacuum System	20
4. Reactant Tanks and Pressurization System	22
5. Constant Temperature Bath With Capillary Flowmeters	23
6. NaOH Flowmeter Calibration	24
7. H ₂ O ₂ Flowmeter Calibration	26
8. CFS/Cl ₂ Delivery System Schematic	28
9. CFS Flowmeter Calibration	29
10. H ₂ O ₂ NaOH Delivery System	31
11. Roller-Drum Reactor Showing the Cl ₂ , CFS, and Premixed H ₂ O ₂ /NaOH Delivery Systems	32
12. On-Line Continuous Base-Peroxide Mixer	34
13. On-Line Base-Peroxide Mixer	35
14. Initial Design for On-Line Continuous Base-Peroxide Mixer . . .	40
15. Initial On-Line Base Peroxide Mixer	41
16. Roller Drum Generator Assembly	217
17. Gas Generator Glass Housing	218
18. Roller-Drum Reactor Glass Housing and Gas Nozzle	46
19. Roller-Drum Reactor Internal Assembly and End Plates	47
20. Large Roller and Components	219
21. CFS, Cl ₂ Nozzle	220
22. Small Roller Assembly	221
23. Solid/Liquid Reaction Byproduct Trap, Roller-Drum Reactor . . .	55
24. Reactor Configuration O, A	57
25. Near-Downstream Vacuum System-Configuration Ø	58
26. Near-Downstream Vacuum System-Configuration A	59
27. Reactor Configuration B	60
28. Near-Downstream Vacuum System-Configuration B	61
29. Reactor Configuration C, D	62
30. Near-Downstream Vacuum System-Configuration C	63
31. Near-Downstream Vacuum System-Configuration D	64

32.	Reactor and Trap 2, Configuration C	65
33.	Middle Section of Flow System	66
34.	Downstream End of Flow System	67
35.	P_1 vs Air Flow (8 February 1979 Data - Corrected for P and T)	69
36.	Pressure vs Flowrate	73
37.	Flow System Schematic For Residence Time Calculations	74
38.	Estimated Residence Time vs Pressure and Flowrate	76
39.	Trap 3 Configuration	78
40.	Amplifier - Digital Display Units and Strip Chart Recorder	80 81
41.	ESR Spectrum of O_2 Products from $ClOSO_2F-H_2O_2-NaOH$ Reactants	87
42.	Field Controller Modification	93
43.	Continuous Wave Laser Laboratory With EPR Interface	94
44.	ESR Spectrometer System Schematic	95
45.	ESR Control Station	96
46.	Optical Schematic of $O_2(^1\Delta, ^1\Sigma)$ Monitor	98
47.	Singlet Oxygen Optical Monitor	99
48.	Optical Calibration-Test 038	100
49.	Kenics Mixer and Reactant Delivery Arrangement for Cyclone Reactor Tests	107
50.	$O_2(^1\Delta)$ Yield, Test 015; Roller at -11C, Configuration A, Liquid Concentration 2, 3	110
51.	Product Flow vs Cl_2 , CFS Flow - Test 015	111
52.	$O_2(^1\Delta)$ Partial Pressure at P_1 vs Cl_2 , CFS Flow - Test 015	112
53.	$O_2(^1\Delta)$ Yield, Test 021	113
54.	Product Flow vs Cl_2 , CFS Flow - Test 021	114
55.	$O_2(^1\Delta)$ Partial Pressure at P_1 vs Cl_2 , CFS Flow - Test 012	115
56.	$O_2(^1\Delta)$ Yield - Test 022	116
57.	Product Flow vs Cl_2 Flow - Test 022	117
58.	$O_2(^1\Delta)$ Partial Pressure at P_1 vs Cl_2 Flow - Test 022	118
59.	$O_2(^1\Delta)$ Yield, Test 023	119

60.	Product Flow vs CFS Flow - Test 023	120
61.	$O_2(^1\Delta)$ Partial Pressure at P_1 vs CFS Flow - Test 023	121
62.	$O_2(^1\Delta)$ Yield, Test 025	122
63.	Product Flow vs CFS, Cl_2 Flow - Test 025	123
64.	$O_2(^1\Delta)$ Partial Pressure at P_1 vs Cl_2 , CFS Flow - Test 025	124
65.	$O_2(^1\Delta)$ Yield, Test 027	125
66.	Product Flow vs CFS, Cl_2 Flow - Test 027	127
67.	$O_2(^1\Delta)$ Partial Pressure at P_1 vs CFS, Cl_2 Flow - Test 027	129
68.	$O_2(^1\Delta)$ Yield vs CFS, Cl_2 Flow - Test 028	131
69.	Product Flow vs CFS, Cl_2 Flowrate - Test 028	132
70.	$O_2(^1\Delta)$ Partial Pressure at P_1 vs CFS, Cl_2 Flow - Test 028	133
71.	$O_2(^1\Delta)$ Yield vs Cl_2 , CFS Flow - Test 029	134
72.	Product Flow vs Cl_2 Flow - Test 029	135
73.	$O_2(^1\Delta)$ Partial Pressure at P_1 vs CFS, Cl_2 Flow - Test 029	136
74.	$O_2(^1\Delta)$ Yield vs Cl_2 , CFS Flow, Test 030	137
75.	Product Flowrate - Test 030	138
76.	$O_2(^1\Delta)$ Partial Pressure at P_1 vs Cl_2 , CFS Flow - Test 030	139
77.	$O_2(^1\Delta)$ Yield vs Cl_2 Flow - Test 031	140
78.	Product Flow vs Cl_2 Flow - Test 031	142
79.	$O_2(^1\Delta)$ Partial Pressure at P_1 vs Cl_2 Flow, Effects of Trap Temperature and Liquid Flow - Test 031	144
80.	$O_2(^1\Delta)$ Yield - Test 034	146
81.	Product Flow - Test 034	148
82.	$O_2(^1\Delta)$ Partial Pressure at P_1 - Test 034	150
83.	$O_2(^1\Delta)$ Yield - Test 035	152
84.	Product Flow, Test 035	153
85.	$O_2(^1\Delta)$ Partial Pressure at P_1 - Test 035	154
86.	$O_2(^1\Delta)$ Yield - Test 036	155
87.	Product Flow - Test 036	157
88.	$O_2(^1\Delta)$ Partial Pressure at P_1 - Test 036	159
89.	$O_2(^1\Delta)$ Yield - Test 037	161
90.	Product Flow - Test 037	163
91.	$O_2(^1\Delta)$ Partial Pressure at P_1 - Test 037	165

92.	$O_2(^1\Delta)$ Yield - Test 038	167
93.	Product Flow - Test 038	169
94.	$O_2(^1\Delta)$ Partial Pressure at P_1 - Test 038	171
95.	$O_2(^1\Delta)$ Yield - Test 039	173
96.	Product Flow - Test 039	175
97.	$O_2(^1\Delta)$ Partial Pressure at P_1 - Test 039	177
98.	Simple Analysis of Reactor Collisions	181
99.	Effect of Liquid Flowrate on Total O_2 Production at Constant Concentration and Temperature, Configuration D	183
100.	O_2/Cl_2 for Various Liquid Concentrations and Flows	184
101.	Effect of Roller Coolant Temperature on Total O_2 Production - Configuration D	185
102.	Effect of Roller Coolant Temperature at Constant Flowrate (0.12 ml/sec), Constant Concentration	186
103.	Qualitative Quenching Efficiencies	190

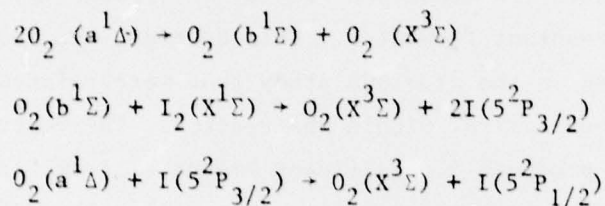
TABLES

1. Viscosity of Chlorine Fluorosulfate	27
2. Basic Hydrogen Peroxide Solutions	33
3. On-Line Mixer Operational Data	37
4. Analyses of On-Line Mixed Basic Peroxide	38
5. Flow System Dimensions and Residence Time Calculations	72
6. Effectiveness of Trap 3 at -160 C in Trapping Cl ₂	79
7. Values of Q and Parameters Used to Calculate Q for O ₂ (¹ Δg) and O ₂ (³ Σg ⁻) at 298.16 K	90
8. Testing Summary	103

SECTION I

INTRODUCTION

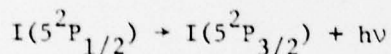
The chemically pumped iodine laser is based on chemical production of oxygen in the $a^1\Delta$ state followed by transfer of the oxygen energy to the iodine according to the following scheme:



The atomic iodine in the $5^2P_{1/2}$ state is the lasing species.

The key to success of this scheme lies in the development of a chemical oxygen generator capable of producing a clean stream of oxygen, a large fraction of which is in the $a^1\Delta$ state, often referred to simply as $^1\Delta$.

Prior to the initiation of this study, a previous study (Ref. 1) showed that the base (NaOH) catalyzed reaction of chlorine fluorosulfate and 90% hydrogen peroxide is capable of producing clean streams of **molecular** oxygen with enough $O_2(^1\Delta)$ to invert the population of the lasing transition.



Subsequent to that study, an iodine laser was demonstrated utilizing an oxygen generator based on the reaction of chlorine with basic hydrogen peroxide (Ref. 2).

2. McDermott, W. E., N. R. Pchelkin, D. J. Benard, and R. R. Bousek, "An Electronic Transition Chemical Laser", Appl. Phys. Lett. 32(8), 469-470 (1978).

The objectives of the present study were to characterize the CFS/H₂O₂/NaOH system on small scale ($\sim 0.1 \times 10^{-3}$ mole/sec O₂), optimize a generator in terms of O₂¹Δ/O₂, scale the generator by one-hundred- to three-hundred-fold, and demonstrate lasing employing the scaled-up generator.

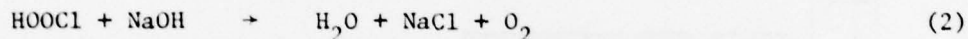
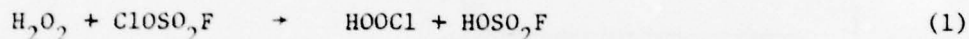
The approach to meeting the objectives was to begin by studying the CFS + H₂O₂/NaOH reaction in a small-scale reactor capable of providing temperature control, surface area control, a means for removal of byproducts, and instantaneous measurement of reactant flowrates. This approach was chosen because of problems encountered in the previous study that were related to surface area control and foam control within the reactor. The reaction of CFS with base and peroxide produces a significant amount of foam, from which the O₂ evolves and through which the O₂(¹Δ) must travel. The difficulties encountered in controlling and reproducing the reaction under these circumstances made it impractical to consider scaling this system until it was better characterized. This report describes the experiments and results by which this characterization was carried out.

The basic chemistry experiments in which the CFS + H₂O₂ reaction was considered are discussed in Section II. Section III is a description of the experimental details of the small-scale reactor testing and setup. The results of the small-scale testing are presented and discussed in Section IV and conclusions are given in Section V.

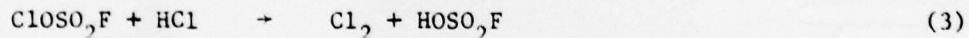
SECTION II

BASIC CHEMISTRY EXPERIMENTS

The reaction of 90% H_2O_2 with CFS followed by immediate contacting of the resulting two phase (gas-liquid) product with 50% NaOH was observed to form $\text{O}_2(^1\Delta)$ (Ref. 1). It had not been determined, however, whether the immediate precursor to $\text{O}_2(^1\Delta)$ resided primarily in the gaseous or liquid phase. Accordingly, some experiments were contemplated in which the liquid phase would be diverted and only the gaseous phase would be contacted with 50% NaOH. The working hypothesis was that the $\text{O}_2(^1\Delta)$ precursor was the as-yet uncharacterized HOOCCl , which would be sufficiently volatile to be present in the gaseous phase (Eq. 1 and 2).



Simultaneous with the buildup of the roller-drum reactor that would be used in continuous flow tests under dynamic vacuum to evaluate the above hypothesis, a series of batch tests was run under dynamic vacuum in the absence of NaOH. In these small-scale experiments, highly purified reactants were used. The CFS was freed of ClF and Cl_2 by refluxing at -78°C until it exhibited a vapor tension < 0.5 torr at -78°C and assayed 102% pure on reaction with excess HCl (Eq. 3).



The H_2O_2 was prepared from 90% H_2O_2 by four crystallizations and assayed 99.95% by permanganate titration. The H_2O was distilled. The reactor (Fig. 1) was a 2.5-cm diameter by 15-cm bed of 5-mm glass beads thermostated in a slush

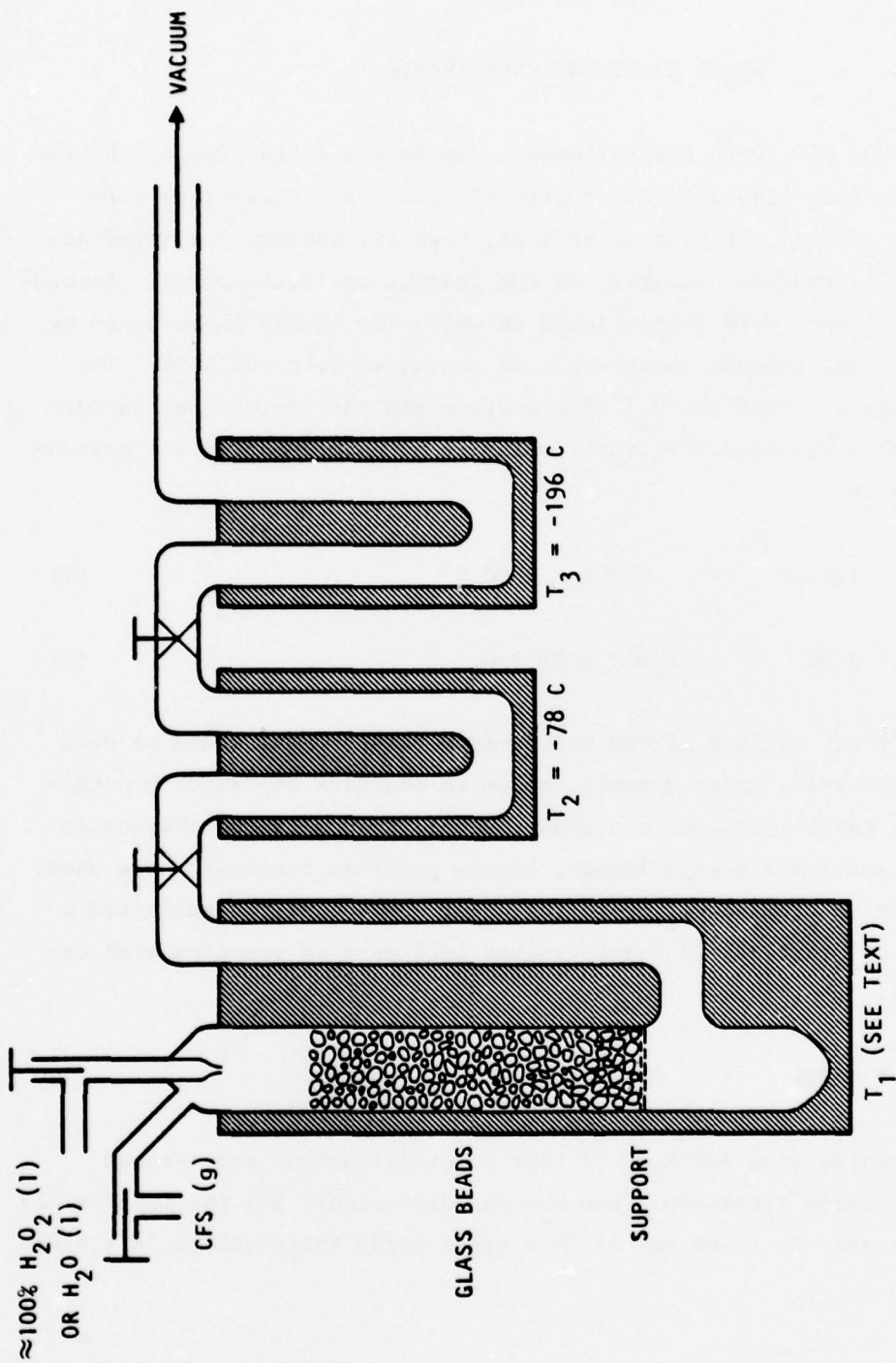
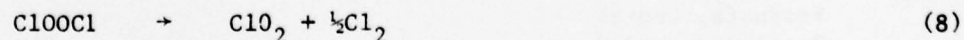
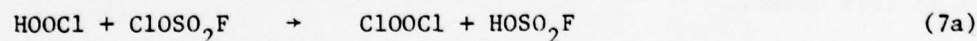
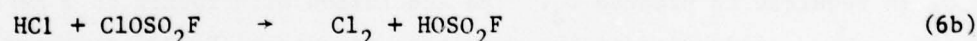
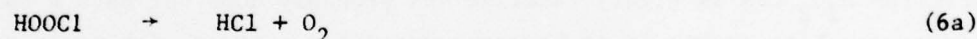
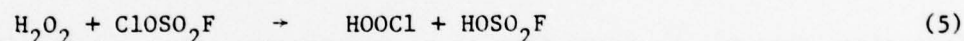
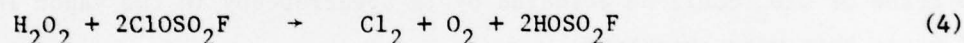


Figure 1. Experimental Apparatus for Basic Chemistry Experiments

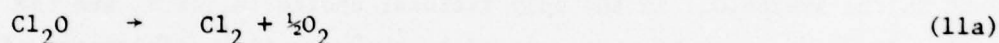
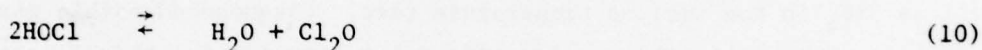
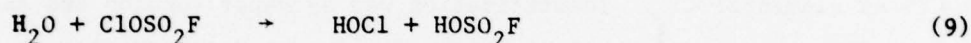
bath and coated with an excess of either pure H_2O_2 or pure H_2O . A measured quantity of pure CFS (ca. 0.5 mmole CFS/30 mmoles H_2O_2) was then allowed to pass through the bed in about 2 minutes under dynamic vacuum and the products (with the exception of O_2) were condensed in cold traps for subsequent purification and identification.

Three experiments with H_2O_2 were run at temperatures of -63°C , -30°C , and 22°C , and one with H_2O at 22°C . The results of each of the H_2O_2 tests were virtually identical with near quantitative recovery of the chlorine content of the CFS as elemental Cl_2 . Identification was by vapor tension and absence of an IR spectrum. A trace impurity of ClO_2 was detected in each test as well as SiF_4 in the ambient temperature test. The noncondensable gas formed was neither collected nor identified but, considering the elements present in the system, O_2 is the only rational choice (H_2 or F_2 are the others). These data may be rationalized by the overall stoichiometry of Eq. 4 which might be realized by either of two mechanisms as indicated in Eq. (5, 6a, 6b) or (5, 7a, 7b).



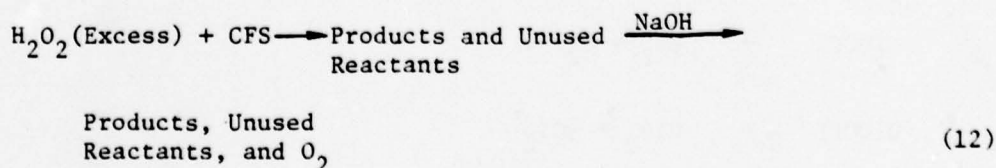
The small amount of ClO_2 may have formed according to Eq. (8).

The experiment using water was similar to those using H_2O_2 in that no CFS passed through the bed. In contrast with the H_2O_2 experiments, little or no noncondensable gas reached the vacuum pump based on changes in its sound of operation. The reaction products were only tentatively identified by their behavior, but appeared to be HOCl in equilibrium with water and Cl_2O (Eq. 9, 10) and decomposition products thereof (Eq. 11a,b). Attempted purification of the products by repeated fractional condensation resulted in significant quantities of water passing a -78°C trap. This may be best rationalized as HOCl actually passing through and disproportionating on warming to ambient temperature (Eq. 10).



Only a trace of ClO_2 could be detected by IR spectroscopy in the vapor (HOCl and Cl_2O are both weak absorbers).

The conclusions that may be drawn from these experiments are: (1) the initial product from $\text{H}_2\text{O}_2/\text{CFS}$ is highly reactive and probably does not have a half-life long enough to enable it to be transported for contact with base, and (2) H_2O_2 is required to produce O_2 . The conclusion with regard to a mechanism for $\text{O}_2(^1\Delta)$ production in the two-stage generator (Eq. 12) reported in Ref. 1 is less clear.



The first stage produces no detectable $O_2(^1\Delta)$. This was demonstrated on this contract and the results are described in Section IV. If the first stage involves total consumption of reactants according to Eq. 4, then every mole of CFS would produce a mole of Cl_2 and O_2 . The subsequent second-stage reaction of Cl_2 with basic peroxide would then produce $O_2(^1\Delta)$ which would be at most 1:1 with ground state O_2 even with 100% stoichiometric production of $O_2(^1\Delta)$ from Cl_2 . If the $O_2(^1\Delta)/Cl_2$ is 0.50 or less, as seems reasonable from subsequent results, then $O_2(^1\Delta)/O_2$ on the order of ≤ 0.25 would be expected. This $O_2(^1\Delta)$ yield is lower than reported in Ref. 1 but is on the order measured in the present effort. If unreacted CFS reaches the NaOH, then direct conversion to $O_2(^1\Delta)$ may be expected.

SECTION III

SMALL-SCALE $O_2(^1\Delta)$ GENERATOR

The major part of the experimental work carried out under the contract was in the Rocketdyne Continuous Wave Laser Laboratory (CWLL) located at the company's Santa Susana Field Laboratory. This section provides a description of the experimental components, installations, calibration, and measurement procedures to facilitate an understanding of the experiments and results described in Section IV.

The experimental setup may be broken down into functions as follows:

Reactant Delivery Systems

Reactor

Product Delivery Systems

Instrumentation and Diagnostics

Each of these functions will be described in the following subsections. Figure 2 shows the installation of these systems on the U-shaped bench with a walk-in fume hood for reactants. The system, connected up as shown, was used to operate the modified Rockwell Science Center generator to provide baseline experimental data. The roller-drum reactor used the same reactant supply and vacuum system.

REACTANT DELIVERY SYSTEMS

The common features of the reactant delivery systems are the storage containers and the flowmeters. The variations in these two common features (directed by the nature of the individual reactants) are discussed. The sodium hydroxide and hydrogen peroxide were premixed either batchwise or continuously (on-line) before contacting with either chlorine fluorosulfate or chlorine in the reactor. A schematic representation of the delivery systems is shown in Fig. 3.

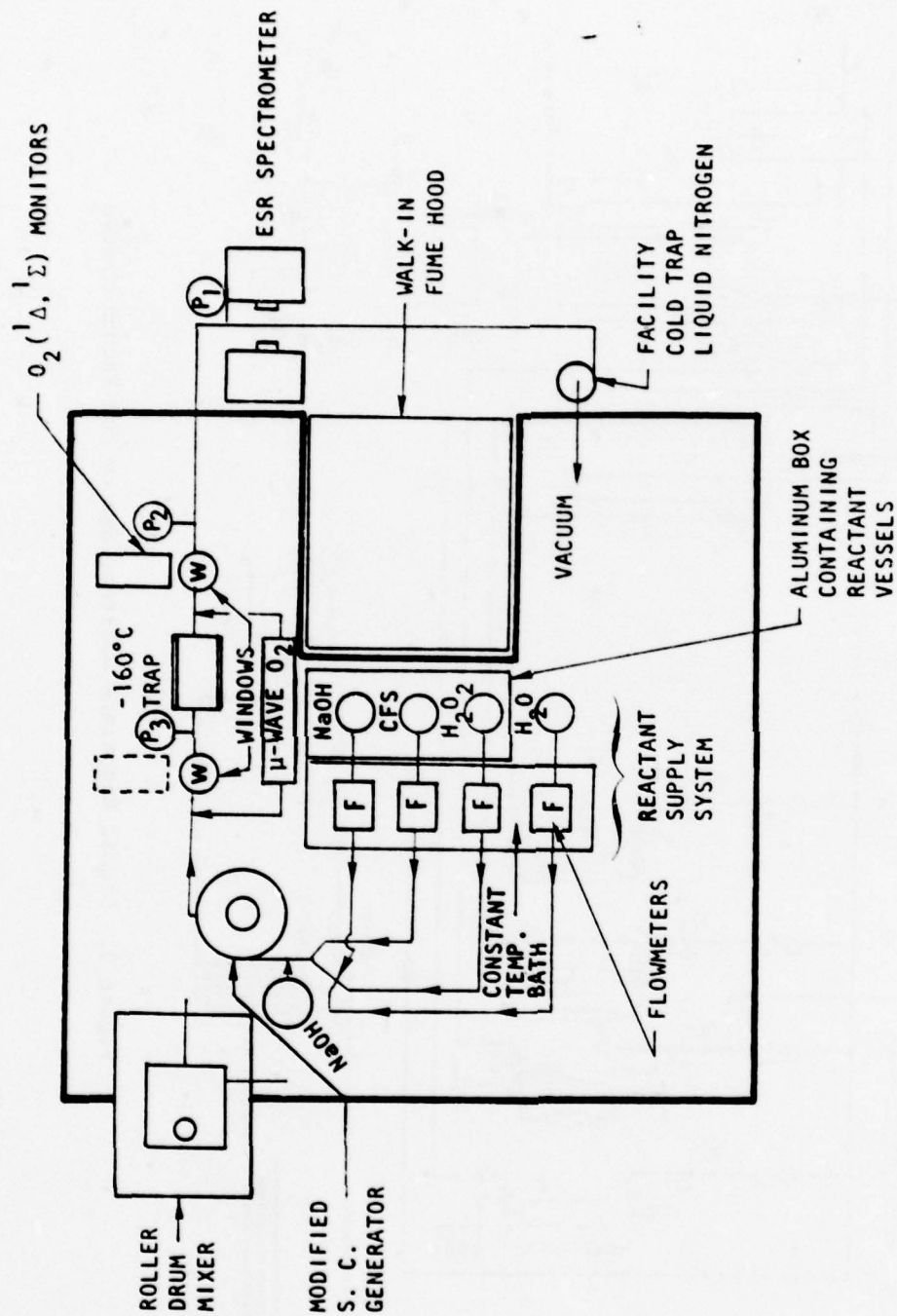


Figure 2 . Tasks 1 and 2 Versatile Experimental Setup Schematic

The Sodium Hydroxide System

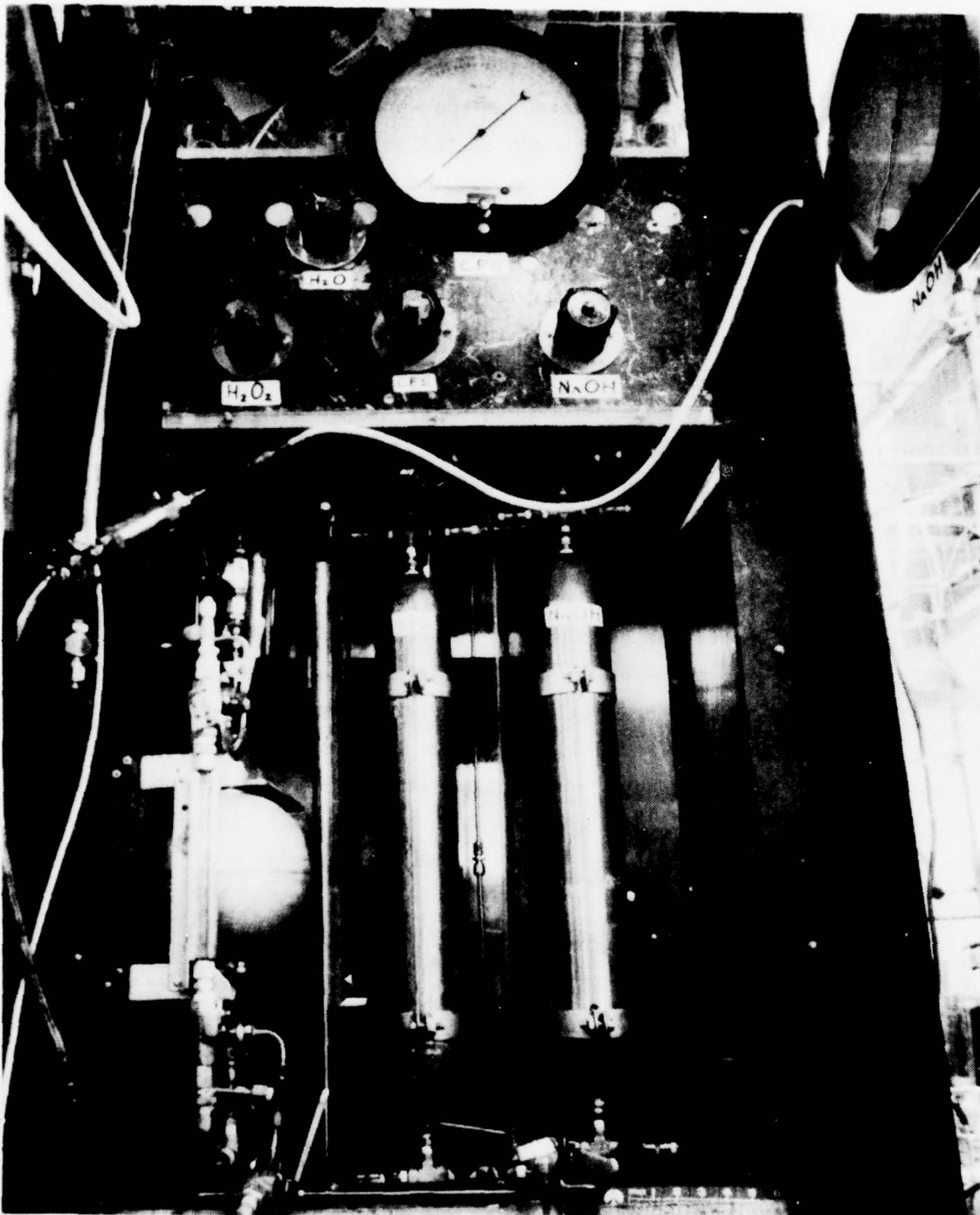
The reactant sodium hydroxide was used in the form of a 50.7% aqueous solution (Baker, reagent). The storage reservoir consisted of a 1-gallon, double-ended stainless-steel Hoke cylinder fitted at the upper end with a fill port, GN_2 pressurization, rupture disk, and vent. A Teflon sight gage connected the upper and lower cylinder ports. All valves and transfer lines were stainless steel (Fig. 4).

The flowrate of the NaOH solution was measured using a capillary viscometric technique. A 17-cm-long, 16 gage (1.194-mm dia) stainless capillary was immersed in a 100 F (37.7 C) thermostat and the pressure drop across the capillary was measured using a variable reluctance differential manometer with both digital readout and recording capability (Fig. 5). The manometer head was ensured to be liquid filled by bleeding both upstream and downstream sides of the diaphragm to the atmosphere. The metered NaOH stream was fed into an on-line mixer together with 90% H_2O_2 .

Calibration of the flowmeter was carried out by determining the time required to deliver a known volume of the NaOH solution at a series of observed differential pressures across the capillary. The apparatus was a 10-ml calibrated tube mounted vertically and filled from the bottom through a horizontal inlet tube. The calibrated tube was rotated about the inlet tube to empty it between measurements. The raw data were converted to the molar flow rates depicted graphically in Fig. 6 according to the formula:

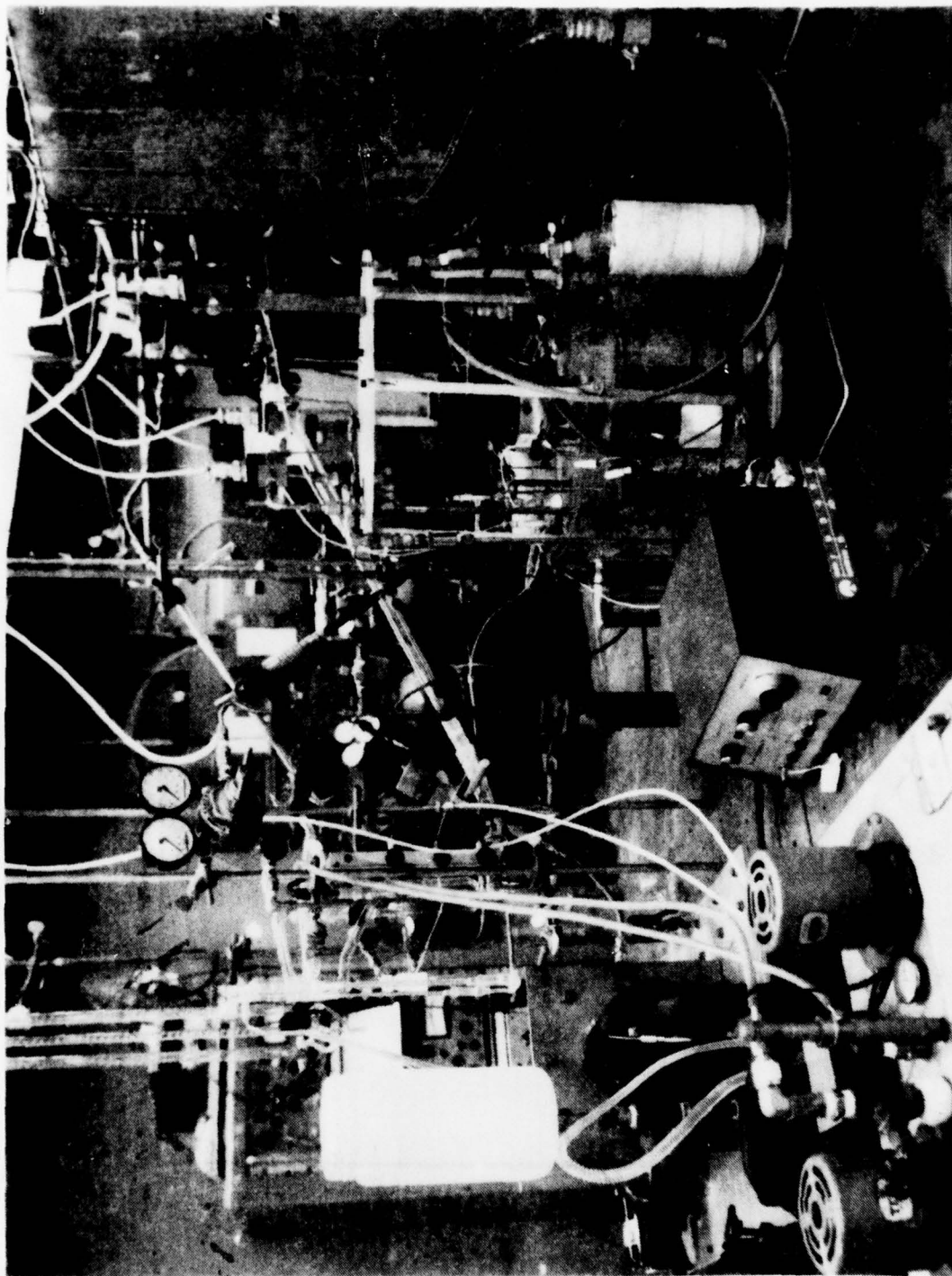
$$\text{mmoles NaOH/sec} = \frac{(\text{ml NaOH solution}) (\text{density}) (\text{assay})}{(\text{seconds}) (\text{mg/mmole})}$$

During testing, the ΔP was recorded. Subsequently, the NaOH flowrate (in millimoles per second) was determined either by inspection of this curve or by calculation using a second-order polynomial in ΔP whose coefficients had been determined from a fit to the data points.



4LC34-11/17/78-S1G*

Figure 4 . Reactant Tanks and Pressurization System



4LC34-11/17/78-SIM*

Figure 5. Constant Temperature Bath With Capillary Flowmeters

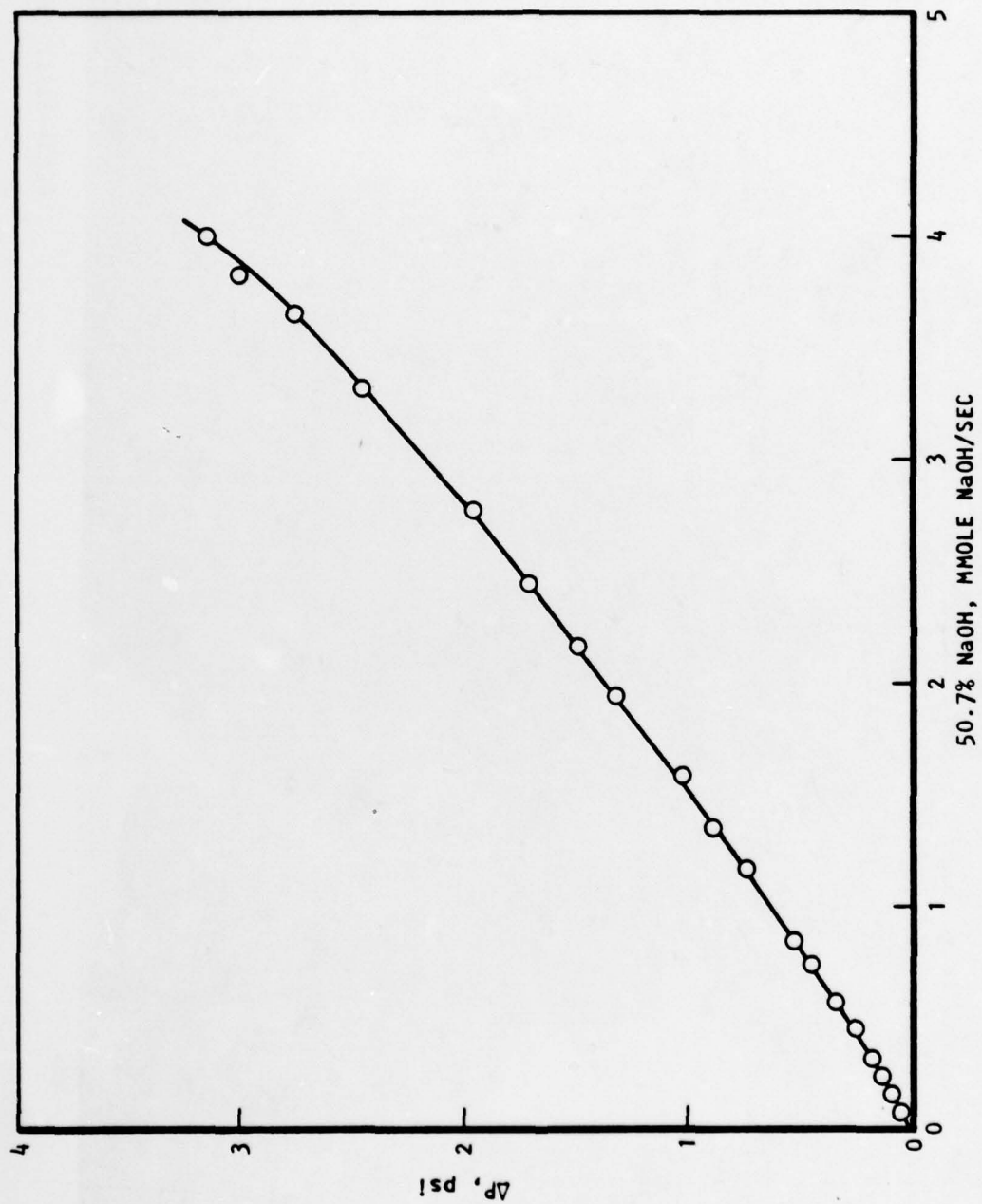


Figure 6. NaOH Flowmeter Calibration

The Hydrogen Peroxide System

The 90% hydrogen peroxide reservoir was a 1-gallon aluminum sphere equipped in the same manner as the 50% NaOH tank (i.e., fill port, GN_2 pressurization, rupture disk, vent, and glass sight gage). In addition, the bottom outlet was fitted so that settled particulate matter could be drained off while the reactant stream passed through a porous Teflon filter (Fig. 3 and 4).

The two-phase flow resulting from slight decomposition of the H_2O_2 to water and oxygen required modification of the capillary viscometric flow-measuring apparatus to achieve satisfactory metering. The initially used stainless-steel system was replaced by a 14-cm-long 0.508-mm glass capillary and Teflon tubing system to decrease the extent of H_2O_2 decomposition. A bleed port was installed immediately upstream of the 100 F (37.7 C) thermostated capillary to prevent entry of O_2 bubbles. The Validyne variable reluctance manometer head used to measure the pressure differential across the capillary was filled with and isolated from the H_2O_2 stream by water to prevent erroneous pressure readouts due to formation of O_2 bubbles in the manometer head.

The metered 90% H_2O_2 stream was mixed continuously with a metered stream of 50% NaOH in an on-line mixer. This flowmeter was calibrated in exactly the same manner and with the same apparatus as was used for the NaOH solution. The H_2O_2 solution used for the calibration assayed 88.8% by permanganate titration. The calibration data are presented graphically in Fig. 7.

The Chlorine Fluorosulfate (CFS) System

The reservoir and thermostated capillary flowmeter were identical in design (but not dimensions) to the sodium hydroxide system with two exceptions. The sight gage was glass rather than Teflon and the manometer head was bled into a cooled evacuated cylinder rather than to the atmosphere (see Fig. 3, 4 and 5). The Celesco manometer head had a Teflon-coated diaphragm and was sealed with Teflon gaskets. The flowmeter capillary was 17.5 cm of 25 gage

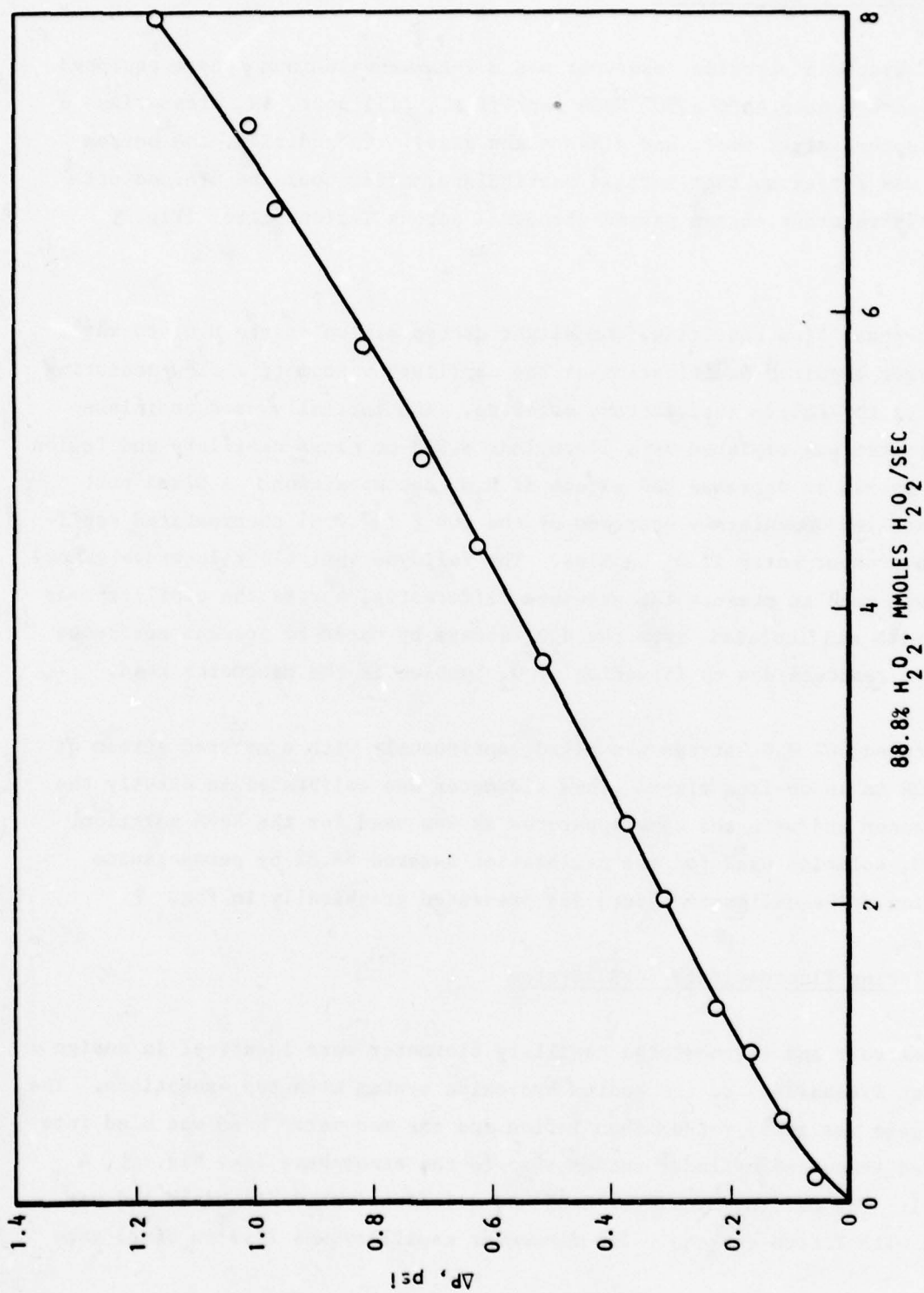


Figure 7. H_2O_2 Flowmeter Calibration

(0.254 mm) stainless steel. Just before entering the $O_2(^1\Delta)$ generator, the metered flow of liquid CFS was vaporized in a 55-cm-long by 13-mm diameter evaporation coil maintained at 47 C by refluxing Freon 113, $CF_2ClCFC1_2$ (Fig. 8).

Calibration of the CFS flowmeter was conducted in the same manner as were the calibrations of the NaOH and H_2O_2 solutions except that the calibrated volume of liquid was collected in a closed system under 10-psig GN_2 pressure rather than open to the atmosphere. The liquid in the calibrated volume was pneumatically transferred through a drain valve to a cooled cylinder between measurements. The graphical presentation of the data is given in Fig. 9 .

In the case of CFS, no published viscosity data were available. This physical constant was required to size the flowmeter capillary using Poiseuille's equation. Accordingly, the viscosity of CFS was determined in a sealed, fused silica Oswald viscometer that had been evacuated and flamed under high vacuum before filling. Five determinations at each of three temperatures (Table 1) were used together with published density data to calculate the viscosity.

TABLE 1. VISCOSITY OF CHLORINE FLUOROSULFATE

Time, seconds	Temperature, C	Density, g/ml*	Viscosity	
			Centistokes	Centipoise
160.8 160.8 161.3 161.0 <u>161.1</u>	30.00	1.686	0.3281	0.5532
161.0 (avg)				
150.3 149.2 149.8 149.9 <u>150.0</u>	37.77	1.667	0.3053	0.5089
149.8 (avg)				
136.5 138.1 135.2 135.4 <u>135.2</u>	50.00	1.544	0.2774	0.4283
136.1 (avg)				
*Gilbreath, W. P. and G. H. Cady, <u>Inorg. Chem.</u> , <u>2</u> , 496 (1963)				

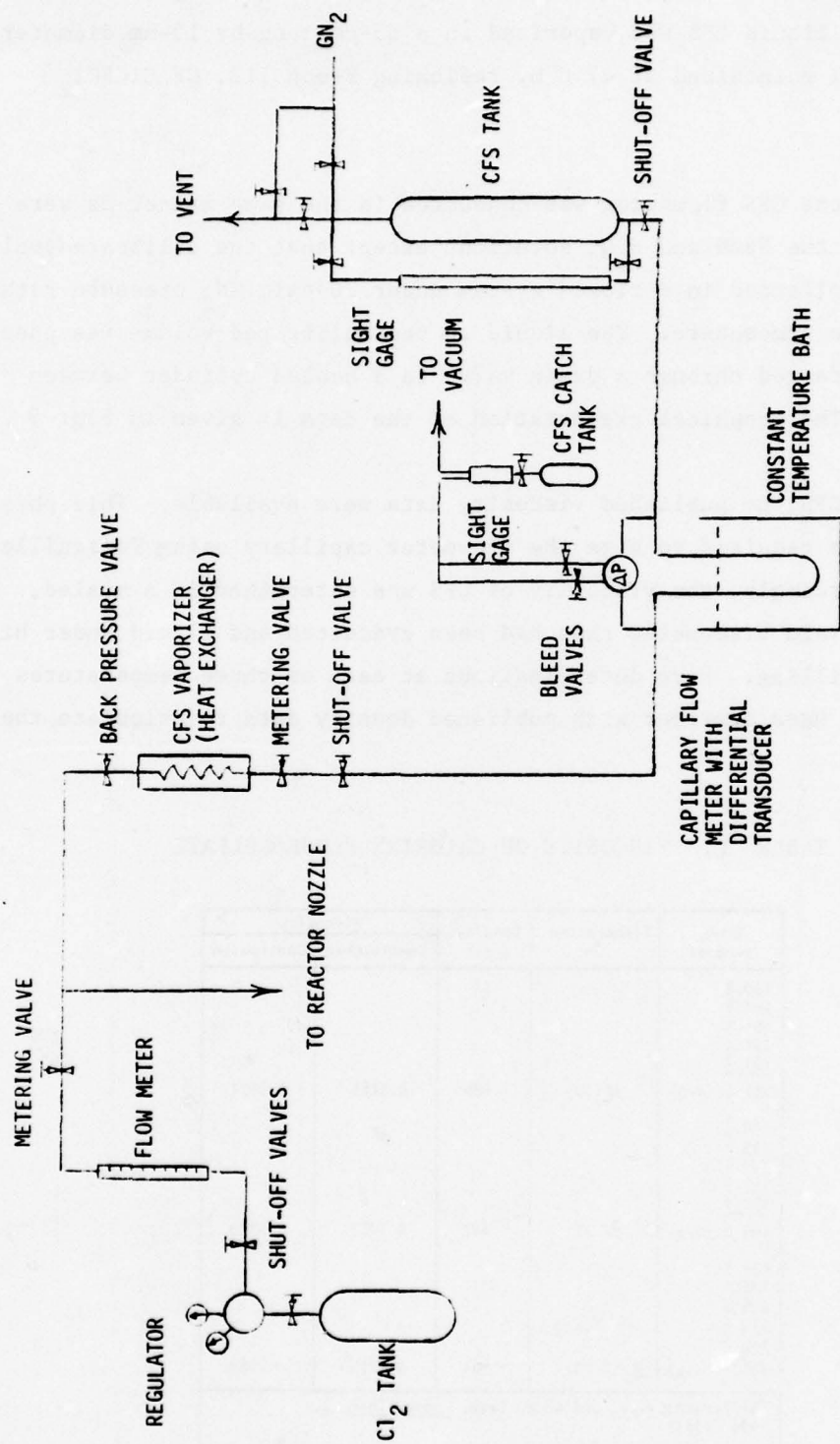


Figure 8. CFS/Cl₂ Delivery System Schematic

The Chlorine System

The chlorine delivery system was quite conventional and consisted of a steel cylinder of liquid chlorine from which gaseous Cl_2 was withdrawn at near atmospheric pressure through a regulator (Fig. 8). The flow to the reactor was measured with an air-calibrated rotameter using a sapphire ball float. The rotameter readings were corrected for density and viscosity but not temperature and pressure to determine the Cl_2 flowrates.

The Premixed Basic Peroxide System

In numerous experiments conducted prior to the development of the on-line continuous basic peroxide mixer, premixed reactant solutions were prepared batchwise and delivered to the $\text{O}_2(^1\Delta)$ generator from a burette under atmospheric pressure (Fig. 10 and 11). Flowrate was determined from periodic volume measurements. The basic peroxide solutions were prepared either from 44% NaOH (to minimize solids precipitation) or solid NaOH admixed with 90% H_2O_2 and maintained in the temperature range of 0 to 25 C. The concentrations of the premixed solutions used are indicated in Table 2 (solutions 1-3).

The On-Line Continuous NaOH/ H_2O_2 Mixer System

The key to successful mixer operation is maintenance of a separation of the peroxide solution and the base solution by means of an oxygen-filled chamber. In operation, the NaOH solution is added dropwise to the magnetically stirred H_2O_2 solution in the thermostated (0 to 5 C) mixer (Fig. 12 and 13). On contact of the NaOH solution with the H_2O_2 , precipitation of solids occurs (probably $\text{NaOOH} \cdot \frac{1}{2}\text{H}_2\text{O}_2 \cdot 2\text{H}_2\text{O}$; Ref. 3) followed by immediate dissolution. Operation of the on-line mixer requires only an infrequent water washdown of the chamber wall when coated by some of the solid which causes excessive decomposition of the H_2O_2 to $\text{O}_2(^3\Sigma)$. The major portion of the ground state oxygen

3. Makarov, S.Z. and N.K. Grigor'eva, Bull. Acad. Sci. U.S.S.R., Div. Chem. Sci., 1955, 15.

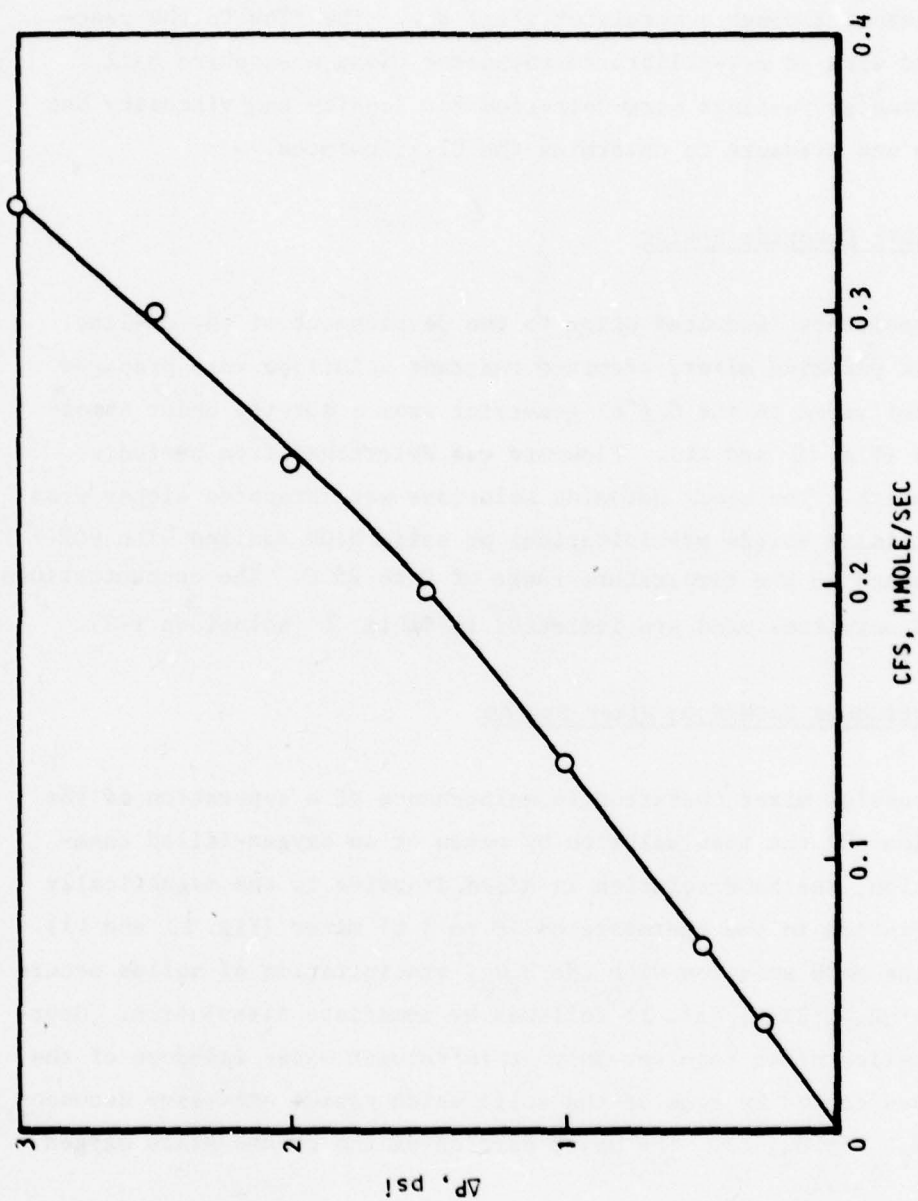


Figure 9. CFS Flowmeter Calibration

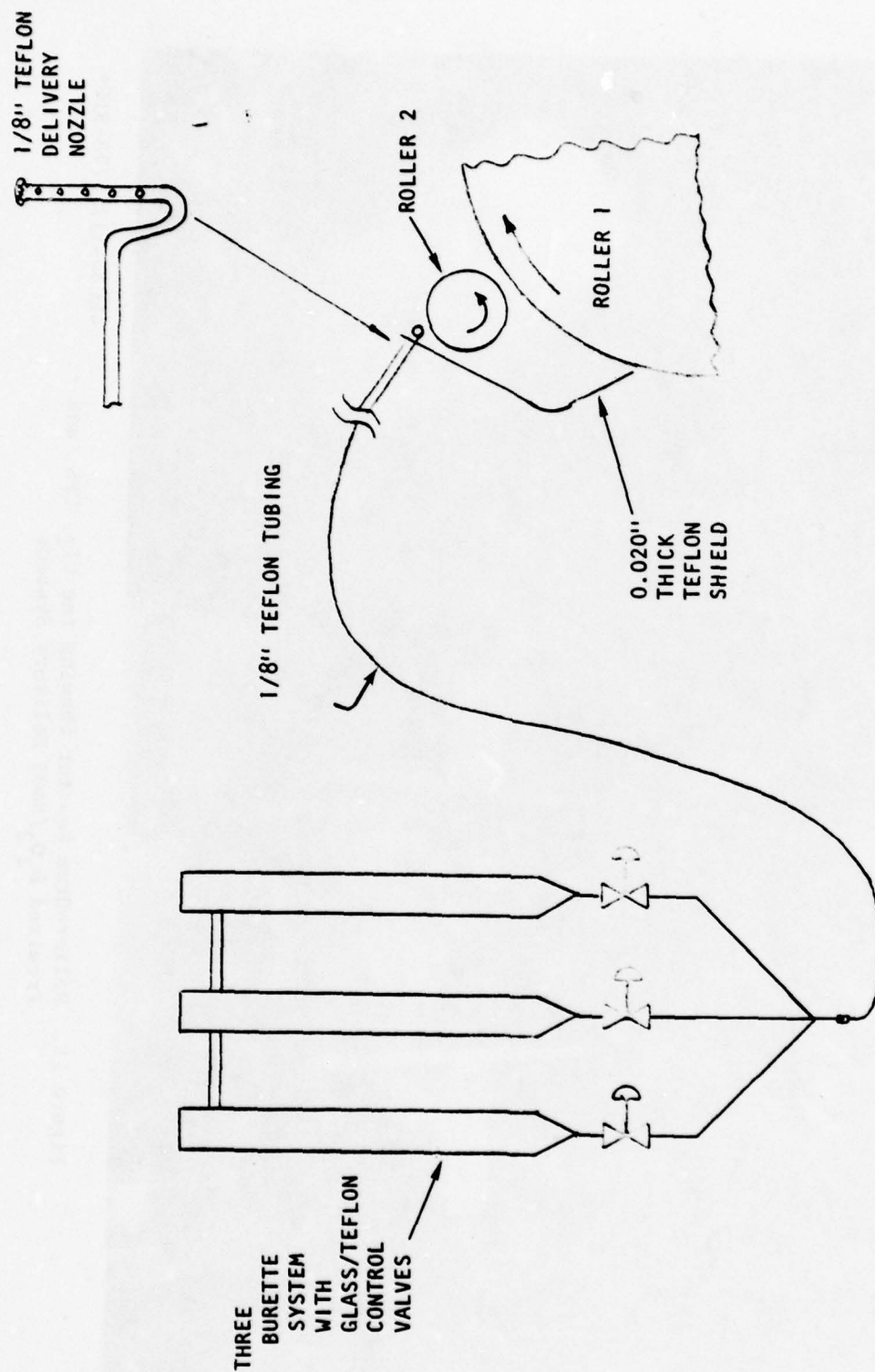
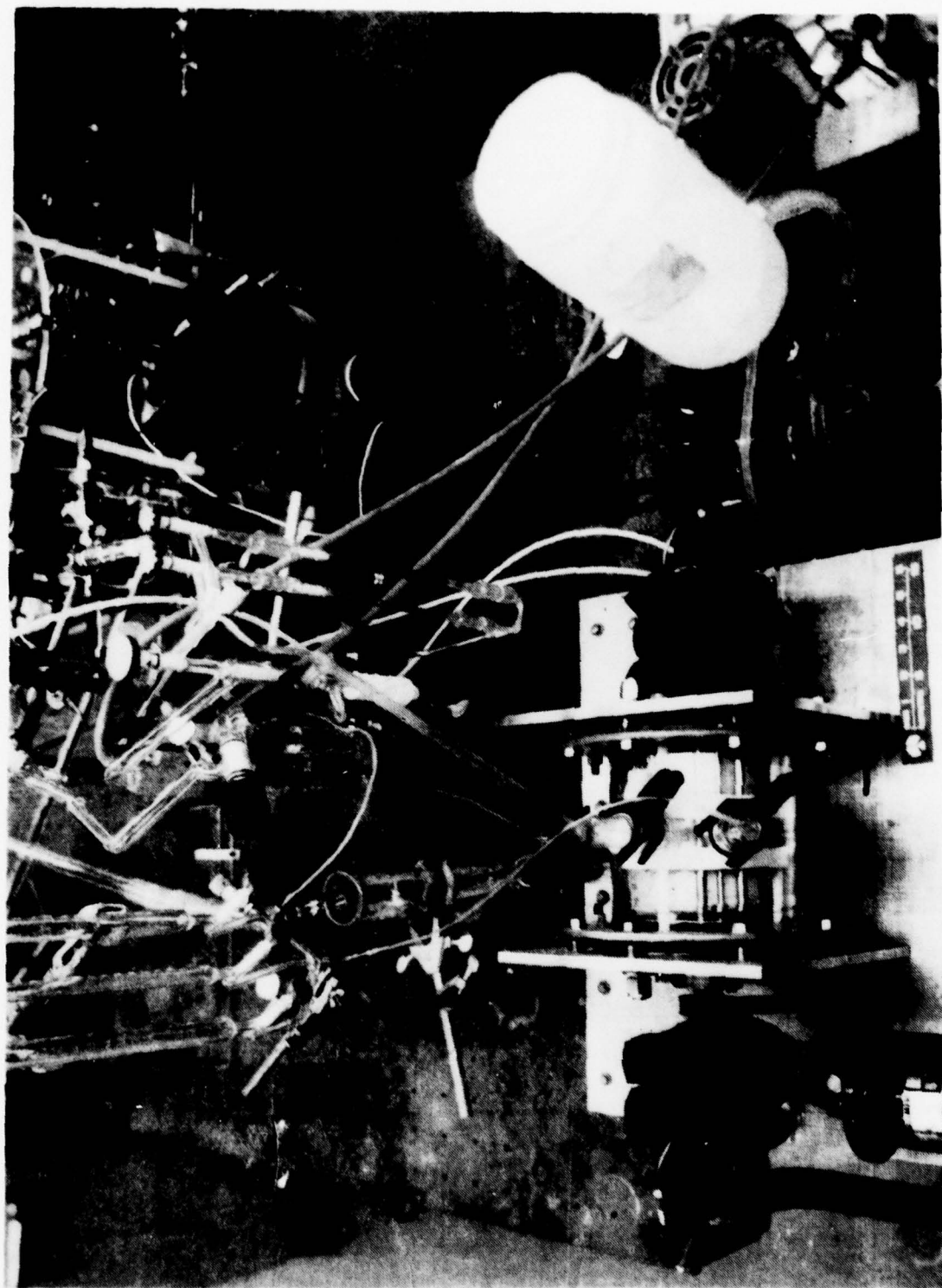


Figure 10. H_2O_2 NaOH Delivery System



4LC34-11/17/78-S1F*

Figure 11. Roller-Drum Reactor Showing the Cl_2 , CFS, and Premixed $\text{H}_2\text{O}_2/\text{NaOH}$ Delivery Systems

TABLE 2. BASIC HYDROGEN PEROXIDE SOLUTIONS

Solution	Preparative Method	Molar Concentration		
		H ₂ O ₂	NaOH	H ₂ O
1	Add 27 g NaOH to 100 ml 90% H ₂ O ₂ while chilling to hold temperature at 0 to 25 C	32.2	6.1	6.8
2	Dilute 50% NaOH 5:1 by volume with H ₂ O and add 70 ml to 100 ml 90% H ₂ O ₂ while chilling to hold to 0 to 25 C temperature	21.1	4.3	17.9
3	Dilute solution No. 2 1:1 by volume with H ₂ O	10.6	2.2	42.6
4	On-line mixing of 1.48 mmoles/sec H ₂ O ₂ (88.8%) and 0.604 mmole/sec NaOH (50.7%) streams while chilled in an ice bath	20.3	8.3	22.7
5	On-line mixing into roller-drum reactor at H ₂ O ₂ ΔP = 0.300, NaOH ΔP = 0.200	27.4	4.4	16.2
6	On-line mixing into roller-drum reactor at H ₂ O ₂ ΔP = 0.600, NaOH ΔP = 0.400	28.0	4.1	15.6

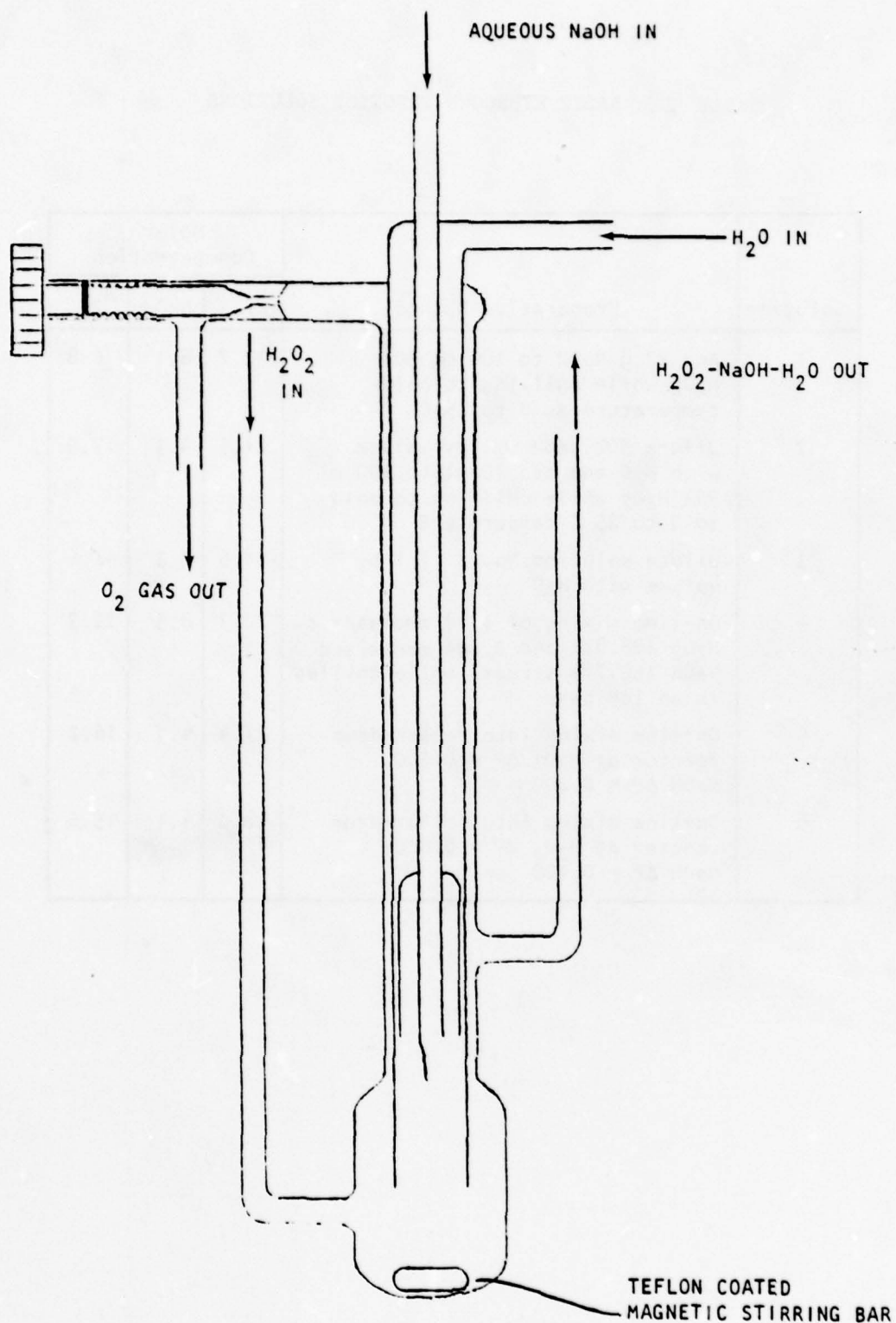
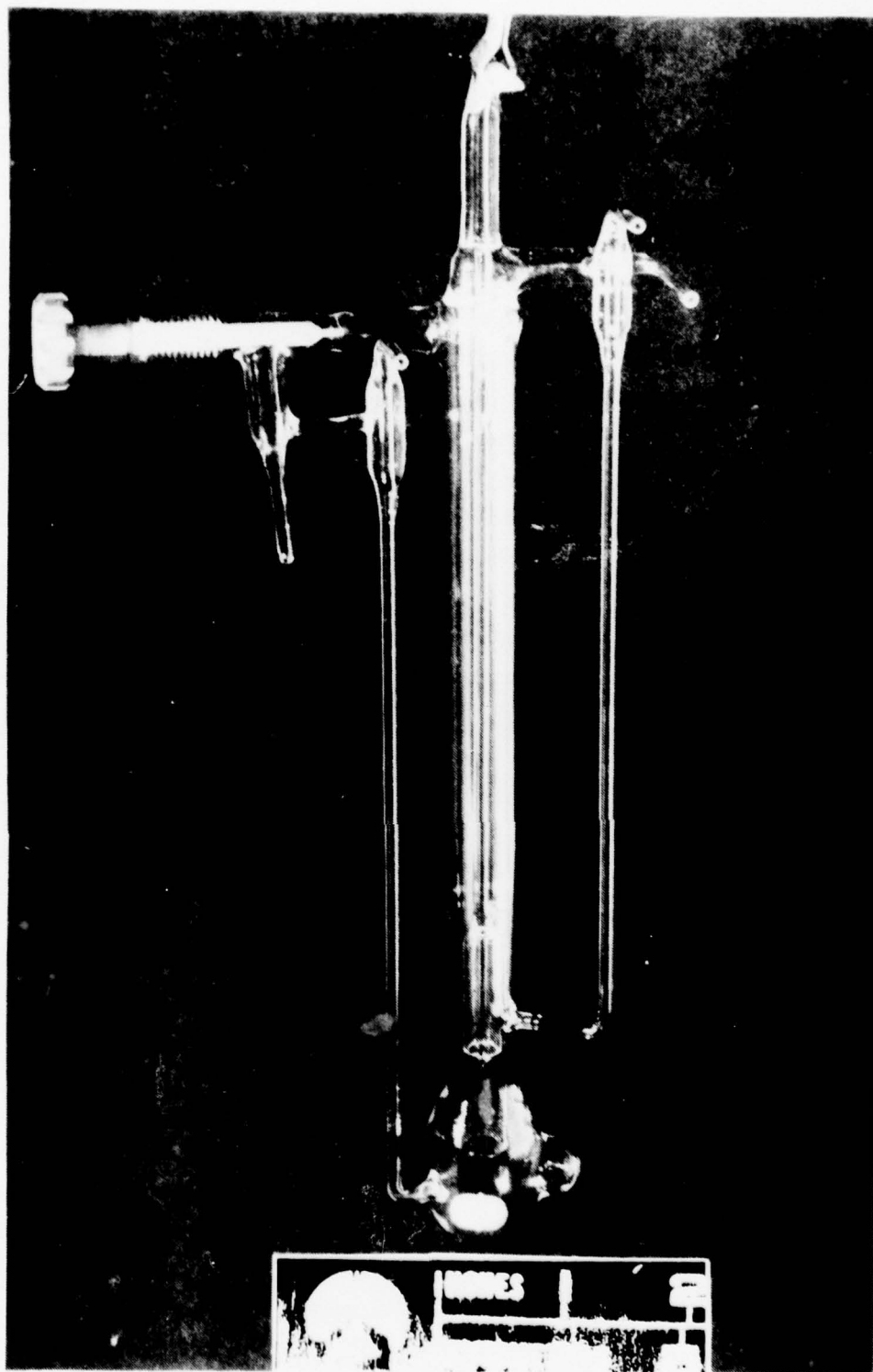


Figure 12. On-Line Continuous Base-Peroxide Mixer



4LZ81-12/21/78-C1

Figure 13. On-Line Base Peroxide Mixer

formed in the mixer is vented through a bypass around the system diagnostics. The remainder, together with the basic H_2O_2 solution, is introduced to the reaction chamber of the $\text{O}_2(^1\Delta)$ generator.

If the mole ratio of $\text{NaOH}/\text{H}_2\text{O}_2$ does not exceed ~ 0.41 , the resulting mixture of basic peroxide does not solidify when the mixer effluent is discharged either to atmospheric pressure or vacuum and the temperature of the thermostat is in the range 0 to 5 C. Qualitatively, it appears that precipitation of solids occurs more readily if the mixer effluent is discharged into the $\text{O}_2(^1\Delta)$ generator under reduced pressure. The factors affecting this behavior have not been elucidated. The near-maximum molar solubility of NaOH , as well as the concentrations of the other components in the on-line mixed basic peroxide stream, are indicated in Table 2 (solution 4).

A check run of the mixer was made with a $\text{NaOH}/\text{H}_2\text{O}_2$ ratio of 0.4 at a series of six flowrates to compare the actual volume of basic peroxide delivered with the volume calculated from the flow calibration of each reactant. The data in Table 3 show a delivered volume of approximately 1 ml in excess of the calculated volume independent of flowrate, suggesting, perhaps, a constant error in the H_2O_2 calibration curve in the low flowrate range.

Another series of mixer tests was run to obtain analytical samples so that the flowrates of H_2O_2 and NaOH calculated from the flowmeter calibrations could be confirmed experimentally. Each analytical sample was collected directly in a tared, magnetically stirred Erlenmeyer flask containing an excess of standardized 2N H_2SO_4 and cooled in an ice bath. The H_2O_2 was determined by permanganate titration and the base by back titration of the excess acid. The data in Table 4 indicate that the experimental sample weights tend to be higher than calculated from the flowmeter calibration curves, as expected, based on the previously observed higher than calculated sample volumes. The values for molar concentrations are less certain because of the estimated basic peroxide solution densities used in the computations. However, no significant amount of decomposition is indicated to have occurred during the mixing process.

TABLE 3. ON-LINE MIXER OPERATIONAL DATA

84.4% H ₂ O ₂ ^(a)			50.7% NaOH			Effluent Flowrate, ^(b) ml/min	
ΔP , psi	mmole/sec	ml/min	ΔP , psi	mmole/sec	ml/min	Observed	Calculated
0.085	0.38	0.67	0.070	0.10	0.22	2.0	0.89
0.125	0.74	1.32	0.160	0.26	0.50	2.8	1.82
0.175	1.00	1.78	0.240	0.39	1.21	4.4	2.99
0.225	1.38	2.45	0.320	0.51	1.59	5.0	4.04
0.280	1.81	3.22	0.400	0.64	1.99	6.3	5.21
0.320	2.12	3.77	0.500	0.79	2.46	7.2	6.23
0.175	1.00	1.78	0.250	0.40	1.25	-- (c)	3.03
0.315	2.08	3.69	0.500	0.79	2.46	-- (c)	6.15
0.300	1.98	3.51	0.200	0.32	1.00	-- (c)	4.51
0.600	4.30	7.64	0.400	0.63	1.96	-- (d)	9.60

^(a) Calibration of flowmeter with 88.8% H₂O₂ is assumed to hold for other concentrations
^(b) Discharging under atmospheric pressure
^(c) Discharging under dynamic vacuum in roller-drum reactor
^(d) Nominal flows used in most O₂(¹ Δ) tests; calculated concentrations 27.4M H₂O₂, 4.4M NaOH, 16.2M H₂O at lower flowrate and 28.0M H₂O₂, 4.1M NaOH, 15.6M H₂O at high flowrate

TABLE 4. ANALYSES OF ON-LINE MIXED BASIC PEROXIDE

Sample No.	Time, seconds	87.6% H_2O_2 *		50.7% NaOH		Sample Weight		Molar Concentrations, (calculated)			Observed H_2O_2
		ΔP	mmole/sec	ΔP	mmole/sec			H_2O_2	NaOH	H_2O_2	
1A	60	0.280	1.81	0.200	0.32	5.738	Calculated	27.8 (26.5)	4.3 (4.7)	-	(17.3)
1B	60	0.300	1.98	0.200	0.32	7.111		27.8 (27.1)	3.9 (4.4)	-	(16.8)
1C	60	0.300	1.98	0.200	0.32	6.849		27.9 (27.1)	4.2 (4.4)	-	(16.8)
2A	60	0.600	4.30	0.398	0.63	13.117		27.3 (27.6)	4.3 (4.0)	-	(16.8)
2B	60	0.580	4.08	0.400	0.63	11.628		27.5 (27.5)	4.4 (4.2)	-	(16.5)
2C	60	0.570	4.04	0.400	0.63	12.451		27.2 (27.4)	4.6 (4.3)	-	(16.5)
3A	60	0.310	2.06	0.402	0.63	7.800		21.4 (20.7)	6.5 (6.3)	-	(19.1)
3B	60	0.300	1.98	0.400	0.63	7.824		20.1 (20.3)	6.8 (6.5)	-	(19.4)
3C	60	0.300	1.98	0.400	0.63	7.792		19.7 (20.3)	6.9 (6.5)	-	(19.4)
4A	75	0.500	3.54	0.700	1.08	17.414		20.3 (20.7)	6.3 (6.3)	-	(19.1)
4B	60	0.500	3.54	0.700	1.08	14.030		20.3 (20.7)	6.1 (6.3)	-	(19.1)
4C	60	0.515	3.66	0.700	1.08	14.242		20.8 (20.9)	6.0 (5.7)	-	(20.1)
5A	60	0.200	1.18	0.400	0.63	6.071		17.6 (16.1)	7.7 (8.6)	-	(22.7)
5B	60	0.200	1.18	0.400	0.63	6.686		17.6 (16.1)	7.6 (8.6)	-	(22.7)
5C	60	0.200	1.18	0.400	0.63	6.399		17.4 (16.1)	7.8 (8.6)	-	(22.7)

*Calibration of flowmeter with 88.8% H_2O_2 is assumed to hold for other concentrations

Prior to testing of the on-line mixer just described, another mixer was designed and tested (Fig. 14 and 15). In this mixer, separately metered streams of 90% H_2O_2 and 50% NaOH combined immediately upstream of a 12-element Kenics mixer. In operation, the mixer was purged with water prior to the sequential flow of the 90% H_2O_2 and 44% NaOH streams. Immediately on contact of the 44% NaOH stream with the 90% H_2O_2 , the incoming NaOH solution solidified for a distance of 2 to 3 cm upstream from the contact point. The same behavior was repeated when the concentration of an estimated 40 to 50% H_2O_2 was increased gradually. No further testing of this design was attempted.

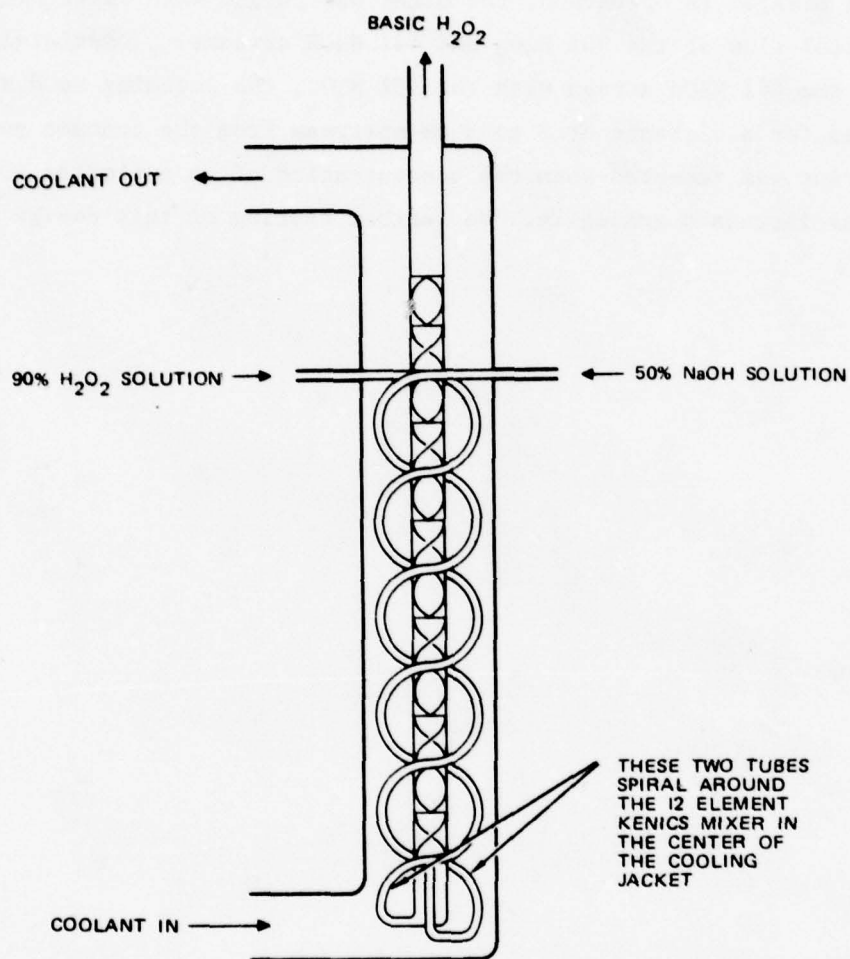
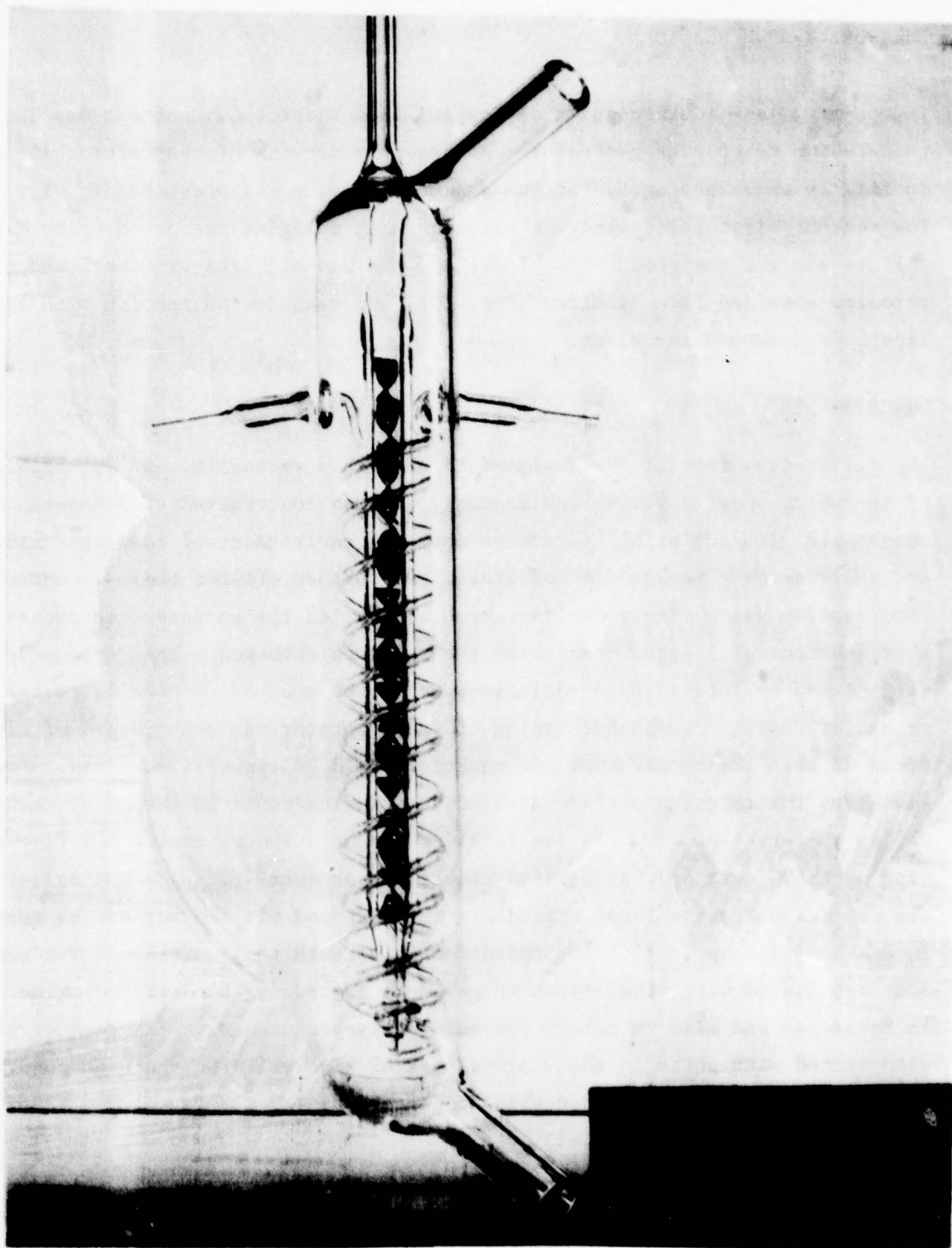


Figure 14. Initial Design for On-Line Continuous Base-Peroxide Mixer



5AL21-12/12/78-C1

Figure 15. Initial On-Line Base Peroxide Mixer

THE ROLLER-DRUM REACTOR

The primary gas-liquid contact device utilized under this contract was the roller-drum reactor or generator. An assembly drawing of the reactor is shown in Fig. 16 and a photograph of the assembled device was presented in Fig. 11. The reactor mixed basic peroxide solution with chlorine gas or chlorine fluorosulfate gas for the production of $O_2(^1\Delta)$. It was utilized with premixed basic peroxide supplied from burettes (Fig. 10), and also in conjunction with an on-line base and peroxide mixer.

Capabilities

The roller-drum reactor was designed to be highly versatile. It is capable of operating under a vacuum environment, and was constructed with materials compatible with the highly corrosive chemical environment of basic peroxide and chlorine or chlorine fluorosulfate. It further offered thermal control of the reaction via a liquid coolant which controlled the surface temperature of a cylindrical Al_2O_3 drum upon which the reaction occurred. The contact drum surface can be rotated by a variable-speed motor mounted externally to the generator casing. The outer casing of the generator was constructed of clear Pyrex so that the progress of the reaction could be visually observed. Additionally, the reaction surface area of the alumina could be varied by changing Teflon spacers that enclosed the reacting volume. The generator was fitted with an Al_2O_3 scraper that scraped reaction byproducts (liquids and salts) off the contact surface. Those byproducts then dropped off the scraper by gravity into a cooled trap ($-78^\circ C$) located directly beneath the generator. The generator was fitted with five 1-inch-ID ports to introduce the basic peroxide and chlorine gas and also to remove the chemically produced O_2 . The reactor was also fitted with ports in the stainless-steel side walls so that the generator interior could be water-washed without disassembly.

Detailed Description

An engineering drawing of the glass housing that encloses the roller contact surface is shown in Fig. 17*. A photograph of that housing and the CFS/ Cl_2

*Figures 16 and 17 are foldouts and are located at the end (pages 217 and 218) of the report.

Figure 16 is a foldout and appears at the back of this book on page 217.

Figure 17 is a foldout and appears at the back of this book on page 218.

Teflon nozzle (to be described later) is shown in Fig. 18. That housing is all Pyrex and was specially manufactured from two pieces of 6-inch ID "double tough" Corning pipe ends. Five 1-inch-ID ports were fitted to the pipe as shown. Those ports were equipped with number 25 Pyrex brand Corning manufactured joints allowing easy and rapid attachment to mating glassware. The larger 2-inch ID port was used to gravity collect solid and liquid reaction byproducts. Attached to that port was a Pyrex trap cooled to -78°C which quenched further reaction and minimized ground-stage oxygen evolution. The ends of the 6-inch pipe were ground flat and parallel to each other. Each glass end sealed up against a stainless-steel end plate, and leakage was prevented by using two Teflon-coated rubber O-rings between each end plate and the glass pipe.

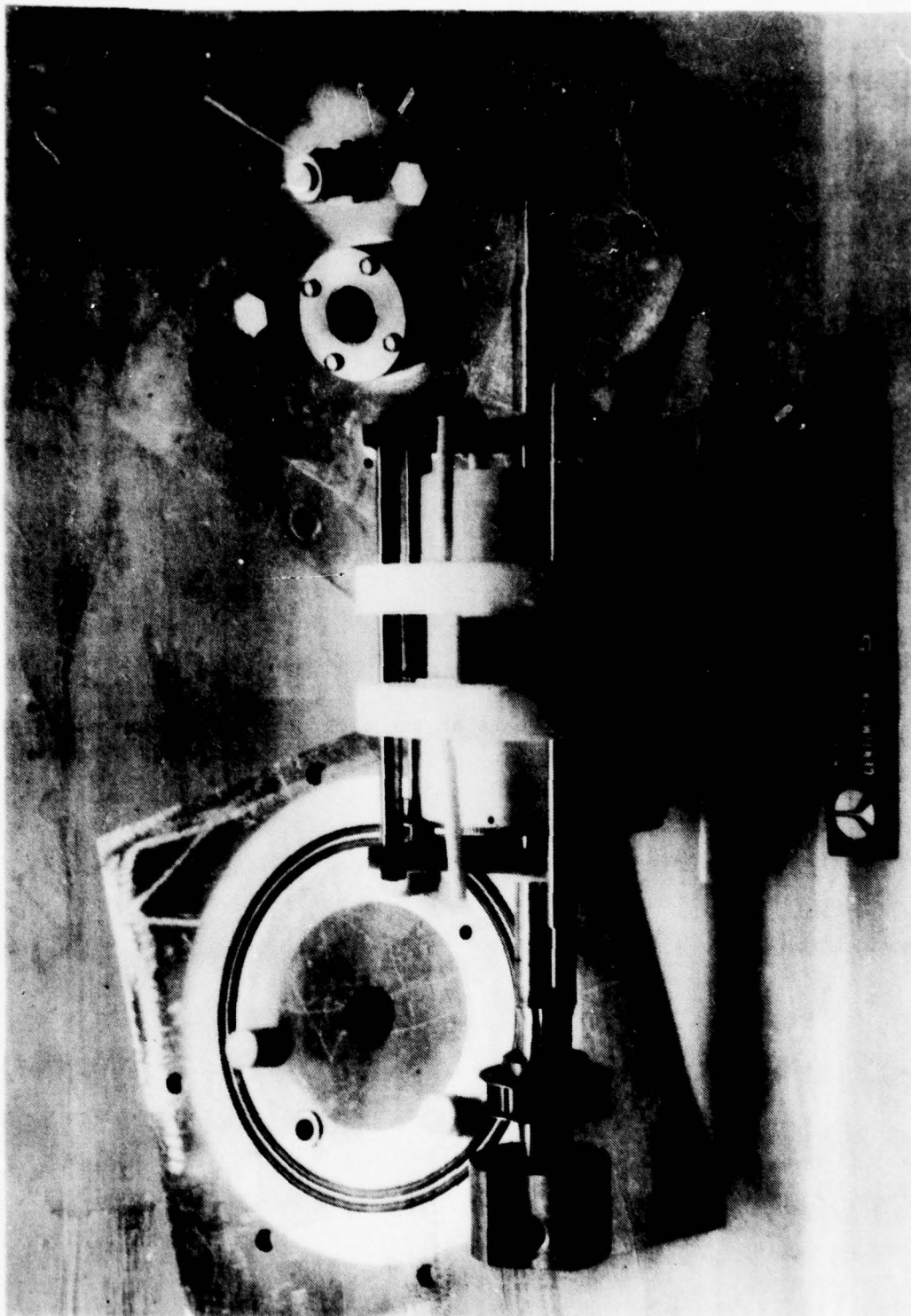
Referring to Fig. 17, we consecutively number the five 1-inch ports from the upper left to the lower right (1,2,3,4,5, respectively). Port 1 was utilized to introduce the basic peroxide mixture; port 2 introduced the CFS or Cl_2 ; and ports 3, 4, and 5 withdrew the gaseous reaction products from the generator. Only one port at a time (usually 3 or 5) was used to withdraw the $\text{O}_2(^1\Delta)$ from the generator. During several early experiments, a three-way pneumatic valve located downstream of ports 3 and 5 allowed O_2 withdrawal from either of those two ports during a run. This effectively varied the $\text{O}_2(^1\Delta)$ residence time within the generator.

The larger roller (Fig. 19 and 20*) is covered with a cylinder of Al_2O_3 which provides the surface upon which the basic peroxide is deposited for reaction with CFS or Cl_2 gas. The alumina cylinder proved difficult to manufacture and two were cracked during final grinding. This caused manufacturing delays and, for this reason, a spare alumina cylinder was manufactured to minimize down time should another breakage occur. Alumina was chosen because it is compatible with the basic peroxide/CFS environment and also because its thermal conductivity was adequate to allow rapid temperature regulation of the reaction surface. Temperature conditioning was achieved by utilizing a commercial bath-type cycling refrigerator employing methanol-water mixtures. The coolant was

*Figure 20 is a foldout, and is located at the end (page 219) of the report.



Figure 18. Roller-Drum Reactor Glass Housing and Gas Nozzle 4LC34-8/23/78-S1B*



4LC34-8/23/78-S1C*

Figure 19. Roller-Drum Reactor Internal Assembly and End Plates

Figure 20 is a foldout and appears at the back of this book on page 219.

pumped through insulated lines and through the large roller within the generator. Thermocouples at the coolant input and exit of the roller indicated the temperature of the reacting surface. Typically, they were not more than 1/2 to 1 degree apart during an experiment. Heat transfer calculations indicated that the reaction surface temperature would be maintained within a 5 C range during an experiment. The temperature range of operation was from ambient to approximately -40 C. To minimize the thermal response time of the large roller, it was constructed hollow in the middle (to minimize total heat content) and the coolant was circulated directly beneath the alumina cylinder. Silicon rubber O-rings prevented coolant leakage at the low temperatures and vacuum environment of operation.

A 1-inch-wide section of the alumina roller was utilized during all tests (see Fig. 19). That reaction width was at the center of the roller and located directly below the five 1-inch glass ports. To conform with the 1-inch reaction width, an alumina scraper and small alumina roller (which applied the basic peroxide to the large roller), both of which are 1-inch wide, were utilized. The 1-inch-wide reaction zone was isolated from the remainder of the drum by Teflon baffles. The baffles extended radially outward from the alumina surface to the inner glass walls of the generator. The fit between the baffle and inner glass wall was not leak sealed or particularly "tight"; however, it served the function of confining the reaction gases to that enclosed section of the generator.

An added refinement that further confined the CFS or Cl_2 to close contact with the wetted alumina surface was the installation of a Teflon shield. The shield followed the contour of the Al_2O_3 and was located a variable distance above the drum surface. It was varied from 10 to 15 cm long and butted up against the Cl_2 /CFS nozzle on one end, and extended to the location of the port which was used to withdraw the O_2 ($^1\Delta$). Several lengths were used depending on the location of the withdrawal port employed. The shield was cut from a sheet of clear Teflon to allow viewing of the reaction surface. It was held in place by grooves cut into the Teflon baffles. Four grooves were cut into each baffle at different radial distances from the drum axis. This allowed the shield to

be located at several heights above the alumina surface. The usual position of the shield was in the groove closest to the drum, thereby providing the most intimate gas-liquid contact. The height of the closest shield position above the alumina surface was approximately 0.66 cm.

CFS or Cl_2 was fed into the generator through an all-Teflon nozzle inserted at port 2. A schematic of the nozzle is shown in Fig. 21.* Note that the nozzle exit orifice is a 1-inch-wide slit and would thus provide a homogeneous flux of CFS or Cl_2 gas across the reaction zone width. The slit height could be varied to help control the gas exit velocity, and it was designed to impinge the gas at an angle on the reaction surface. Slit heights used during the tests were in the 0.020-inch range. The height of the nozzle above the alumina drum was variable to allow the wetted surface to pass beneath without scraping off the basic peroxide reactant. This height control was achieved by threading the nozzle head onto the nozzle body; thus, by screwing the nozzle body deeper into the head, the gap between the roller and nozzle was increased. The separation height commonly used was about 0.050 inch. This gap does afford a pathway for the CFS or Cl_2 to escape the reaction volume and react with the basic peroxide earlier than desired. However, the gap height is fairly small and about 1-inch long, thus minimizing this problem. Also, the $\text{O}_2(^1\Delta)$ removal port sets up the opposite direction as the primary flow path.

The basic peroxide was applied in an even layer to the large alumina roller by wetting a small alumina roller that travelled at the same surface velocity. The small roller was geared to the large roller to ensure identical surface velocities and the gap between the two rollers was adjustable. It was nominally kept at approximately 0.020 inch for most of the experiments. An engineering drawing of the small roller assembly is shown in Fig. 22.*

The small alumina roller was wetted by dripping basic peroxide onto it as it rolled with the large Al_2O_3 drum (see Fig. 10). The nozzle that dripped the

*Figures 21 and 22 are foldouts and are located at the end (pages 220 and 221) of the report.

Figure 21 is a foldout and appears in the back of this book on page 220.

Figure 22 is a foldout and appears in the back of this book on page 221.

basic peroxide was simply a piece of 1/16-inch Teflon spaghetti tubing bent parallel to the axis of the small roller and located 1/4-inch vertically above it. The end was heat sealed and five evenly spaced holes were pierced through the tubing by a wire, and the basic peroxide dripped out of those holes onto the surface of the small roller. It was found during early runs that the bubbling basic peroxide would splash from both the nozzle exit and small roller surface onto the inner glass casing and obscure the visible operation of the generator. To alleviate this problem, a small, nearly transparent Teflon splash plate or shield was installed over the nozzle and small roller. That shield confined the splashing and was used on all of the later roller-drum tests.

In the reaction volume region between the large Teflon baffle plates, the materials exposed to the $O_2(^1\Delta)$ species included the alumina drum surfaces and alumina scraper, the Teflon baffles, Teflon nozzles and Teflon shield and, finally, the inner glass wall. Only a small amount of stainless steel was exposed within the reaction volume of the Teflon baffles. That included the support and strut for the alumina scraper and the shaft for the small alumina roller, both of which were not centrally located in the reaction zone. External to the reaction volume, the side plates of the generator and the shaft of the large roller had exposed stainless surfaces. Those surfaces were halocarbon greased and all components of the generator showed no corrosive effects from the CFS, Cl_2 , and basic peroxide reactants.

The roller-drum was powered by a high-torque, low-speed electric motor that belt drove the drum axis external to the generator housing. The variable speed motor had a maximum speed of 10 rpm, at which most of the experiments were carried out.

The alumina scraper was tension-controlled via a spring mechanism. One side of the scraper shaft extended through the generator side plate and was sealed from leakage via an O-ring. A lever arm was attached to the end of the shaft and, at its end, a spring allowed various scraper tensions to be applied.

The solid/liquid reaction byproduct trap at the bottom of the generator was kept at -78°C and was easily removable for cleaning. The trap had added to it a port with a number 25 purex O-ring joint that could be used to withdraw O_2 from the generator (Fig. 23). This modification was added to help remove water vapor as soon as possible and prior to the next downstream trap, which was also at -78°C .

Both side plates of the reactor had capped, 1/2-inch-diameter holes that could be opened after a test run and used for washing the interior of the generator. This was done with a simple nozzle made of Teflon tubing with holes drilled into its end. Pressurized distilled water from the distilled water tank was used for washing. Prior to washing, the reaction byproduct trap was removed and a pail placed beneath the 2-inch ID port to collect the wash residue. Washing was efficient and rapid.

Several problems did occur with the generator and most of them were related to bushing failure problems on the main shaft. The bushing failure problems then resulted in failure of the neighboring rotating seals with subsequent leaks. These failures occurred both where the main shaft entered the side plates and also where the coolant entered and exited the shaft. The problem was solved at the side plates by adding fluorocarbon-lubricated needle bearings and putting a hardened sleeve on both sides of the main shaft at those points. This same fix was applied where the coolant enters and leaves the main shaft but failure occurred once again when running at low temperatures. The coolant washed the lubricant off those end bearings which then ran "dry" and galled on the shaft. This problem was solved by using a Teflon sleeve in place of the bearings. Once these minor fixes were employed, mechanical operation of the generator was quite satisfactory.

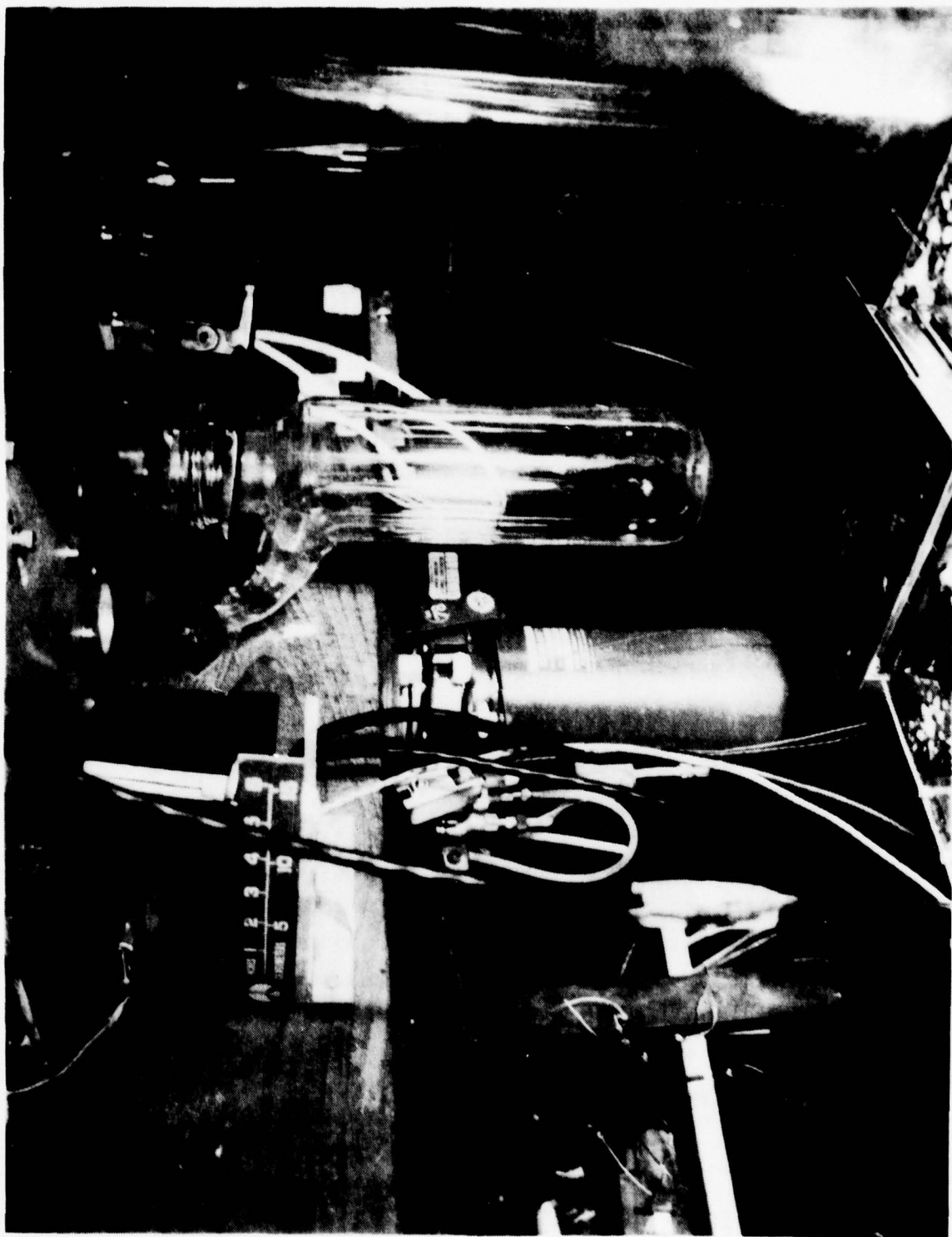


Figure 23. Solid/Liquid Reaction Byproduct Trap, Roller-Drum Reactor 4LC34-11/17/78-S1L*

PRODUCT DELIVERY SYSTEM

The product delivery system refers to the vacuum system downstream of the reactor.

Flow System Description

A number of system configurations were employed and these are shown schematically and identified by Fig. 24 through 31. Results with different configurations and rationale for changing are discussed in Section IV. Trap 1, where the solid and liquid product is collected, was shown in Fig. 23. Figure 32 shows trap 2 as used in configuration C. The middle section of the flow system, including the three-way valve and trap 3, is shown in Fig. 33. Figure 34 shows the downstream end of the flow system, from the $O_2(^1\Delta)$ optical monitor, through the ESR spectrometer, through the facility trap, and to the 4-inch facility vacuum system inlet.

Pumping System Description

The facility vacuum system consists of three positive-displacement, roots-type, blower pumps backed by a $9.9 \text{ m}^3/\text{min}$ (350 cfm) piston-type Stokes pump. When the system is activated, the nominal volume flowrate is $58 \text{ m}^3/\text{min}$ (2050 cfm) at the vacuum pumps, and the pressure range is from 0.27 to 18.1 kPa (0.3 to 20 torr). The blowers are driven by electric motors via belts. An interstage heat exchanger is utilized to take out the heat load produced by the blower pumps. The exhaust from the Stokes pump is passed through a caustic scrubber prior to venting to the atmosphere. The scrubber is intended to provide aqueous sodium hydroxide scrubbing of the exhaust gases in the concurrent shower, liquid-drop tower of minimum exhaust back pressure on the vacuum system. System blankoff pressure is $<45 \times 10^{-3} \text{ kPa}$ ($<50 \text{ mtorr}$). System performance in terms of pressure versus flowrate is described in the next section.

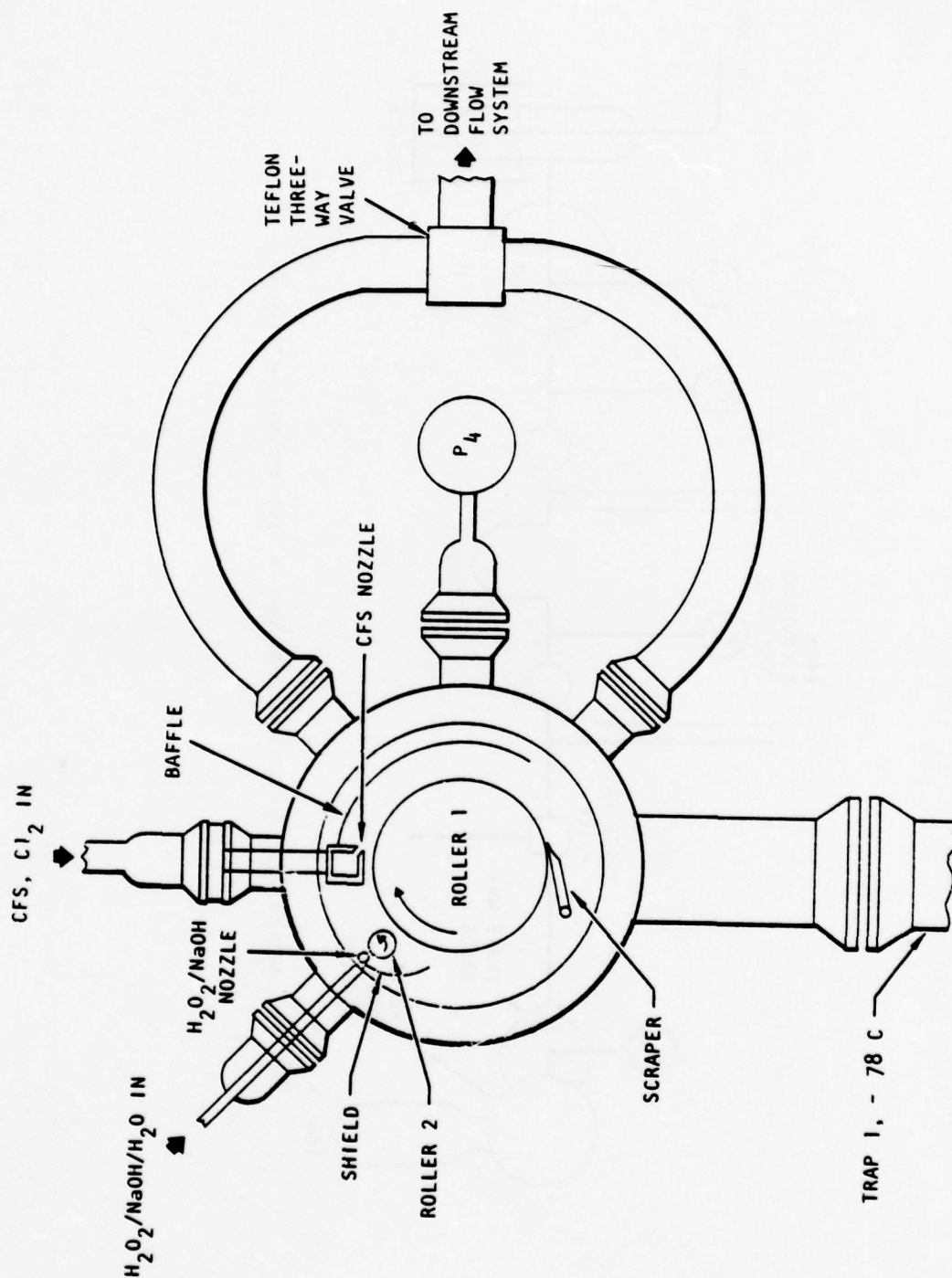


Figure 24. Reactor Configuration O, A

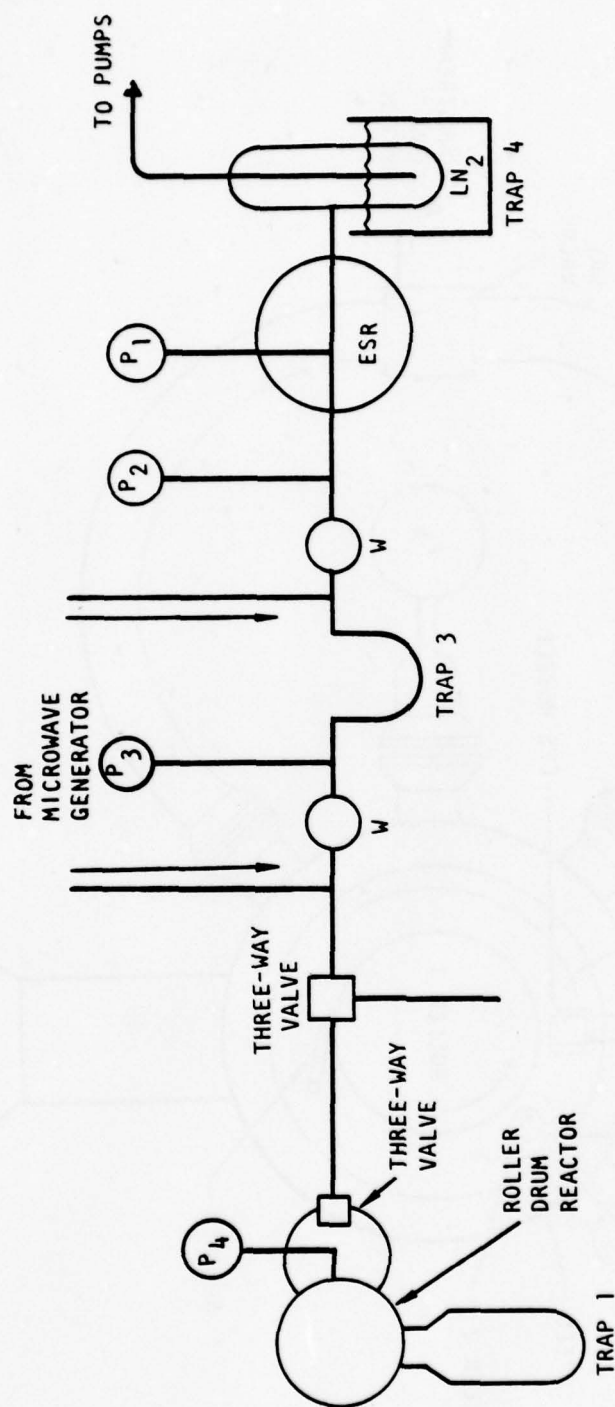


Figure 25. Near-Downstream Vacuum System-Configuration Ø

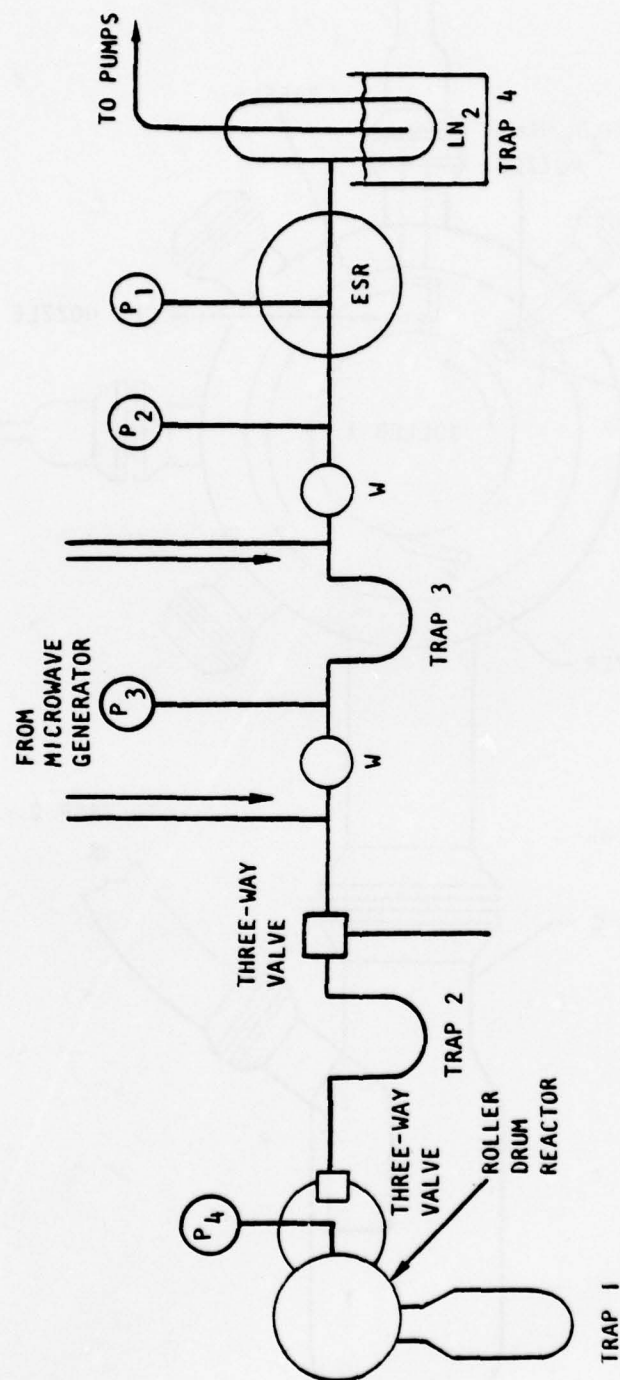


Figure 26. Near-Downstream Vacuum System-Configuration A

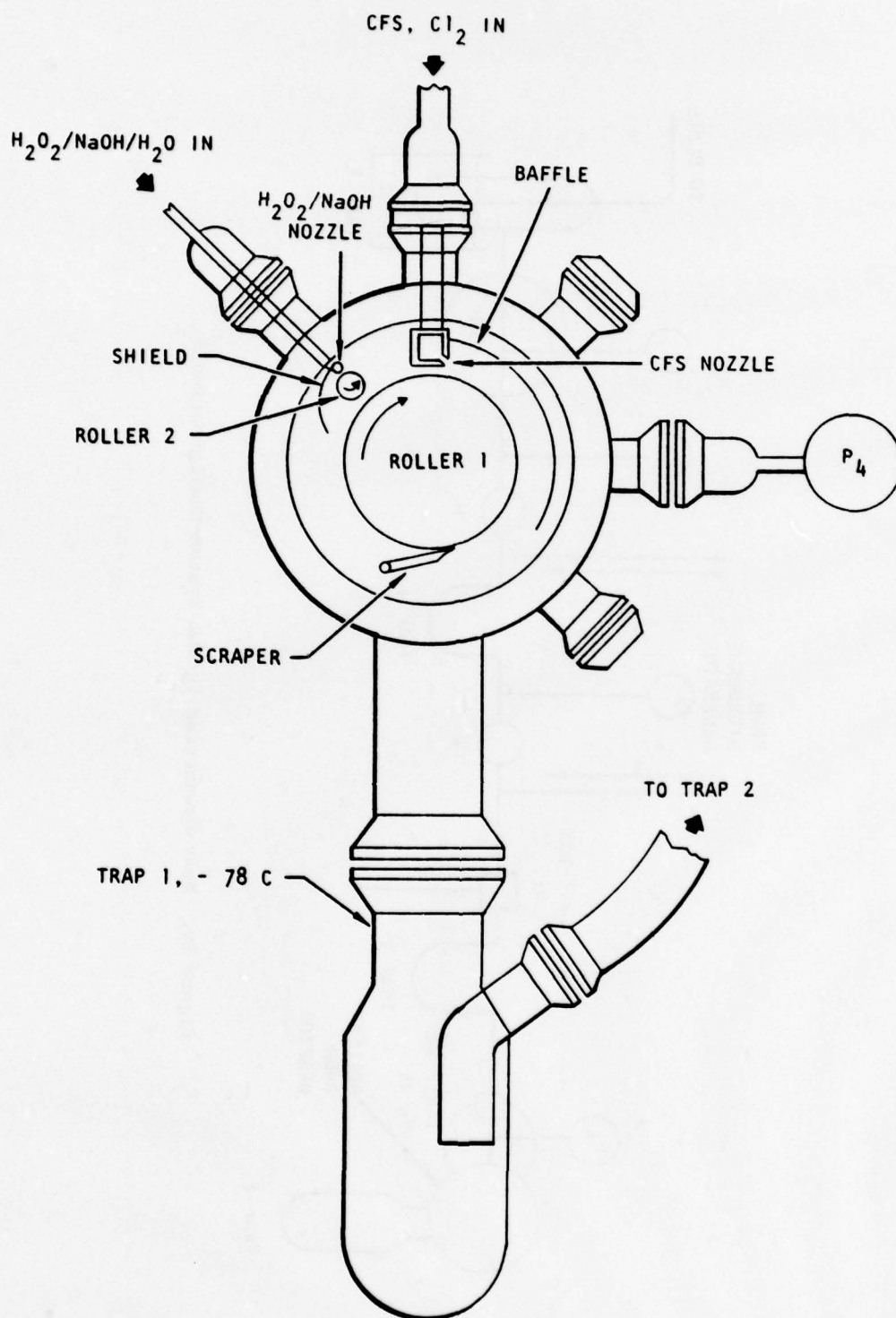


Figure 27. Reactor Configuration B

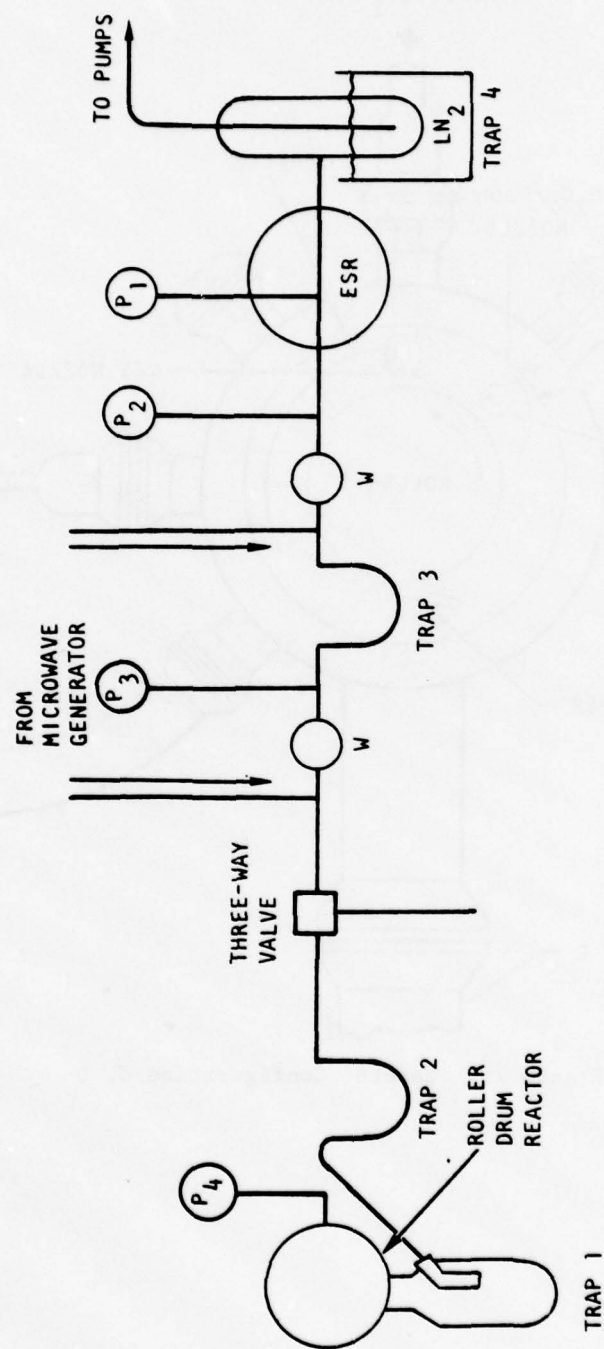


Figure 28. Near-Downstream Vacuum System-Configuration B

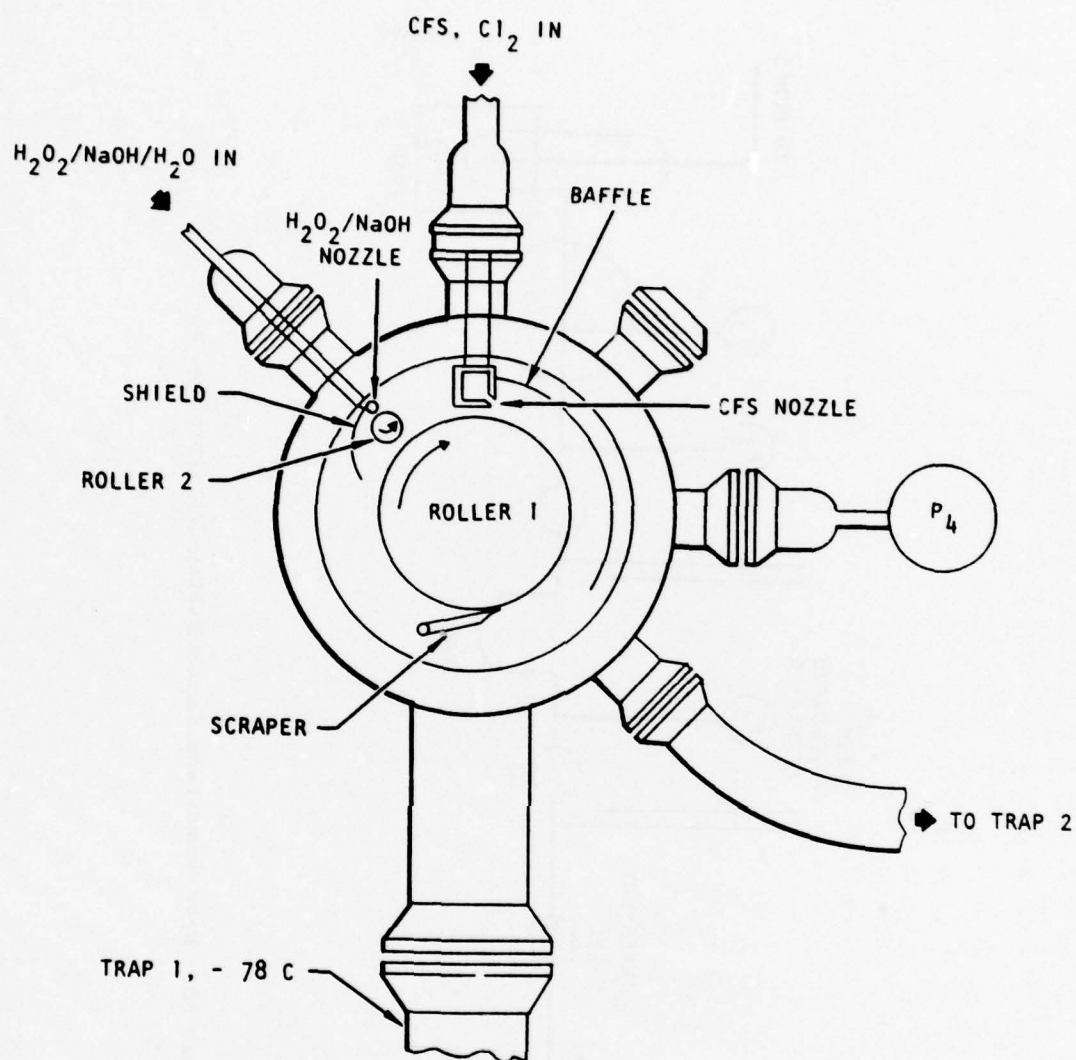


Figure 29. Reactor Configuration C, D

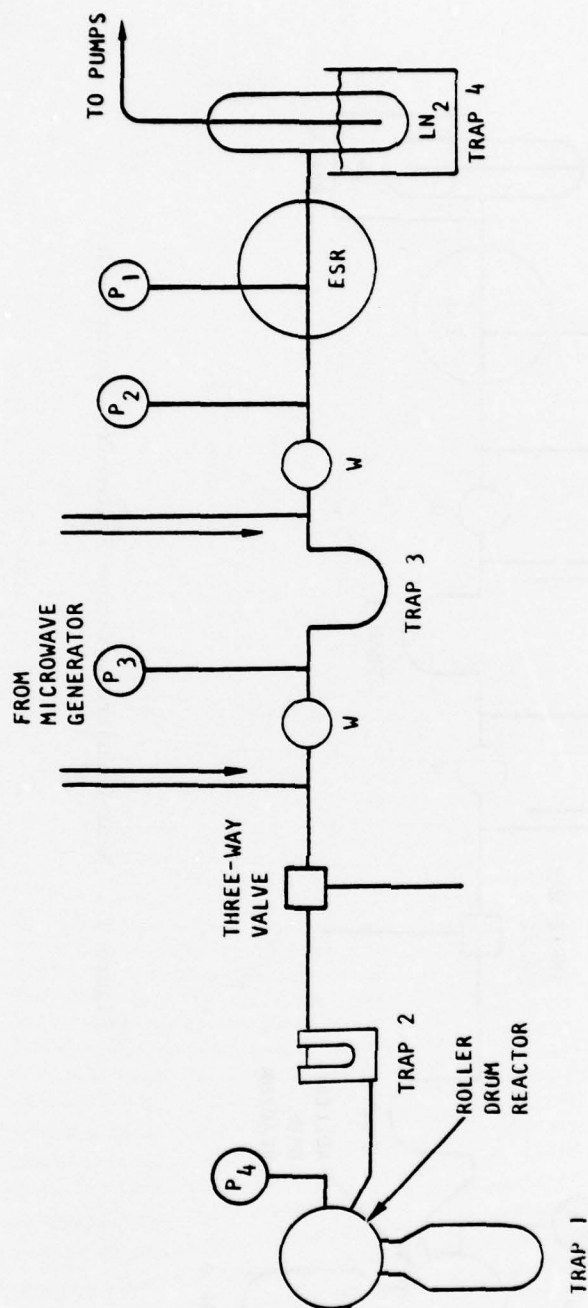


Figure 30. Near-Downstream Vacuum System-Configuration C

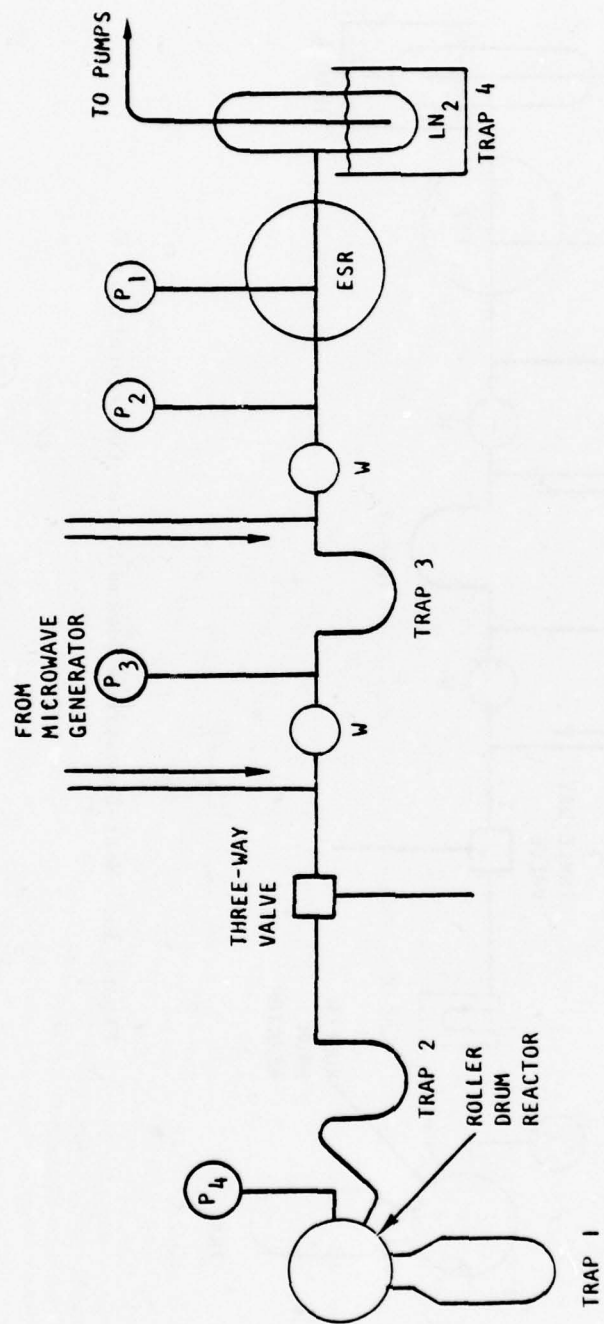
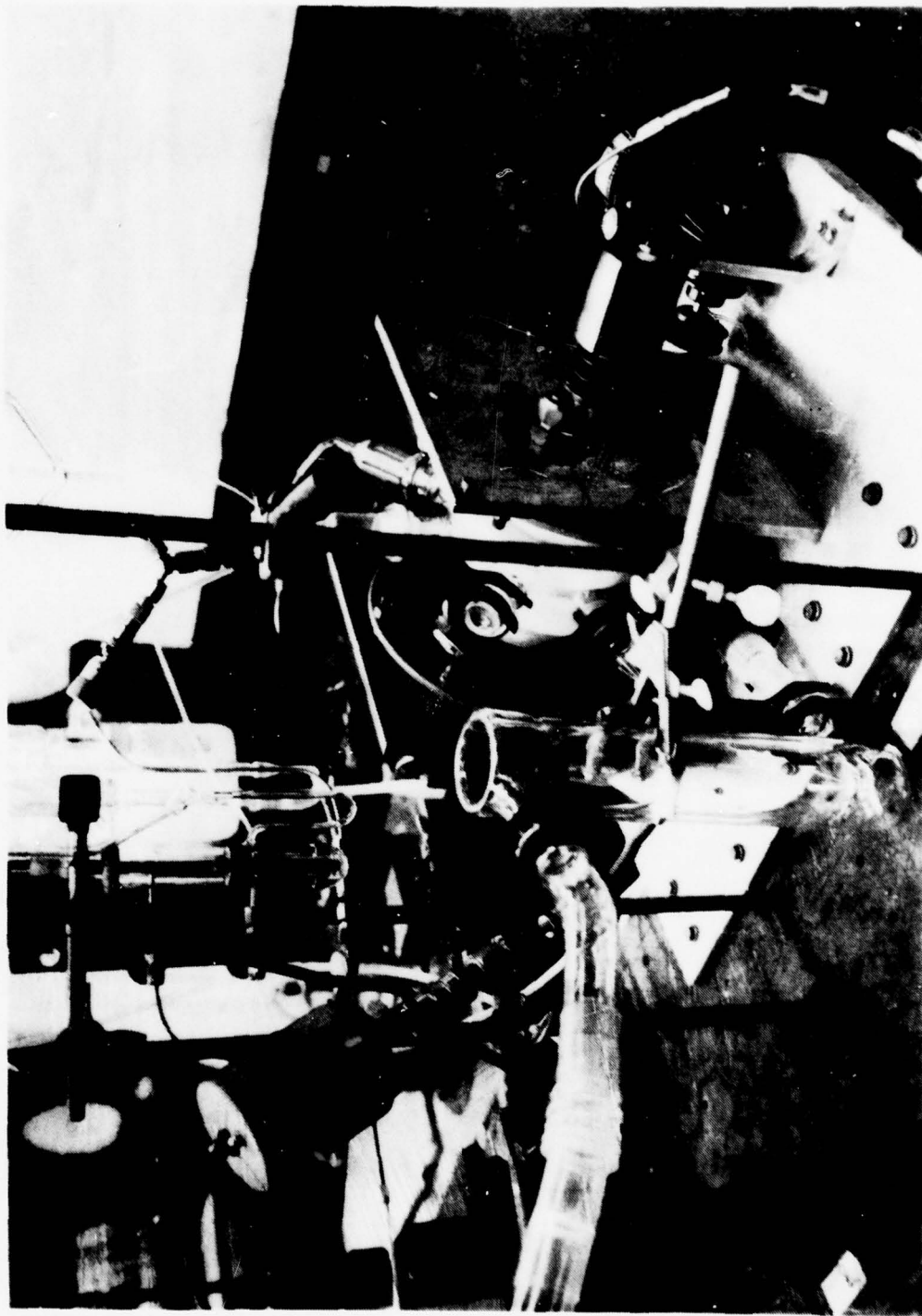
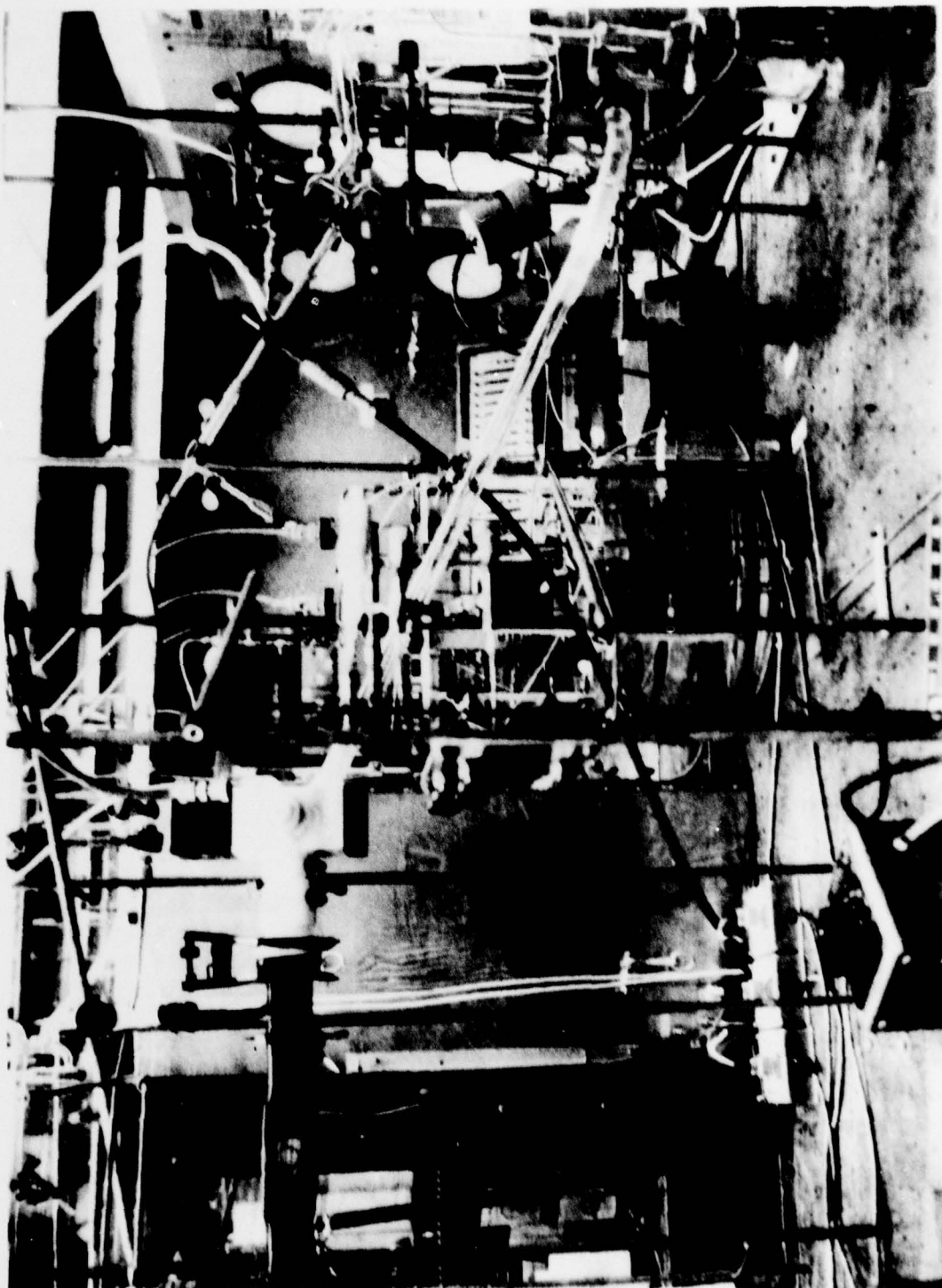


Figure 31. Near-Downstream Vacuum System-Configuration D



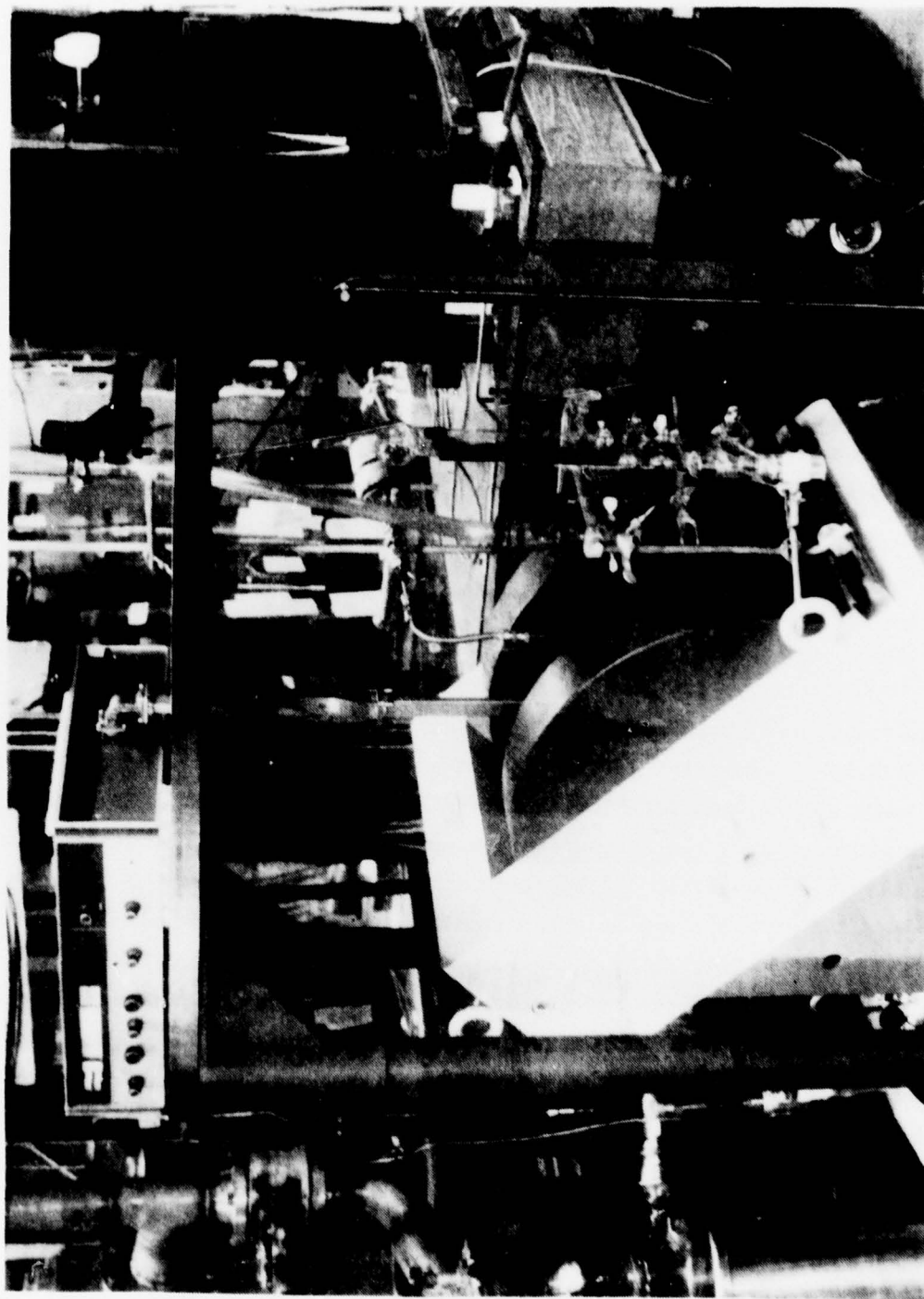
4LC34-11/17/78-S1D*

Figure 32. Reactor and Trap 2, Configuration C



4LC34-11/17/78-S1B*

Figure 33. Middle Section of Flow System



4LC34-11/17/78-S1C*

Figure 34. Downstream End of Flow System

Product Flow Determination and Vacuum

System Performance

To evaluate and analyze generator performance, one must know the flowrate of the oxygen produced. This section describes the procedures used for determining that flowrate. The determination is based on the assumption that the pressure at any point in a low-pressure flow system is a function of the volumetric flowrate past that point; also, that the functional dependence is independent of what is upstream of the point as long as the downstream system remains unchanged with respect to temperature, geometry, and pumping system performance. The various downstream flow systems employed and identified above are identical downstream of the three-way valve. This common section includes two capacitance manometers, both downstream of trap 3 (the -160 Cl₂ trap). The most downstream of these is at the ESR and is considered as the primary pressure measurement in the system and is designated as P₁. This manometer was calibrated at intervals during the experimental effort.

Figure 35 shows the pressure at P₁ versus flowrate past P₁. The flowrate was determined by admitting air to the system through two different flowmeters (Manostat Predictability Flowmeters, Models 36-541-08, 36-541-13). The flowrate was corrected for pressure and temperature dependence of density, but not viscosity, as described in the operating instructions (Ref. 4). This yields flowrate of standard air in ml/min, which was converted to moles/sec.

It may be noted that the curves for the two flowmeters do not coincide in the region of their overlap but that the curves agree within the limits of accuracy of the instruments. These data have been fitted to a third-order polynomial of the form:

$$\text{Flow (moles/sec of air)} = a_0 + a_1 P_1 + a_2 P_1^2 + a_3 P_1^3$$

4. Operating Instructions - Flowmeters, Manostat Bulletin 0577.

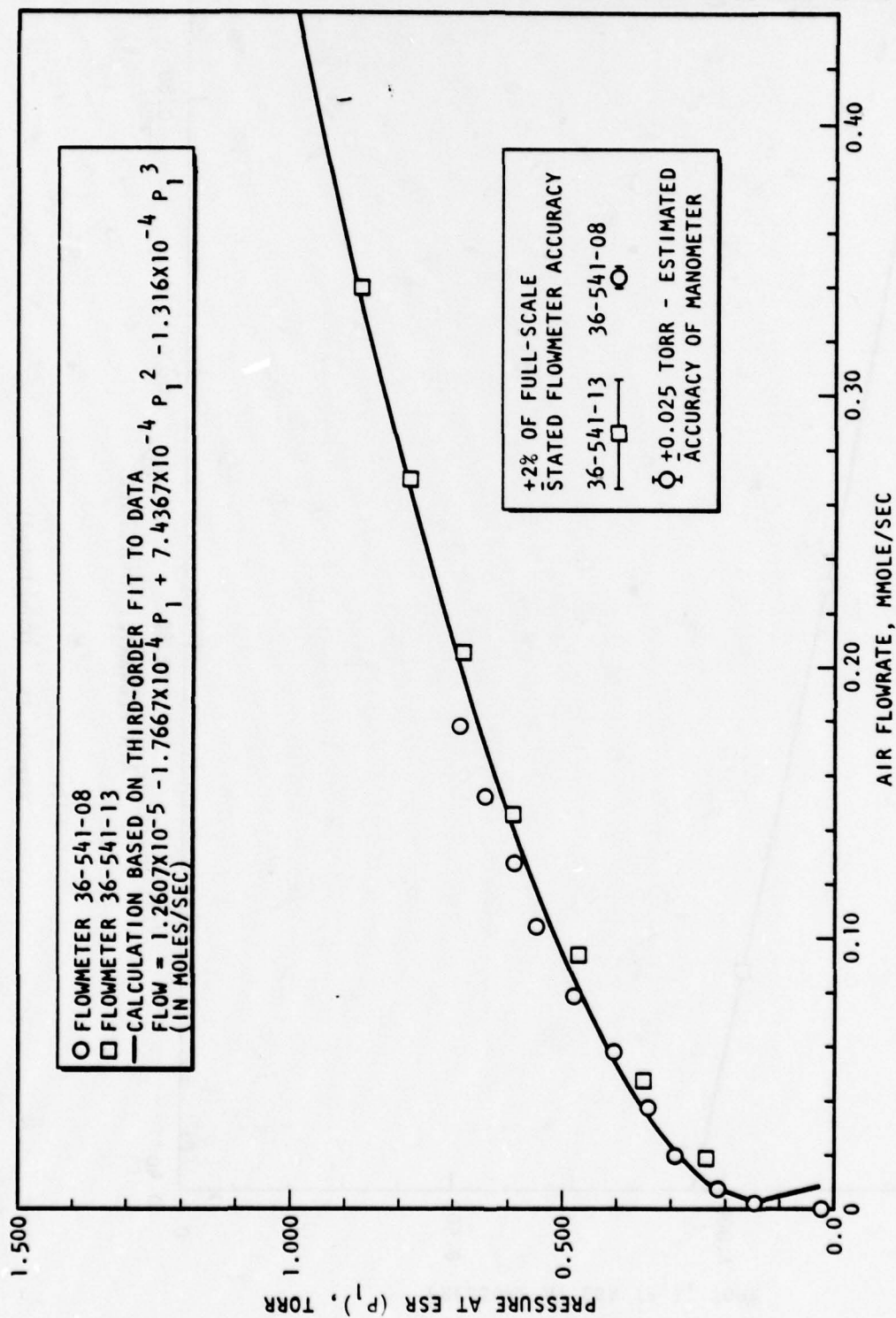


Figure 35. P_1 vs Air Flow (8 February 1979 Data - Corrected for P and T)

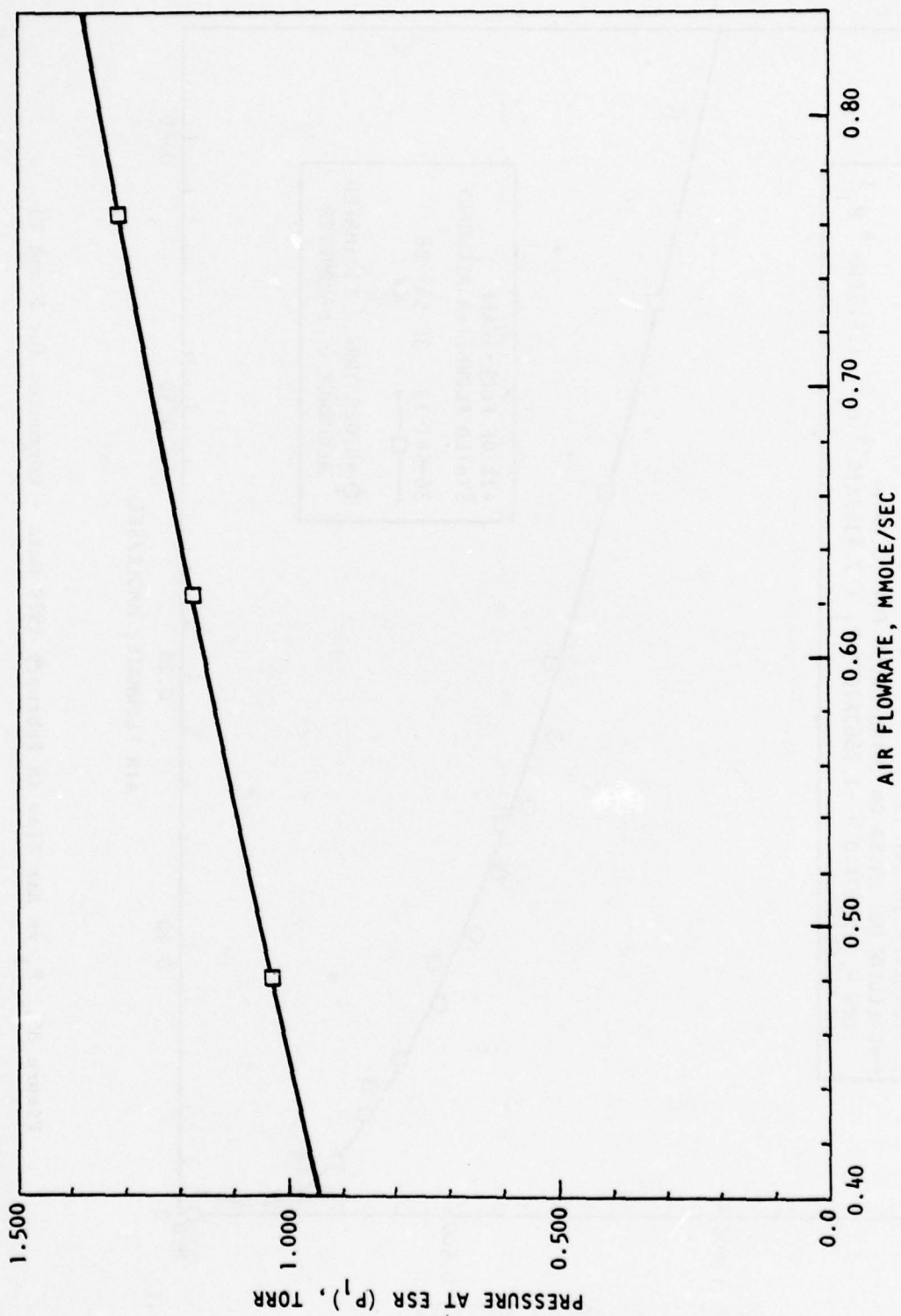


Figure 35. (Concluded)

to provide a single flow versus pressure curve, shown in Fig. 35. The coefficients a_0, a_1, a_2, a_3 are then used to determine the product flowrate whenever the pressure P_1 is known. No corrections were made for gases other than air flowing past P_1 , and all product flowrates given are in terms of air equivalents.

Flow Velocities and Residence Times

Wall quenching and gas-phase quenching are significant loss mechanisms for $O_2(a^1\Delta)$. Wall quenching may be expected to go roughly as flow distance and gas-phase quenching roughly as flow time. Thus, both distance and cross-sectional area are important features of the product delivery system and are discussed here.

The product residence time in the system is just the sum of the residence times in the individual sections, which are related to the gas velocities and flow distances:

$$T = \sum_i t_i = \sum_i l_i / v_i \quad (12)$$

$$v_i = \frac{(\text{volume flowrate})_i}{A_i} = \frac{\dot{V}_i}{A_i} \quad (13)$$

$$T = \sum_i \frac{l_i A_i}{\dot{V}_i} \quad (14)$$

$$\dot{V}_i = \dot{m} \text{ (gm mole/sec)} \times 22.421 \times 10^3 \times \frac{P_o}{P_i} \times \frac{T_i}{T_o} \quad (15)$$

$$T = \left(\frac{P_o}{T_o} \times \dot{m} \times 22.421 \times 10^3 \right)^{-1} \sum_i l_i A_i P_i / T_i \quad (16)$$

Since the pressure is a function of \dot{m} , as described in the preceding section, then the residence time is a function only of mass flow, geometry, and temperatures. The pressure P_1 versus air flow data described in the preceding section were obtained with the configuration D system shown schematically in Fig. 31. The pressures at the four stations versus flow are plotted in Fig. 36. These plots may be used to estimate pressure at any part in the system as a function of flowrate for noncondensable flow. System geometry for configuration D is described in Fig. 37 and Table 5.

TABLE 5. FLOW SYSTEM DIMENSIONS AND RESIDENCE TIME CALCULATIONS

Leg*	Length, cm	Diameter, cm	Pressure,** torr	Temperature, K	Time, seconds
ef	15	1.4 x 2.54	0.780	294	2.52×10^{-2}
fd	79	2.2	0.740	294	1.34×10^{-1}
DE	51	4.0	0.700	244	3.27×10^{-1}
EF	37	2.2	0.680	294	5.79×10^{-2}
FW	143	4.0	0.620	249	7.96×10^{-1}
WG	43	4.0	0.590	294	1.93×10^{-1}
GH	114	2.2	0.540	294	1.41×10^{-1}
e w					1.34
e h					1.67
*Refer to Fig. 37					
**Estimated pressure when $P_1 = 0.500$ torr, $\dot{m} = 9.0 \times 10^{-5}$ mole/sec					

The table also includes an example of residence time estimates for the case of $P_1 = 0.500$ torr, $\dot{m} = 9.0 \times 10^{-5}$ mole/sec. The residence time from the reactor inlet to the window and to the ESR spectrometer is 1.34 and 1.67 sec, respectively. The distance to the ESR is 482 cm, so the average velocity is

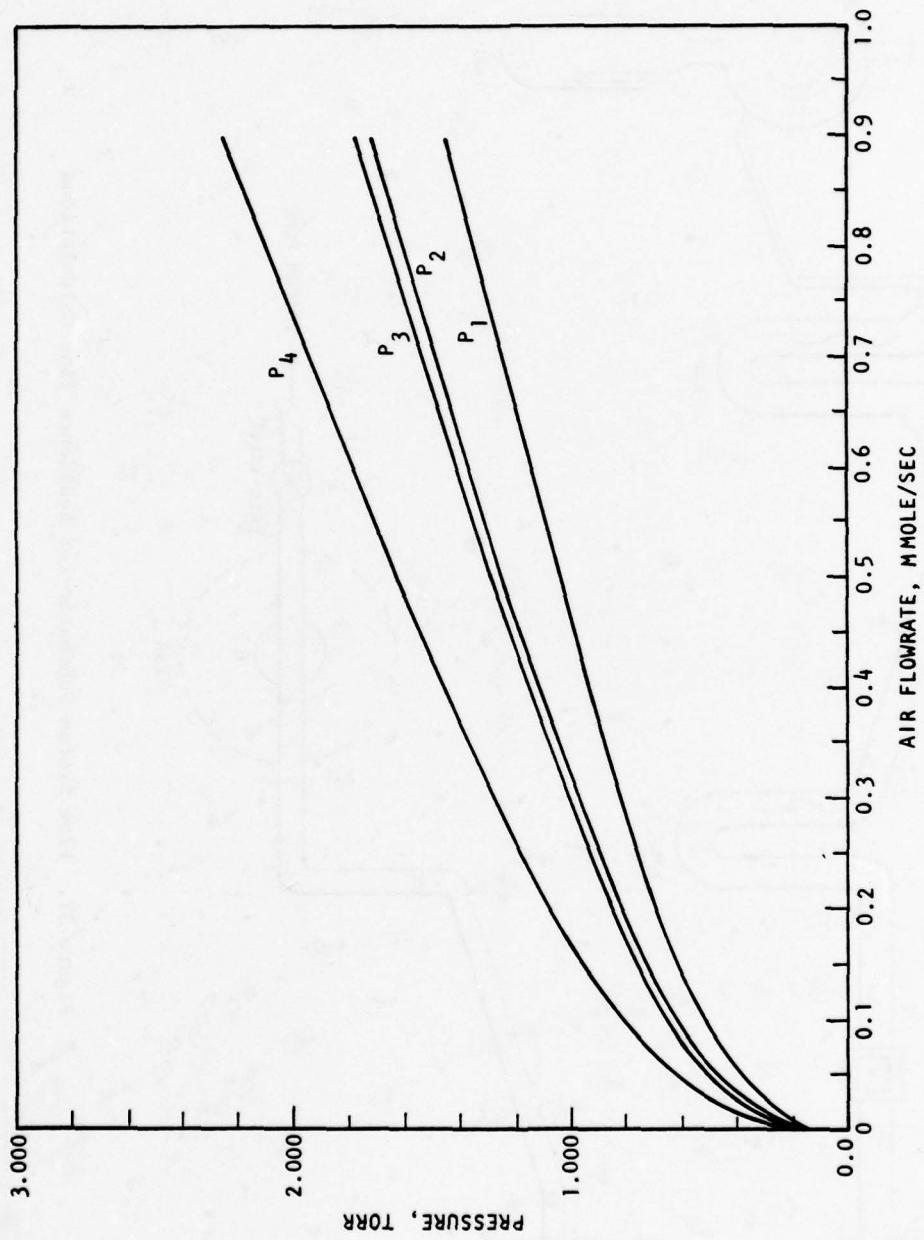


Figure 36. Pressure vs Flowrate

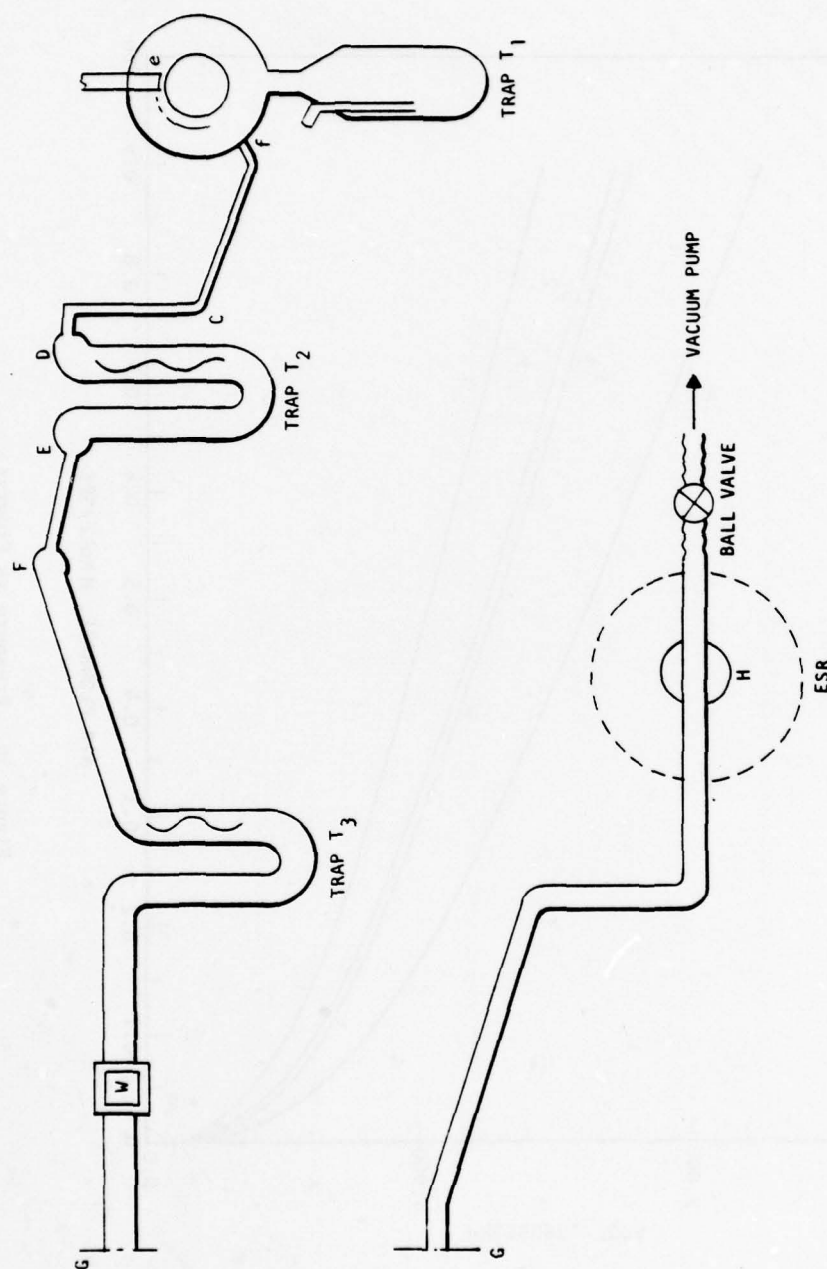


Figure 37. Flow System Schematic For Residence Time Calculations

288 cm/sec. The data from Fig. 36 and 37, and Table 5 allow the estimation of residence time for any flowrate. A reasonable estimate can be had by using average values for the area, pressure, and temperature:

$$\bar{A} = \frac{\sum \ell_i A_i}{\sum \ell_i} = 8.1 \text{ cm}^2$$

$$\bar{P} \equiv 1.3P_1$$

$$\bar{T} \equiv 265 \text{ K}$$

$$\text{Thus, } T \approx \left(\frac{P_o}{T_o} \times \dot{m} \times 22.421 \times 10^3 \right)^{-1} \times \frac{\bar{A} \times \bar{P}}{\bar{T}} \times \sum \ell_i$$

and since \dot{m} versus P_1 is known, the residence time can be estimated as a function of P_1 only, or of \dot{m} only. These estimates are shown in Fig. 38. These estimates do not include consideration of condensation in the cold traps, but are intended to characterize the system for noncondensable flow.

Traps

Traps perform the important function of removing unwanted gases and aerosols from the reactor effluent stream. Both unused reactants and unwanted products may be present. Trap design is important in that trap walls can play a significant role in quenching $O_2(^1\Delta)$. This section describes the traps employed in this study. A total of six cryogenic trap configurations were used at three temperatures. The traps were located at positions 1-4, as indicated in Fig. 26.

Trap 1 (Fig. 23) was primarily for gravity collection of the solid and liquid products and reactants scraped from the roller. This trap was always operated at -78 C (dry ice-slush). Two configurations were used. Configuration B

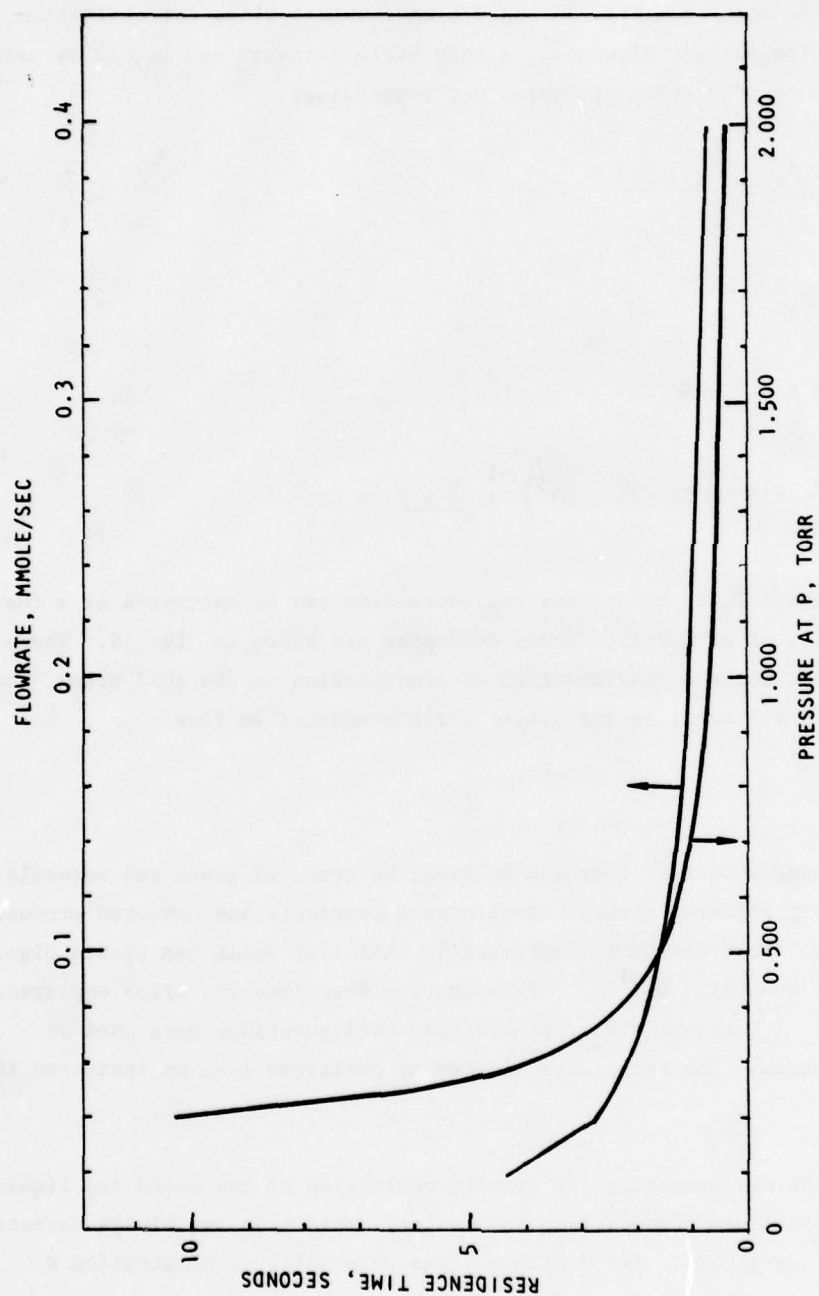


Figure 38. Estimated Residence Time vs Pressure and Flowrate

(Fig. 29) was a simple dead-end trap. Configuration C (Fig. 27) was tried to get the product to the cold zone more quickly for removal of potential quenchers. This configuration had the effect of slightly improving $O_2(^1\Delta)$ yield from CFS and slightly decreasing the yield from Cl_2 . This result is reasonable since quenching by the condensibles in the CFS system is very serious and the benefit of removing these a little faster more than offsets the added residence time (estimated ~ 0.4 sec) and quenching by noncondensibles. This is not the case for the Cl_2 system. Trap 1 was cleaned by removing and washing.

Trap 2 was for removing condensible vapors (primarily H_2O and H_2O_2) and aerosols which came out of the reactor. This trap was operated at $-78^\circ C$. A U trap with swirler plates was used in configuration B (Fig. 26). Significant quantities of aerosols were carried to this trap with CFS operation. Under high flow conditions, some aerosols were carried downstream. The U was replaced with a bottom-entry trap (Fig. 30) to reduce residence time for the aerosols and other quenchers. The annular area was the same as the cross section of the U trap but, since the linear dimensions were smaller, some blockage was experienced in the longer Cl_2 tests, and the U trap was returned. Trap 2 was cleaned by removing and washing.

Trap 3 was for removing Cl_2 and CFS and was operated at $-160^\circ C$ (isopentane slush). The trap was a U tube with swirler blades in the inlet side (Fig. 39). Tests were conducted to measure the efficiency of this trap in removing Cl_2 . Table 6 shows the results of a test in which O_2 was passed through the trap and various amounts of Cl_2 were added. P_1 is downstream of the trap and P_4 is at the reactor. The readings at zero Cl_2 flow represent O_2 flow. As may be seen, the trap was very effective at removing Cl_2 . This trap remained the same for all tests. It was cleaned either by removal and washing or by warming and transferring the material to trap 4 under vacuum.

Trap 4 was for collecting material passing the other traps, for collecting the Cl_2 from trap 3 after a run, and for protecting the vacuum pumps from Cl_2 . The trap may be seen in Fig. 34. This trap was always maintained at $-196^\circ C$ by liquid nitrogen; it was cleaned by removing and washing.

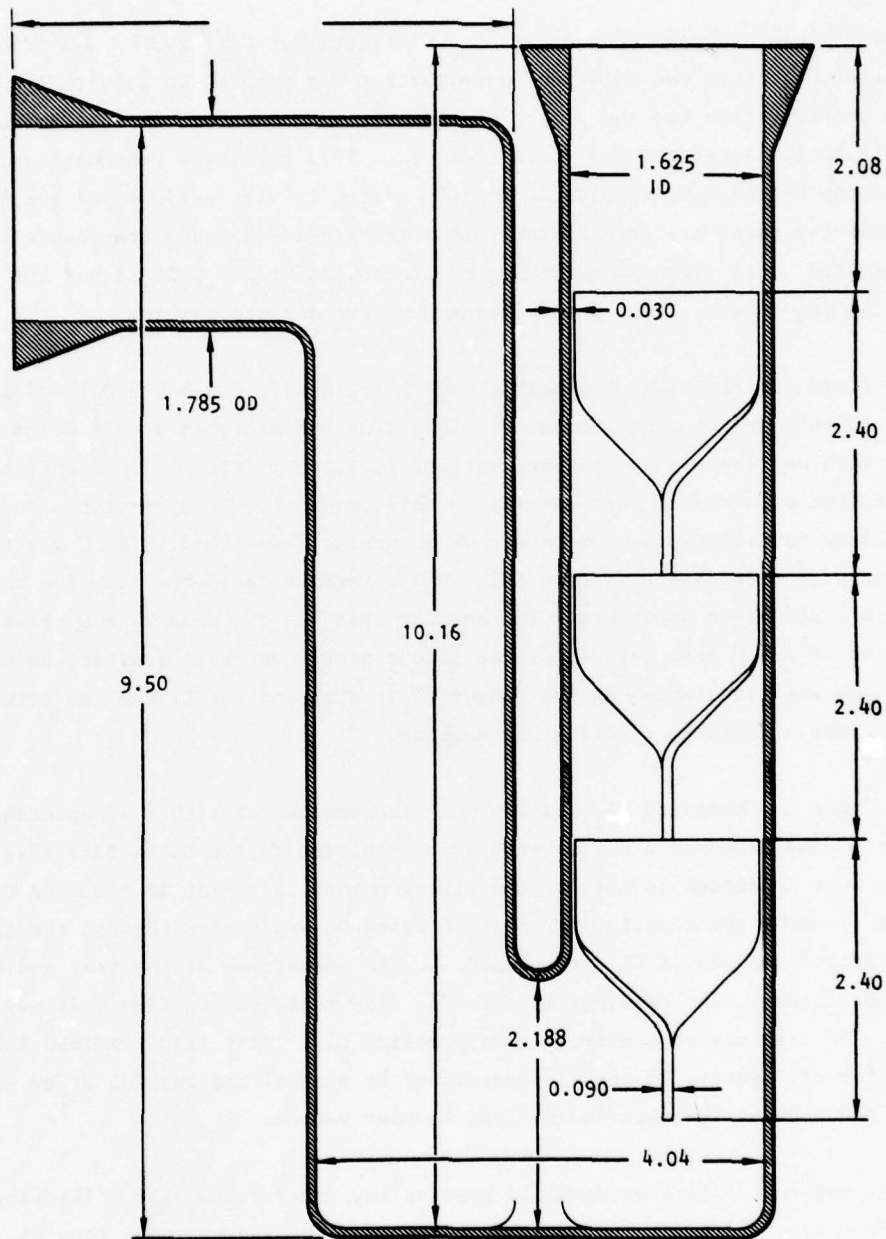


Figure 39. Trap 3 Configuration

TABLE 6. EFFECTIVENESS OF TRAP 3 AT -160 C
IN TRAPPING Cl_2

Cl_2 Flow		P_1 , torr*	P_4 , torr
Reading	Flowrate, mmole/sec		
0	0.025	0.275	0.287
6		0.275	0.348
8		0.277	0.378
10		0.276	0.408
12		0.275	0.436
14	0.1	0.275	0.465
16		0.275	0.491
18		0.275	0.520
20		0.275	0.549
Max	1	0.279	2.499

*Background = 0.064

INSTRUMENTATION AND DIAGNOSTICS

This section describes the components, systems, and procedures employed for obtaining the quantitative data presented in Section IV. Total pressures, $\text{O}_2(^1\Delta)$ and $\text{O}_2(^3\Sigma)$ partial pressures, product flows, and reactant flows were determined from measurements employing the instrumentation and diagnostic system described below.

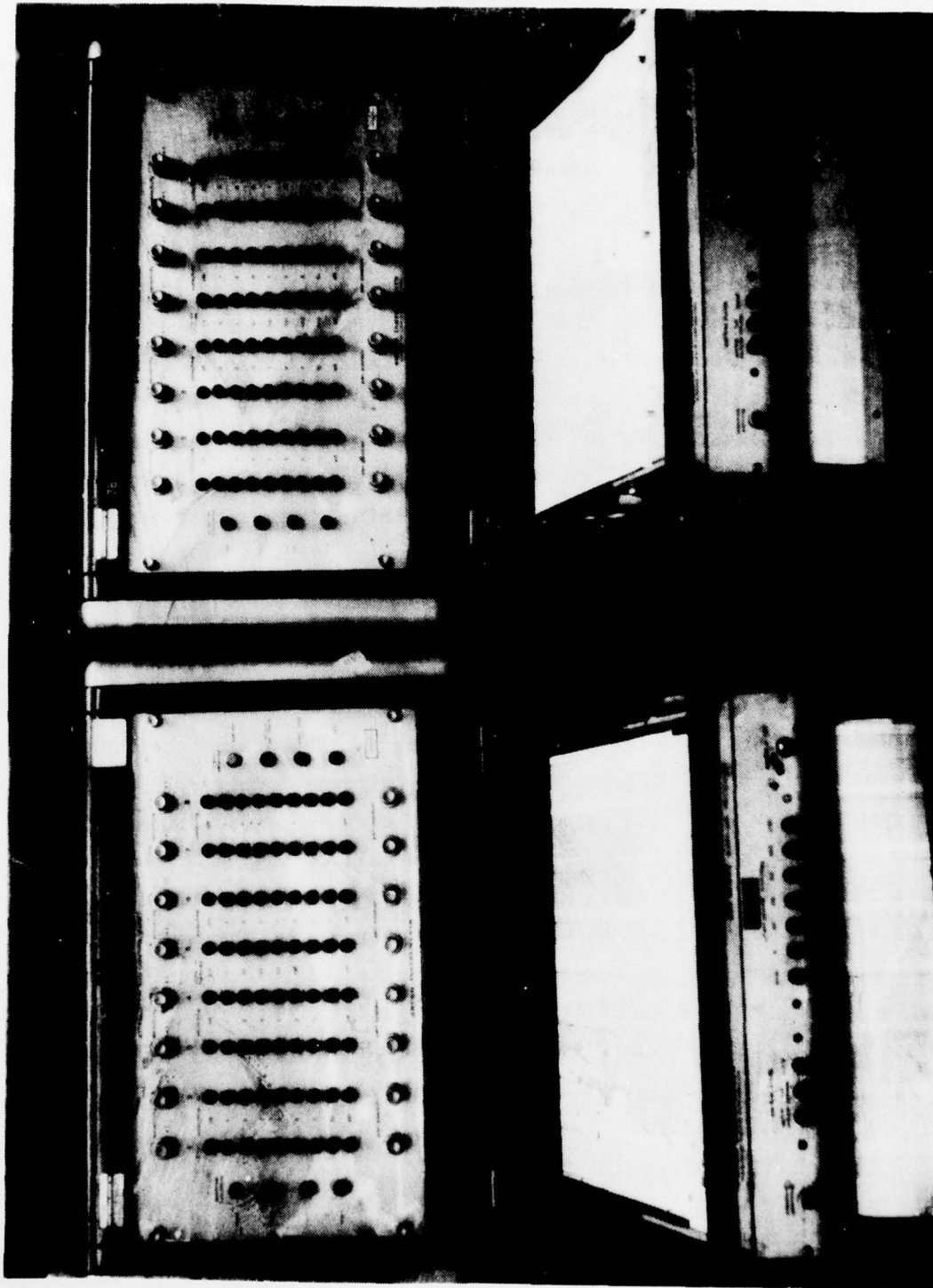
Signal Processing, Display, and Recording

Signals from all of the instruments described below (except the ESR spectrometer) were routed to the amplifier-display units shown in Fig. 40a. These units provide for zero and span adjustment as well as independent adjustment of the gain on the signal out, which is compatible with chart recorders. Zero voltage (short circuit) and calibration voltage could be applied to the units. Data recording was accomplished with the Brush strip chart recorders shown in Fig. 40b. These recorders received signals either directly from the instrument (with or without a voltage divider in line) or from the amplifier units just described.



41C34-11/17/78-S1N*

Figure 40a. Amplifier - Digital Display Units



4LC34-11/17/78-S1K*

Figure 40b. Strip Chart Recorder

Pressure Measurements

Pressures at various points in the vacuum system were measured using capacitance manometers: Baratron Model 221AHS-A-10 (0 to 10 torr) and Model 221AHS-A-100 (0 to 100 torr) with readout on Baratron Model PDR-5, five-channel power supply, one digital readout.

The manometers were calibrated by Baratron and recalibrated at the Rocketdyne Instrument Laboratory. P_1 , the manometer at the ESR spectrometer, was considered as the primary pressure measurement, and this manometer was recalibrated at intervals during the test program. Prior to each test, O_2 was admitted into the vacuum system and the amplifier-digital readout units and chart recorders were adjusted, if necessary, to correspond to the Baratron readout unit. It was noted that the readings from this system were sensitive to sensor orientation, pressure on the case of the sensor (such as by a three-finger clamp), and proximity of the sensor, sensor cable, or signal processing unit to the 2450 MHz μ -wave transmission line.

Differential pressures across the flowmeter capillaries (described previously) were measured in the range 0 to 5 psi using variable reluctance manometers. The H_2O , H_2O_2 , and NaOH flowmeter employed Validyne Model DP215 differential pressure sensors (0 to 3.0 psid) with CD-18 carrier demodulators and MC1-3 power supply. The CFS flowmeter employed a Celesco special differential pressure sensor (0 to 5 psid) with Teflon gaskets and a Teflon-coated diaphragm. These systems were calibrated with gaseous nitrogen at the beginning of the test program, and the carrier-demodulator units and power suppliers were not changed from the duration of the testing. Prior to each test, the zero and span on the digital readouts were adjusted, if necessary, to correspond to the calibration.

Electron Spin Resonance Diagnostic

Electron spin resonance (ESR) has been used extensively to identify, detect, and measure the concentration of atoms and diatomic molecules in the gas phase.

Species that exhibit quantized spin or orbital angular momentum can be studied by ESR. Thus, the four major species in the O_2 to I energy transfer laser-- $I(^2P_{1/2})$, $I(^2P_{3/2})$, $I(^2P_{3/2})$, $O_2(^3\Sigma_g^-)$ and $O_2(^1\Delta_g)$ --are amenable to analysis by ESR spectroscopy. In fact, ESR provides one of the few ways of detecting ground state oxygen, and is the only unequivocal means of determining the concentrations of $O_2(^1\Delta_g)$ and $O_2(X^3\Sigma_g^-)$. For this reason, an on-line ESR Spectrometer was utilized in CWLL for this contract.

ESR has four major advantages for its use as a means of calibration of optical detection schemes. Its sensitivity is comparable to that of atomic absorption methods. It is accurate to better than $\pm 1.5\%$ in most cases; it is unequivocal in that the absorptions are unique to a given species; it permits any gas of known concentration of paramagnetic species to be used to calibrate the instrument, such as ground state O_2 , thus reducing the difficulty of standardization as well as the number of measurements required. The disadvantage of the ESR technique is that a steady-state concentration is required for measurement since each analysis requires that an absorption line be recorded. However, it is ideal for calibrating the fast-response, direct-detection optical methods also utilized in this contract.

ESR Theory. The theory of quantitative ESR measurements has been discussed by Goldberg and Bard (Ref. 5), Westenberg and deHaas (Ref. 6 through 8), and

5. Goldberg, I.B., and A.J. Bard, "Analytical Applications of Electron Spin Resonance," I.M. Kolthoff, P.J. Elveng and M.M. Bursey editors, Treatise on Analytical Chemistry; Magnetic Measurements, Vol 6, 2nd Ed., John Wiley, N.Y.
6. Westenberg, A.A., "Use of ESR for Quantitative Determination of Gas Phase Atom and Radical Concentrations," Prog. React. Kinetics, 7, 23 (1973)
7. Westenberg, A.A., and N. DeHaas, "Quantitative Measurements of Gas Phase O and N Atom Concentrations by ESR," J. Chem. Phys., 40, 3087 (1964).
8. Westenberg, A.A., "Intensity Relations for Determining Gas Phase OH, Cl, Br, I, and Free Electron Concentrations by Quantitative ESR," J. Chem. Phys., 43, 1544 (1965).

Evenson and Burch (Ref. 9). A summary of general applications and methods to obtain accurate results is provided in Ref. 5.

For reasons of sensitivity and ease of operation, ESR spectrometers present the first derivative of the microwave absorption. Since the transition dipole intensity is related to the integral of the absorption, it is necessary to doubly integrate the ESR signal to obtain the concentration of a particular species. The double integral of the ESR signal is related to the concentration of atoms or molecules according to Eq. 17. This double integration procedure was carried out on the Nicolet Signal Averager provided for this contract by the Air Force Weapons Laboratory.

The concentration of $C(i)$ of species i is given by Eq. 17:

$$C(i) = \left[\frac{K_I}{A \cdot H_m \cdot p^{1/2}} \right] \left[\frac{2kT}{h\nu_o \beta} \right] \left[\frac{g_{eff}^2}{g_J^2 (J-M_J)(J+M_J+1) \exp(-E_{J,M_J}/kT)} \right] X$$

$$\left[\int_{H_1}^{H_2} \int_{H_1}^H \right] \mathcal{J}(H) dH dH' \quad (17)$$

$$C(i) = A \cdot B \cdot Q \cdot D \quad (18)$$

where

K_I = instrumental constant determined by standardization

A = amplification of ESR signal

-
9. Evenson, K.M., and D.S. Burch, "Use of O_2 for ESR Calibration for Quantitative Measurement of Gas Concentrations," J. Chem. Phys., 44, 1715 (1965).

- H_n = modulation amplitude
 p = microwave power
 k = Boltzmann's constant
 T = absolute temperature, K
 h = Planck's constant
 ν_0 = microwave frequency (Hz)
 β = Bohr magneton
 g_J = spectroscopic splitting factor
 J = angular momentum quantum number
 M_J = azimuthal quantum level of J
 E_{J,M_J} = energy above ground state of the electronic state of the species undergoing a transition (does not include the Zeeman or field dependent energy)
 (H) = ESR signal intensity
 H_1, H_2 = beginning and ending field of sweep (0 and ∞)
 $g_{eff} = (h/\beta) dv/dH \sim g_J$
 Z = partition function including spin degeneracy

This equation may be broken down into the product of four terms (A , B , Q and D). The parameter Q is selected to be consistent with Ref. 5 through 8. Q was taken to be 36.6 for $O_2(^1\Delta)$ and 58.5 for $O_2(^3\Sigma)$. The parameter A depends only on instrumental parameters that are accurately measurable or are preset. These include the microwave power, modulation amplitude, and signal amplification. The instrumental constant can be determined by standardization with known concentrations of paramagnetic materials and will only depend on the geometry of the sample container and cavity. The parameter B is known accurately since it contains only the temperature of the sample and the microwave frequency. The parameter Q is dependent only on the specific transition used in the analysis and on the electronic states of the molecule or atom. This is accurately calculated and many values have been tabulated by Westenberg

(Ref. 6). The last term, D, is the double integral of the lineshape. Since it is never possible to carry out an infinite scan, a correction factor can be applied to the finite scan (Ref. 10). Since these lines are Lorentzian,

$$\int_0^\infty \int_0^H S(H) dH' dH = \frac{\pi}{2} \tan^{-1} \left\{ \left[\frac{(H_0 - H_a)}{\frac{\sqrt{3}}{2} \Delta} \right] - \frac{\frac{2}{\sqrt{3}} \frac{(H_0 - H_a)}{\Delta}}{1 - \frac{2(H_0 - H_a)}{\sqrt{3} \Delta}} \right\} \times$$

$$\int_{H_0 - H_a}^{H_0 + H_a} \int_{H_0 - H_a}^H S(H') dH' dH$$

where the scan is taken from the $H_0 - H_a$ to $H_0 + H_a$, H_0 being the resonance field, and Δ is the peak-to-peak width of the derivative curve. These methods have been used extensively in this laboratory with excellent success.

$O_2(^1\Delta)$

In polyatomic molecules, the rotational angular momentum couples to the orbital and spin momentum such that each rotational level exhibits ESR absorption. The spectrum of $O_2(^1\Delta)$ has been observed in the $J = 2$ and $J = 3$ states (Ref. 11 and 12). $J = K + L + S$, where K is the rotational level, $L = 2$, and $S = 0$. For most ESR spectrometers, such as those operating in the region of 9 GHz, only the transitions corresponding to $J = 2$ can be observed. The spectra of the $J = 2$ level consist of four transitions between each of the $(2J + 1) = 5$ states corresponding to different values of M_J . The relative intensities of the transitions are 2:3:3:2. This is shown in Fig. 41. Depending on the frequency, this is near to two $O_2(^3\Sigma_g)$ lines, and thus the ground-state and excited-state species can be recorded in succession.

10. Goldberg, I.B., "Improving the Analytical Accuracy of Electron Spin Resonance Spectrometry," submitted to Analytical Chemistry
11. Falick, A.M., B.H. Mahan, and R.J. Myers, "Paramagnetic Resonance of the $^1\Delta_g$ Oxygen Molecule," J. Chem. Phys., **42**, 1837 (1965).
12. Miller, T.A., "Rotational Moment, Rotational g-factor, Electronic Orbital g-Factors, and Anisotropy of the Magnetic Susceptibility of $^1\Delta O_2$," J. Chem. Phys., **53**, 909 (1971).

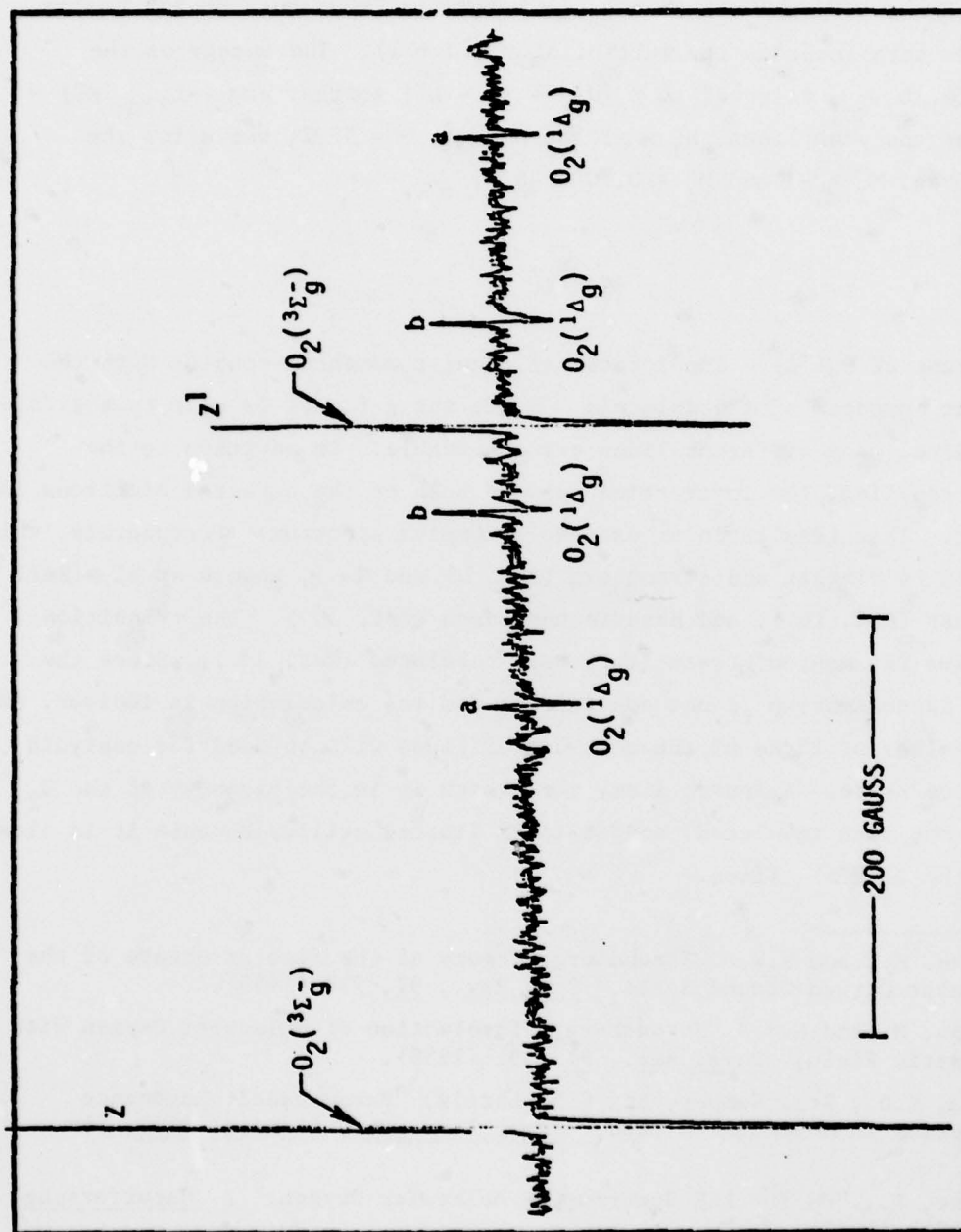
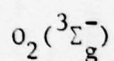


Figure 41. ESR Spectrum of O_2 Products from $ClOSO_2F-H_2O_2-NaOH$ Reaction

The spectrum is suitable to be considered a high-field approximation, and thus the parameters are given precisely by Eq. 17. The rotational partition function is given by kT/hB , since only one-half of the states are allowed by symmetry. The rotational constant B_0 is 1.4178 cm^{-1} , so that at 296 K, $Z = 145.1$. This term includes the multiplicity $(2J + 1)$. The energy of the lowest state, E_{J, M_J} is equal to $B_0[J(J + 1) - L^2]$ so that $\exp(-E_{J, M_J}/kT) = 9.9863$. For the weak lines, $M_J = -2$ and $M_J = 1$, $Q = 55.2$, while for the stronger lines, $M_J = -1$ and $M_J = 0$, $Q = 36.8$.



As in the case of $O_2(^1\Delta)$ the rotational angular momentum couples with the spin angular momentum of the molecule. Since the g factor is near to the free electron value, many different lines are observable. In addition to the rotational coupling, the interaction between both of the unpaired electrons is significant. This results in an extremely complex spectrum. Fortunately, this was analyzed by Tinkham and Strandberg (Ref. 13 and 14), Bowers et al. (Ref. 15), Tischer (Ref. 16), and Hendrie and Kusch (Ref. 17). The transition probabilities for many of these lines were tabulated (Ref. 15). Since the high-field approximation is not applicable, and the calculation is tedious, the tabulated values of three of the most useful lines will be used for analysis of the ground state. A fourth line, that which is in the vicinity of the $O_2(^1\Delta)$, has not been tabulated, and it is of limited utility because it is close to one of the $O_2(^1\Delta)$ lines.

13. Tinkham, M., and M.W.P. Strandberg "Theory of the Fine Structure of the Molecular Oxygen Ground State," Phys. Rev., 97, 937 (1955).
14. Tinkham, M., and M.W.P. Strandberg, "Interaction of Molecular Oxygen With a Magnetic Field," Phys. Rev., 97, 951 (1955).
15. Bowers, K.D., R.A. Kamper, and C.D. Lustig, "Paramagnetic Resonance Absorption in Molecular Oxygen," Proc. Roy. Soc., (London) A251, 565 (1959).
16. Tischer, R., "On the ESR Spectrum of Molecular Oxygen," Z. Naturforschg., A22, 1711 (1967).
17. Hendrie, J. M., and P. Kusch, "Radio-Frequency Zeeman Effect in O_2 ," Phys. Rev., 107 (1957).

The transition probabilities of the lines of the O_2 spectrum are given in terms of the parameter $p = J_{\pm}^2 \exp(-E_J/kT)$, which replaces the parameter $(J-M_J)(J+M_J+1) \exp(-E_{J,M_J}/kT)$ in Eq. 17. The partition function is equal to $(2S+1) \cdot kT/(2hB)$, where $B = 1.4377 \text{ cm}^{-1}$. At 296 K, this is 214.6

Required for the quantitative determinations of both the excited and ground state oxygen species is a theoretical calculation of the matrix elements for the ESR transitions in question. Such calculations of the transition probabilities require solving the Hamiltonian for the interaction of both oxygen species with the applied magnetic fields. The calculations were conducted at the Rockwell Science Center under the direction of Dr. Ira Goldberg. A computer program was written to calculate the required transition probabilities and to define their magnetic field and temperature dependence over our range of operating conditions. A summary of that effort with the required background information follows.

The analysis of O_2 by ESR can be precise to $\pm 1\%$. Since O_2 in its ground state also is used to calibrate the spectrometer, the limiting factor in the accuracy of the ESR determination is the accuracy of the matrix elements of the spin transitions which have only been calculated (Ref. 14) for one microwave frequency (9430 MHz) at 300 K. We have, therefore, undertaken to recalculate these transition probabilities for different fields and frequencies and different temperatures. Because the O_2 molecule is in a triplet state, where the spin-spin interactions are of the same order as the Zeeman energies, the electron spin wave functions are expected to be strongly dependent on the resonant field of a particular transition.

Equation 19 relates the pressure of the gas, P , to the doubly integrated ESR signal, D ,

$$P = \frac{2kT}{h\nu_o \mu_B} \cdot Q \cdot K_I \cdot D \quad (19)$$

where k is Boltzmann's constant, T is the temperature, h is Planck's constant, ν_o is the microwave frequency of the spectrometer, μ_B is the Bohr Magneton,

and K_I is the instrumental constant determined from calibration. Q is a function of the molecule and the particular spin transitions as given by Eq. 20.

$$Q = \frac{g_{\text{eff}}^2 Z}{g_j^2 |J_{\pm}|^2 \exp(-E_j/kT)} \quad (20)$$

where g_{eff} is the conversion of the magnetic field to frequency units, Z is the rotational partition function, g_j is the g-factor $|J_{\pm}|^2$ is the transition matrix element, and E_j is the rotational energy. The results of preliminary calculations are given in Table 7. These values agree closely with the values presented by Westenberg (Ref. 6) calculated from the data from Tinkham and Strandberg (Ref. 14). It appears that values for the ratio of $^1\Delta_g$ to $^3\Sigma_g^-$ oxygen are approximately 1.5% lower than that calculated from the commonly used values.

TABLE 7. VALUES OF Q AND PARAMETERS USED TO CALCULATE Q FOR $O_2(^1\Delta_g)$ AND $O_2(^3\Sigma_g^-)$ AT 298.16 K

Parameters	$O_2(^1\Delta_g)$	$O_2(^3\Sigma_g^-)$
B_O (GH)	42.51297	43.1029
Z	146.46	215.53
g_{eff}	0.6667	0.929
g_j	0.66662	2.0023
Transition K	2	3
J		4
M	-1 \rightarrow 0; 0 \rightarrow 1	3 \rightarrow 4
J_{\pm}^2	6.000	1.027
Q	36.6	58.53
ν	9.35	9.35
H_O (Oe)	9978; 10081	9507

ESR Setup at CWLL and Calibration Techniques. Prior to the testing described in Section IV, Rocketdyne transported its Varian 9-inch magnet, associated power supply and ESR console and recorder from its previous location at Canoga Park to the CWLL laboratory. To prepare for acceptance of the equipment, the required power and water cooling modifications were made at CWLL. A vacuum flow system was connected through the magnet and coupled with CWLL's pumping facilities. The design of the ESR installation was versatile and, although it is currently attached to the iodine laser oxygen generator, it is easily adapted for evaluating new production sources of electronically excited oxygen ($O_2(^1\Delta)$).

Once installed, the ESR hardware was checked out using microwave-generated $O_2(^1\Delta)$ and ground state oxygen. The hardware was calibrated against known concentrations of the ground state species ($O_2(^3\Sigma)$) and instrumental constants were calculated for the spectrometer.

Determination of the instrumental constants were carried out at numerous pressures ranging from 0.250 to 4.0 torr and, also, at several modulation amplitudes, covering the range over which the instrument would be used for unknown determinations. As part of the instrumental constant determination, measurements of the field modulation amplitudes were made to determine the accuracy of the indicated instrumental values. Some were found to be in error and corrected values are now used to eliminate this problem. Also, the Lorentz curves were corrected for line shape via the standard procedure described earlier, and this line shape correction procedure was utilized on all quantitative ESR determinations. The resulting instrumental constants determined under the various conditions were averaged to generate one value which is used for unknown determinations. A pretest check of the instrumental constant was carried out to ensure no major deviations from previous constant determinations. The equation utilized for the determination of $O_2(^1\Delta)$ and $O_2(^3\Sigma)$ pressures was given (Eq. 17).

By flowing oxygen through a microwave discharge, excited oxygen can be produced along with the ground state species. At the ESR microwave cavity, a Baratron accurately measures the total pressure of the two gases. The pressure of each species is then determined via Eq. 17 and the sum of the calculated pressures should add up to the measured Baratron pressure. This procedure serve as a check of the ESR calculation procedure. However, it is necessary to ensure that any oxygen atoms produced in the discharge are recombined to form O_2 molecules before making the measurement. This can be ensured by using a catalytic layer of HgO to facilitate recombination and by monitoring O atom presence via ESR. Additionally, because Hg atom recombination yields broadband radiation, the ESR was utilized to determine the presence of O atoms prior to each test. If O atoms were found, the HgO catalytic layer was replenished.

A quick change field switch was added to the console which permitted rapid switching of the magnetic field between any two values between 0 and 10,000 gauss. Rapid field switching is desirable to minimize the time required to manually set the field and, thus, it reduces the time required to record two ESR spectra at different fields. Figures 42a and 42 b show the modifications made to the spectrometer to accomplish this field switching.

The recorder was interfaced with a storage oscilloscope and a signal averager which gave the capability for rapid integration and data reduction of acquired spectra. The integration capability of the signal averager allowed for rapid calculations of species concentrations. A floor schematic of the installation at CWLL is shown in Fig. 43 and a block diagram indicating the integrated ESR components is shown in Fig. 44. Figure 45 shows the ESR recorder, power supply, Nicolet signal averager, and oscilloscope in the CWLL laboratory. The ESR magnet and Klystron within the facility may be seen in Fig. 34.

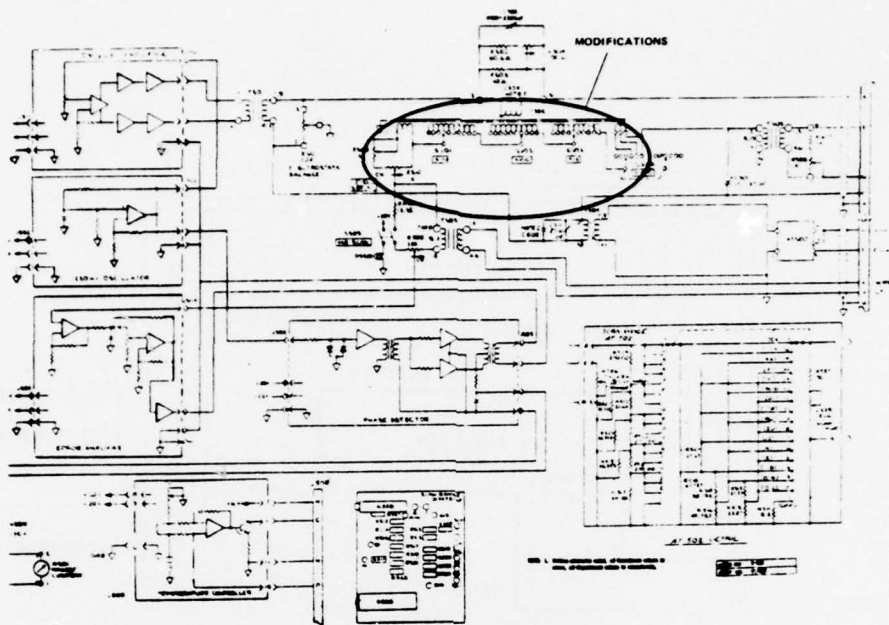


Figure 42a. Field Controller Modification Location

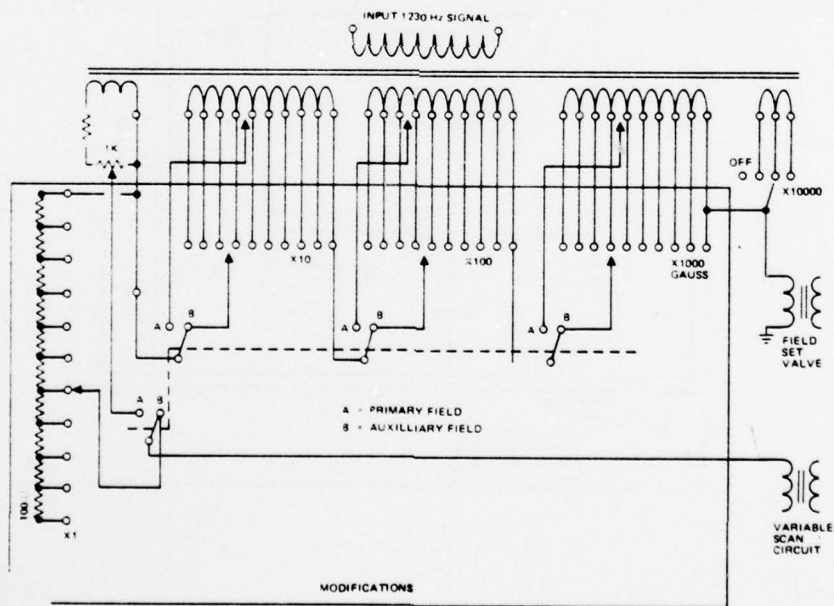


Figure 42b. Field Controller Modification

AD-A078 919

ROCKWELL INTERNATIONAL CANOGA PARK CA ROCKETDYNE DIV
CHEMICALLY PUMPED IODINE LASER.(U)

F/6 20/5

SEP 79 S HURLOCK , H LAEGER , R WAGNER

F29601-78-C-0023

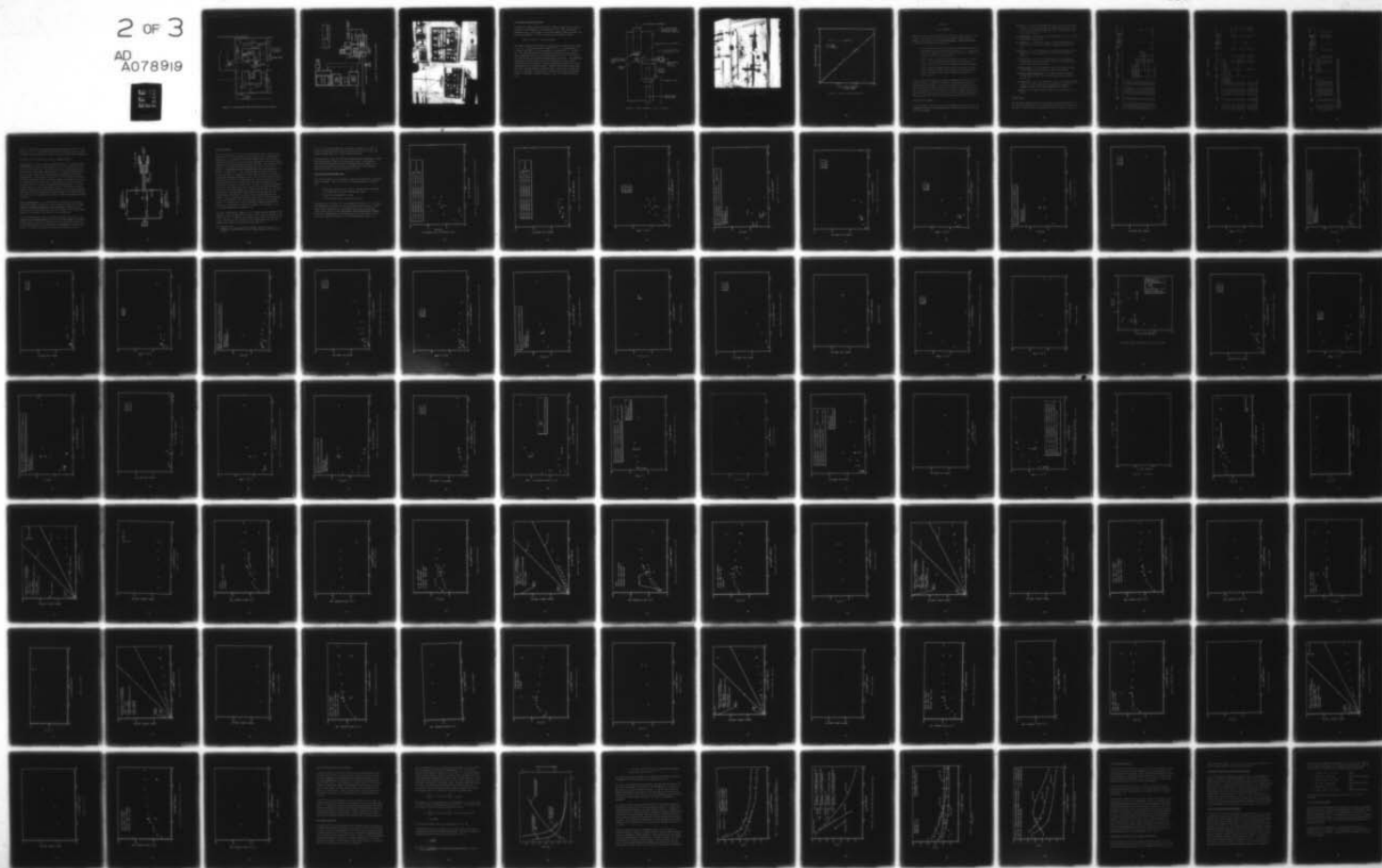
UNCLASSIFIED

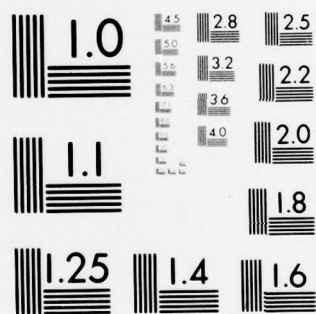
AFWL-TR-79-52

NI

2 OF 3

AD
A078919





MICROCOPY RESOLUTION TEST CHART
NATIONAL BUREAU OF STANDARDS-1963-A

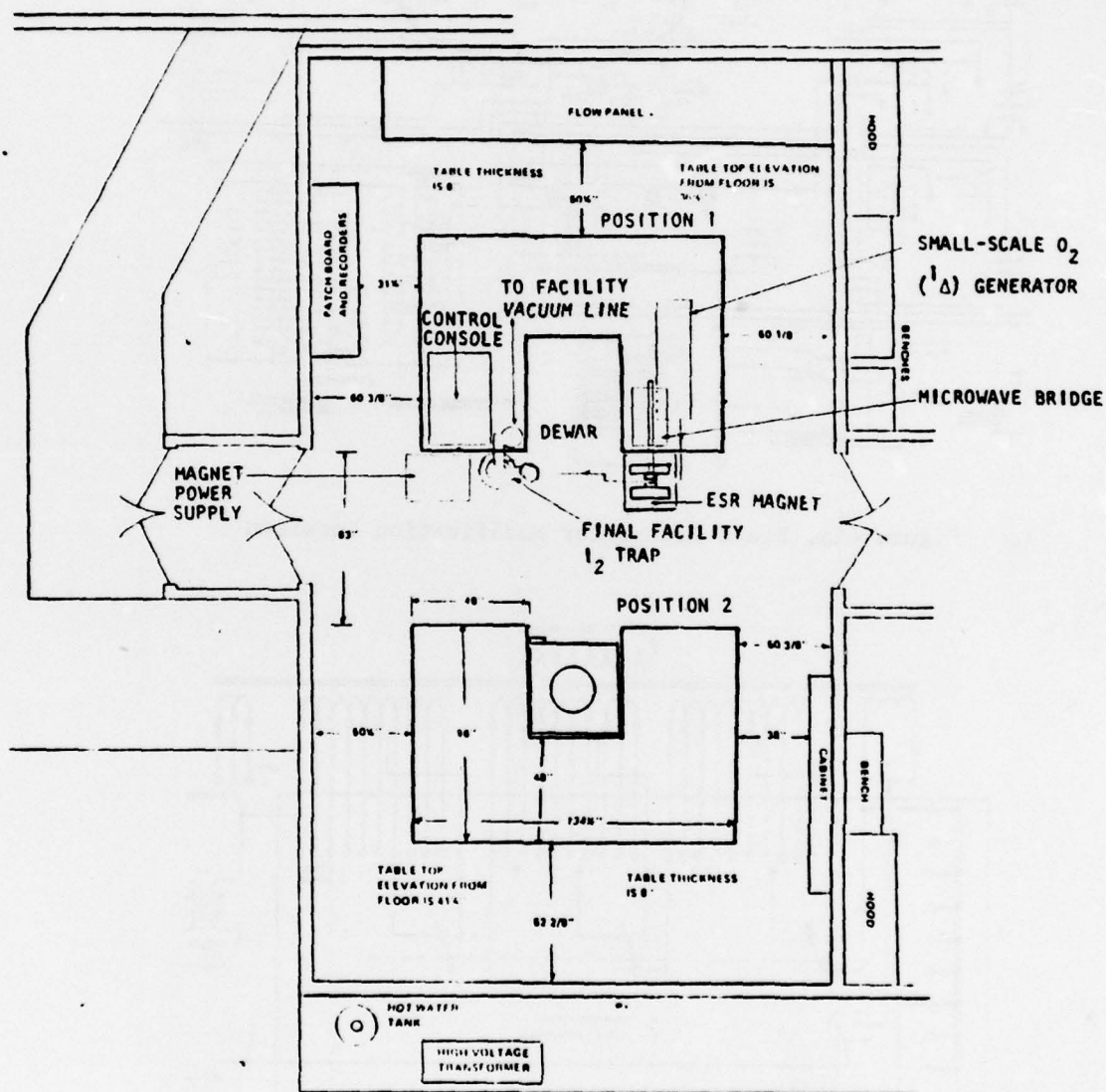


Figure 43. Continuous Wave Laser Laboratory With EPR Interface

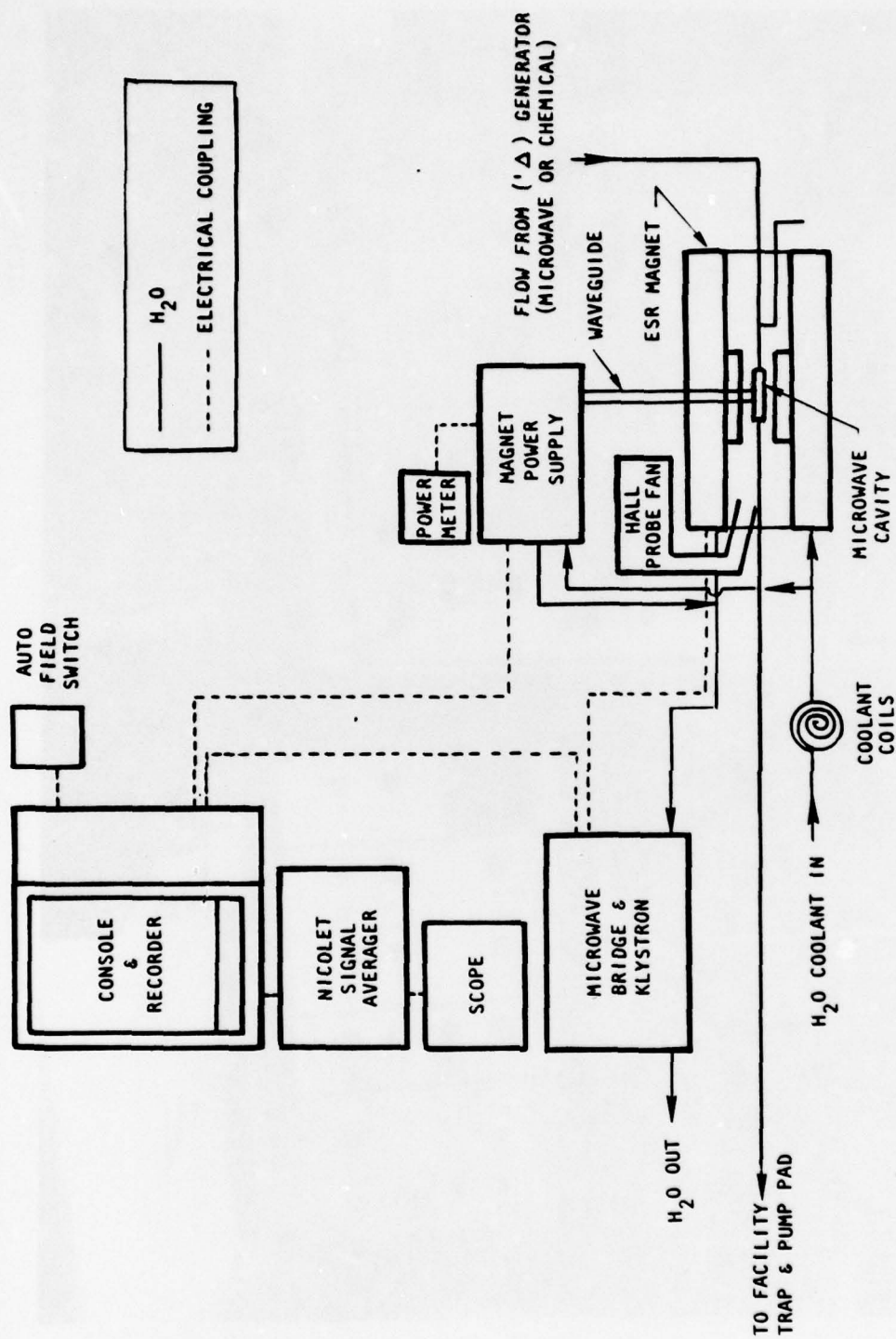
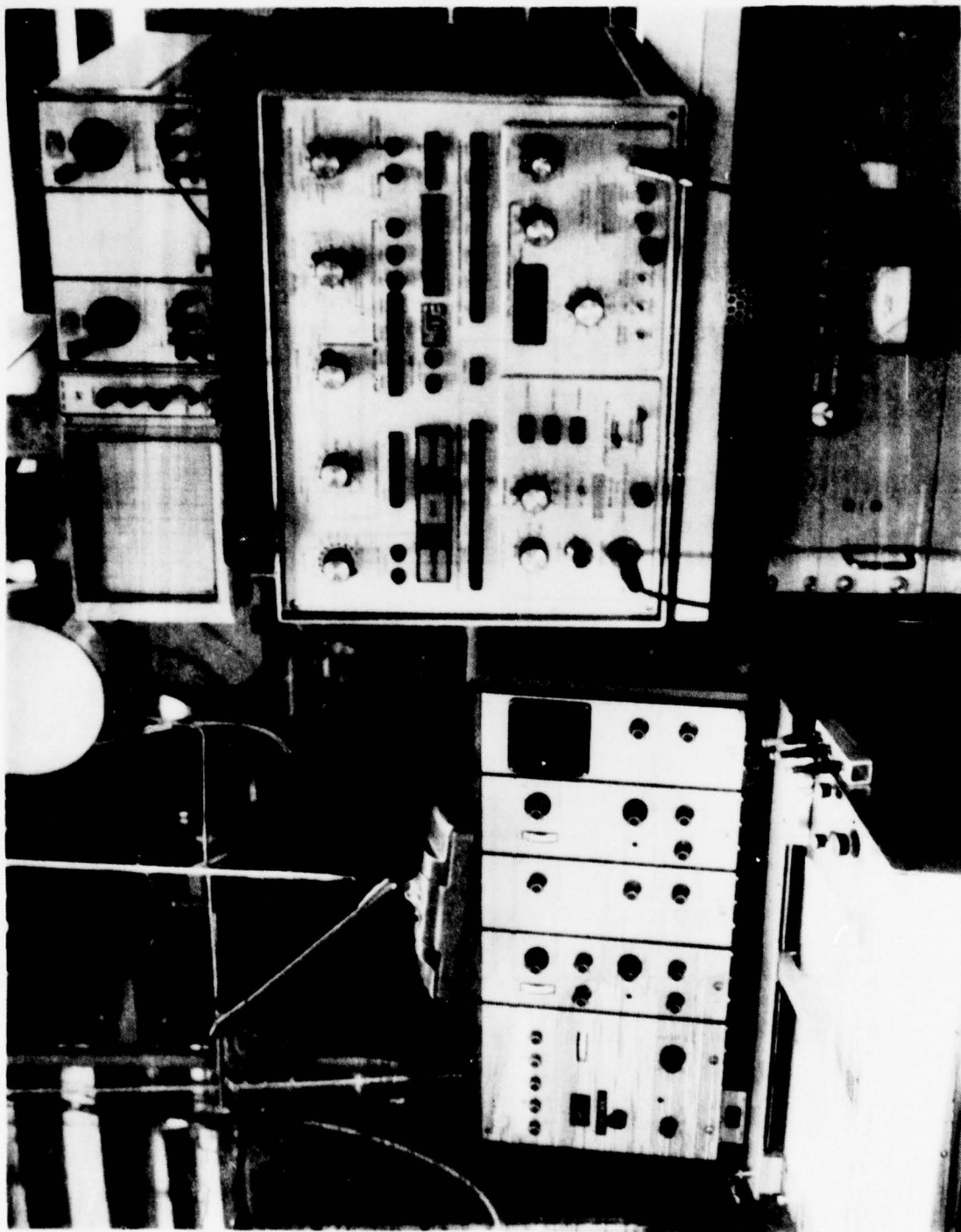


Figure 44. ESR Spectrometer System Schematic



4LC34-11/17/78-S1 I*

Figure 45. ESR Control Station

The Singlet Oxygen Optical Monitor

The spectra of singlet oxygen have been of interest for many years, originally because of their appearance as the atmospheric ($b^1\Sigma_g^+ - X^3\Sigma_g^-$) and infrared atmospheric ($a^1\Delta_g - X^3\Sigma_g^-$) bands. Both of these bands are seen in emission from gas containing $O_2(^1\Delta)$. The $b^1\Sigma$ is formed via the "pooling" reaction:



The singlet oxygen spectral features of interest to this study are the 0-0 band of the $^1\Delta_g - X^3\Sigma_g^-$ system centered at 7882.39 cm^{-1} ($\lambda = 1.26830 \text{ }\mu\text{m}$) and the 0-0 band of the $b^1\Sigma_g^+ - X^3\Sigma_g^-$ system centered at $13120.9085 \text{ cm}^{-1}$ ($\lambda = 0.7619.13 \text{ }\mu\text{m}$). The system constructed for measuring the emission from these bands is shown schematically in Fig. 46 and photographically in Fig. 47. This system was calibrated against the ESR spectrometer described earlier. The calibration consisted of a fit to the data points comprising optical monitor voltage versus $O_2(^1\Delta)$ partial pressure. Pretest calibrations were made using μ -wave generated $O_2(^1\Delta)$ at various pressures. ESR data taken during the tests were also used in the calibrations. Figure 48 shows a typical set of calibration data. The $O_2(^1\Delta)/O_2$ was determined by using the slope (and intercept when nonzero) to determine the $O_2(^1\Delta)$ pressure in torr at the ESR and dividing by P_1 .

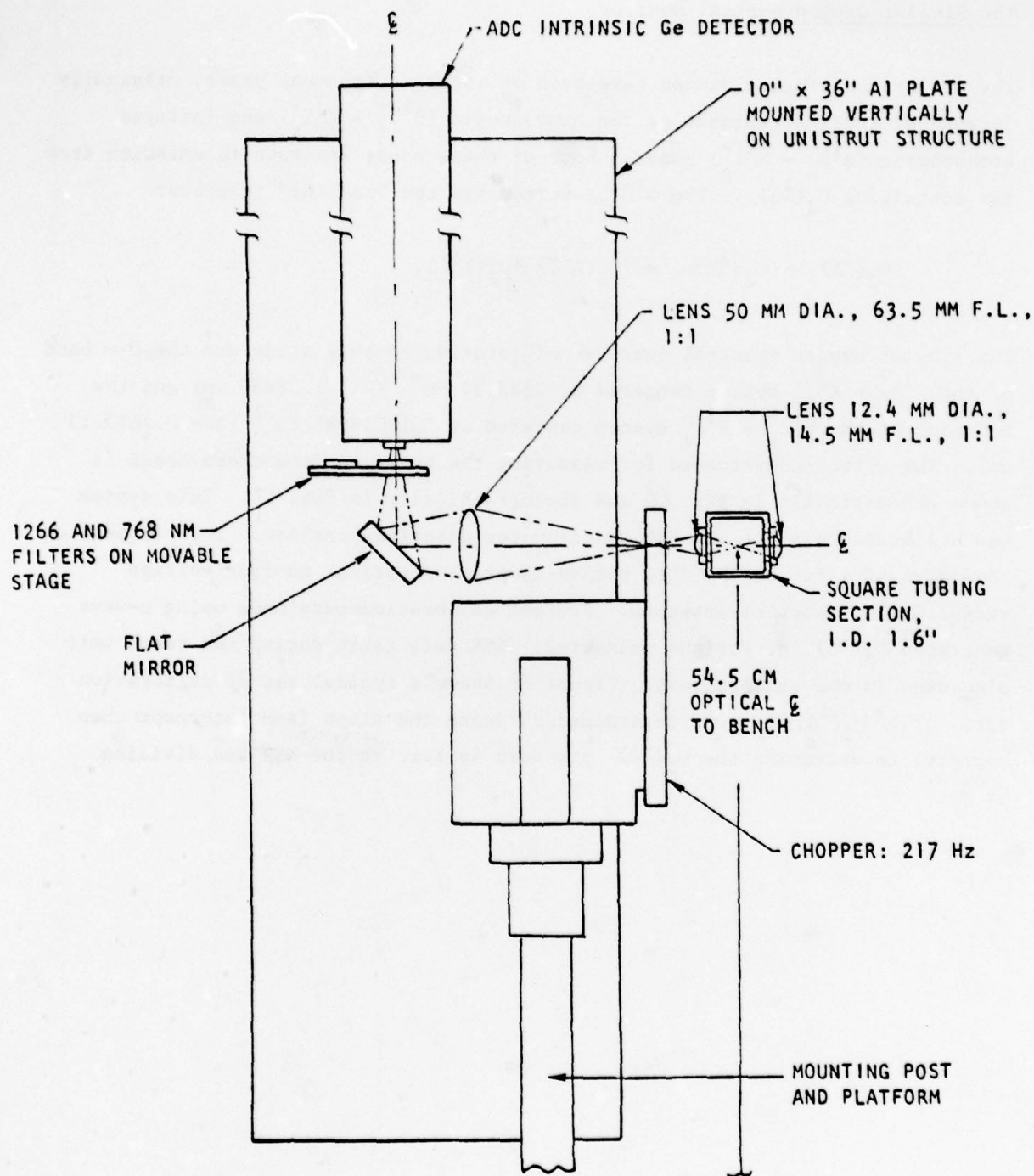
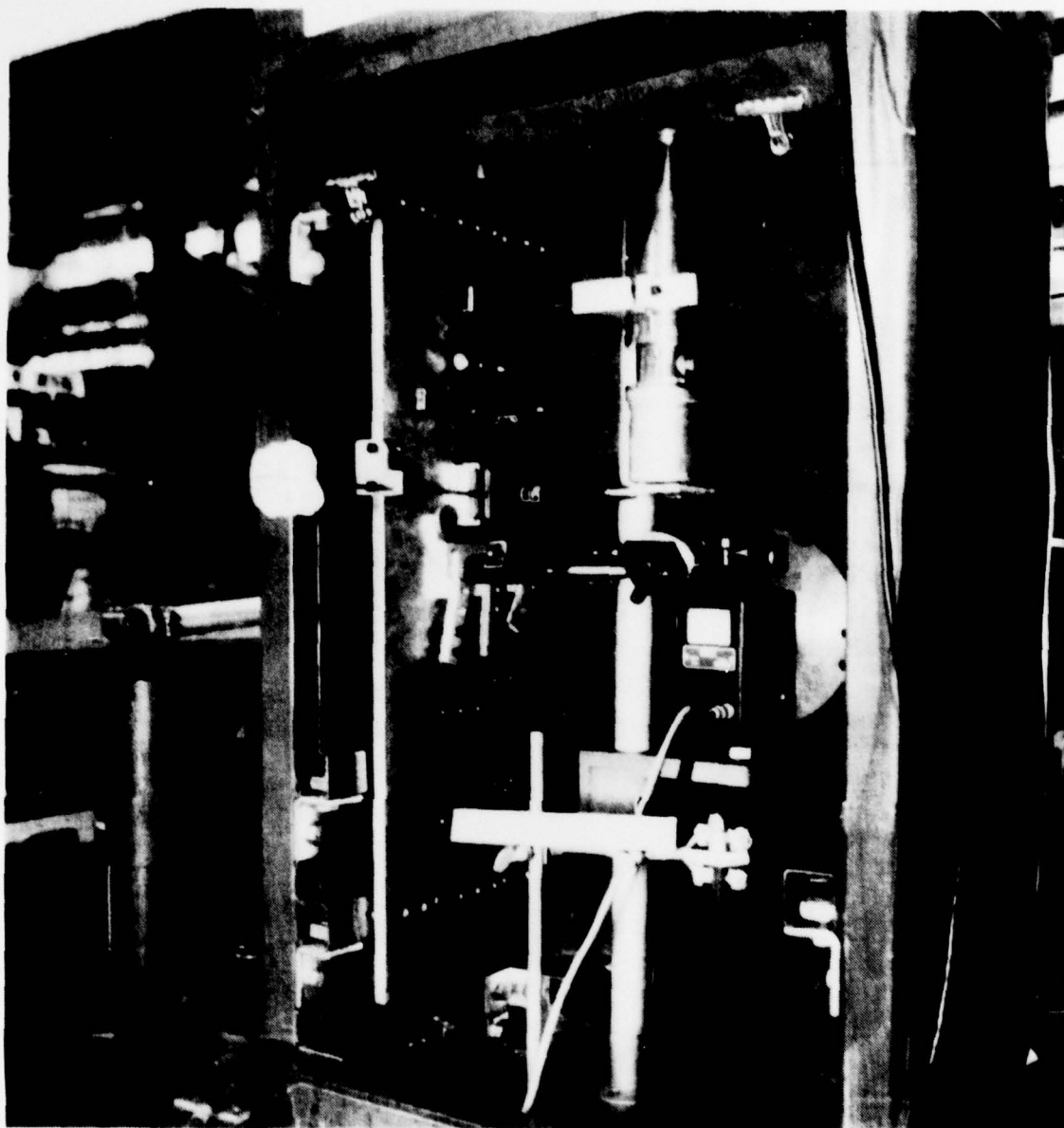


Figure 46. Optical Schematic of $O_2(^1\Delta, ^1\Sigma)$ Monitor



4LC34-11/17/78-S1H*

Figure 47. Singlet Oxygen Optical Monitor

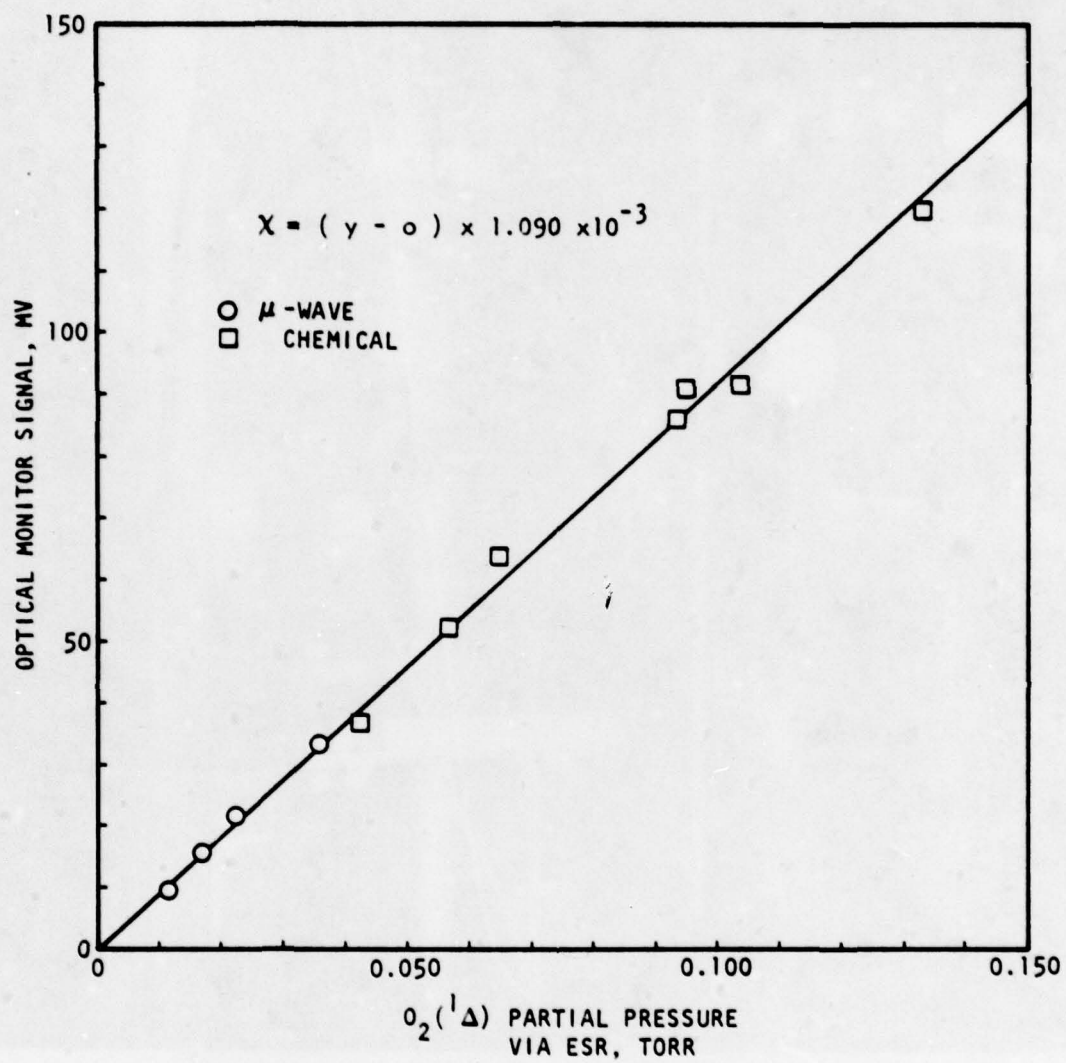


Figure 48. Optical Calibration-Test 038

SECTION IV

$O_2(^1\Delta)$ EXPERIMENTS

Production of good yields of singlet delta oxygen was a major objective of the contract. This section describes and discusses the experiments in which production and quenching of $O_2(^1\Delta)$ were investigated. Three different types of production experiments were carried out:

1. $O_2(^1\Delta)$ production using CFS and peroxide, with and without base, in the Rockwell Science Center cyclone reactor (Ref. 1). These experiments were intended to provide a baseline as well as to establish the necessity for base in producing $O_2(^1\Delta)$.
2. $O_2(^1\Delta)$ production using Cl_2 and basic peroxide in the roller-drum reactor. These experiments were intended to characterize the reactor and to provide a basis for comparison with the CFS system.
3. $O_2(^1\Delta)$ production using CFS and basic peroxide in the roller-drum reactor. These experiments were intended to evaluate and characterize this chemical system and to optimize the production of $O_2(^1\Delta)$ from it.

In this section, the overall test program is summarized in terms of tests conducted, rationale for changing configurations and parameters, general performance, and data obtained. These brief discussions of cyclone reactor and roller-drum reactor testing and results are followed by presentation of the data. Interpretation of the roller-drum reactor data includes discussions of the sensitivity of O_2/Cl_2 and $O_2(^1\Delta)/O_2$ to various operating parameters, both with Cl_2 and with CFS. The final discussion deals with quenching of $O_2(^1\Delta)$.

TESTING AND DATA SUMMARY

Table 8 provides a summary of the testing carried out under this effort. The parameters listed on the following page are identified for each test in which $O_2(^1\Delta)$ was produced.

- Reactor. This identifies whether the cyclone reactor or the roller-drum reactor was used and whether the premixed basic peroxide system or the on-line base-peroxide mixer was used to deliver the liquid to the roller-drum reactor.
- Configuration. This refers to the configurations O, A, B, C, D which are described in Section III.
- Temperature. The temperature (given in degrees centigrade) is the average of the coolant in and coolant out temperature during the test.
- R_1 - R_2 gap. This is the distance (in cm) between the surface of the large roller R_1 and the surface of the small liquid applicator roller R_2 .
- R_1 -shield gap. This is the radial distance (in cm) between the surface of the large roller and the concentric Teflon shield which was held in place above the roller.
- Shield length. This is the length of the Teflon shield from where it butted against the gas nozzle to the end of the shield.
- Basic peroxide concentration. This number identifies the basic peroxide solution used. The solutions were described in Table 2, (Section III).
- Liquid flows. This is the flowrate (in ml/sec) of the basic peroxide solution. To get the molar flows (in mmoles/sec), multiply the flowrate in ml/sec by the molar concentrations of Table 2.
- Reactant. This simply specifies whether the test used CFS, Cl_2 , or both.

Cyclone Reactor

The experiments conducted here were very similar to those described in Ref. 1. The same six-element Kenics mixer, cyclone separator/reactor, and -160 C trap were used. CFS and 90% H_2O_2 were admitted to the Kenics mixer, as shown in

TABLE 8. TESTING SUMMARY

DATE	TEST NUMBER	DESCRIPTION	REACTOR	CONFIGURATION	TEMPERATURE °C	R ₁ -R ₂ GAP-CH	R ₁ -SHIELD GAP-CH	SHIELD LENGTH-CM	BASIC PEROXIDE CONCENTRATION	LIQUID FLOWS (NOM)	REACTANT
5 Jul 78	001	Check-out	Cyclone								
26 Jul 78	002	Performance	Cyclone								
3 Aug 78	003	Performance	Cyclone								
31 Aug 78	004	Performance	Cyclone								
12 Sep 78	005	Cold Flow	Roller								
13 Sep 78	006	Cold Flow	Roller								
14 Sep 78	007	Cold Flow	Roller								
18 Sep 78	008	Cold Flow	Roller								
20 Sep 78	009	Check-out	Roller		22	0.054	No Shield		2		CFS
21 Sep 78	010	Demonstration	Roller		2	0.054	No Shield		2		CFS
26 Sep 78	011	Cold Flow	Roller								
27 Sep 78	012	Performance	Roller								
29 Sep 78	013	Performance	Roller								
2 Oct 78	014	Performance	Roller		-14	0.054	1.40	13.2	2		CFS
6 Oct 78	015	Performance	Roller		-11	0.054	1.40	13.2	2,3	0.04-015	Cl ₂ , CFS
7 Oct 78	016	Cold Flow	Roller		Trap 3 Effectiveness						

TABLE 8. (Continued)

DATE	TEST NUMBER	DESCRIPTION	REACTOR	CONFIGURATION	TEMPERATURE °C	R ₁ -R ₂ GAP-CM	R ₁ -SHIELD GAP-CM	SHIELD LENGTH-CM	BASIC PEROXIDE CONCENTRATION	LIQUID FLOWS (NOM) ML/SEC	REACTANT
16 Oct 78	017	Quenching	Roller	By { H ₂ O, NaOH, H ₂ O ₂ , H ₂ O ₂ /NaOH/H ₂ O, Cl ₂ , CFS, Cl ₂ /H ₂ O, CFS/H ₂ O Air, N ₂ , O ₂ , He, CO ₂ , H ₂ SO ₄ , HSO ₃ F	-12	0.54	1.40	12.4	2	0.05-0.13	Cl ₂ , CFS
17 Oct 78	018	Quenching	Roller		-16	0.54	1.40	12.4	3	0.16	Cl ₂
18 Oct 78	019	Quenching	Roller		-14	0.054	1.40	12.4	3	0.02-0.10	Cl ₂ , CFS
19 Oct 78	020	Quenching	Roller		-14	0.054	1.40	12.4	3	0.02-0.10	Cl ₂ , CFS
20 Oct 78	021	Performance	Roller	By Reactor and Flow System	-14	0.054	0.66	12.4	3	0.13	Cl ₂ , CFS
23 Oct 78	022	Performance	Roller		-14	0.054	0.66	12.4	3	0.13	Cl ₂ , CFS
24 Oct 78	023	Performance	Roller		22	0.054	0.66	12.4	1, 1+50% H ₂ O ₂	0.12	Cl ₂ , CFS
25 Oct 78	024	Quenching	Roller		-18	0.054	0.66	12.4	1	0.06	Cl ₂ , CFS
27 Oct 78	025	Performance	Roller	C	-42	0.054	0.66	12.4	1	0.12	Cl ₂ , CFS
30 Oct 78	026	Performance	Roller		-42	0.054	0.66	10.0	1	0.12	Cl ₂ , CFS
31 Oct 78	027	Performance	Roller		-18	0.054	0.66	10.0	1	Varied	Cl ₂
3 Nov 78	028	Performance	Roller								
10 Nov 78	029	Performance	Roller	C	-42	0.054	0.66	12.4	1	0.12	Cl ₂ , CFS
14 Nov 78	030	Performance	Roller		-42	0.054	0.66	10.0	1	0.12	Cl ₂ , CFS
20 Nov 78	031	Performance	Roller		-18	0.054	0.66	10.0	1	Varied	Cl ₂

Δ No data, unsteady flows and O₂ (Δ) Production

TABLE 8. (Concluded)

DATE	TEST NUMBER	DESCRIPTION	REACTOR	CONFIGURATION	TEMPERATURE °C	R ₁ -R ₂ GAP-CM	R ₁ -SHIELD GAP-CM	SHIELD LENGTH-CM	BASIC PEROXIDE CONCENTRATION	LIQUID FLOWS (NOM) ML/SEC	REACTANT
5 Jan 79	032	Performance	Roller/M ^a	C	Aborted Trap 2 Blocked						
8 Jan 79	033	Performance	Roller/M	D	Aborted-Bearings Siezed						
19 Jan 79	034	Performance	Roller/M	D	-19	0.054	0.66	10.0	5	0.075	Cl ₂
22 Jan 79	035	Performance	Roller/M	D	1	0.054	0.66	10.0	5	0.075	Cl ₂
26 Jan 79	036	Performance	Roller/M	D	-1	0.054	0.66	10.0	5	0.075	Cl ₂
29 Jan 79	037	Performance	Roller/M	D	-15	0.054	0.66	10.0	5	0.075	Cl ₂
30 Jan 79	038	Performance	Roller/M	D	21	0.054	0.66	10.0	5	0.075	Cl ₂
2 Feb 79	039	Performance	Roller/M	D	-17	0.054	0.66	10.0	6	0.16	Cl ₂

^aRoller/M signifies the roller-drum reactor with the on-line base peroxide mixer. The other roller tests were with the premixed basic peroxide mode of operation.

Fig. 49. Thermostatically controlled heaters maintained the CFS at $\sim 50^\circ\text{C}$ and the H_2O_2 at $\sim 50^\circ\text{C}$. The 50% NaOH could be added to the H_2O_2 stream, as shown, or could be added downstream of the mixer, as in the Science Center experiments.

The results of the cyclone reactor tests are summarized below.

$\text{O}_2(^1\Delta)$ Yield. At reactor operating conditions similar to the nominal Science Center operation, $\text{O}_2(^1\Delta)/\text{O}_2$ was observed to be 0.24 at a pressure of 0.400 torr and 0.19 at 0.675 torr. These data points were via ESR spectroscopy and are below the optimum values reported in Ref. 1. However, qualitative estimates of $\text{O}_2(^1\Delta)$ yield from the optical monitor (uncalibrated during these tests) were that $\text{O}_2(^1\Delta)/\text{O}_2$ was as high as 0.30 to 0.35 at 0.400 to 0.500 torr. Both total pressure and $\text{O}_2(^1\Delta)$ signal were erratic during these tests because of irregular delivery of CFS and H_2O_2 . The objective of these tests was to verify the ability to reproduce the experiments reported in Ref. 1 with our reactant delivery, vacuum, and diagnostic systems. This objective was met. Attempts to optimize this system were not made because the two-stage operation ($\text{CFS} + \text{H}_2\text{O}_2$ followed by NaOH addition) had been shown to be at least partially equivalent to $\text{Cl}_2 + \text{H}_2\text{O}_2/\text{NaOH}$ during the basic chemistry experiments described in Section II.

Effect of NaOH Addition. Two experiments were conducted in which the base addition was varied. In the first, base was added upstream as well as simultaneously upstream and downstream of the Kenics mixer. Effects on O_2 production were not noted because addition of the 50% NaOH to the 90% H_2O_2 caused plugging of the system by the solids which were precipitated.

In the second experiment, no base was added to the $\text{CFS} + \text{H}_2\text{O}_2$ stream. This resulted in no detectable amount ($\sim 1\%$) of $\text{O}_2(^1\Delta)$ being present in the reactor effluent stream. Carrying this experiment out with the ESR spectrometer and the germanium detector on-line provided direct confirmation of the hypothesis of Ref. 1 that base was required to catalyze the production of $\text{O}_2(^1\Delta)$.

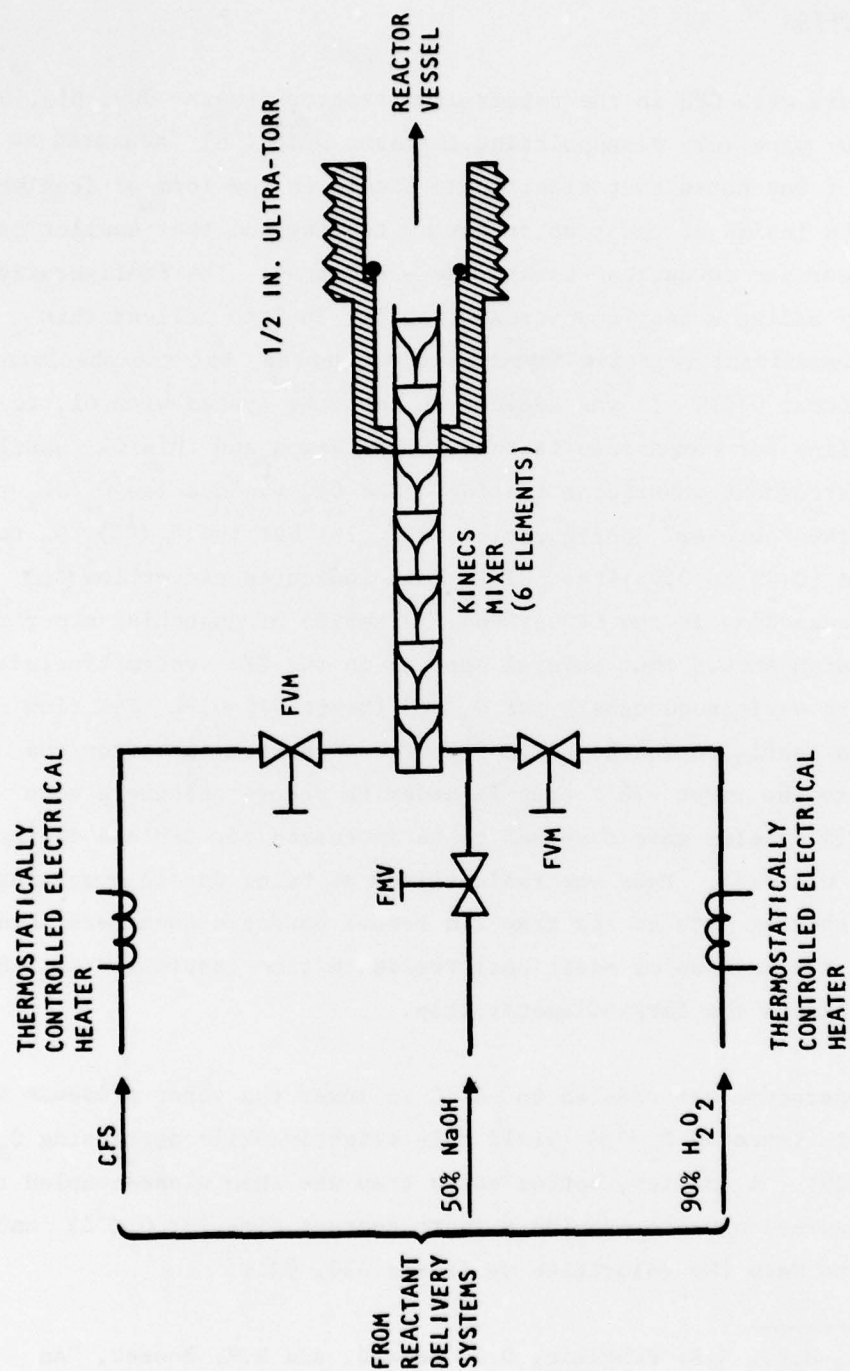


Figure 49. Kenics Mixer and Reactant Delivery Arrangement For Cyclone Reactor Tests

Roller-Drum Reactor

The initial tests with CFS in the roller-drum reactor (tests 009, 010, 012, configuration 0) were very disappointing in terms of $O_2(^1\Delta)$ measured at the diagnostics. It was noted that significant liquid in the form of droplets collected on the inside of the reactor during testing and that smaller droplets (aerosol) had carried downstream toward the -160C trap. The configuration was changed to A by adding a near-downstream trap at -78 C to collect this material. A significant relative improvement was noted, but the absolute ($^1\Delta$) was still low (test 014). It was decided to test the system with Cl_2 to provide a baseline for comparison to the CFS operation and this Cl_2 baseline was provided throughout subsequent testing. The Cl_2 yielded low O_2/Cl_2 ratios compared with the "bubbler" configuration (Ref. 10) but the $O_2(^1\Delta)/O_2$ ratios were comparable (0.25 to 0.45)(test 015). This indicated either low ($^1\Delta$) production or quenching in the CFS system. A series of quenching experiments in the flow system showed that several species in the CFS system (including CFS itself) were serious quenchers for $O_2(^1\Delta)$ (tests 016-019). The flow system was modified to configuration B, which featured a shorter path from the reaction zone to the first -78 C trap in order to remove quenchers more rapidly. $O_2(^1\Delta)$ yields were observed to be increased for CFS and decreased for Cl_2 (tests 021-028). This was rationalized as being due to competing effects. The shorter path to the trap did remove unwanted quenchers more quickly but at the expense of additional residence time (estimated at ~0.4 sec) passing through the large-diameter trap.

The roller temperature was reduced to -42 C to lower the vapor pressure of the quenchers. This improved $O_2(^1\Delta)$ yield only slightly while decreasing O_2/CFS ratios (test 029). A smaller, bottom entry trap was then close-coupled to the reactor (configuration 0) to provide a short contact time for $O_2(^1\Delta)$ and quenchers and to keep the velocities up (tests 030, 031).

-
18. McDermott, W.E., N.R. Pchelkin, D.J. Benard, and R.R. Bousek, "An Electronic Transition Chemical Laser", Appl. Phys. Lett. 32(8), 469-470 (1978).

In all of the tests mentioned above, the general procedure was to hold the liquid flow and concentration fixed while varying the CFS or Cl_2 flow. The system pressures and $\text{O}_2 (^1\Delta)$, $\text{O}_2 (\text{X}^3\Sigma)$ signals were noted.

The final series of tests (034-039) were conducted using configuration D, which was adopted because blockage of the bottom entry trap of configuration C. These tests had the primary objective of characterizing performance of the reactor when coupled with an on-line base peroxide mixer, which had been developed and shown to operate successfully off-line.

Data From Roller-Drum Reactor Tests

This section consists of a presentation of the data obtained in the roller-drum reactor experiment. Three sets of data are presented graphically for each test:

1. $\text{O}_2 (^1\Delta) / \text{O}_2$ versus CFS or Cl_2 flowrate. The data points are marked as to whether ESR or optical techniques were used.
2. Product flow versus CFS or Cl_2 flow.
3. $\text{O}_2 (^1\Delta)$ partial pressure versus CFS or Cl_2 flow.

The graphs (Fig. 50 through 97) are presented in the order 1, 2, 3 for each test starting with test 015, with the tests being in numerical order. Additional data on configuration, roller temperature, gaseous reactant used, liquid volume flowrate, liquid concentration, liquid reactant molar flowrate, and special configurational or operational notes are located either on one or more of the graphs from each test or in the Testing Summary (Table 9).

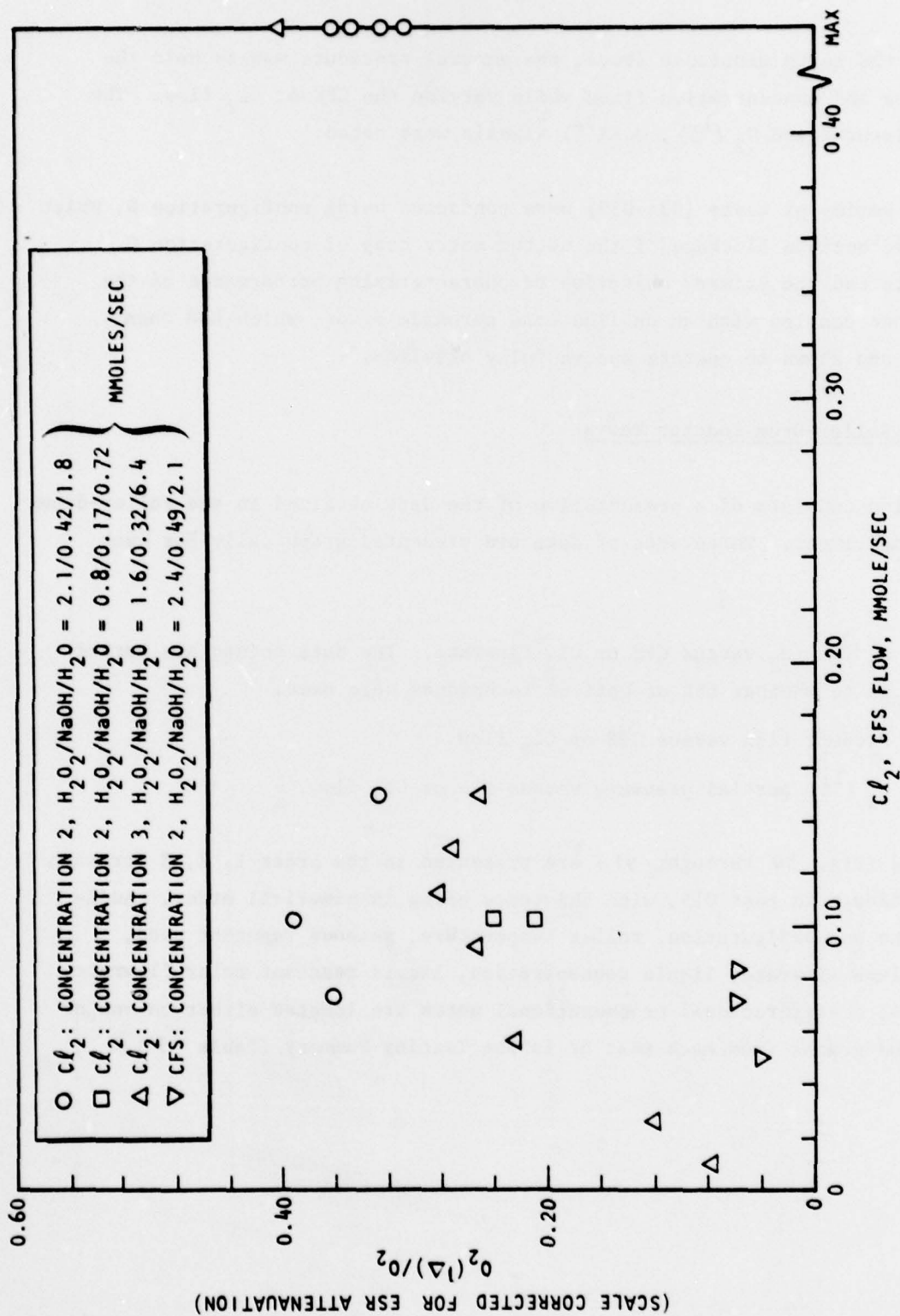


Figure 50. $O_2(^1\Delta)$ Yield, Test 015; Roller at -11C, Configuration A, Liquid Concentration 2, 3

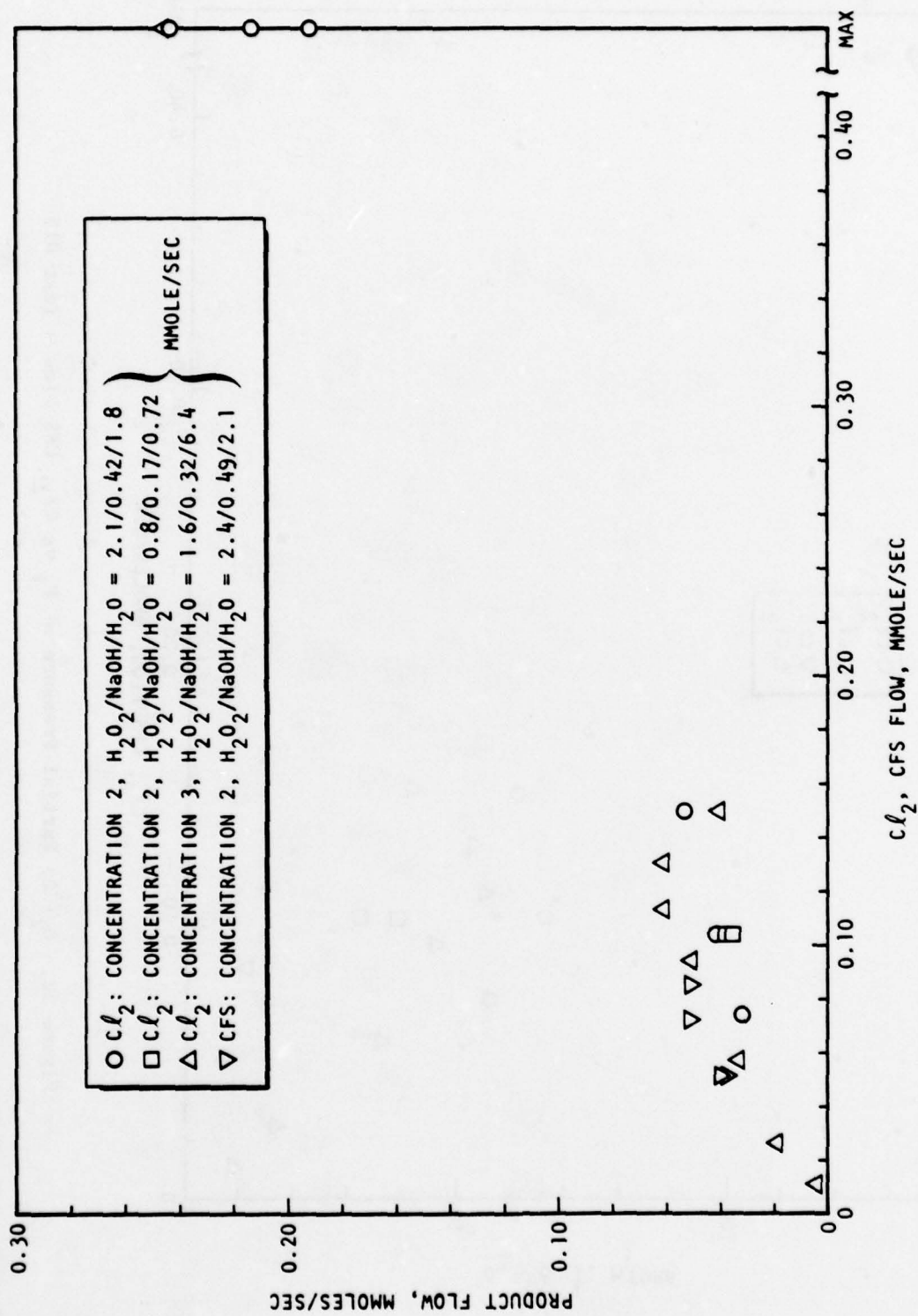


Figure 51. Product Flow vs Cl_2 , CFS Flow - Test 015

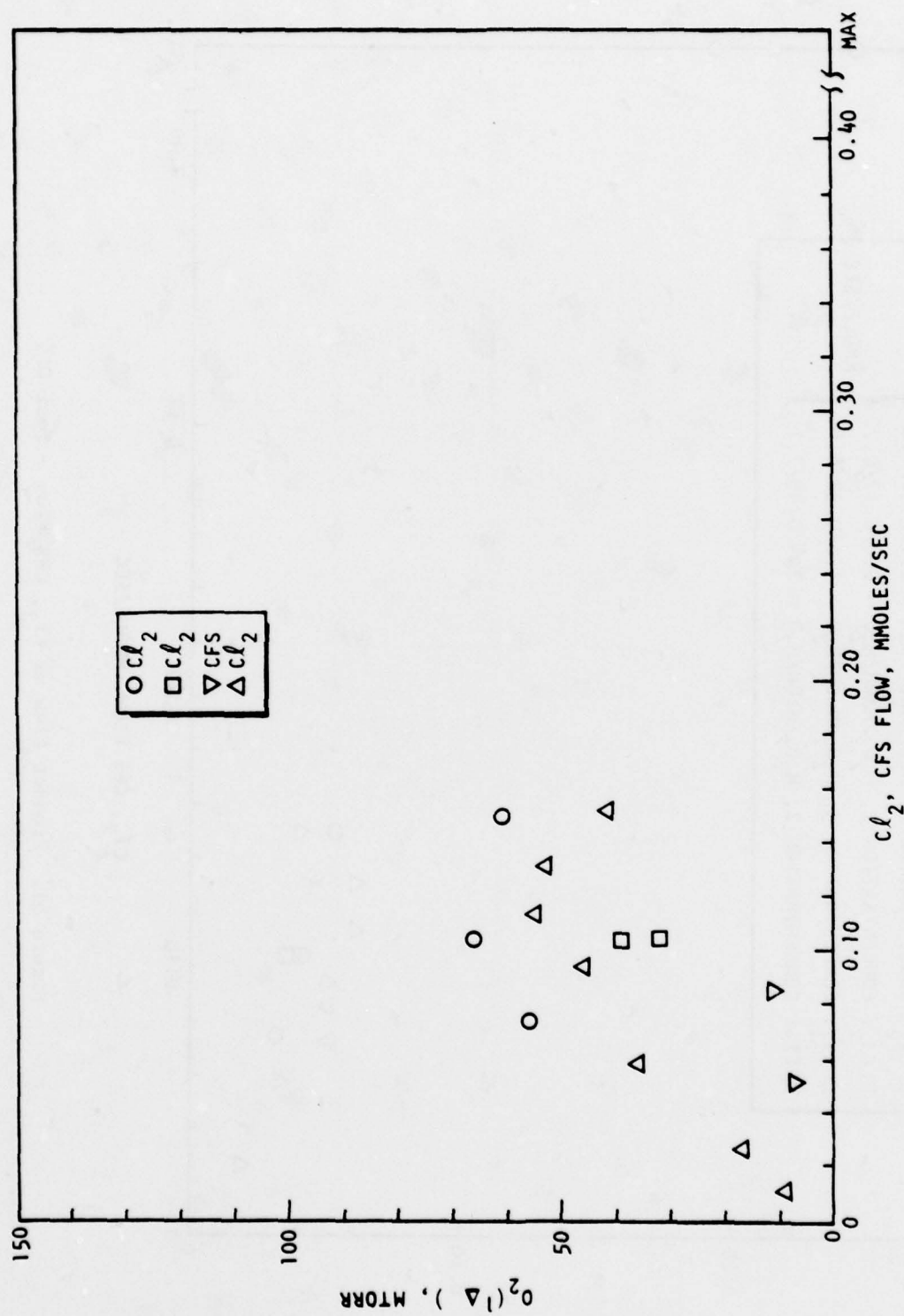


Figure 52. O_2 (Δ) Partial Pressure at P_1 vs Cl_2 , CFS Flow ~ Test 015

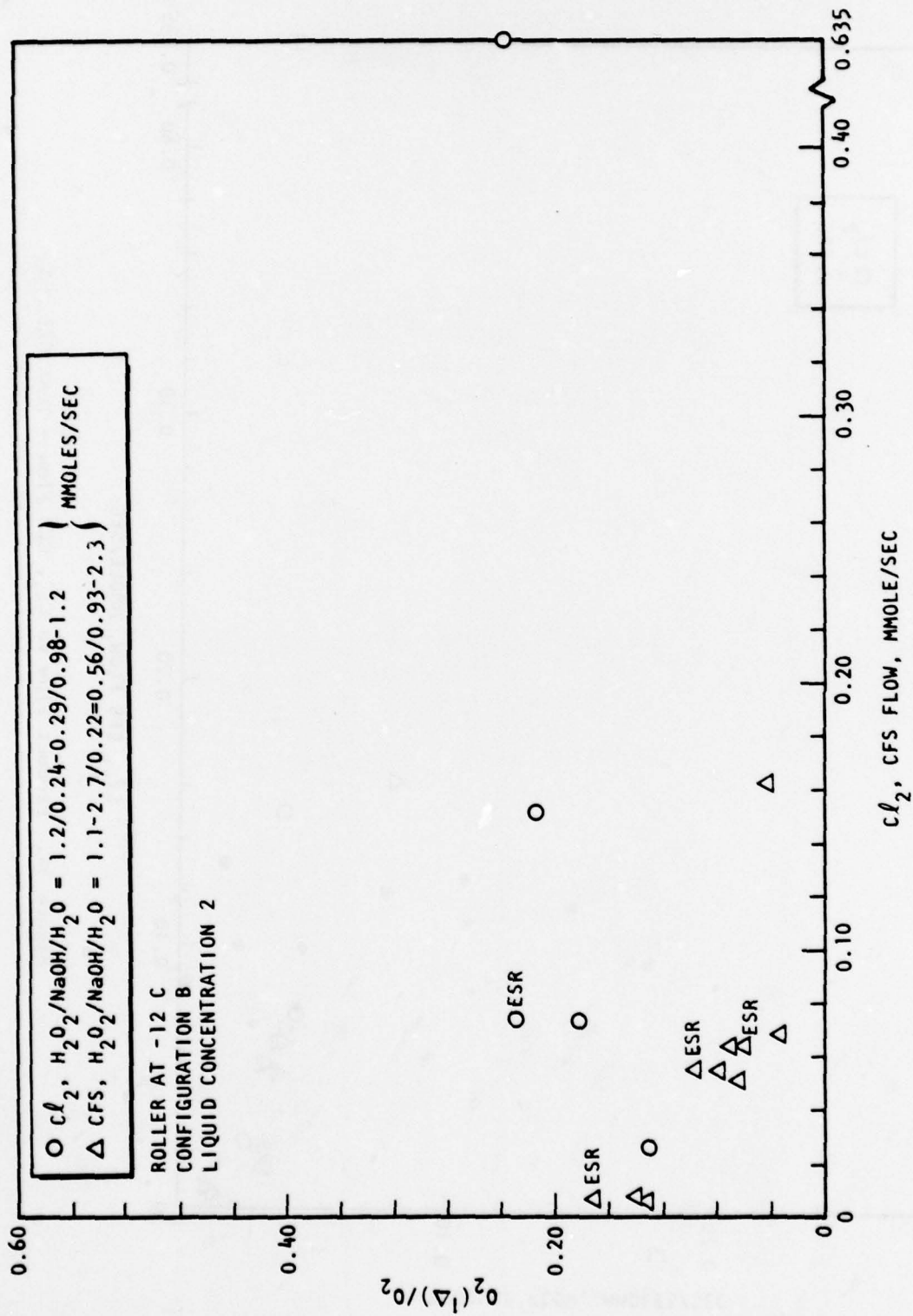


Figure 53. $O_2(\Delta)$ Yield, Test 021

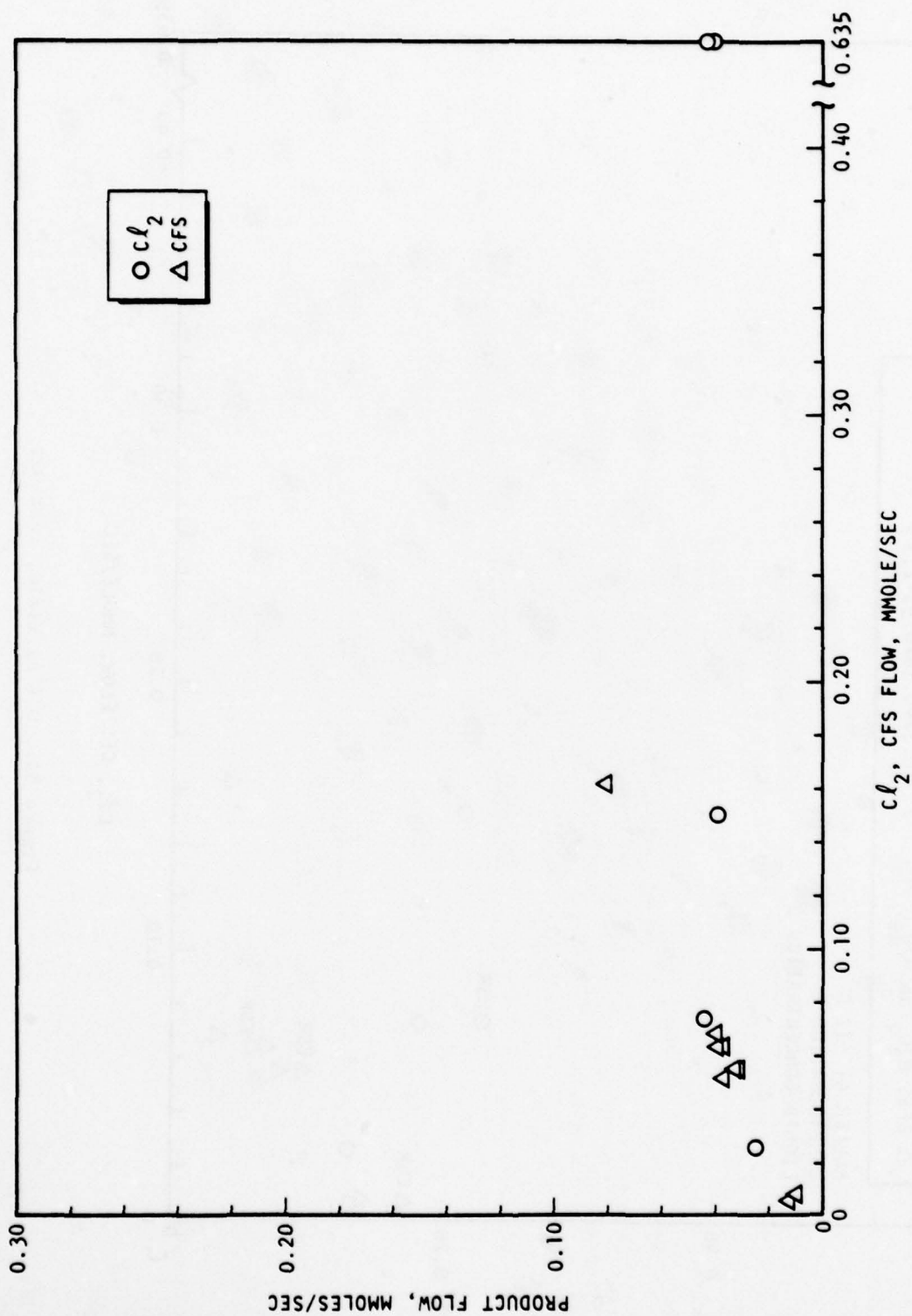


Figure 54. Product Flow vs Cl_2 , CFS Flow - Test 021

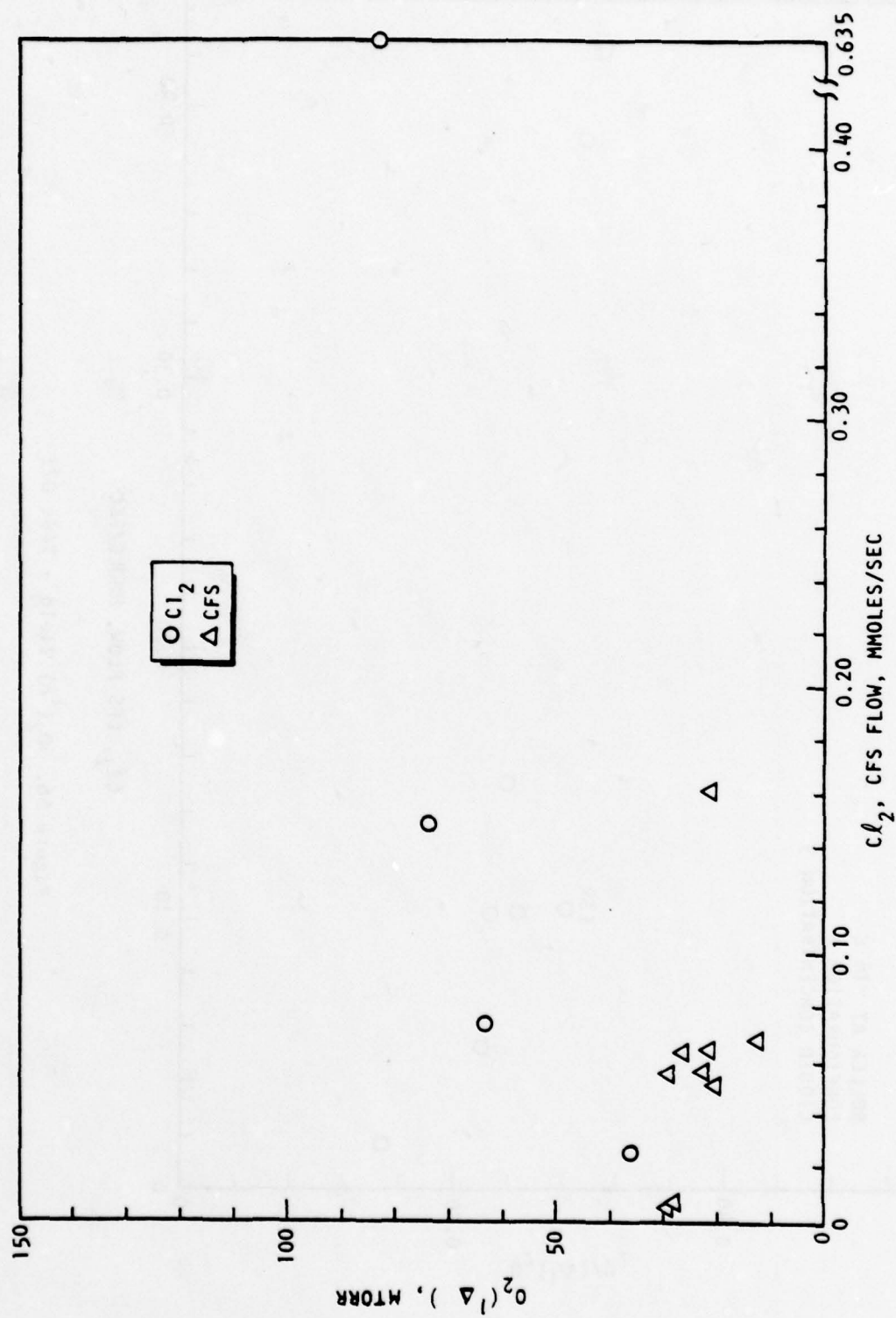


Figure 55. $\text{O}_2(\Delta)$ Partial Pressure At P_1 vs Cl_2 , CFS Flow - Test 021

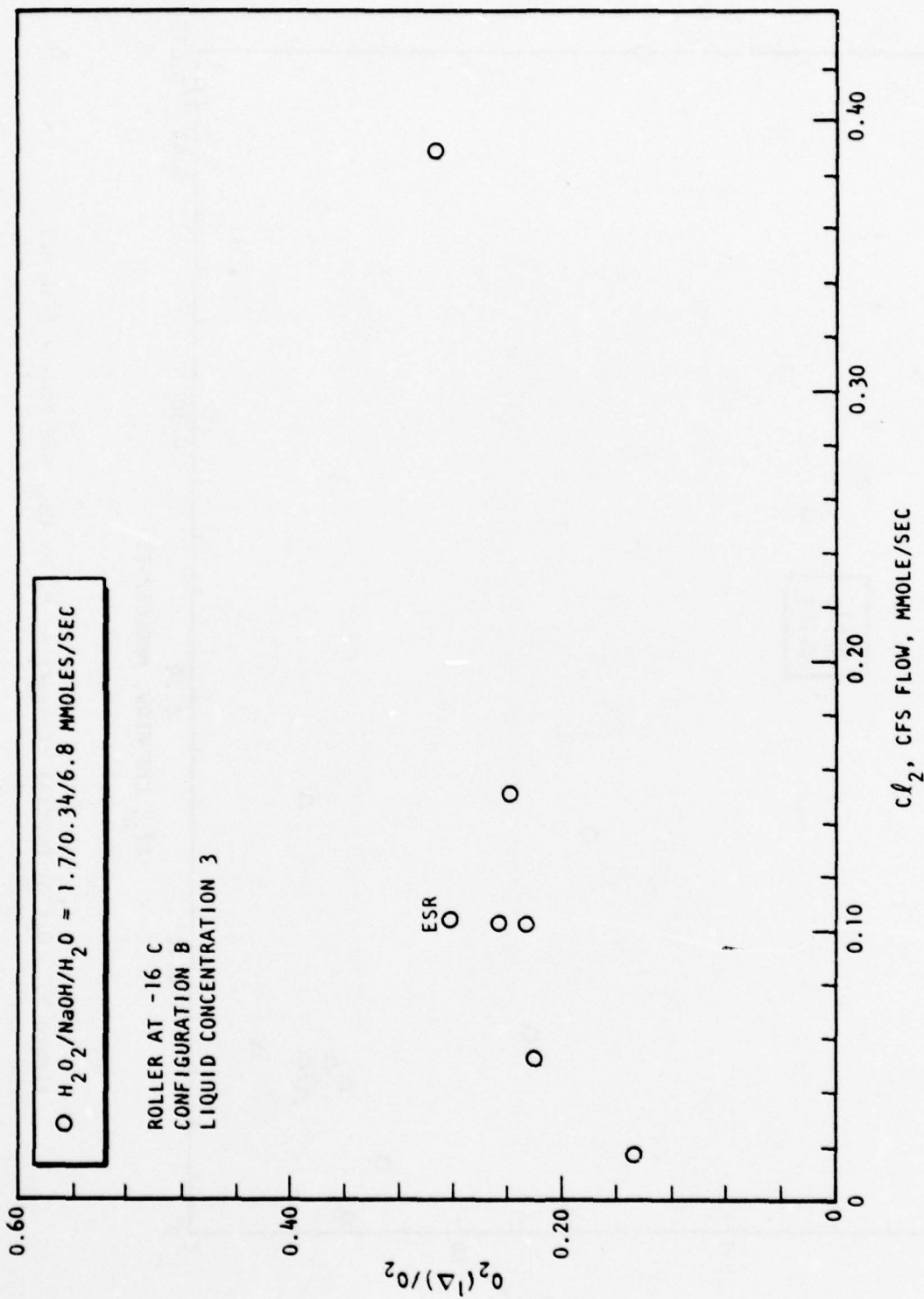


Figure 56. $\text{O}_2(1\Delta)$ Yield - Test 022

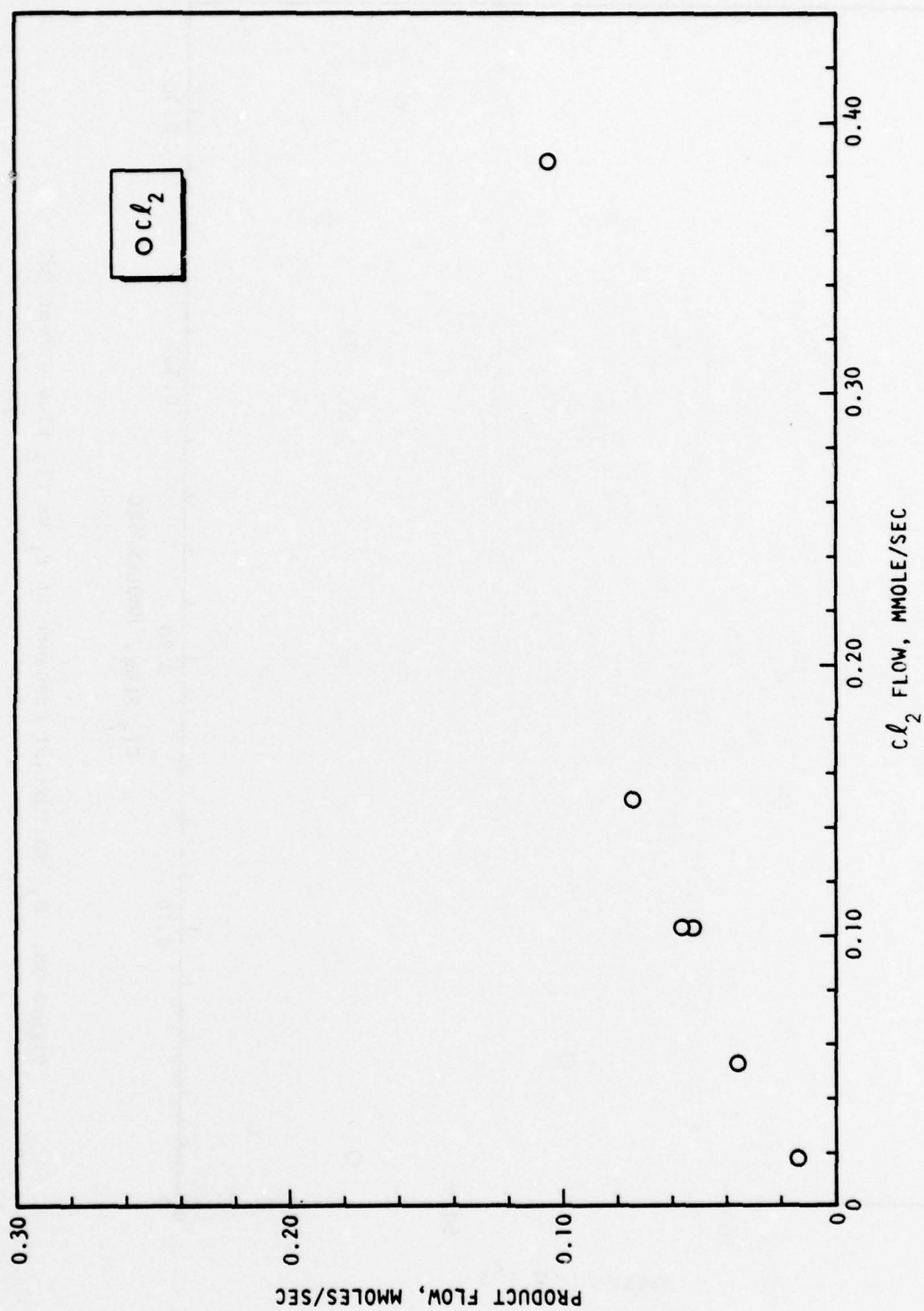


Figure 57. Product Flow vs Cl_2 Flow - Test 022

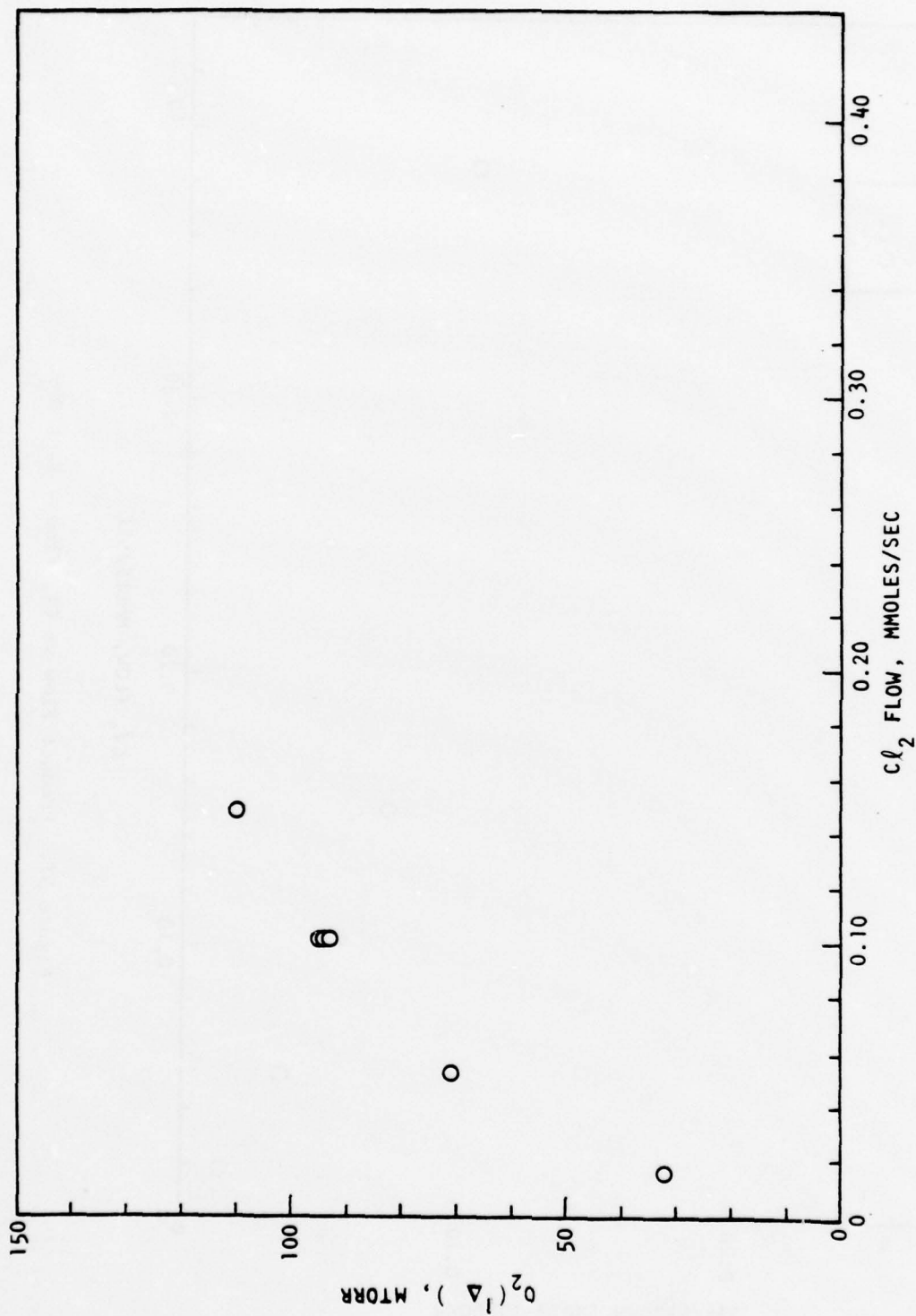


Figure 58. $O_2(^1\Delta)$ Partial Pressure at P_1 vs Cl_2 Flow - Test 022

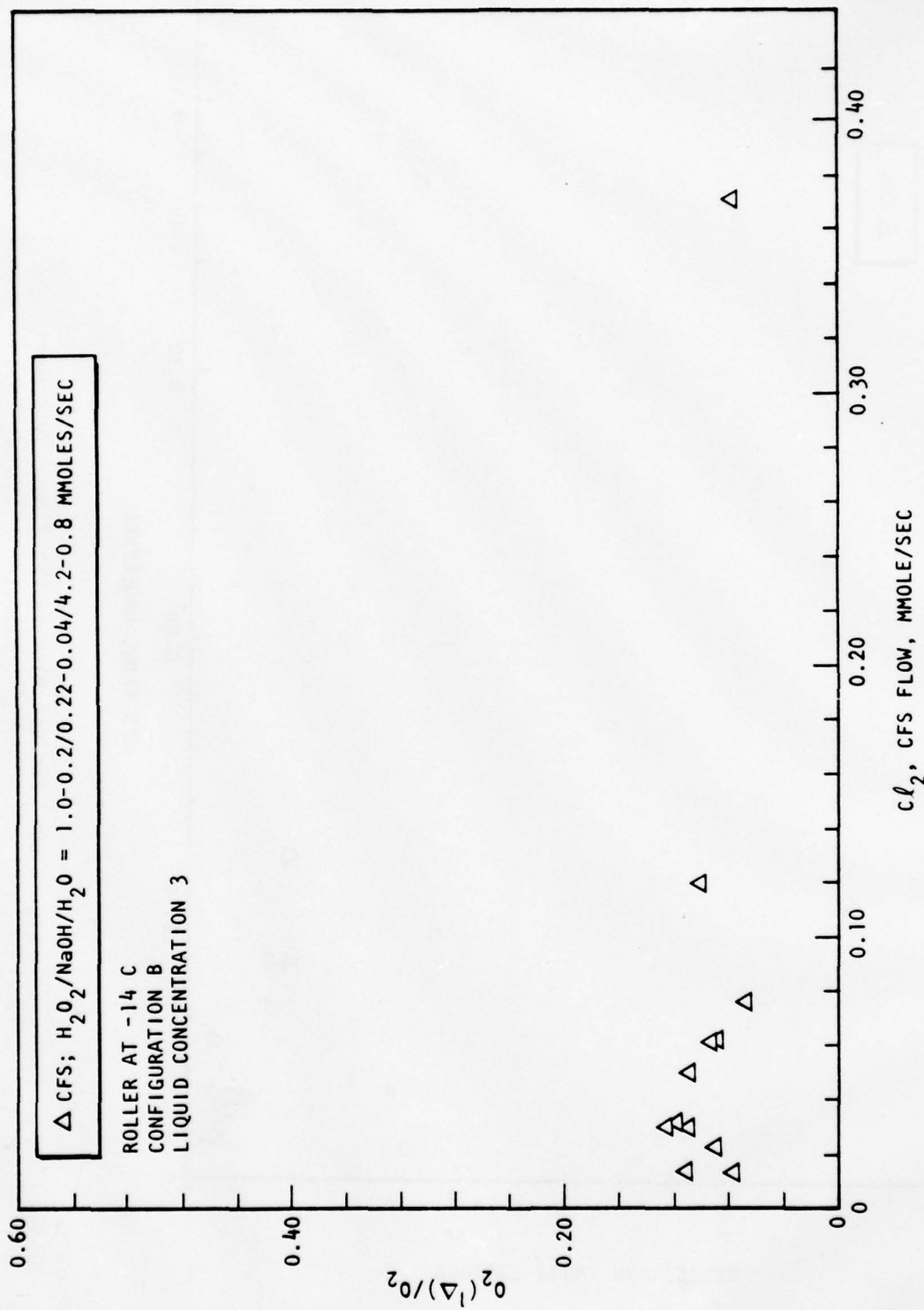


Figure 59. $O_2(l\Delta)$ Yield, Test 023

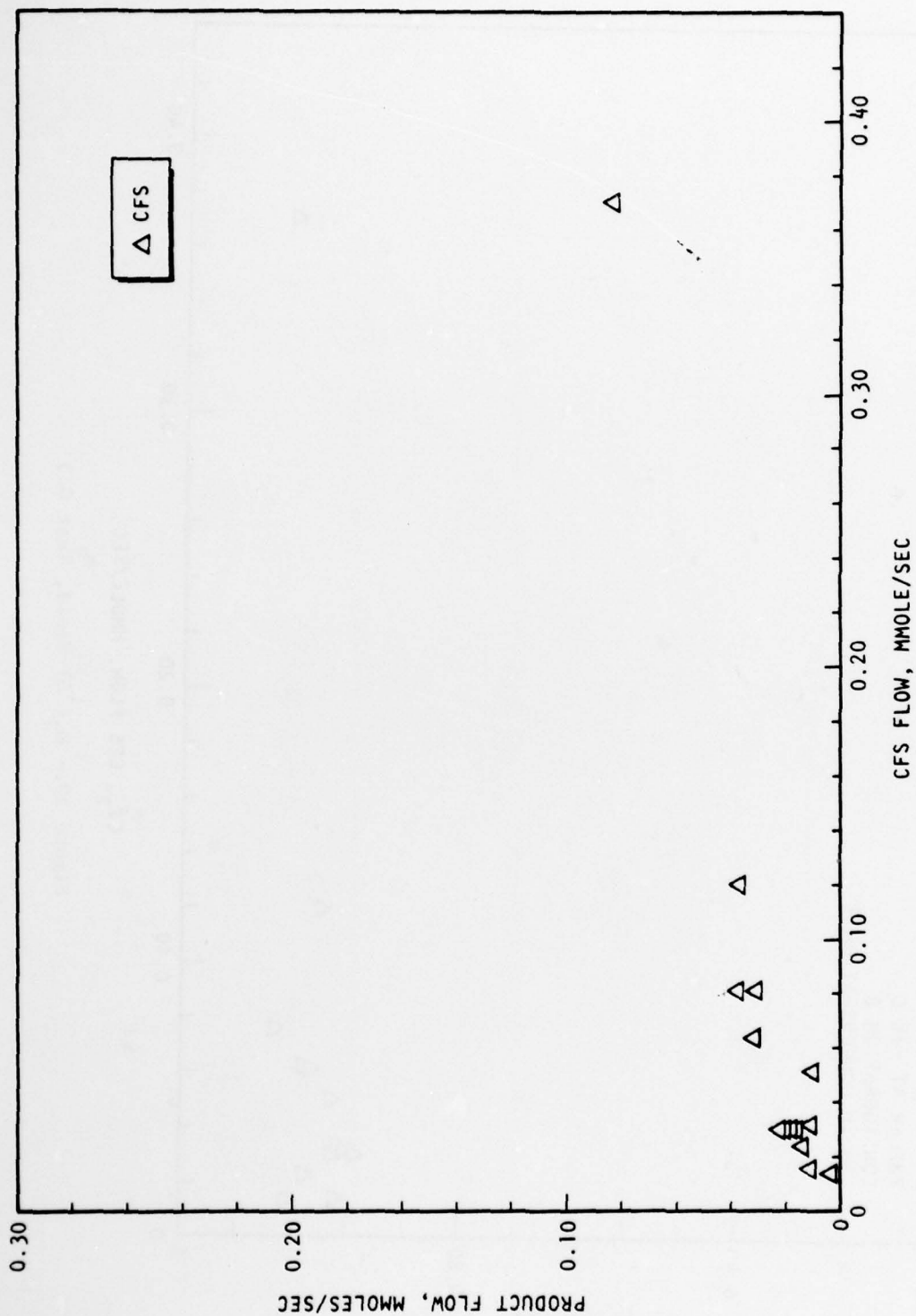


Figure 60. Product Flow vs CFS Flow - Test 023

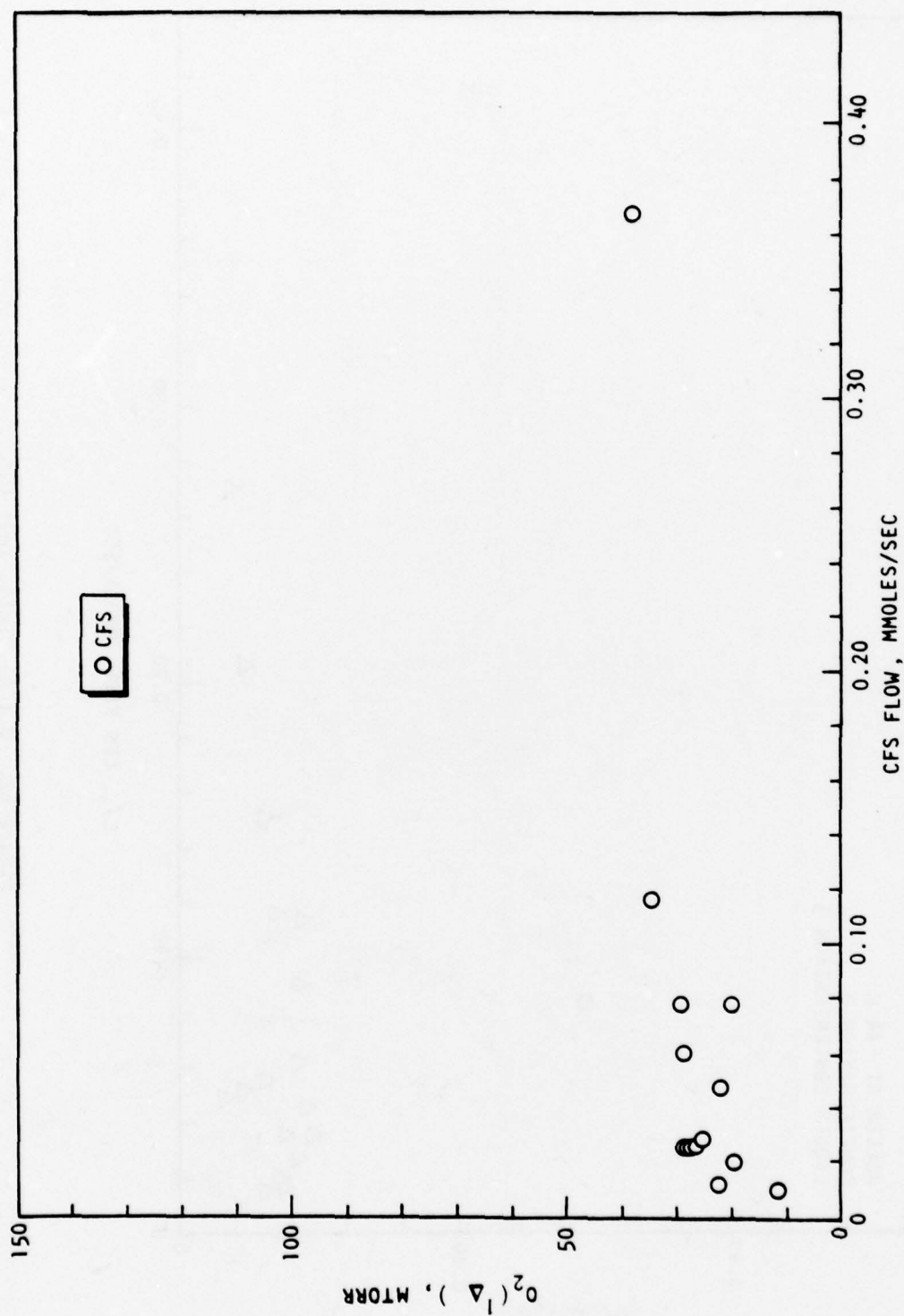


Figure 61. $O_2(\Delta)$ Partial Pressure at P_1 vs CFS Flow - Test 023

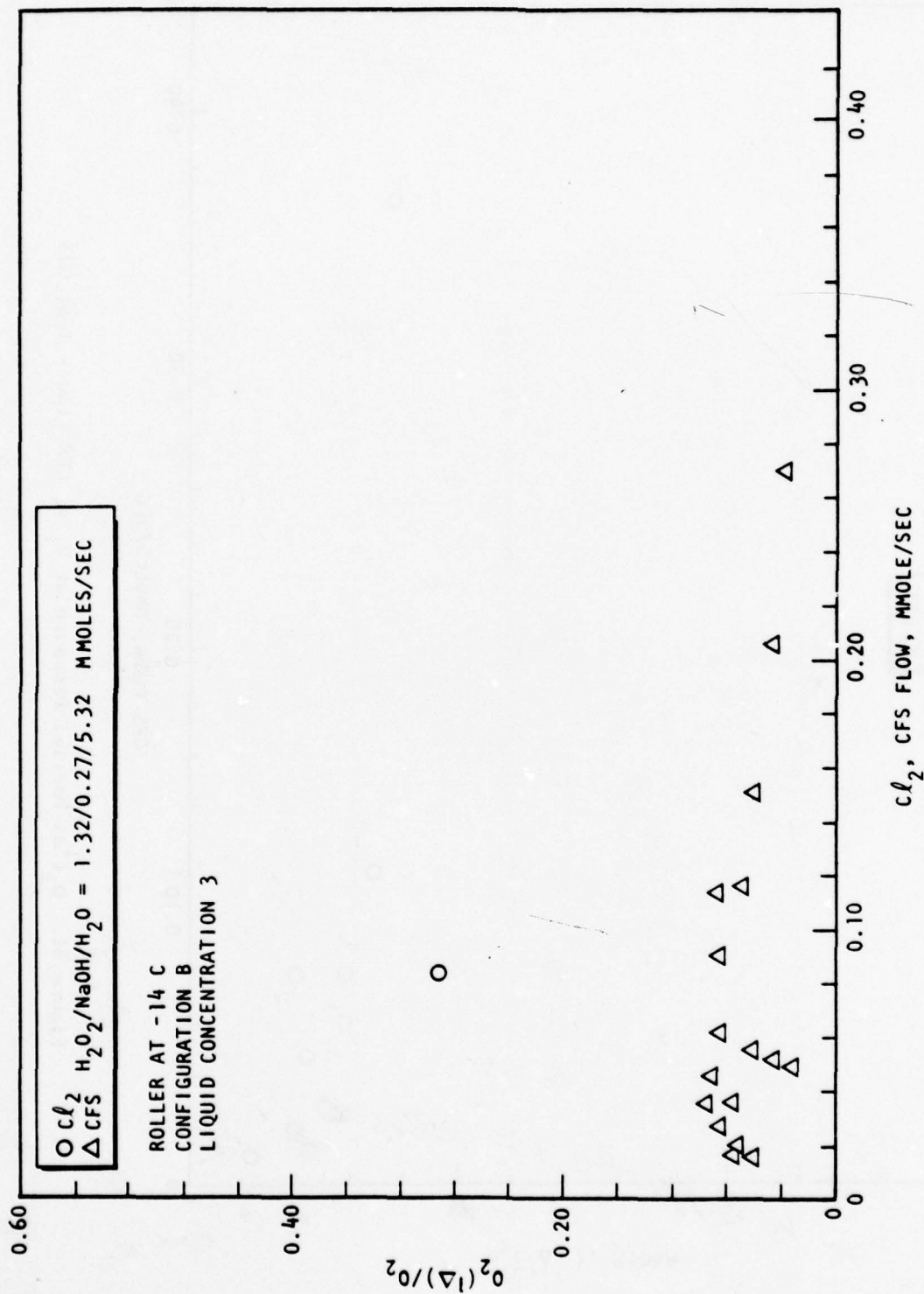


Figure 62. $O_2(\Delta)$ Yield, Test 025

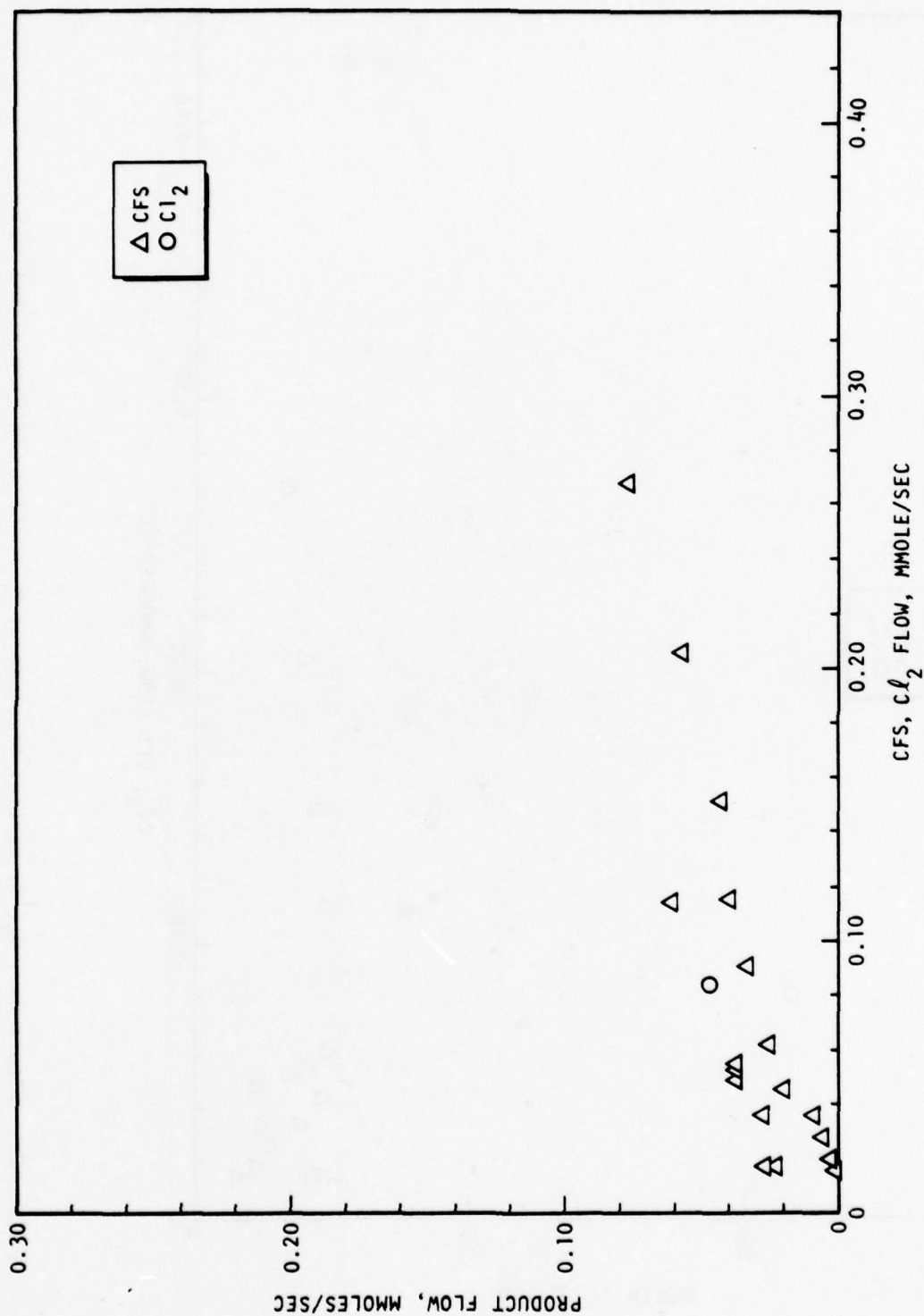


Figure 63. Product Flow vs CFS, Cl_2 Flow - Test 025

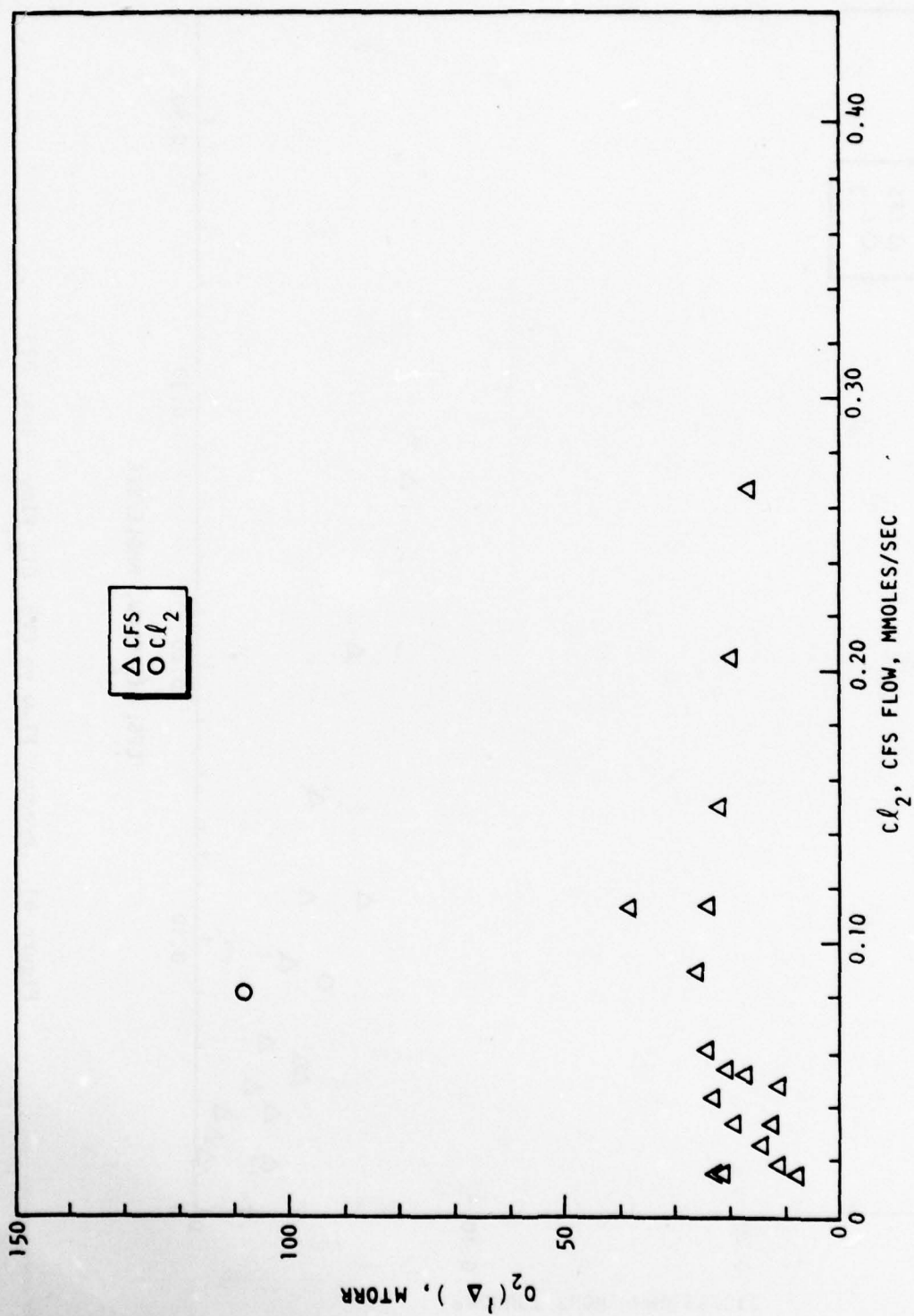


Figure 64. O_2 (Δ) Partial Pressure at P_1 vs Cl_2 , CFS Flow - Test 025

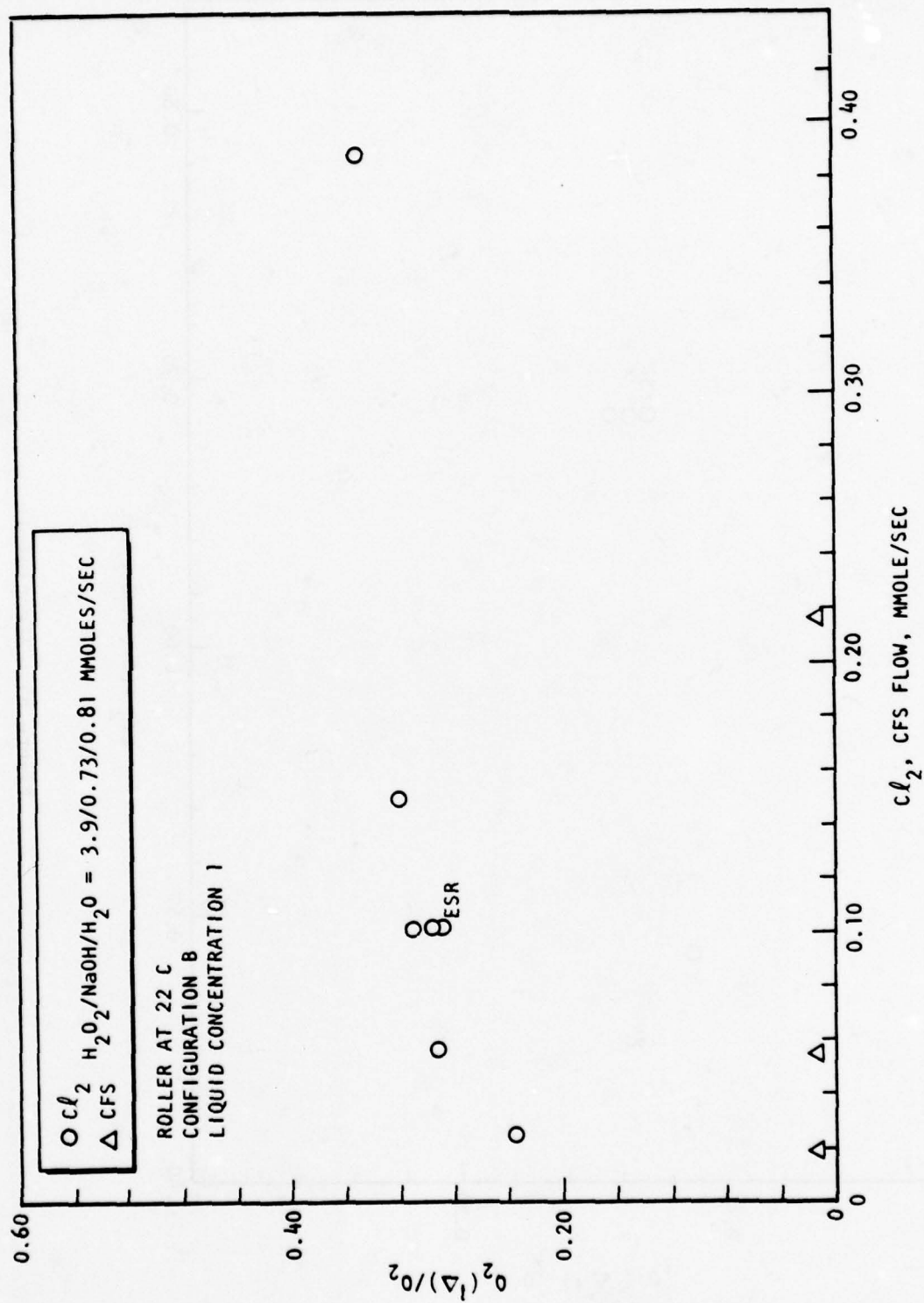


Figure 65. $O_2(1\Delta)$ Yield, Test 027

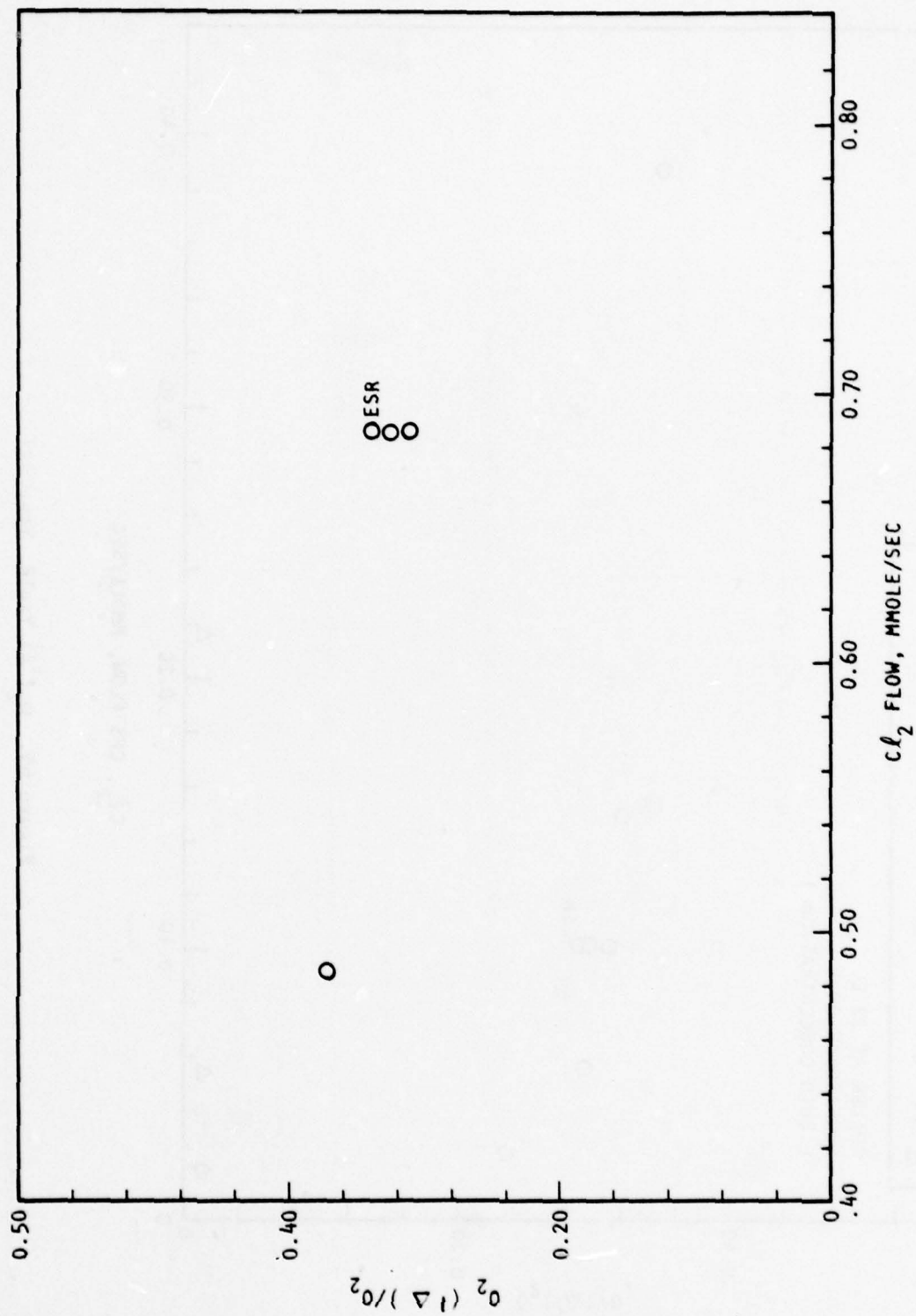


Figure 65. (Concluded)

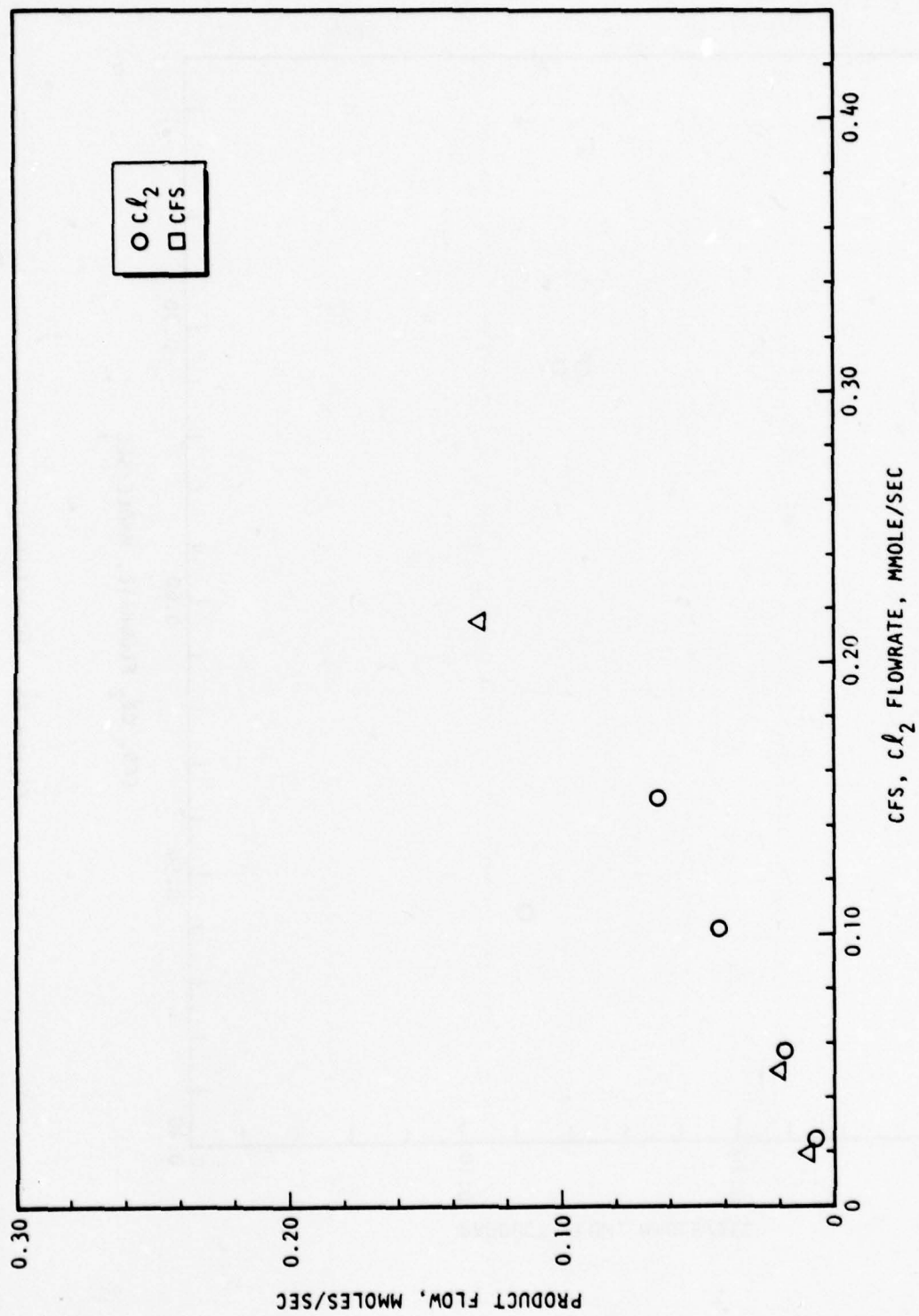


Figure 66. Product Flow vs CFS, Cl₂ Flow - Test 027

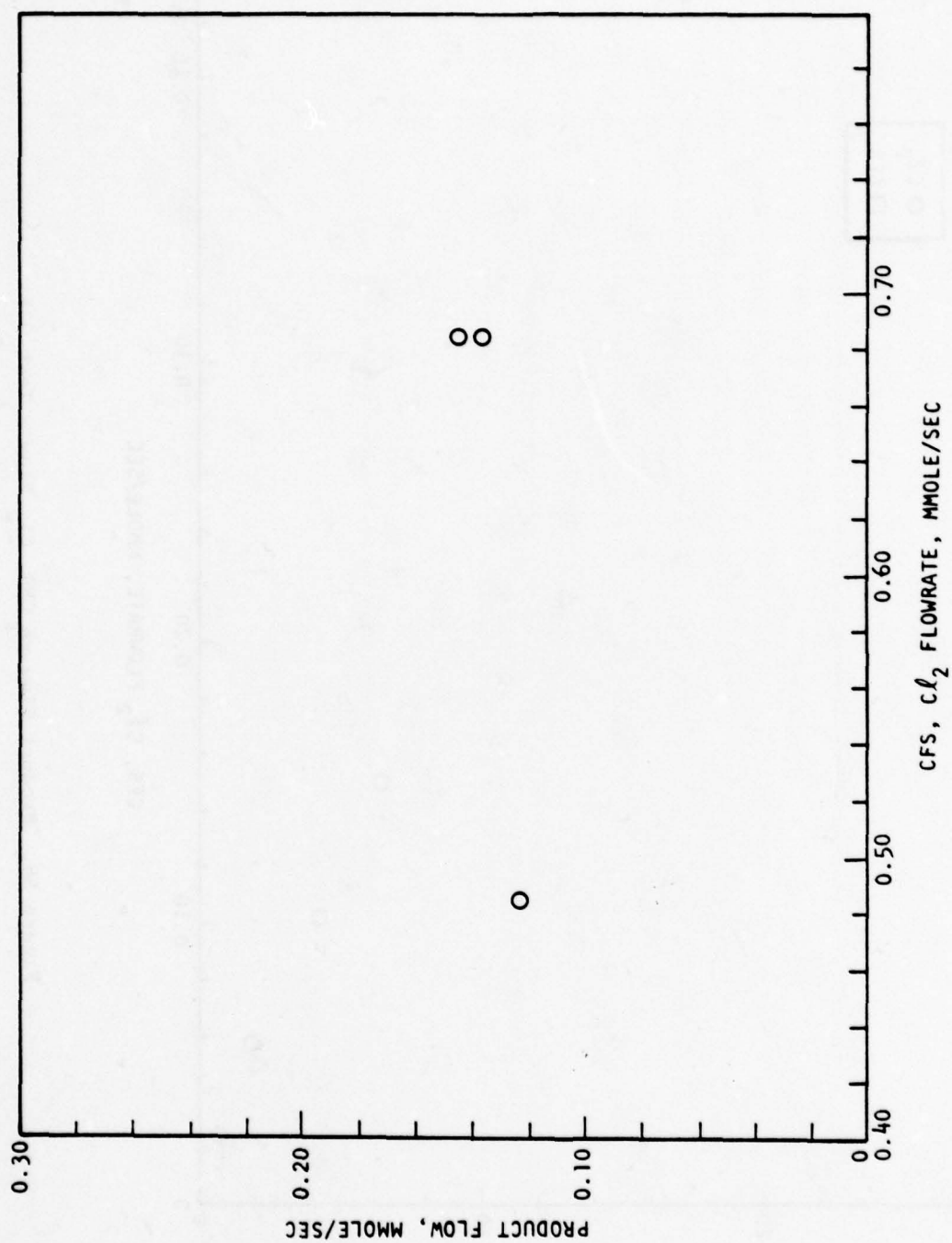


Figure 66. (Concluded)

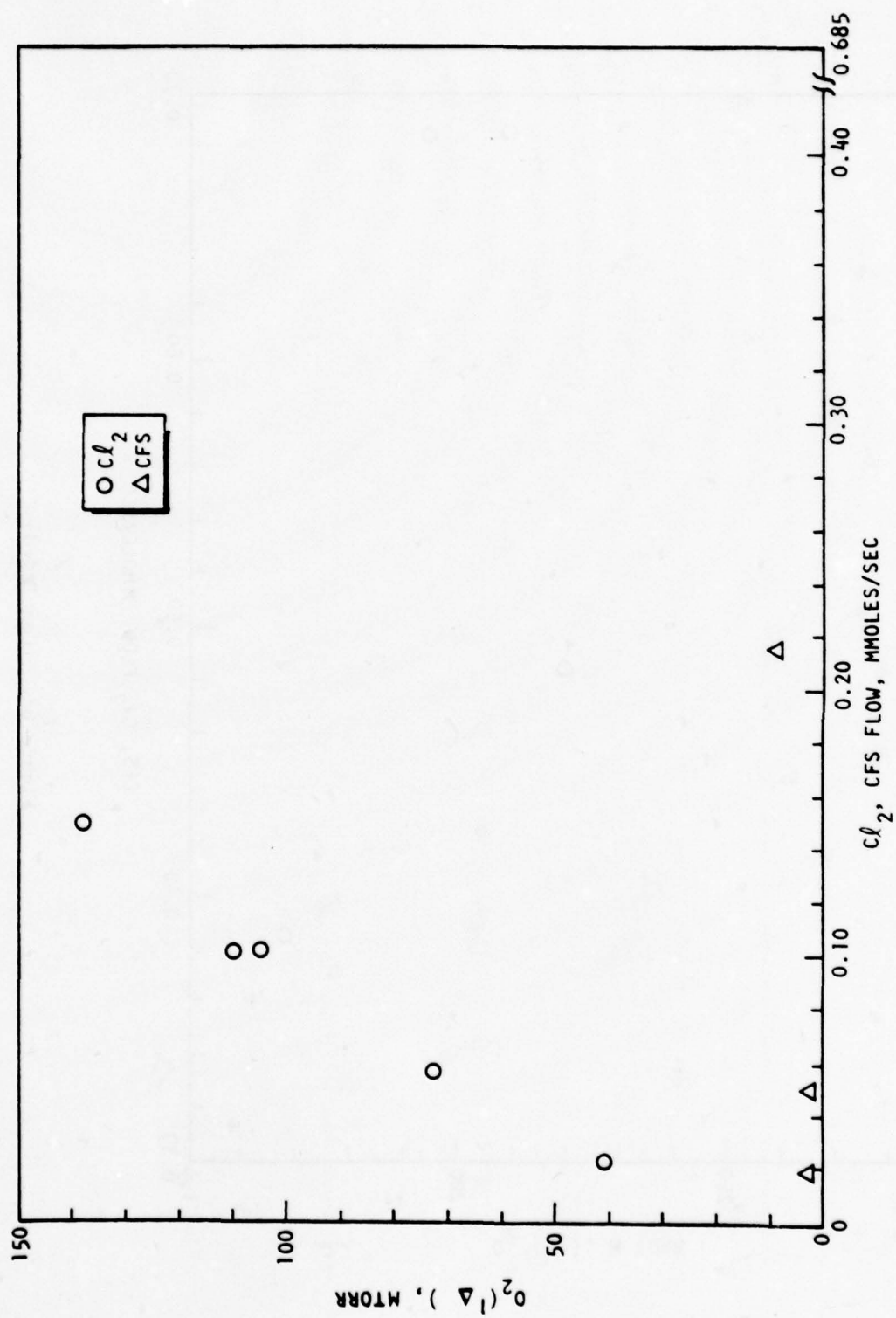


Figure 67. O_2 (Δ) Partial Pressure at P_1 vs CFS, Cl_2 Flow - Test 027

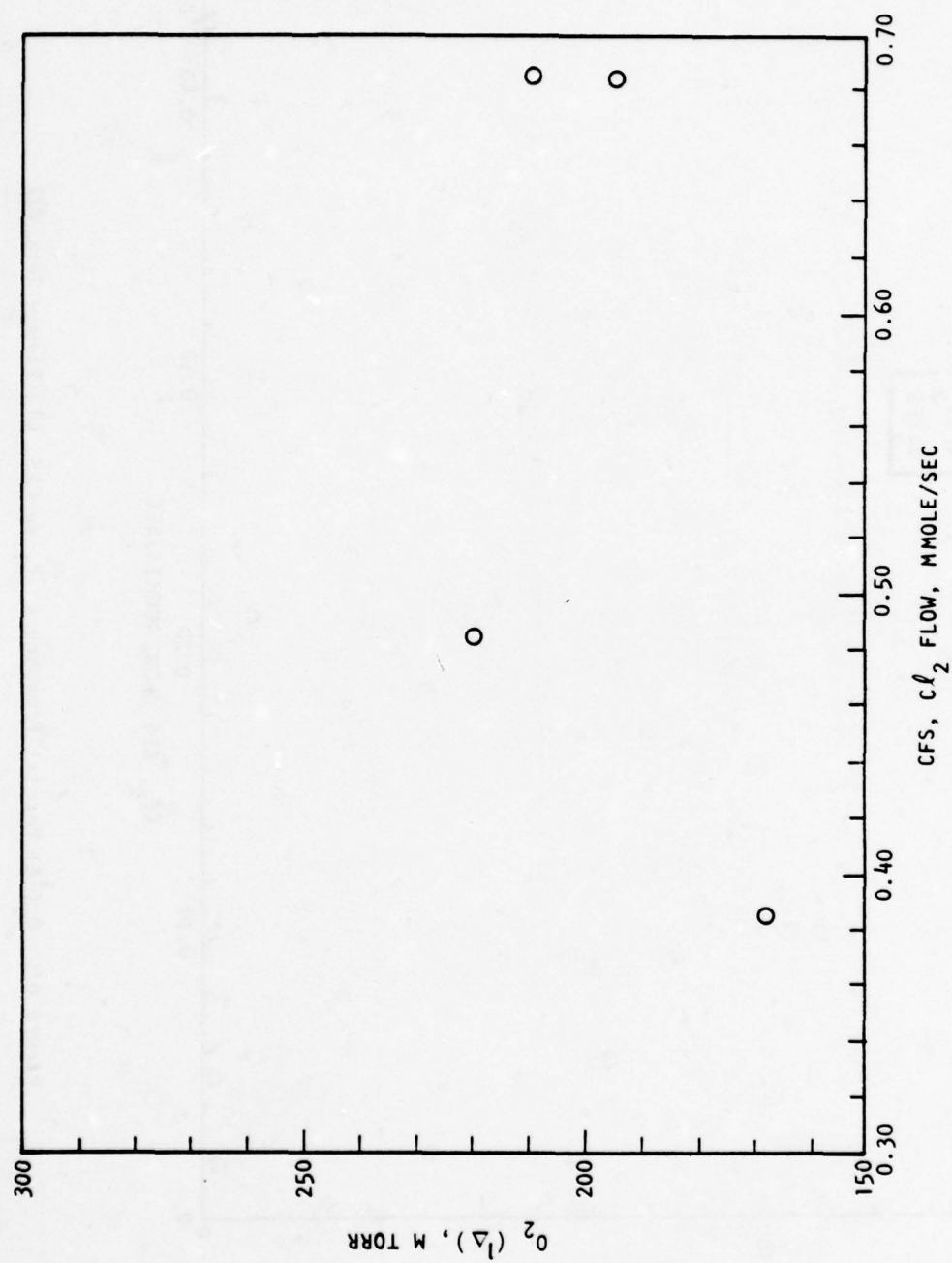


Figure 67. (Concluded)

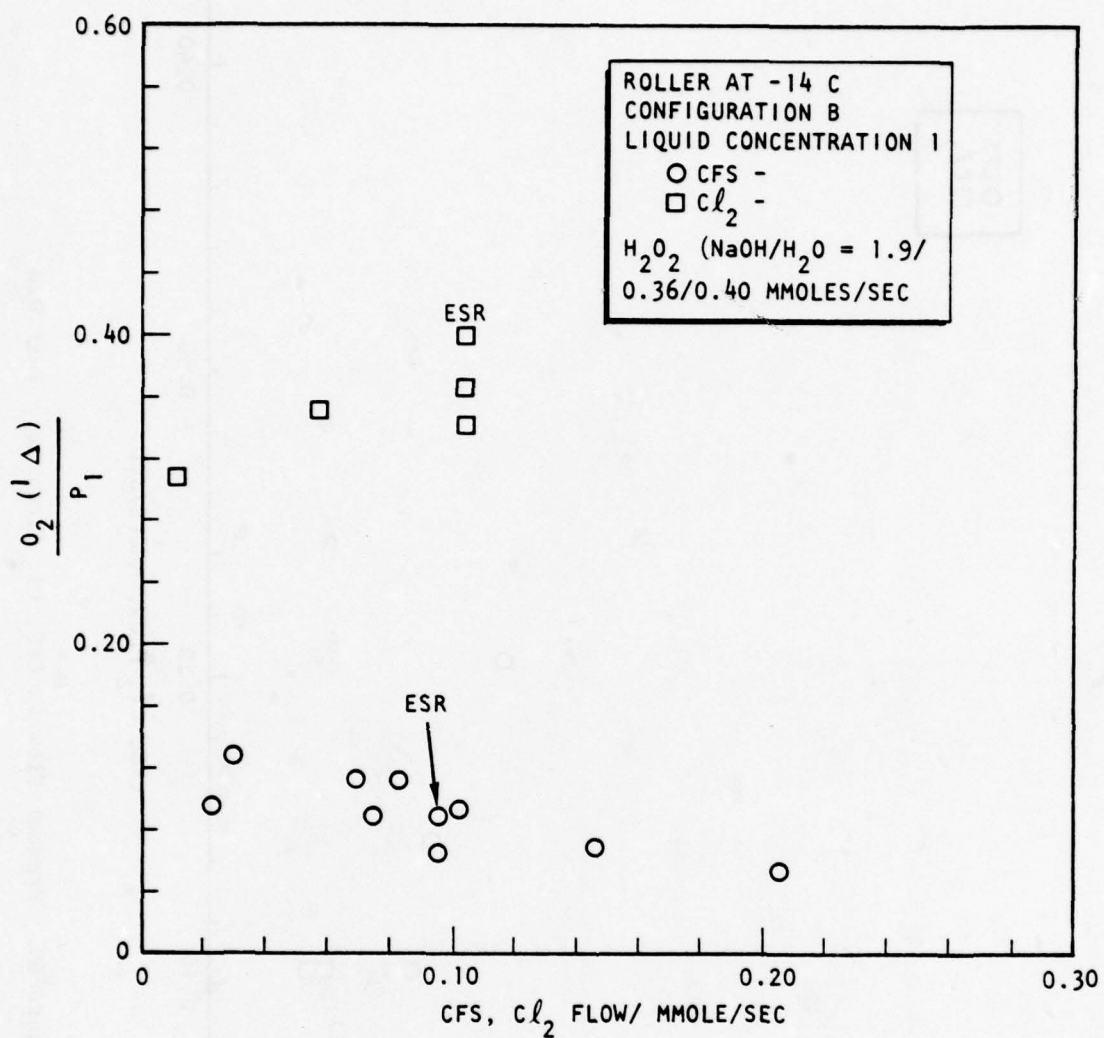


Figure 68. O₂(¹Δ) Yield vs CFS, Cl₂ Flow - Test 028

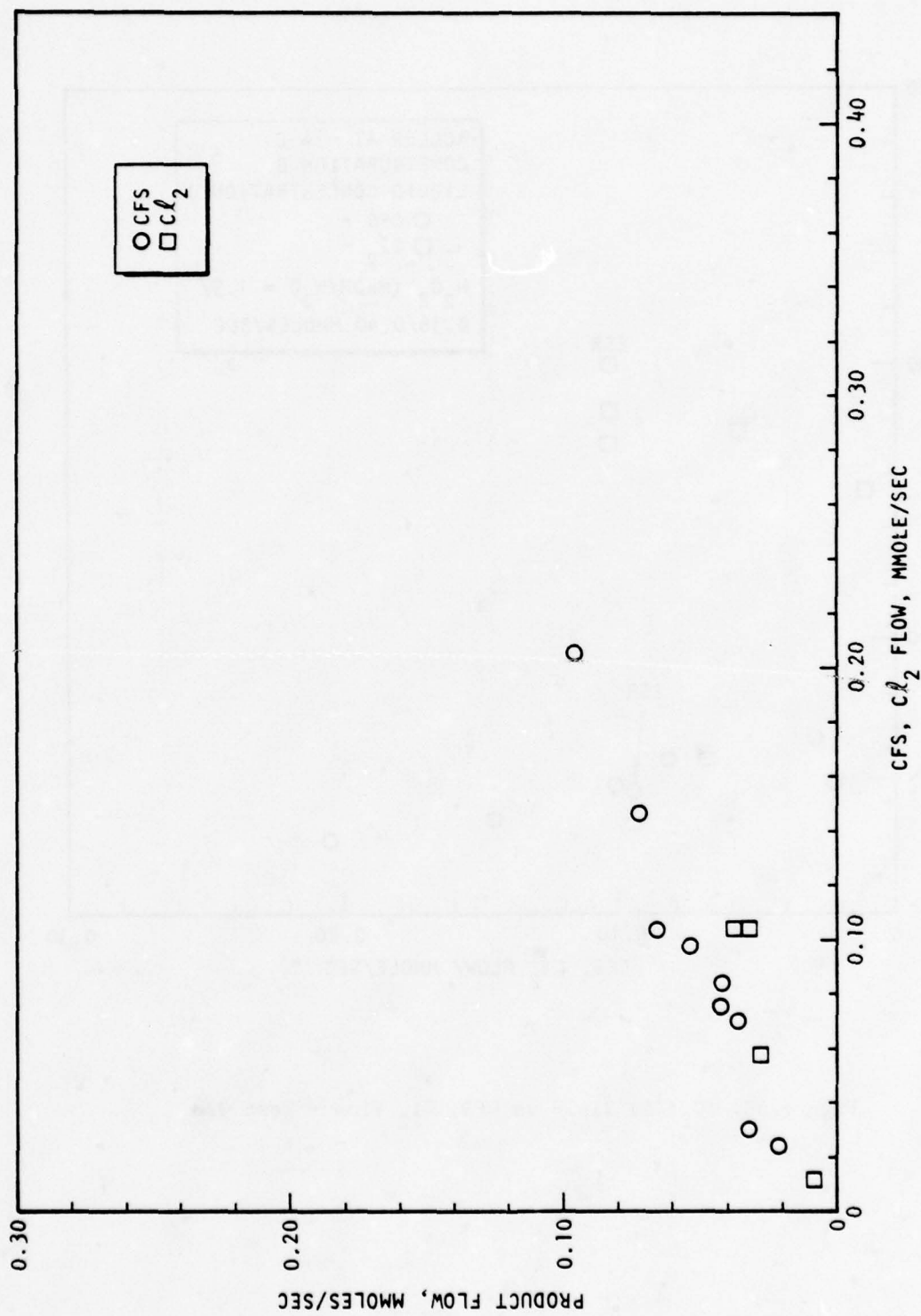


Figure 69. Product Flow vs CFS, Cl_2 Flowrate - Test 028

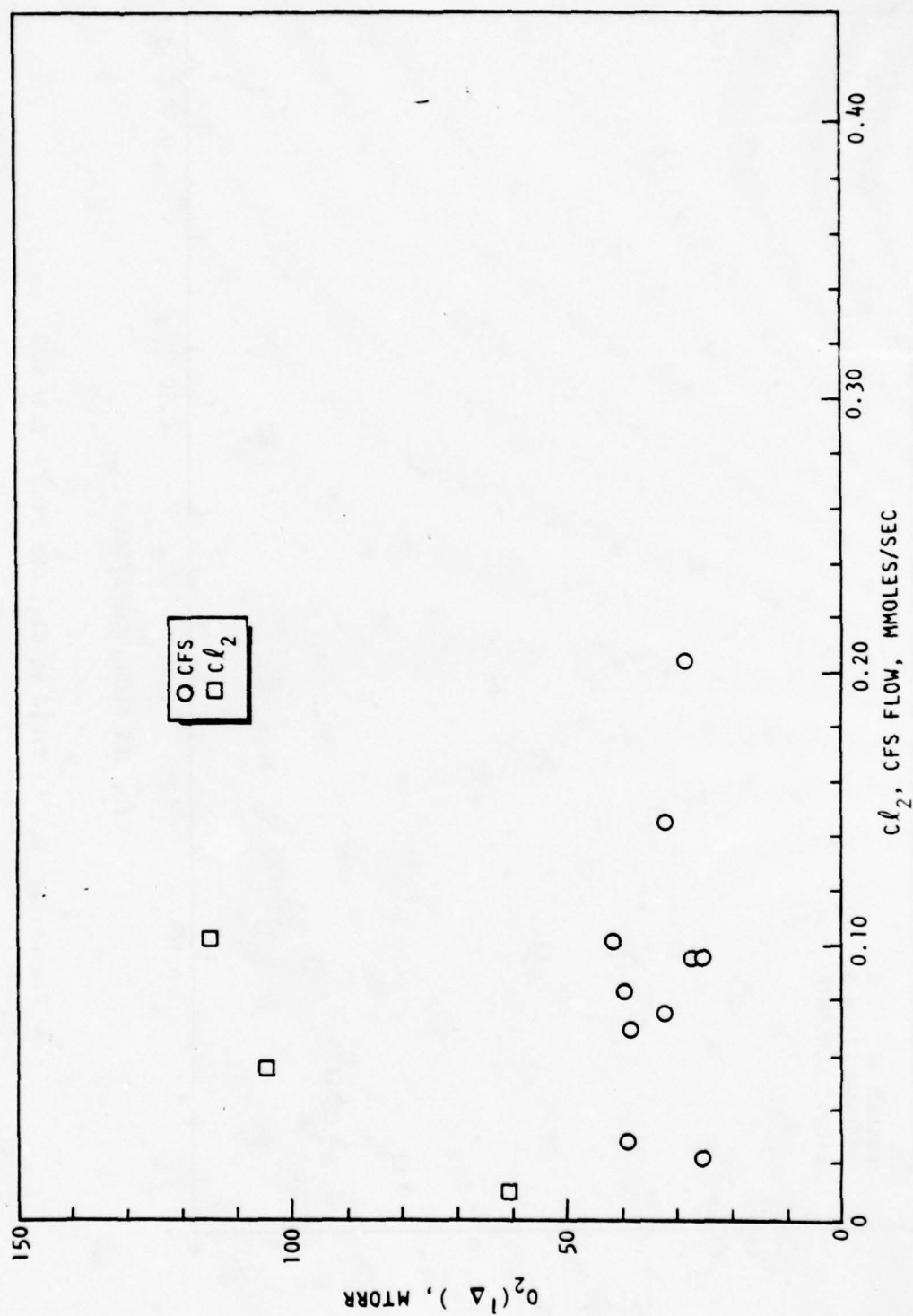
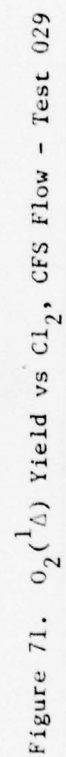


Figure 70. O_2 (Δ) Partial Pressure at P_1 vs CFS, Cl_2 Flow - Test 028



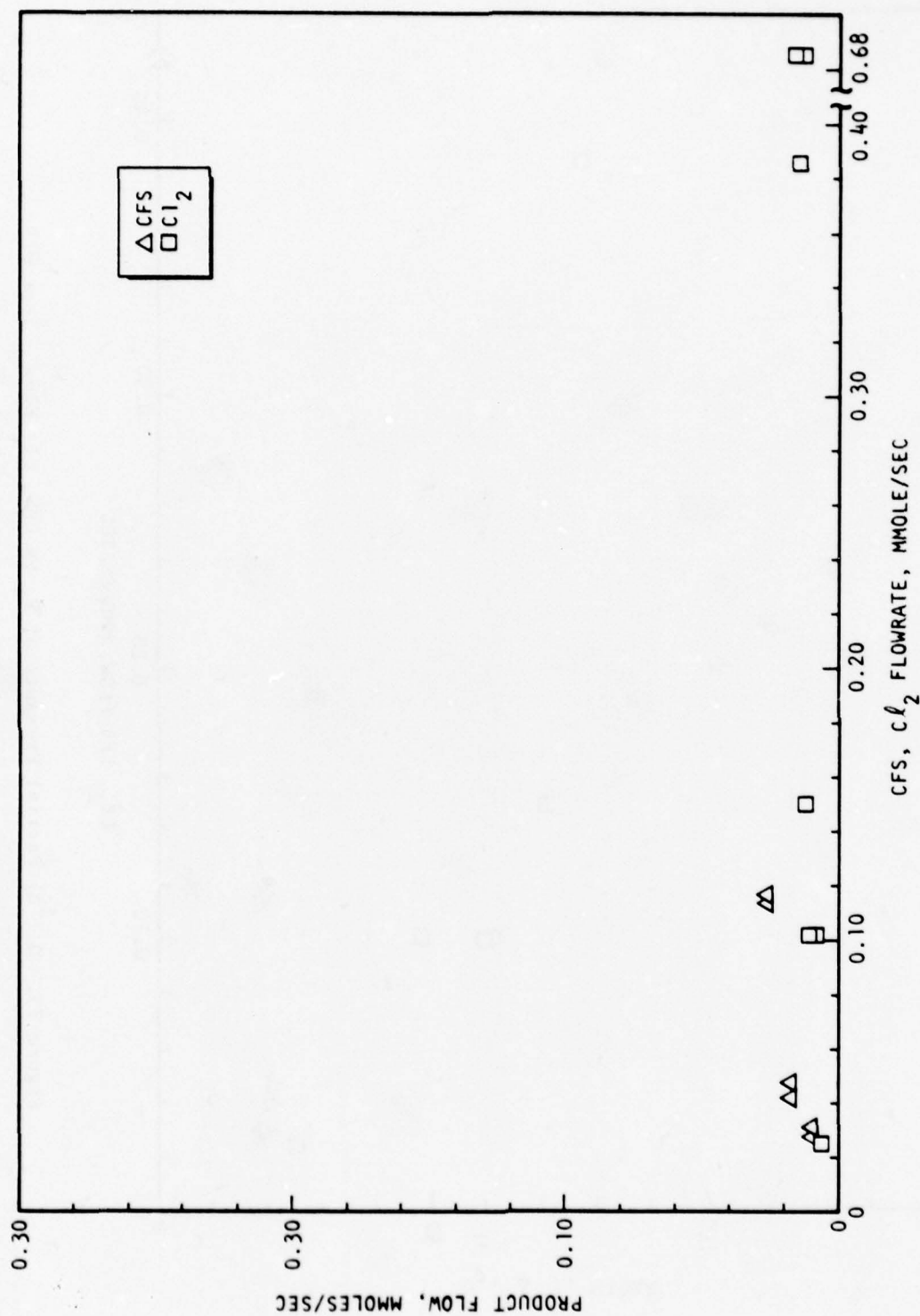


Figure 72. Product Flow vs Cl_2 Flow - Test 029

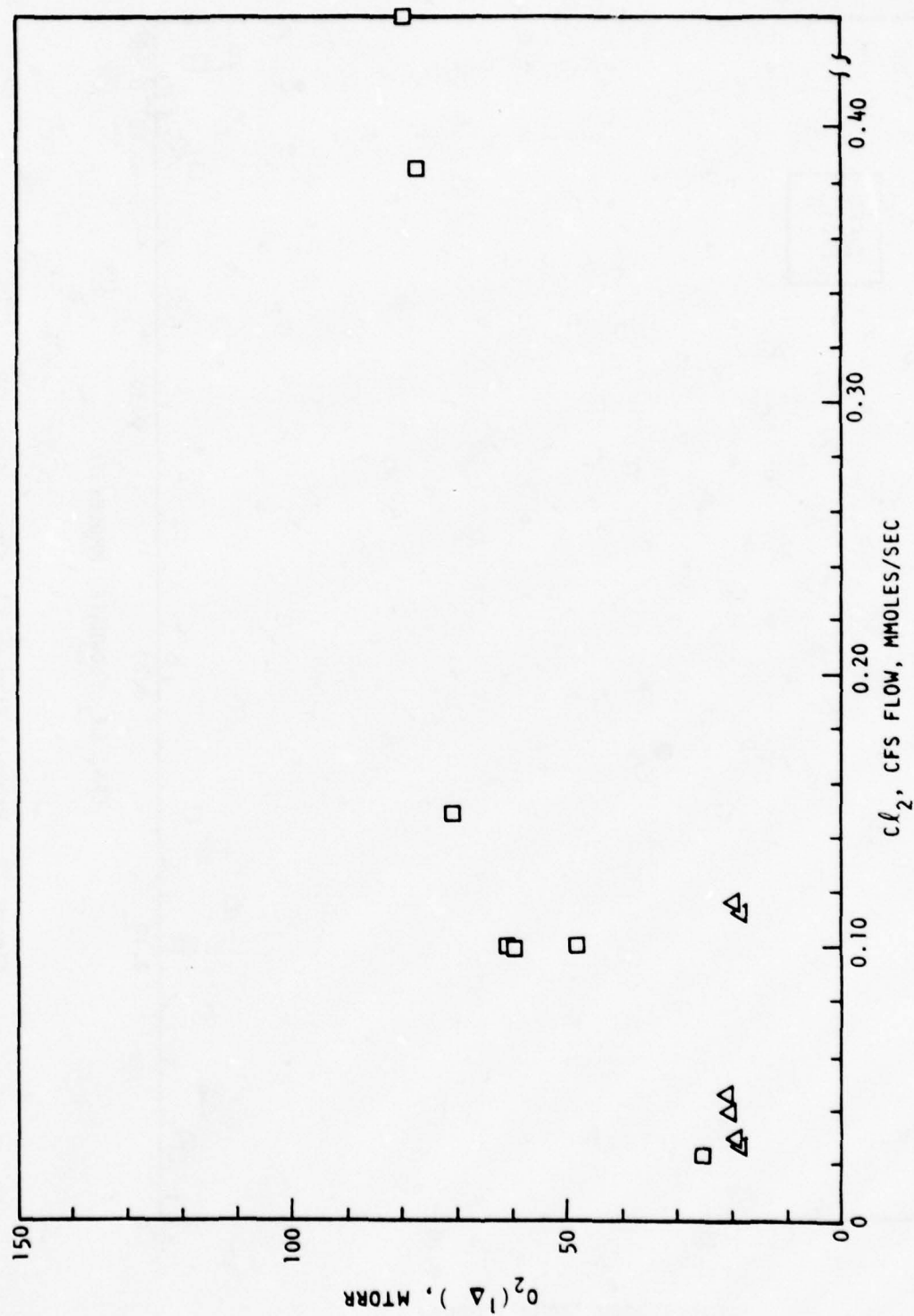


Figure 73. $O_2 (\Delta)$ Partial Pressure at P_1 vs Cl_2 Flow - Test 029

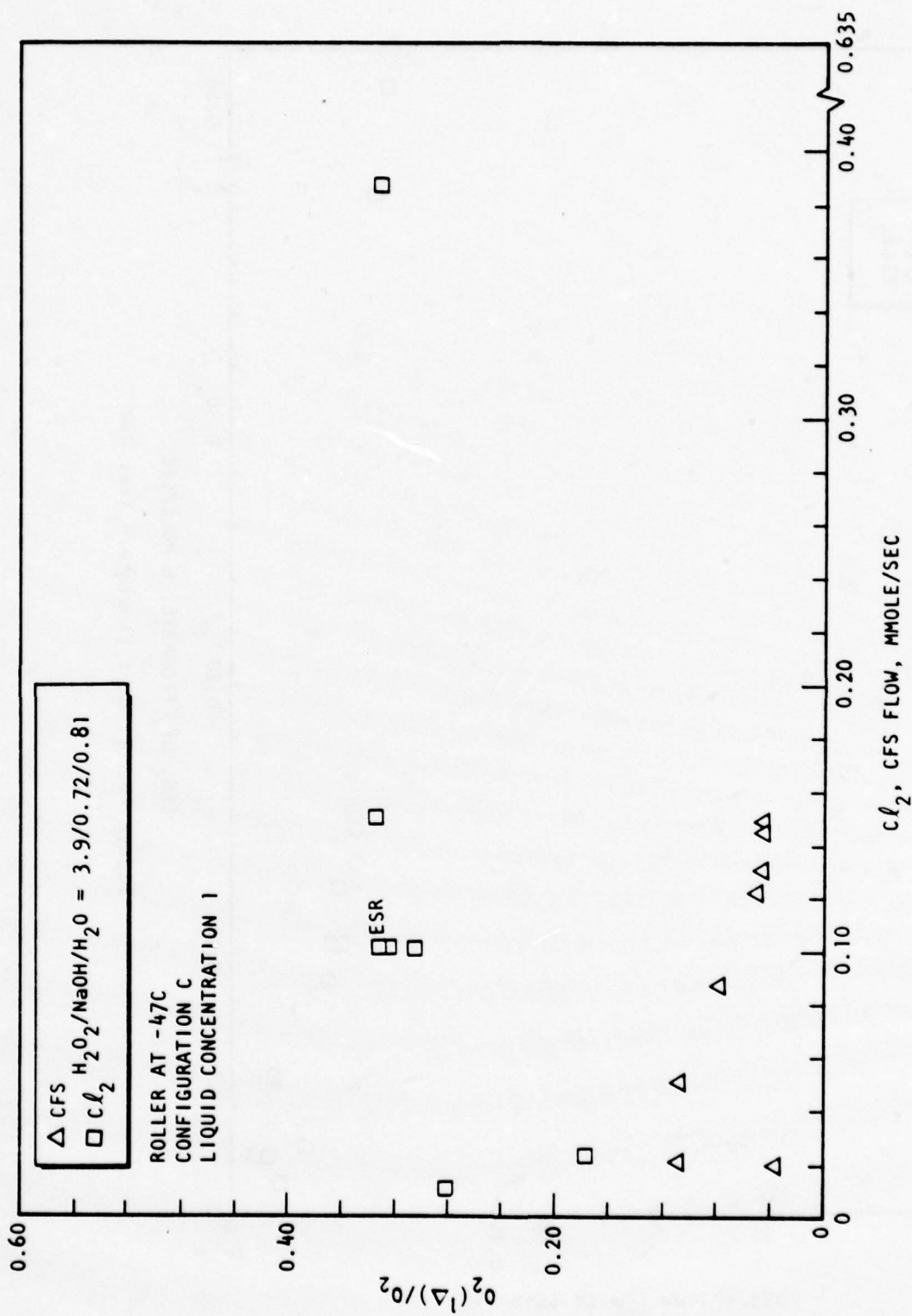


Figure 74. $\text{O}_2(^1\Delta)$ Yield vs Cl_2 , CFS Flow, Test 030

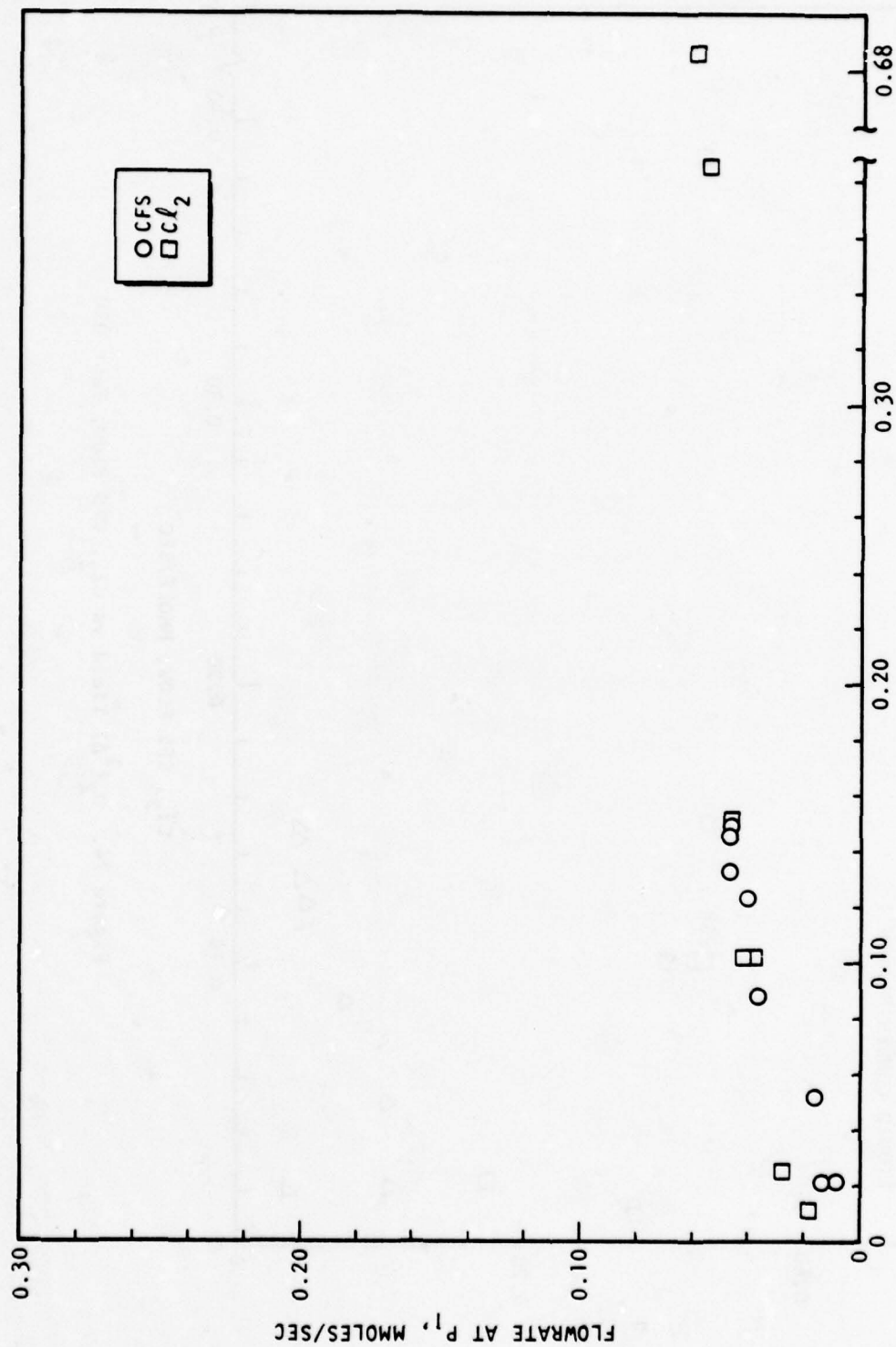


Figure 75. Product Flowrate - Test 030

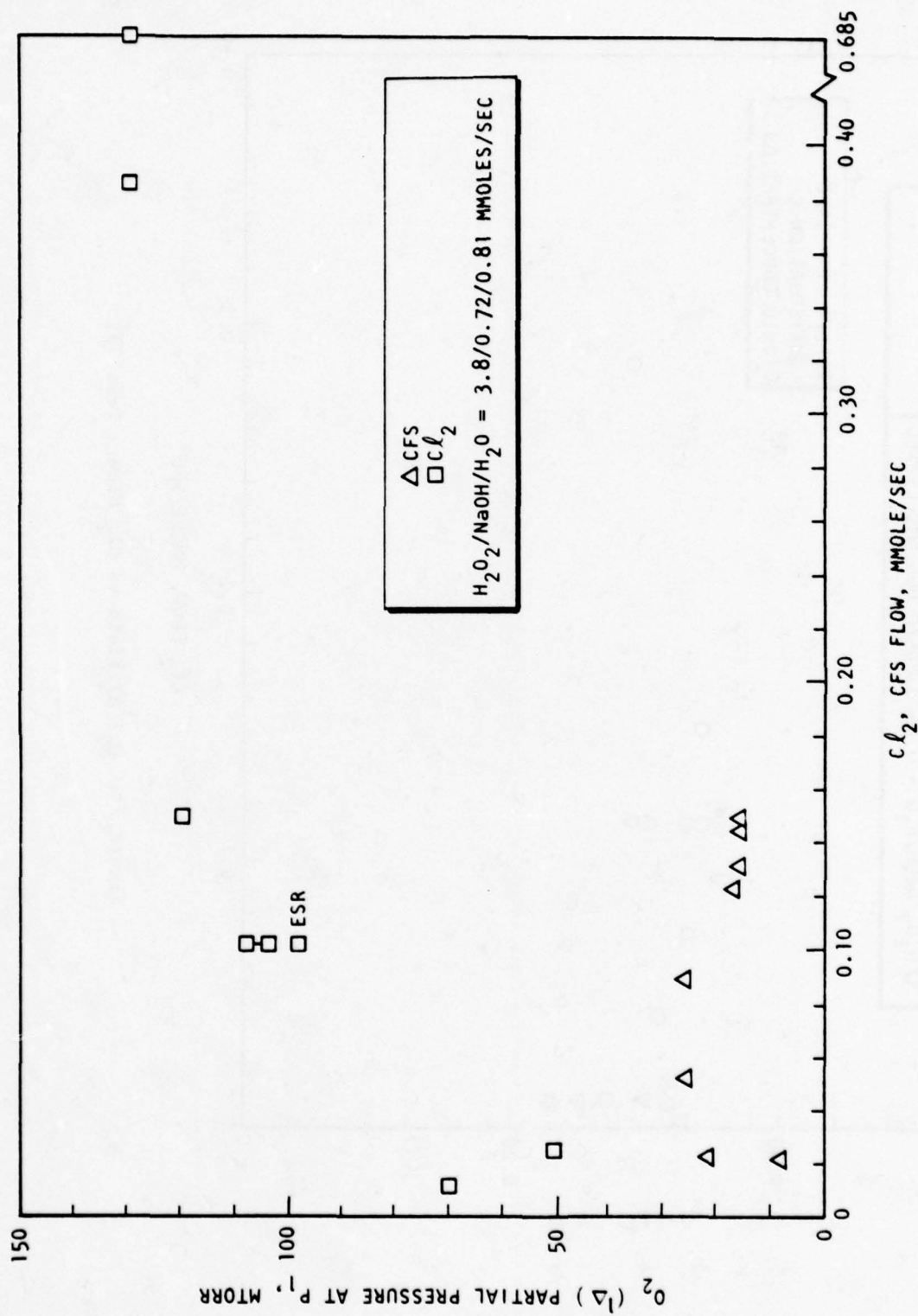


Figure 76. O_2 (Δ) Partial Pressure at P_1 vs Cl_2 , CFS Flow - Test 030

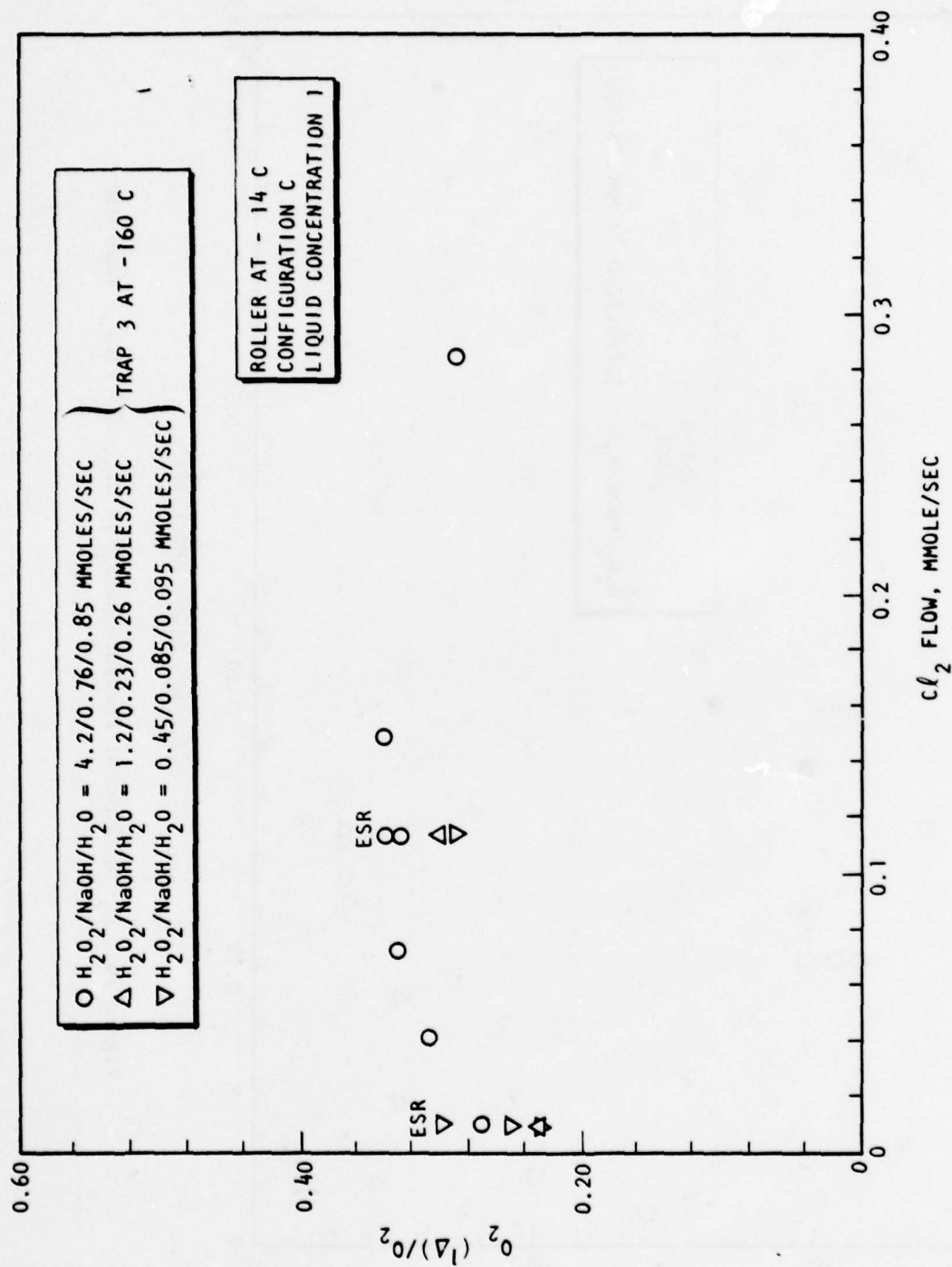


Figure 77. $\text{O}_2 ({}^1\Delta)$ Yield vs Cl_2 Flow - Test 031

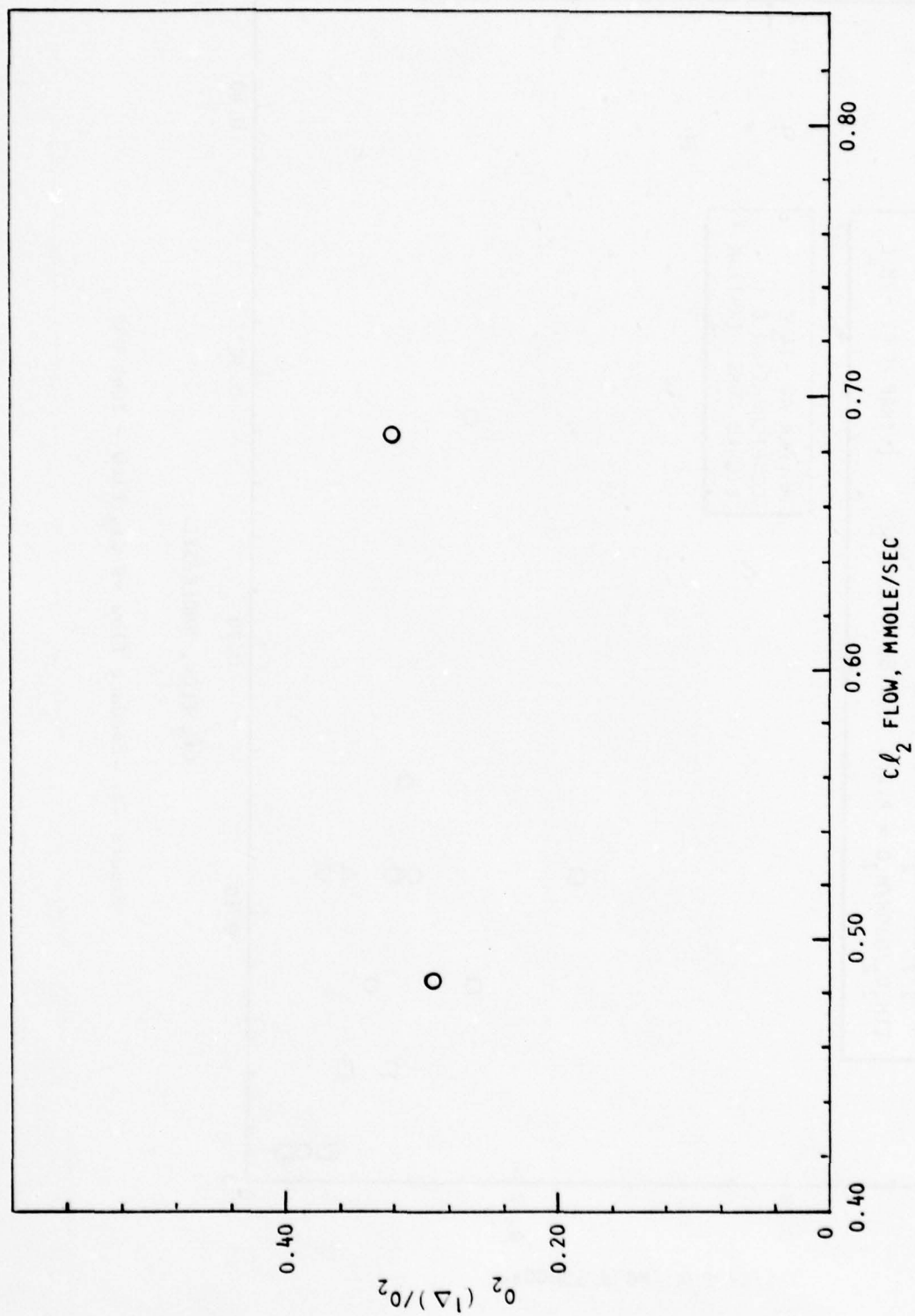


Figure 77. (Concluded)

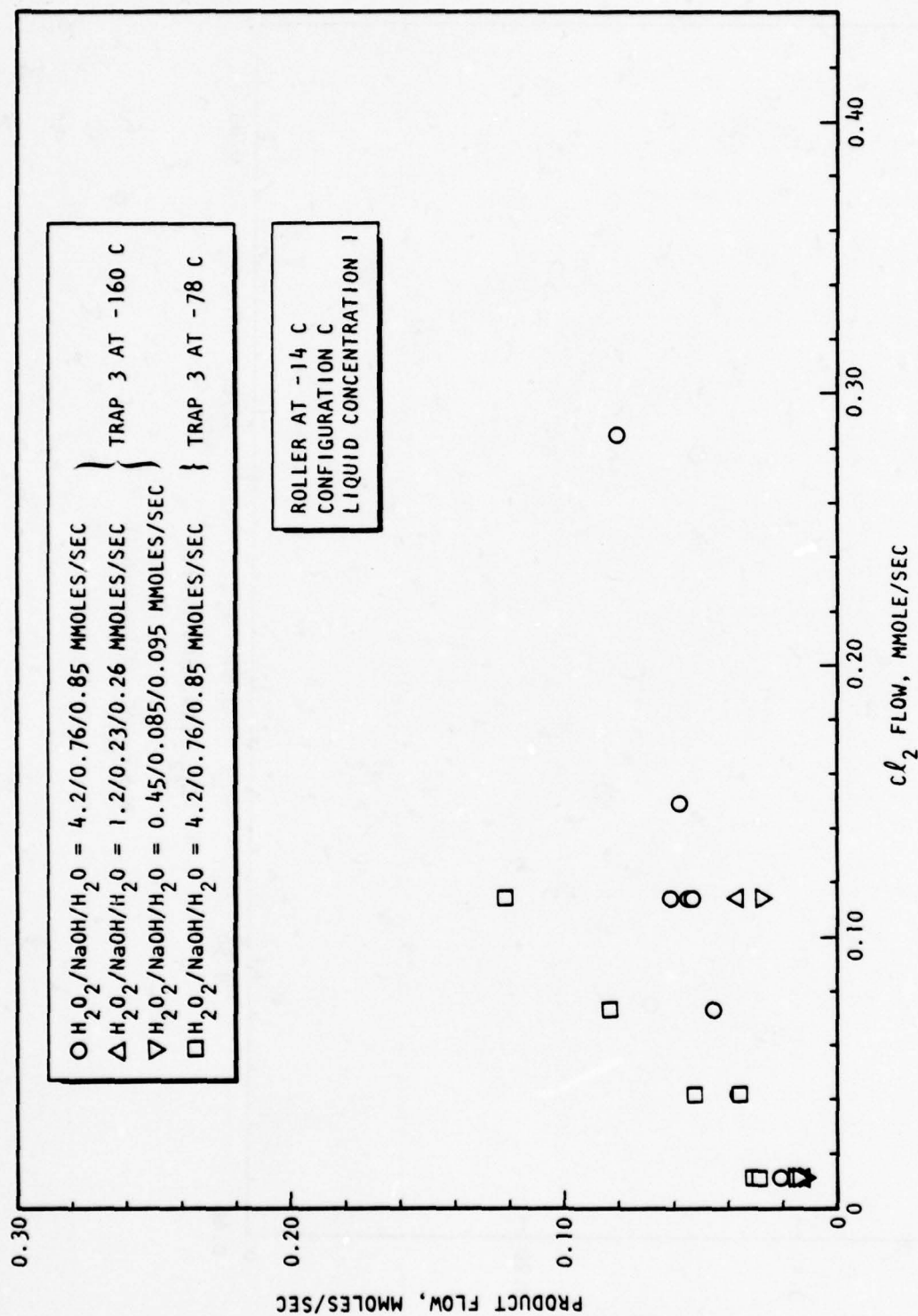
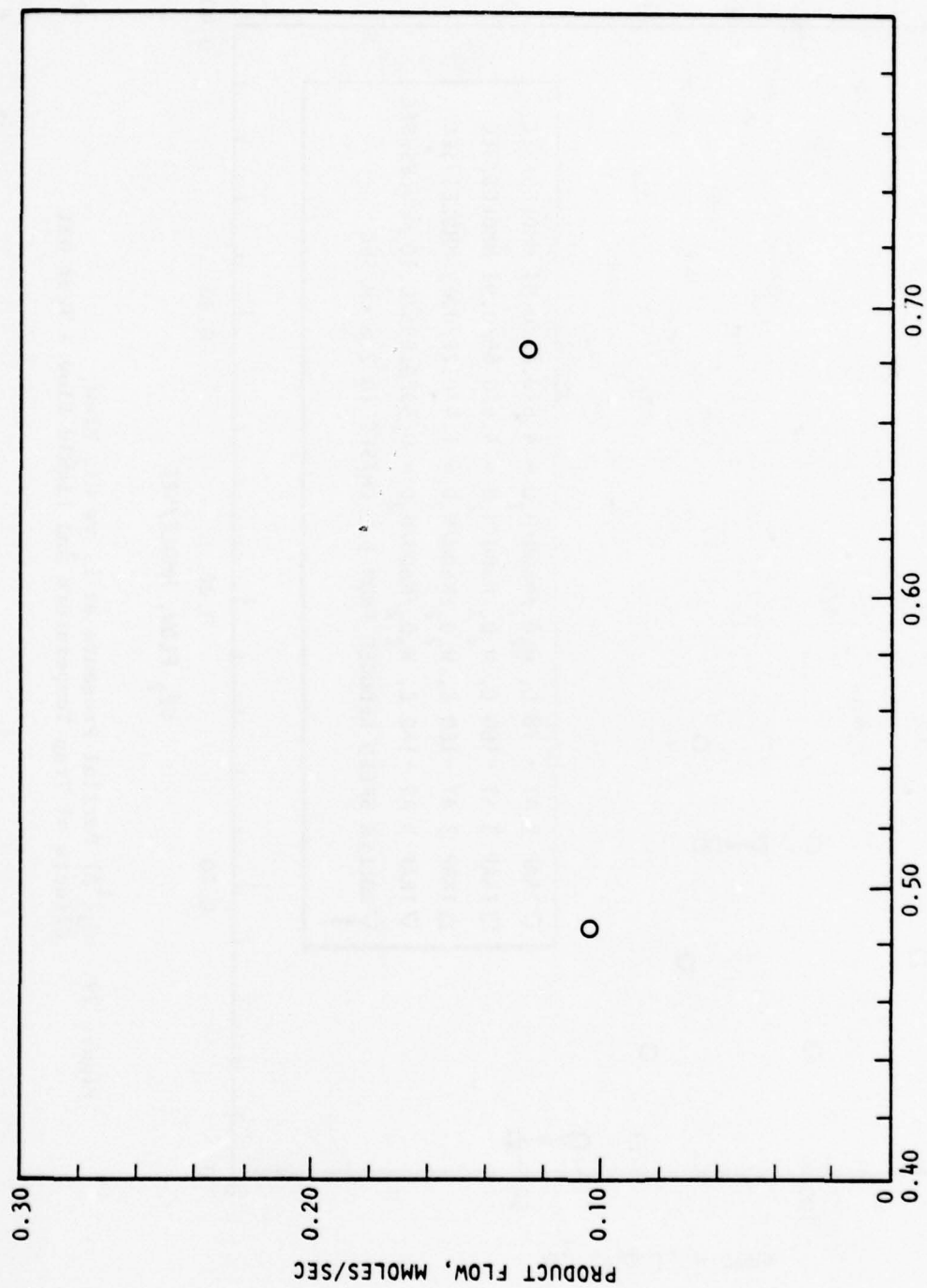


Figure 78. Product Flow vs Cl_2 Flow - Test 031



Cl_2 FLOWRATE, MMOLE/SEC

Figure 78. (Concluded)

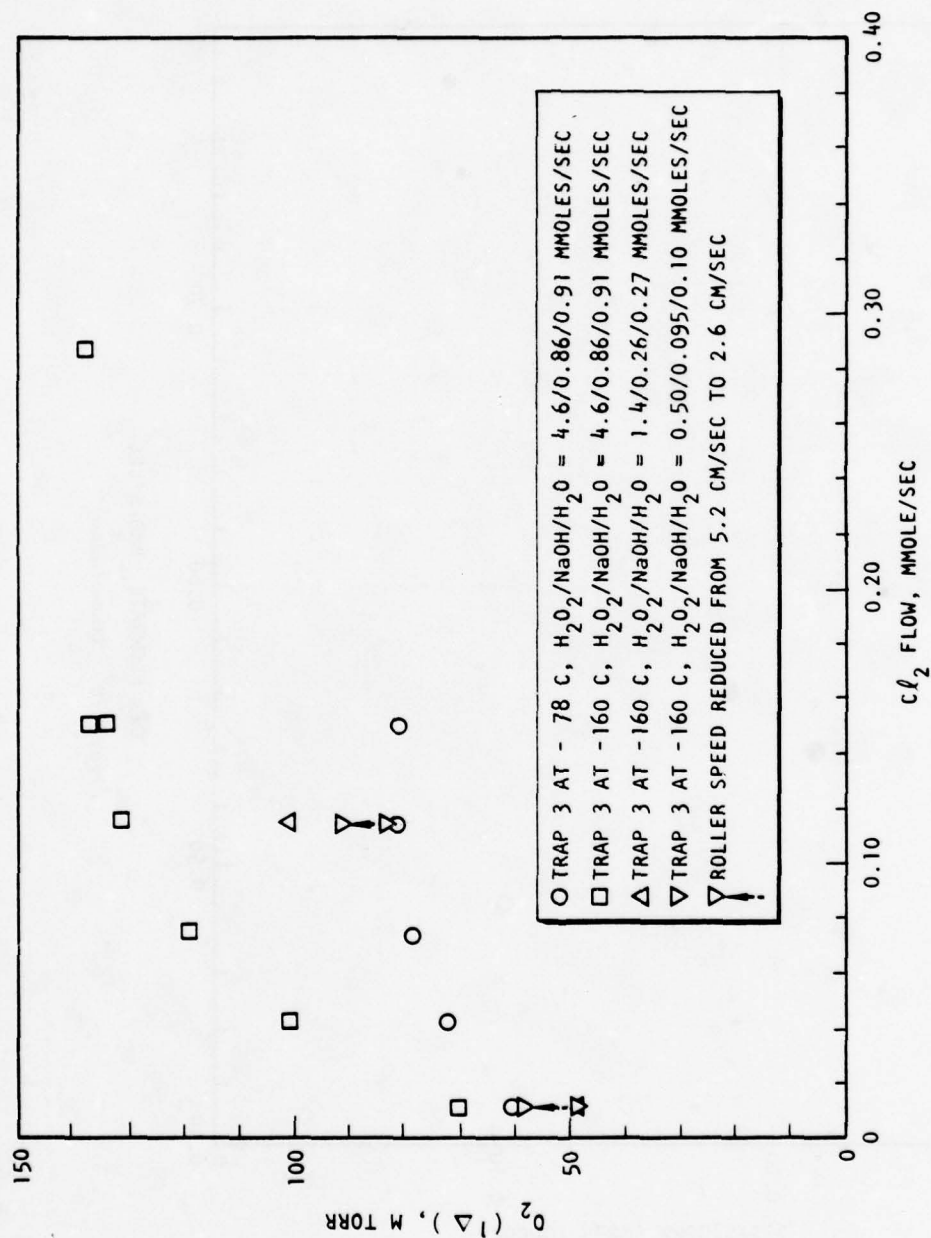


Figure 79. O_2 (Δ) Partial Pressure at P_1 vs Cl_2 Flow,
Effects of Trap Temperature and Liquid Flow - Test 031

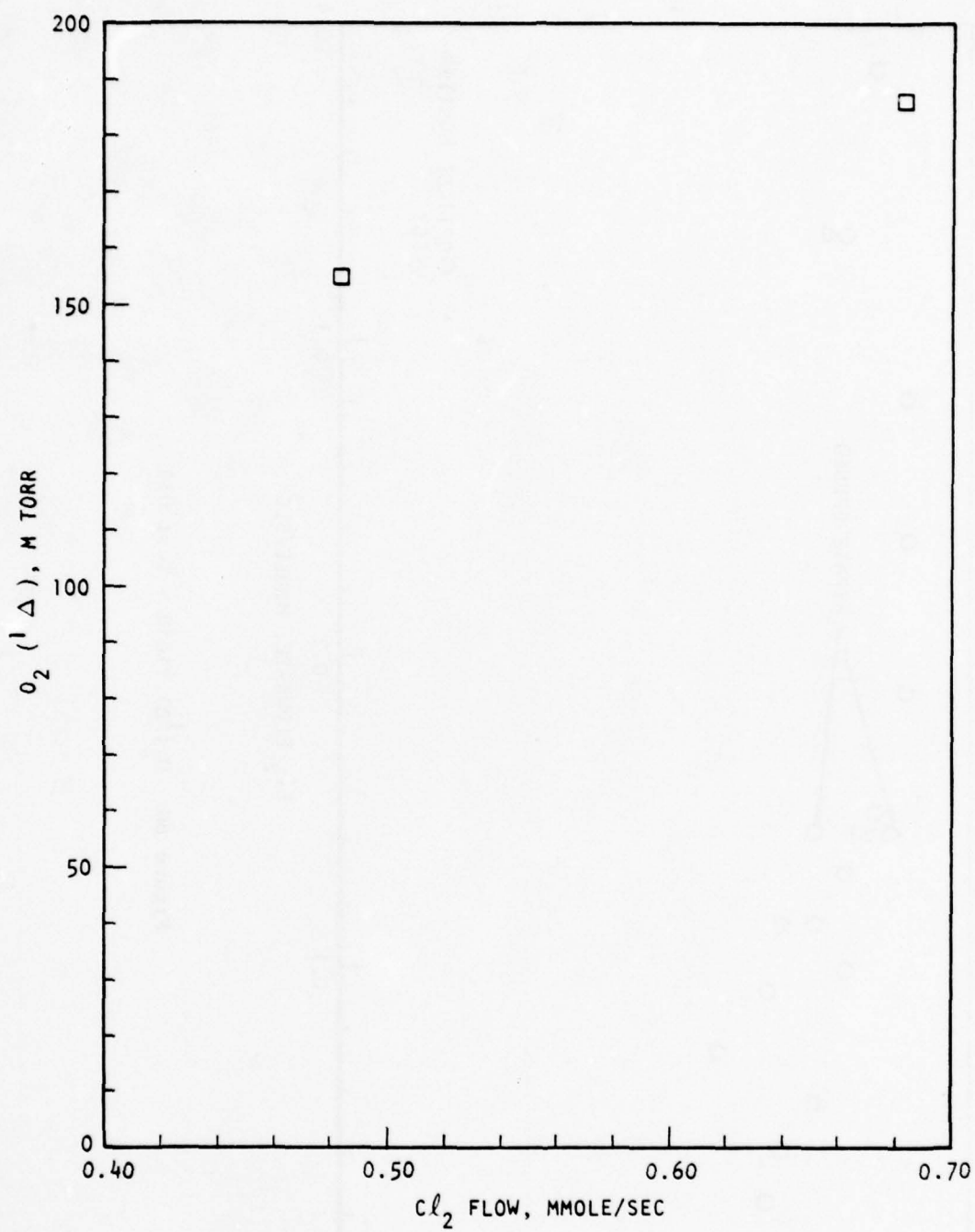


Figure 79. (Concluded)

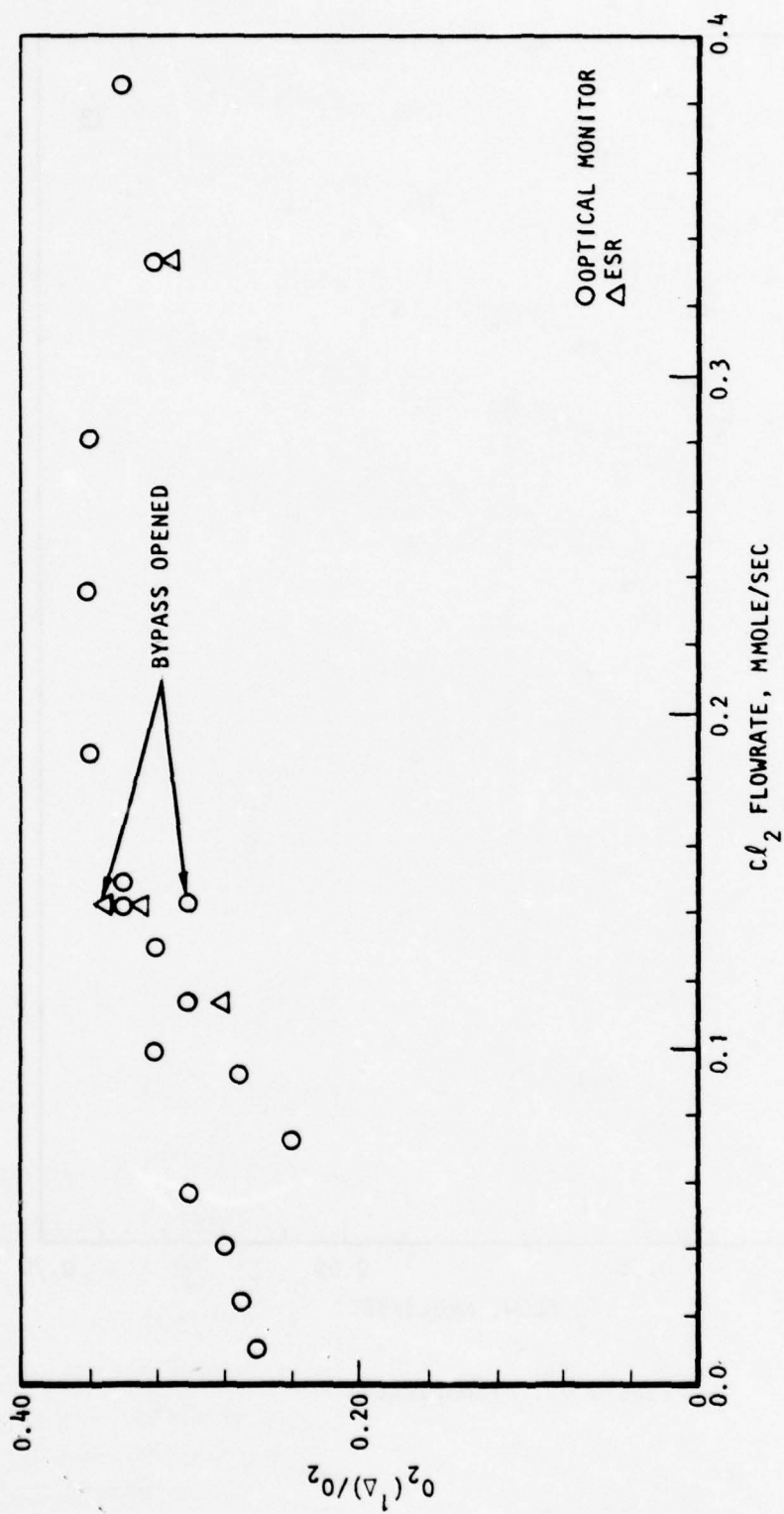


Figure 80. O₂(¹Δ) Yield - Test 034

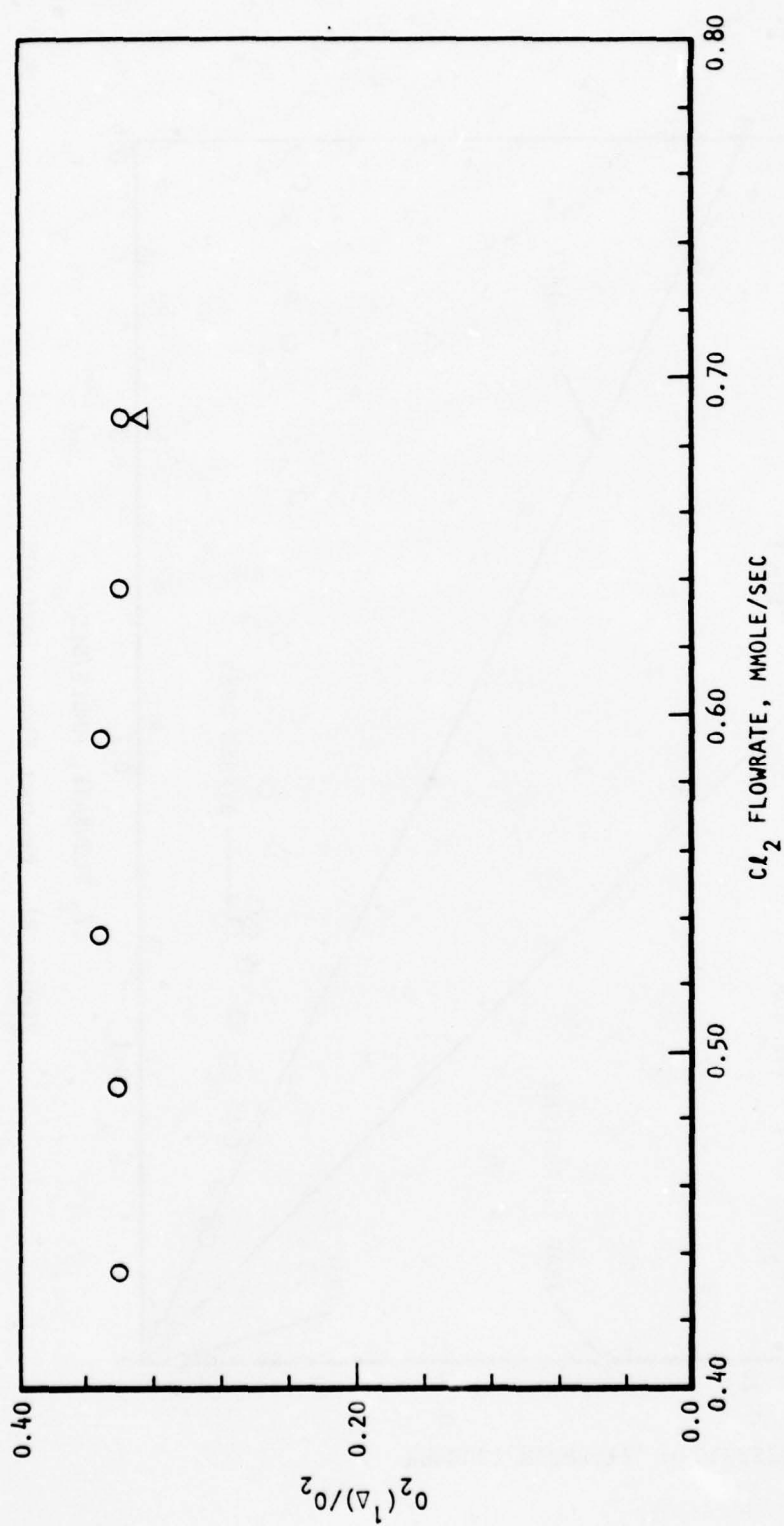


Figure 80. (Concluded)

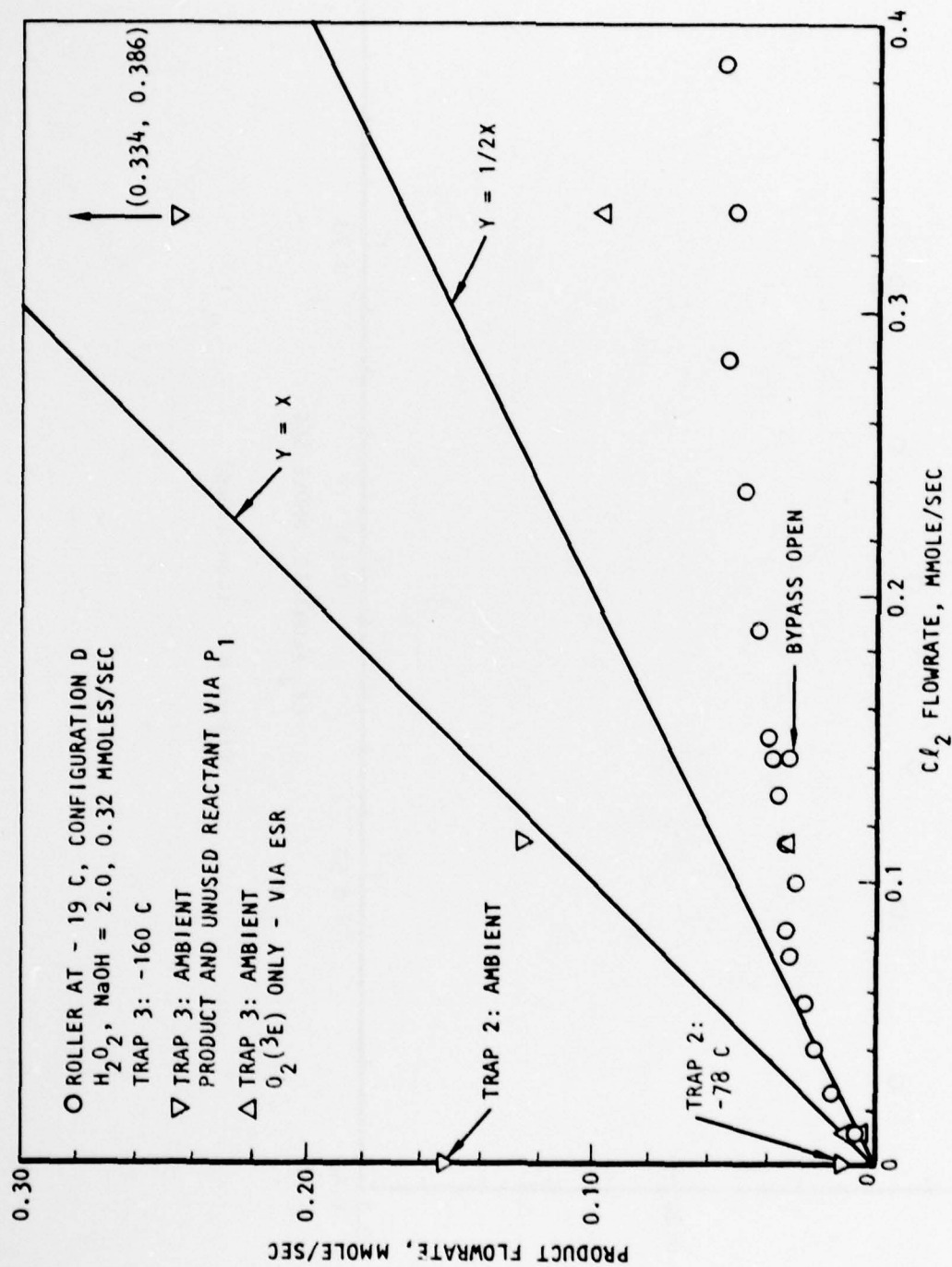


Figure 81. Product Flow - Test 034

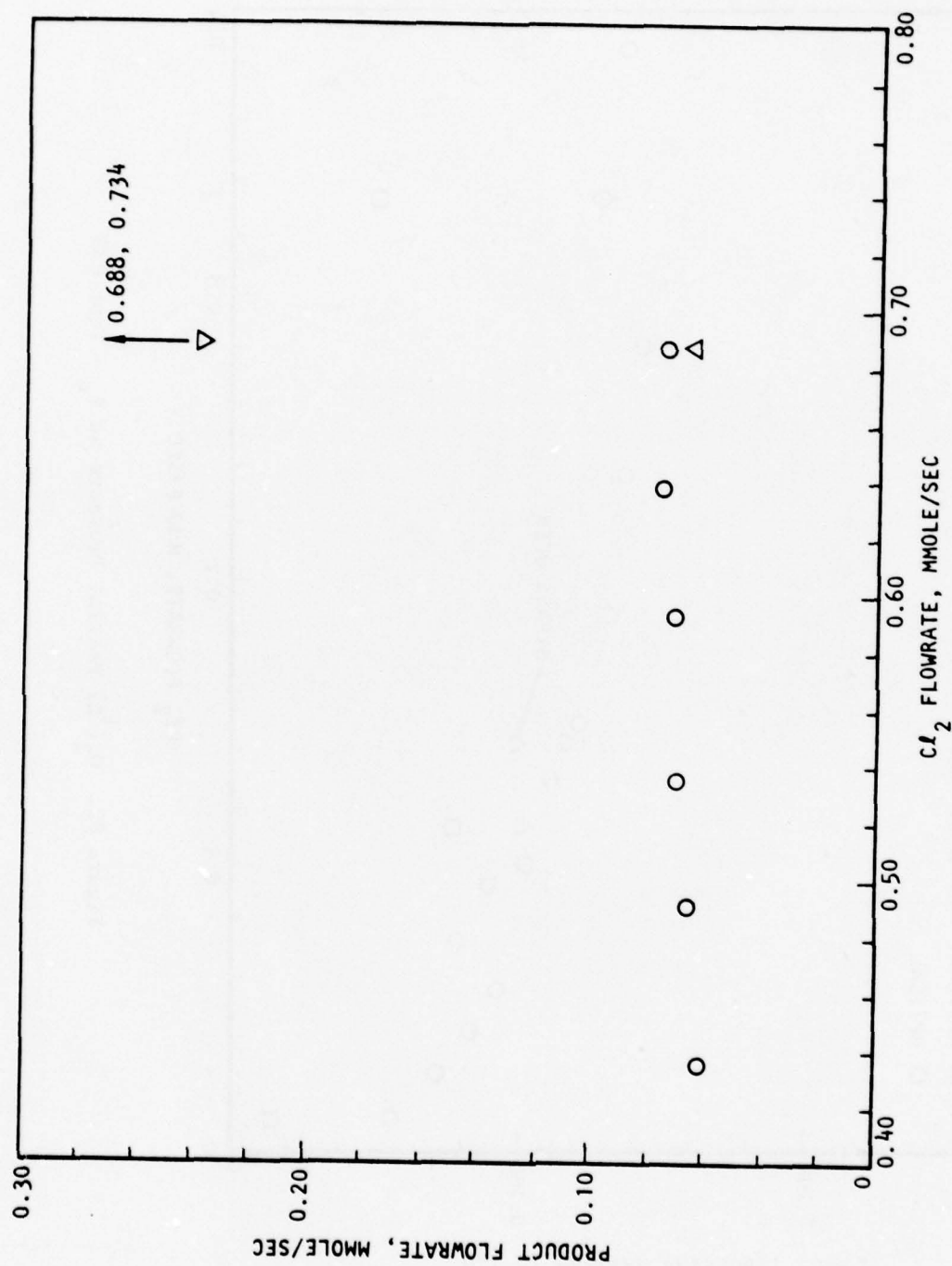


Figure 81. (Concluded)

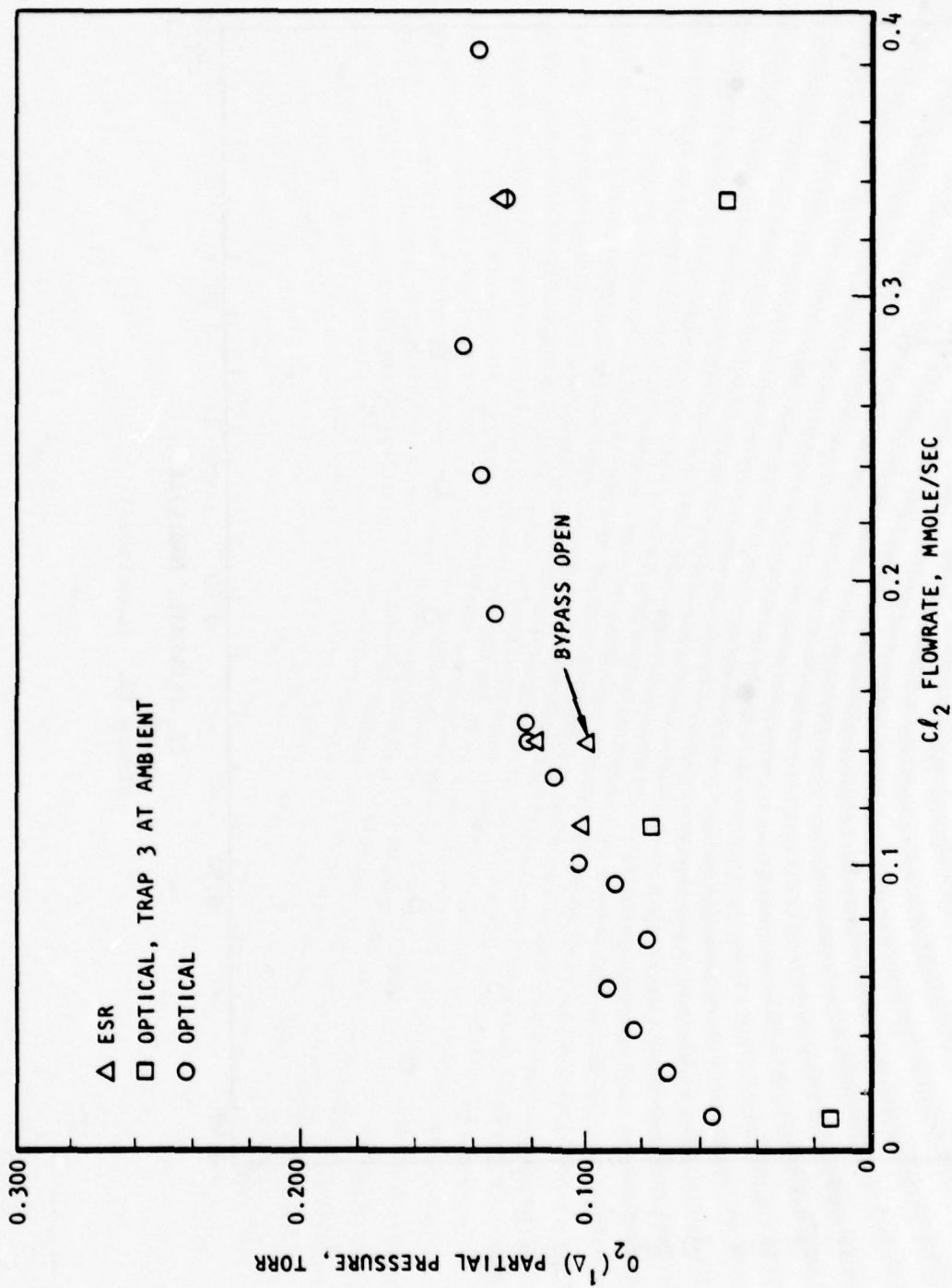


Figure 82. $O_2(\Delta)$ Partial Pressure at P_1 - Test 034

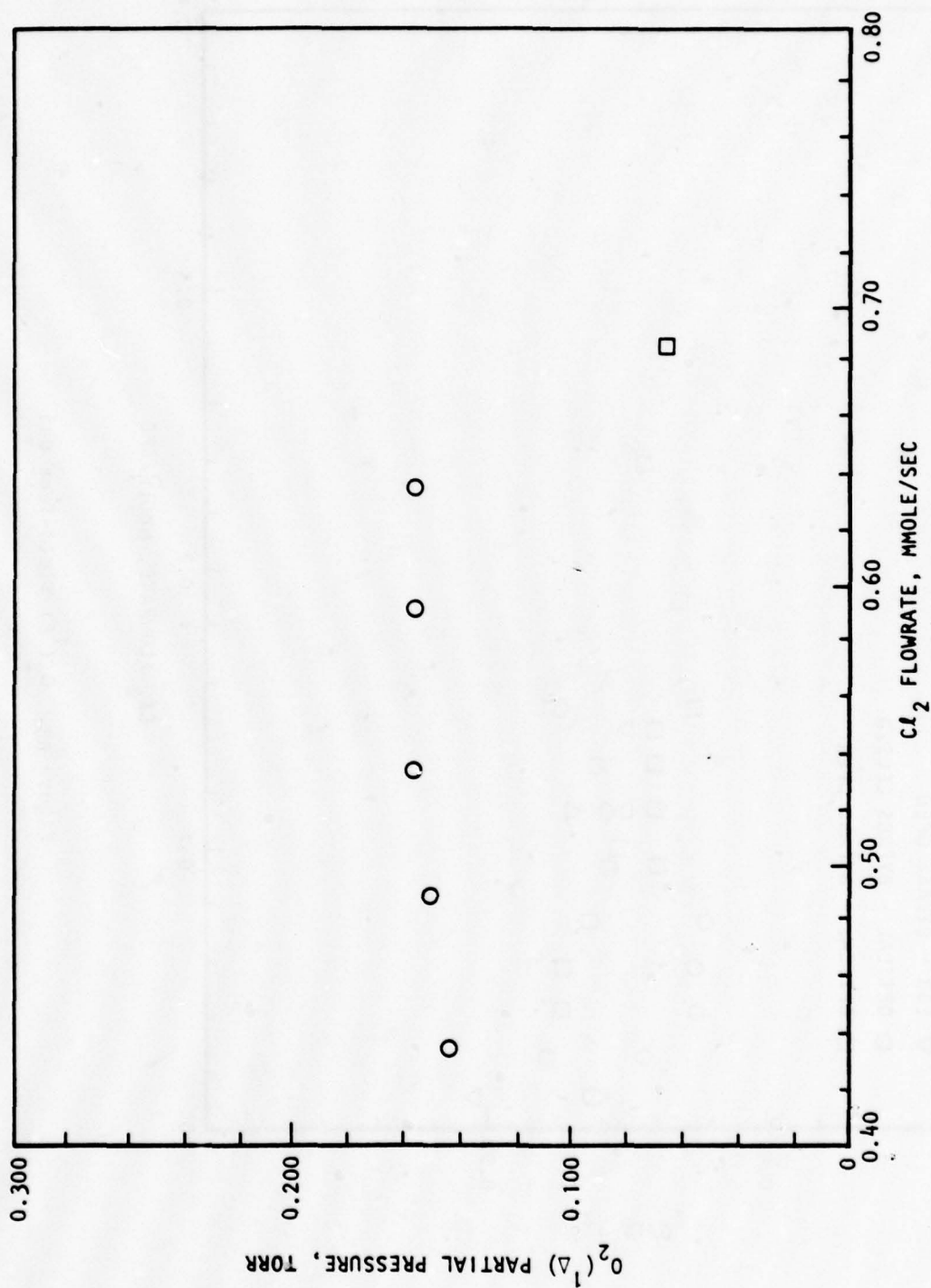


Figure 82. (Concluded)

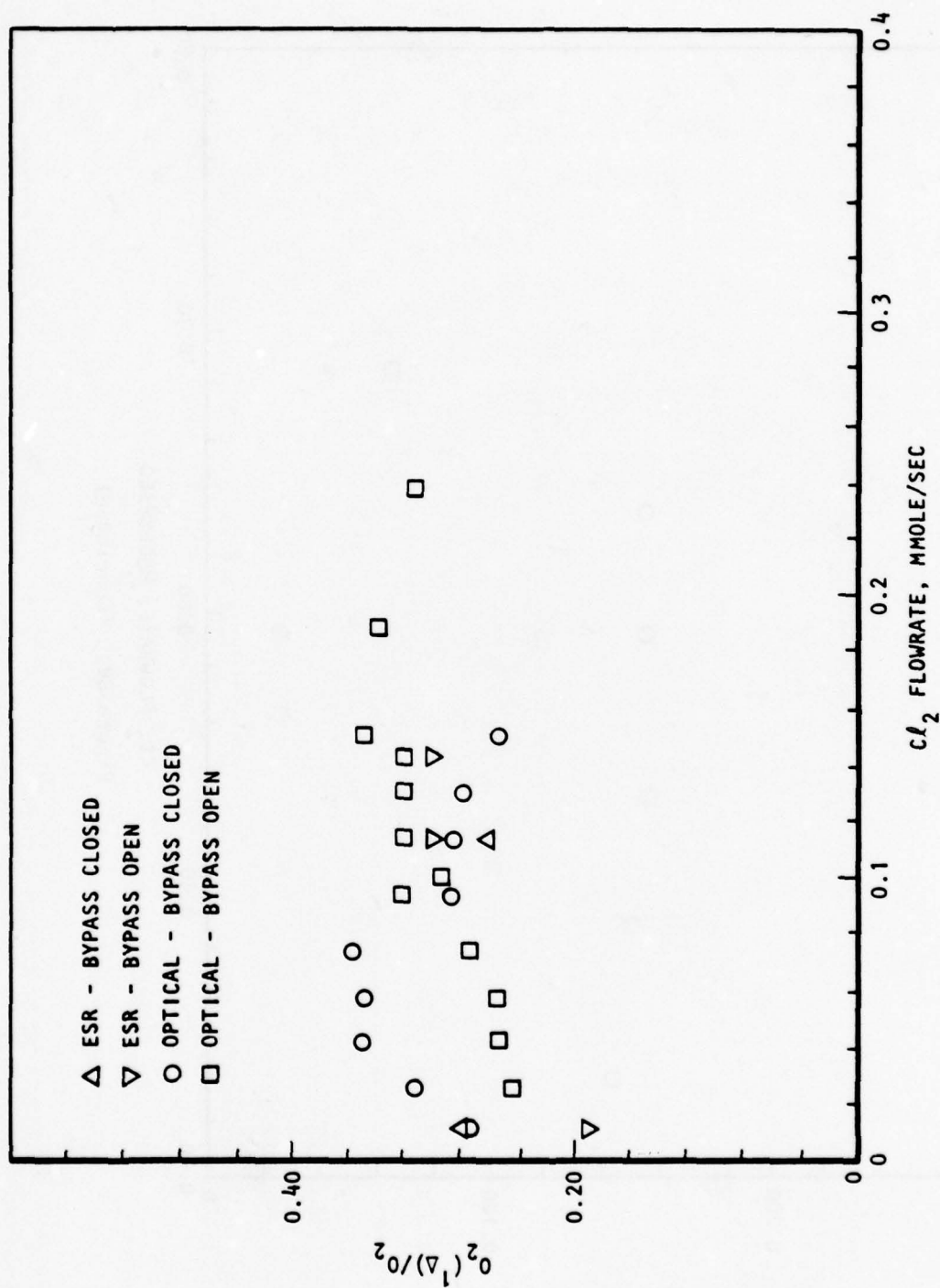


Figure 83. $O_2(^1\Delta)$ Yield-Test 035

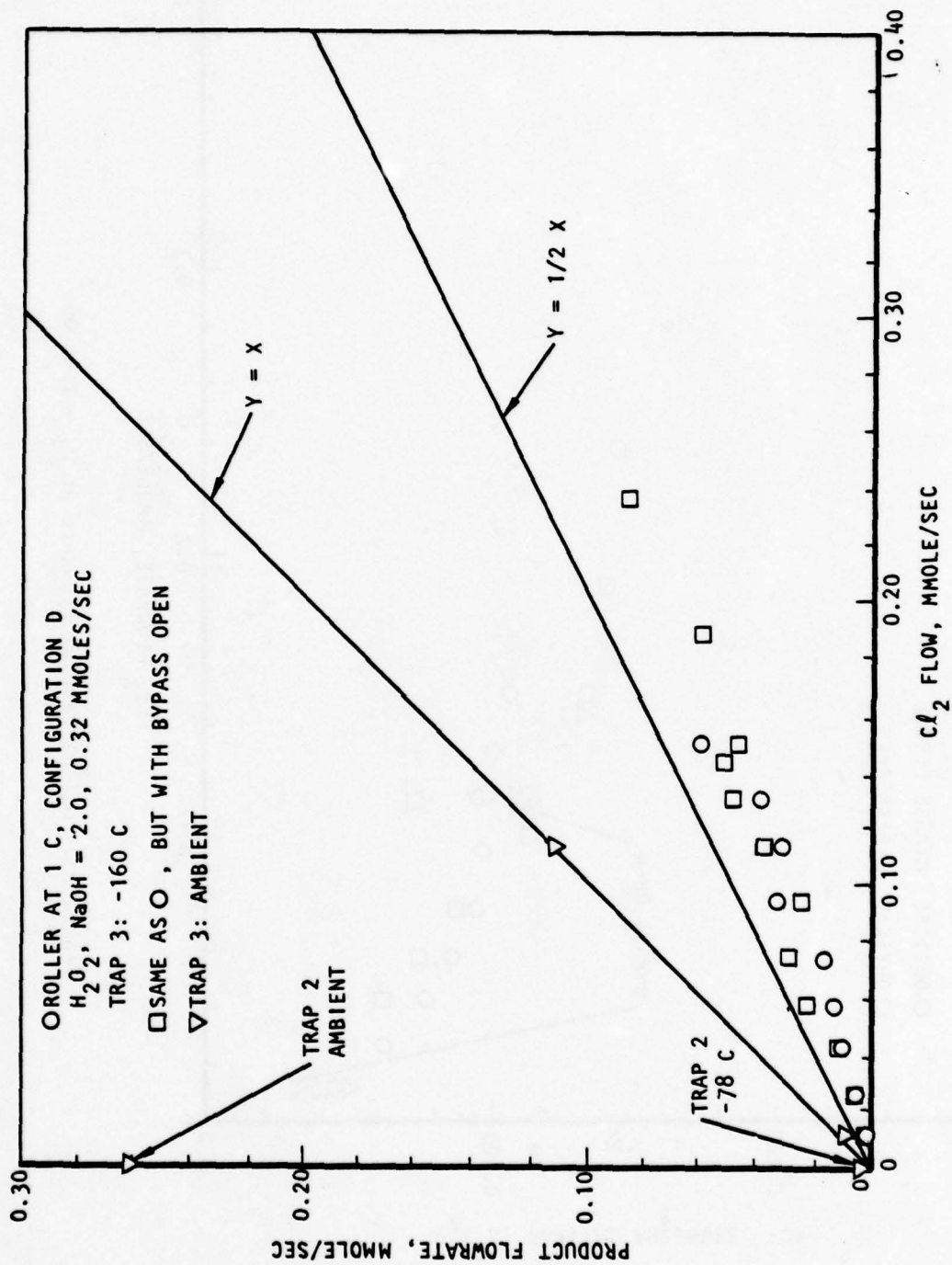


Figure 84. Product Flow, Test 035

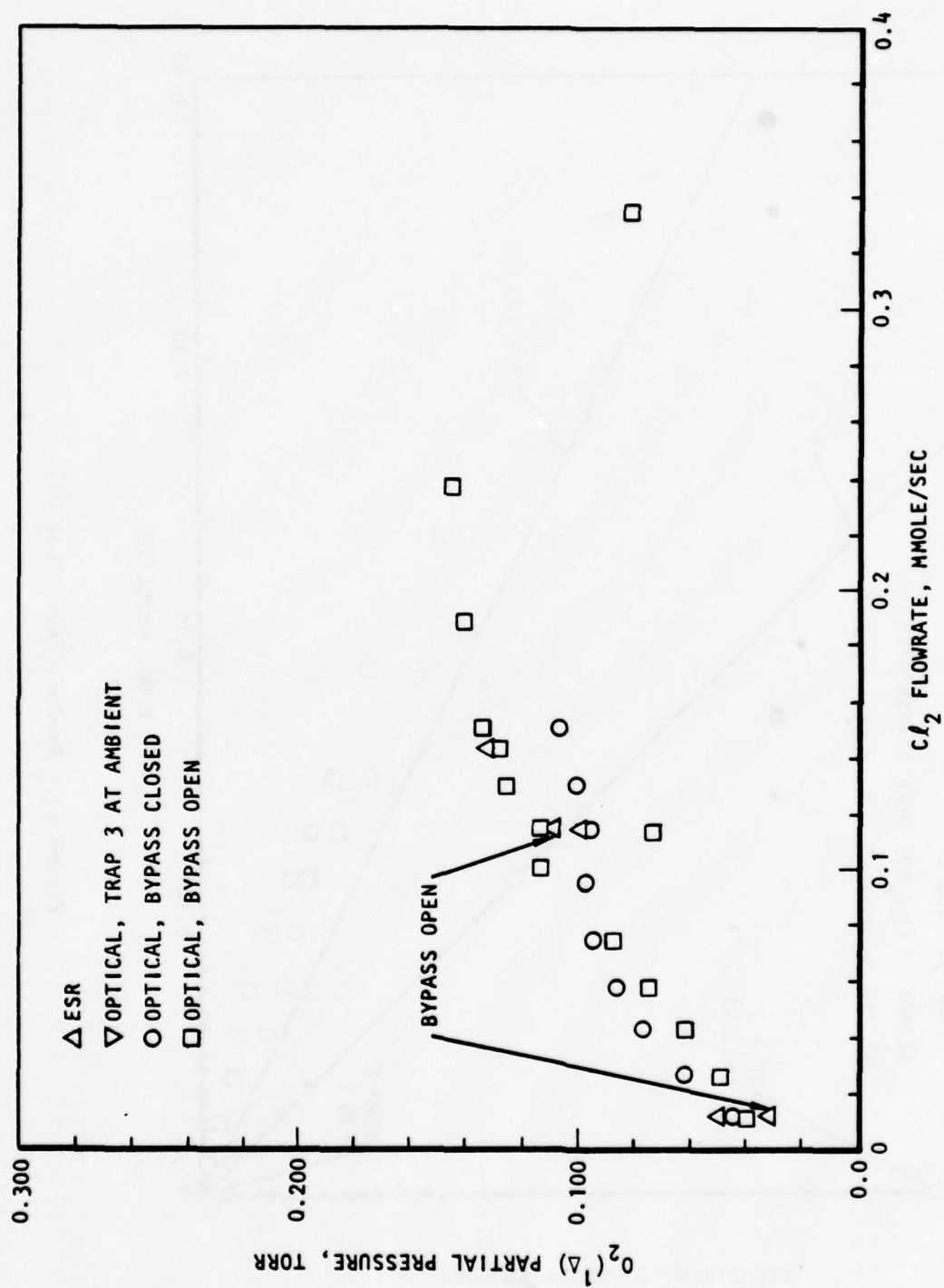


Figure 85. $O_2(\Delta)$ Partial Pressure at P_1 - Test 035

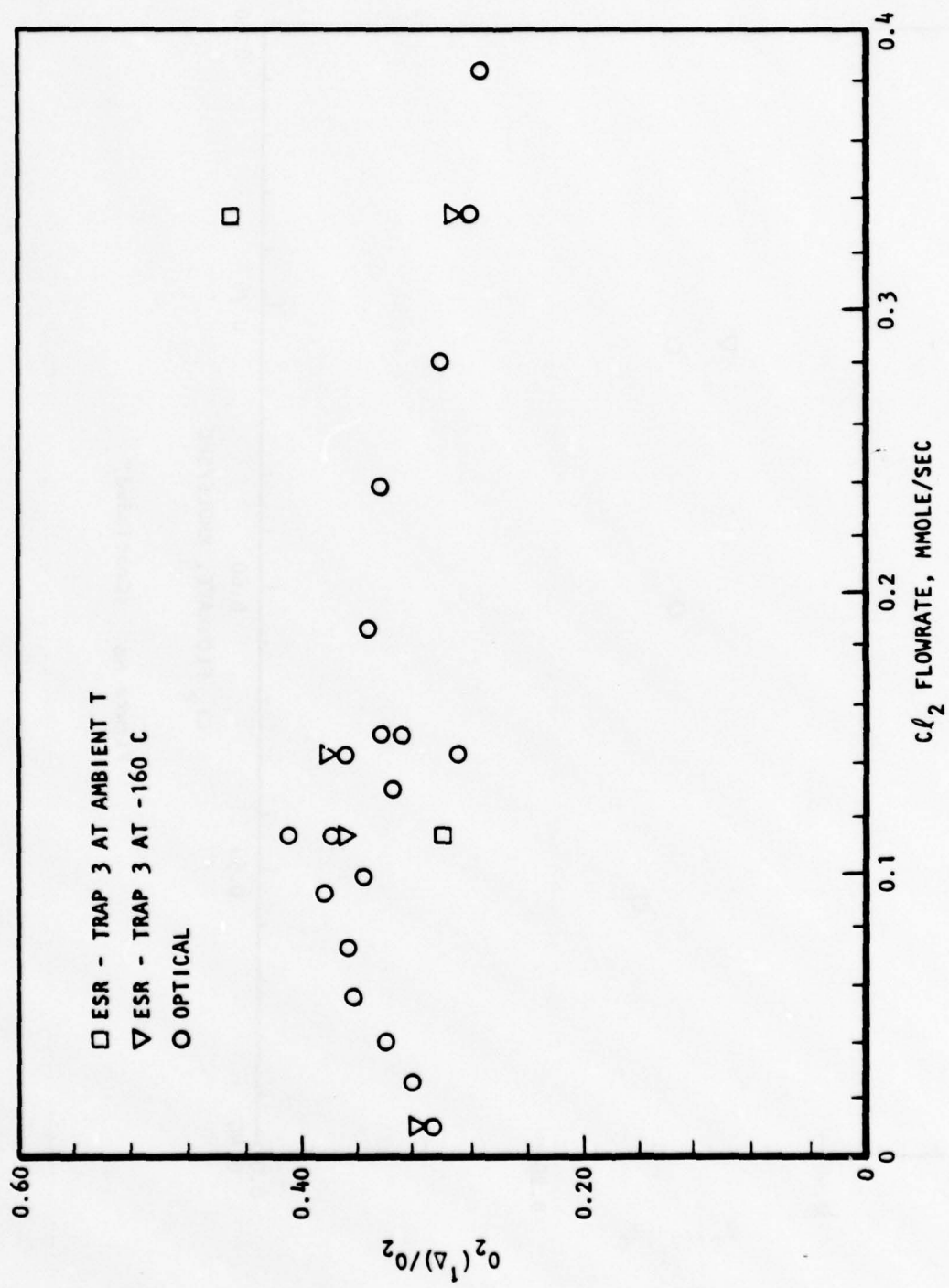


Figure 86. $O_2(^1\Delta)$ Yield - Test 036

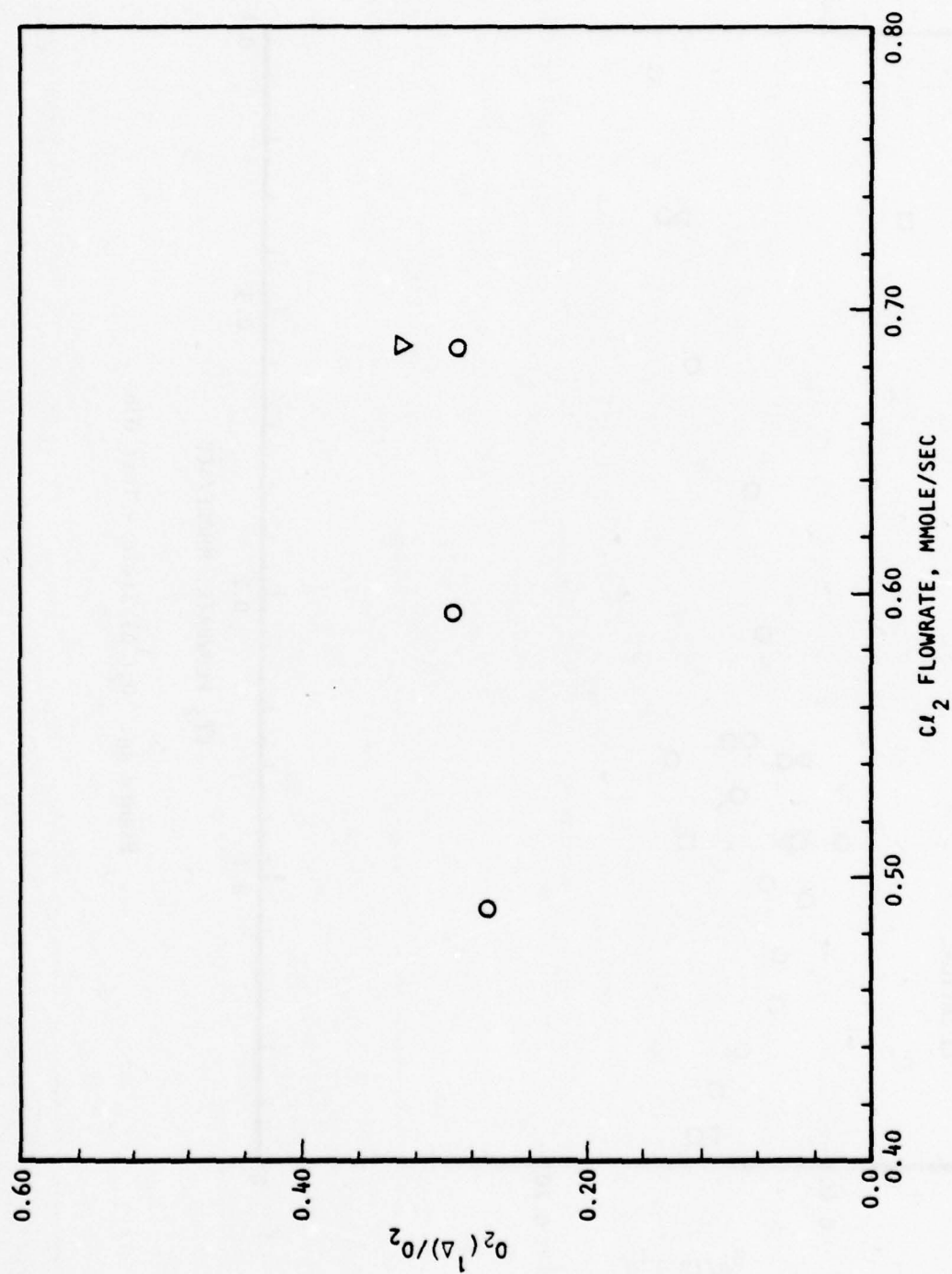


Figure 86. (Concluded)

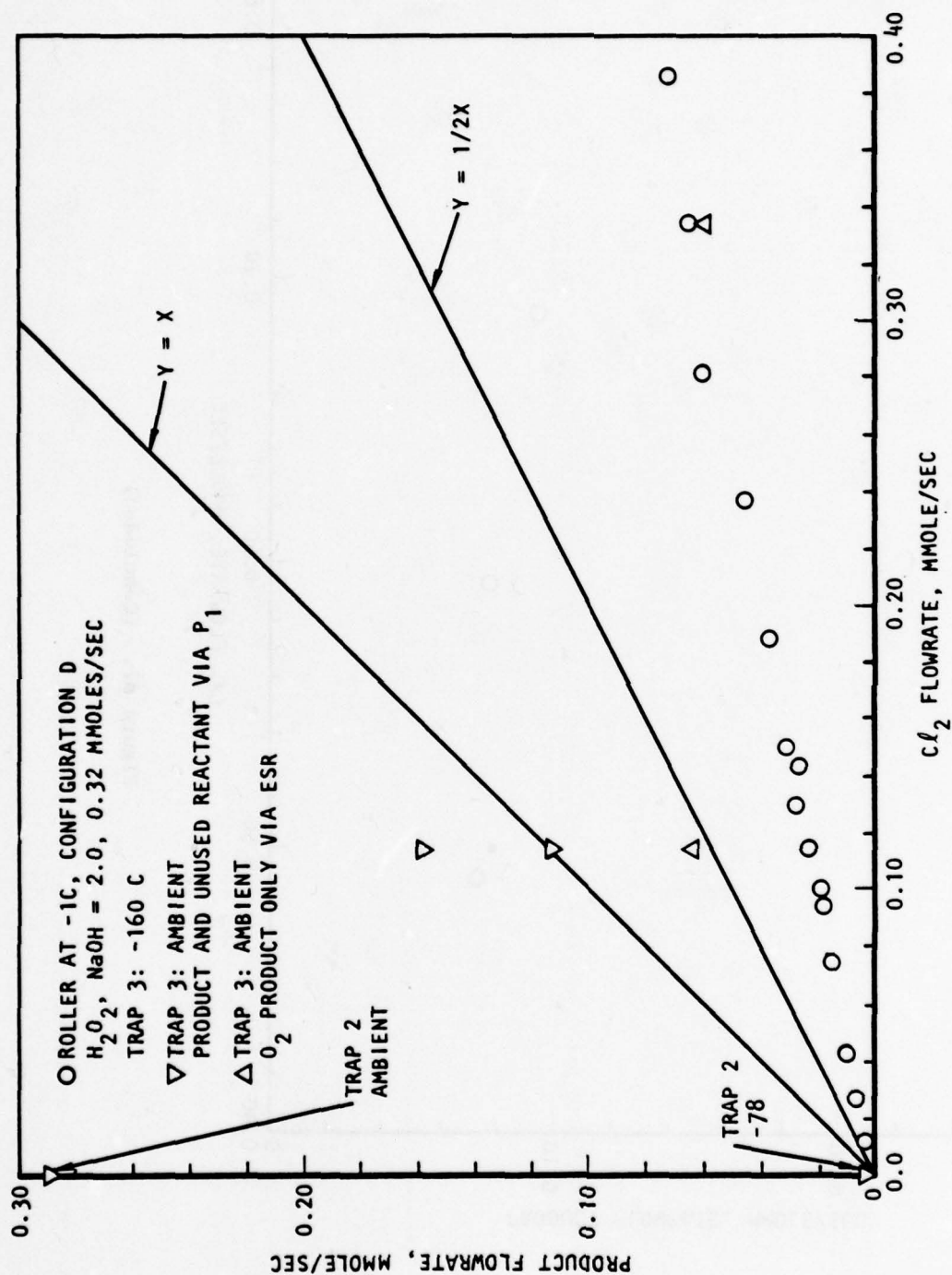


Figure 87. Product Flow - Test 036

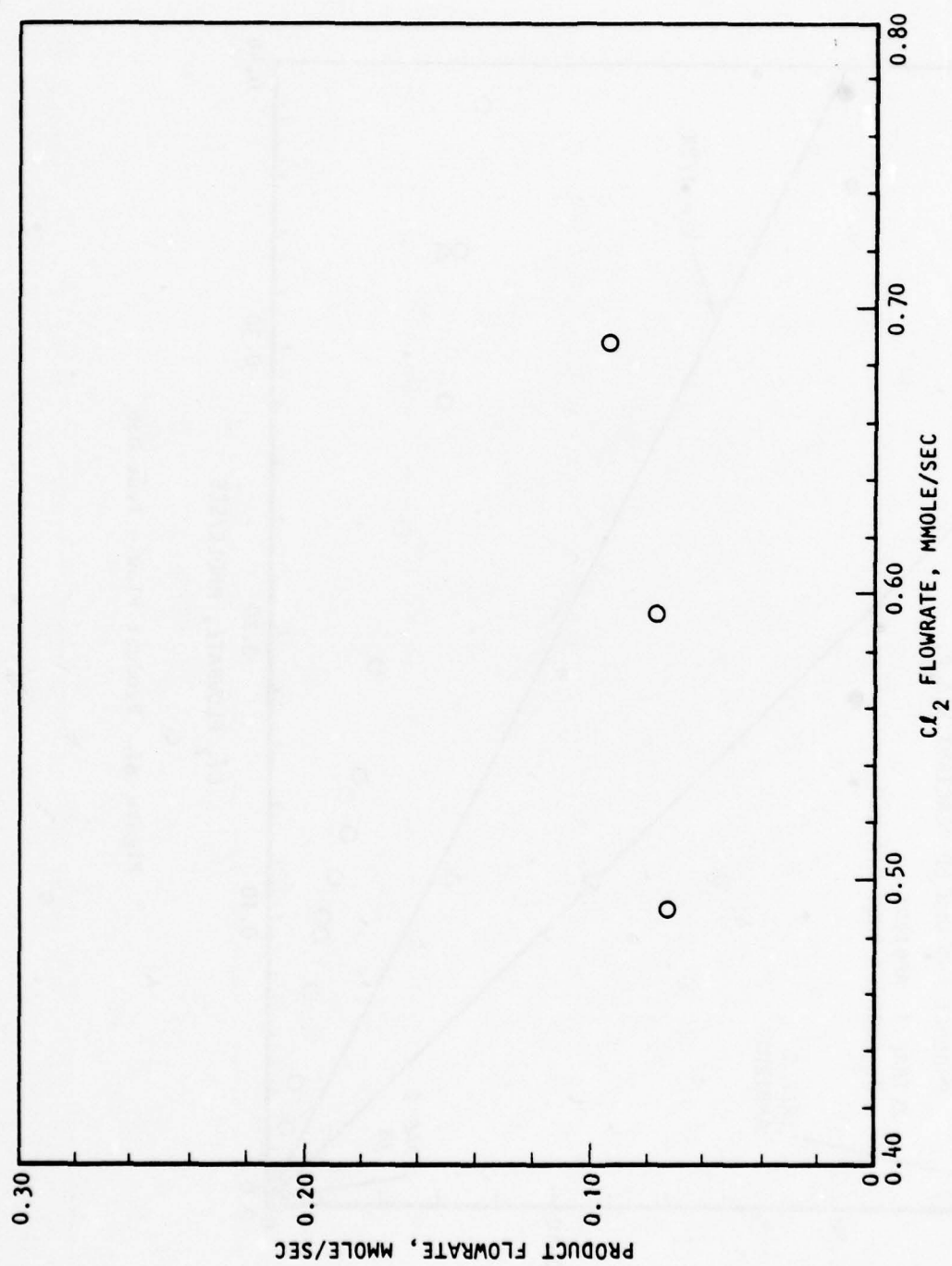


Figure 87. (Concluded)

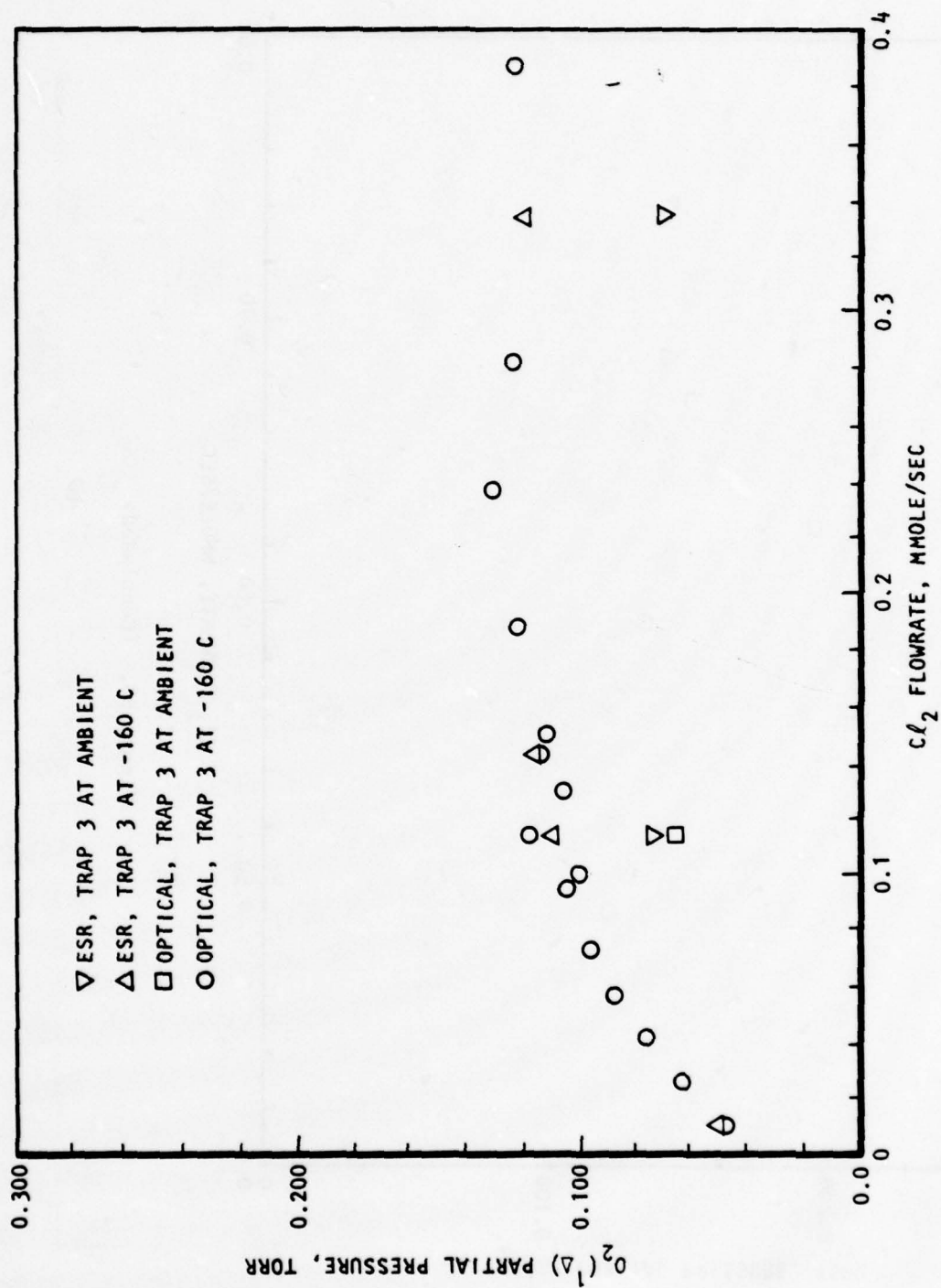


Figure 88. $\text{O}_2(^1\Delta)$ Partial Pressure at P_1 - Test 036

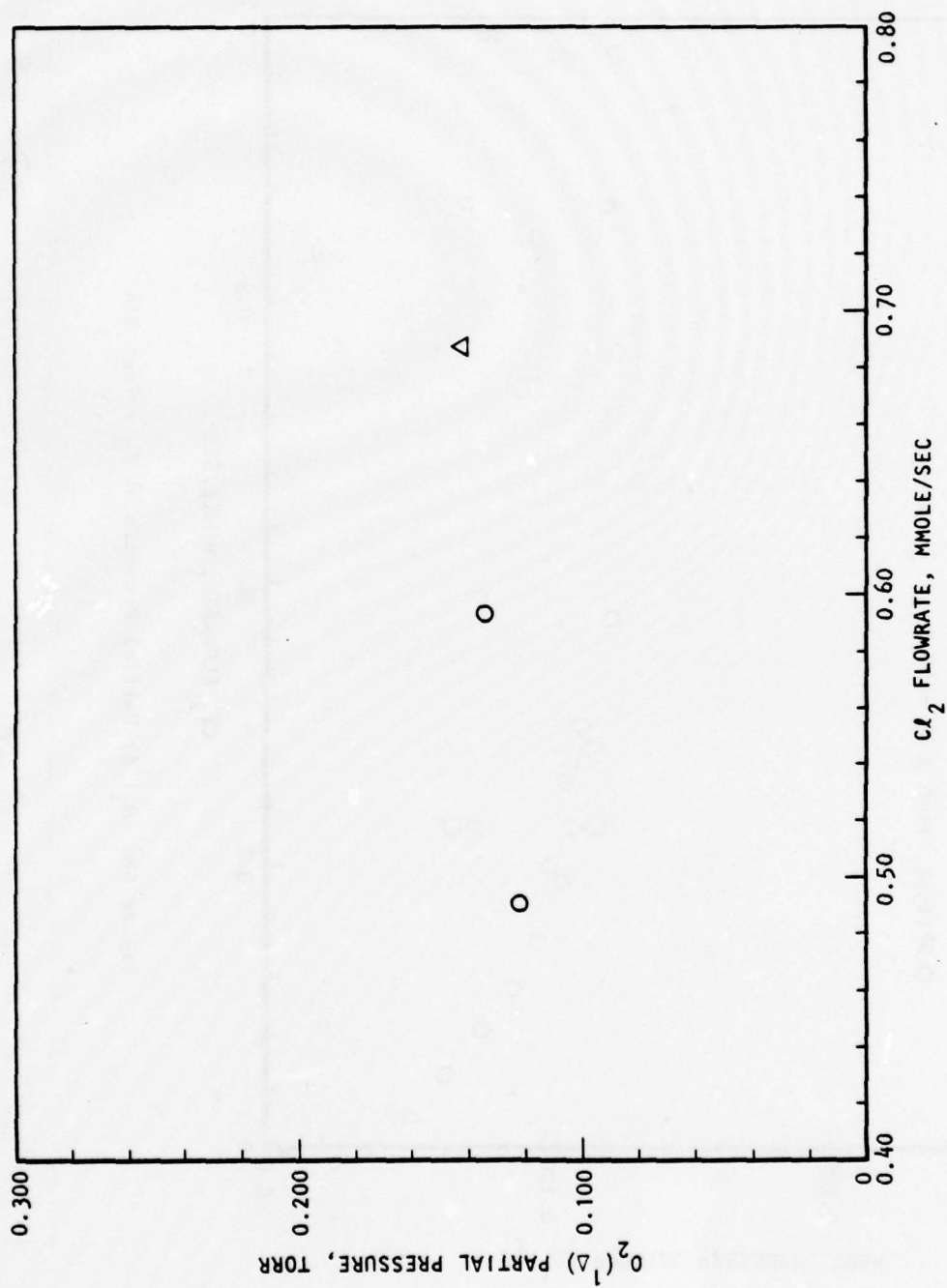


Figure 88. (Concluded)

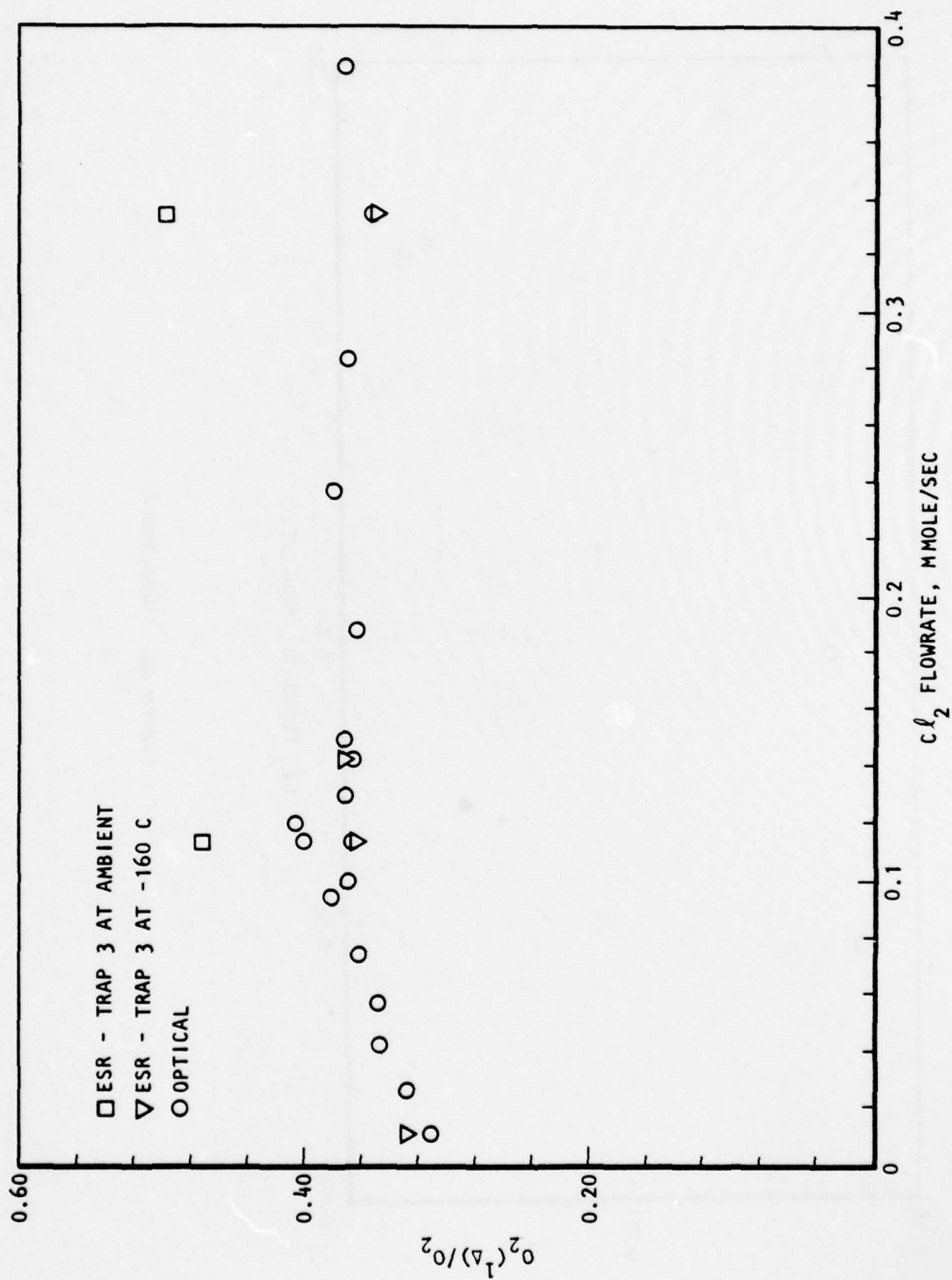


Figure 89. O₂(¹Δ) Yield-Test 037

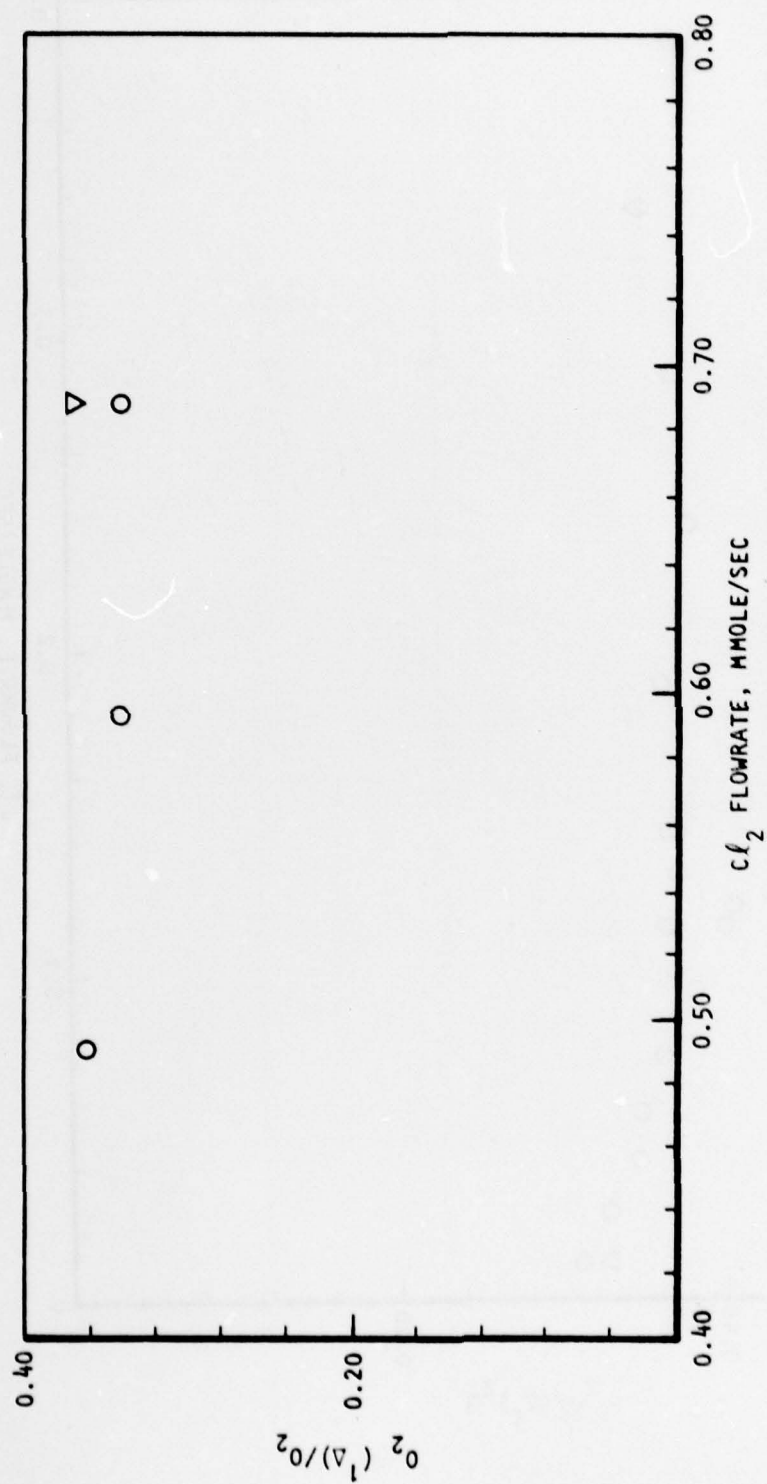


Figure 89. (Concluded)

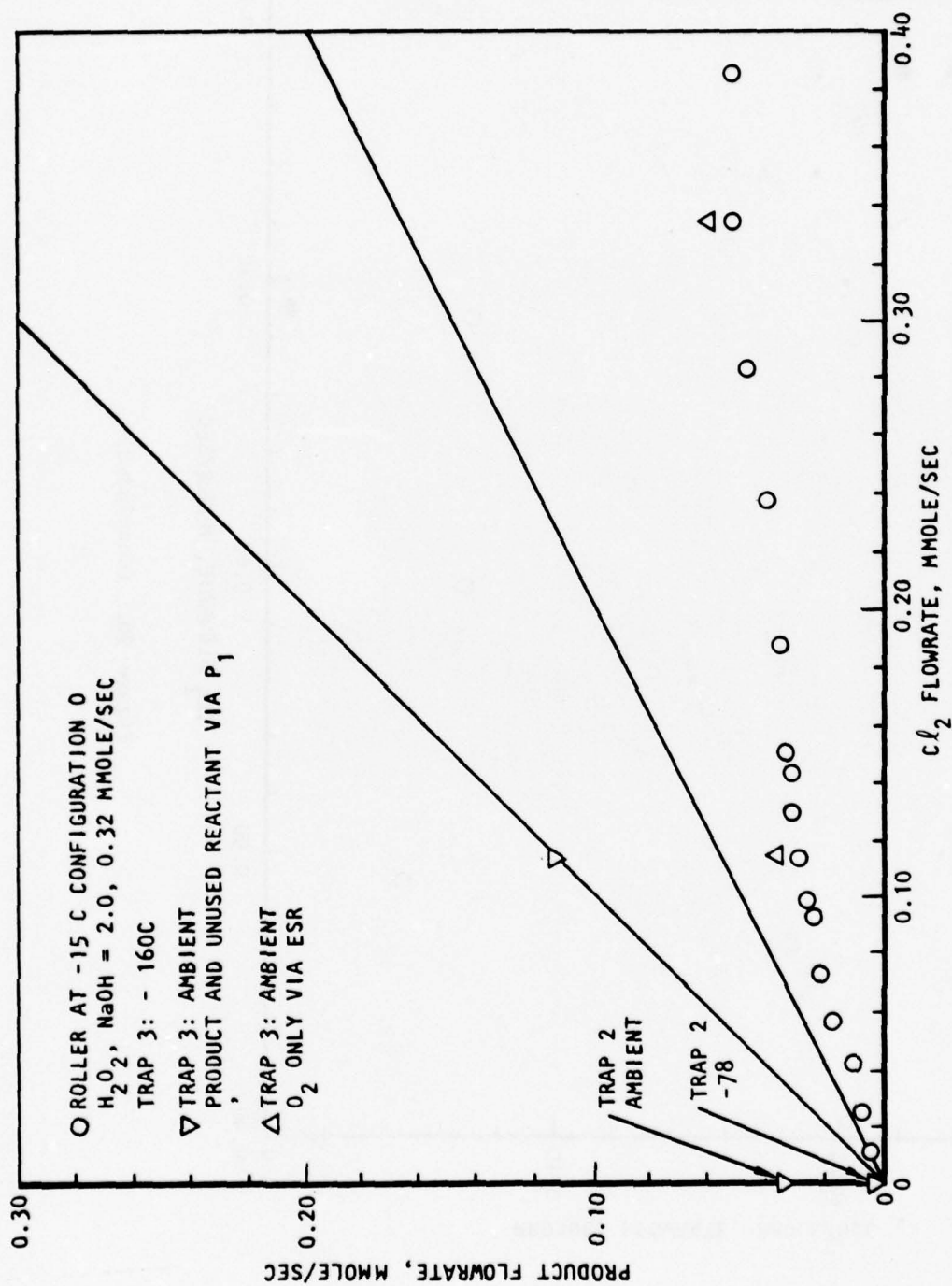


Figure 90. Product Flow - Test 037

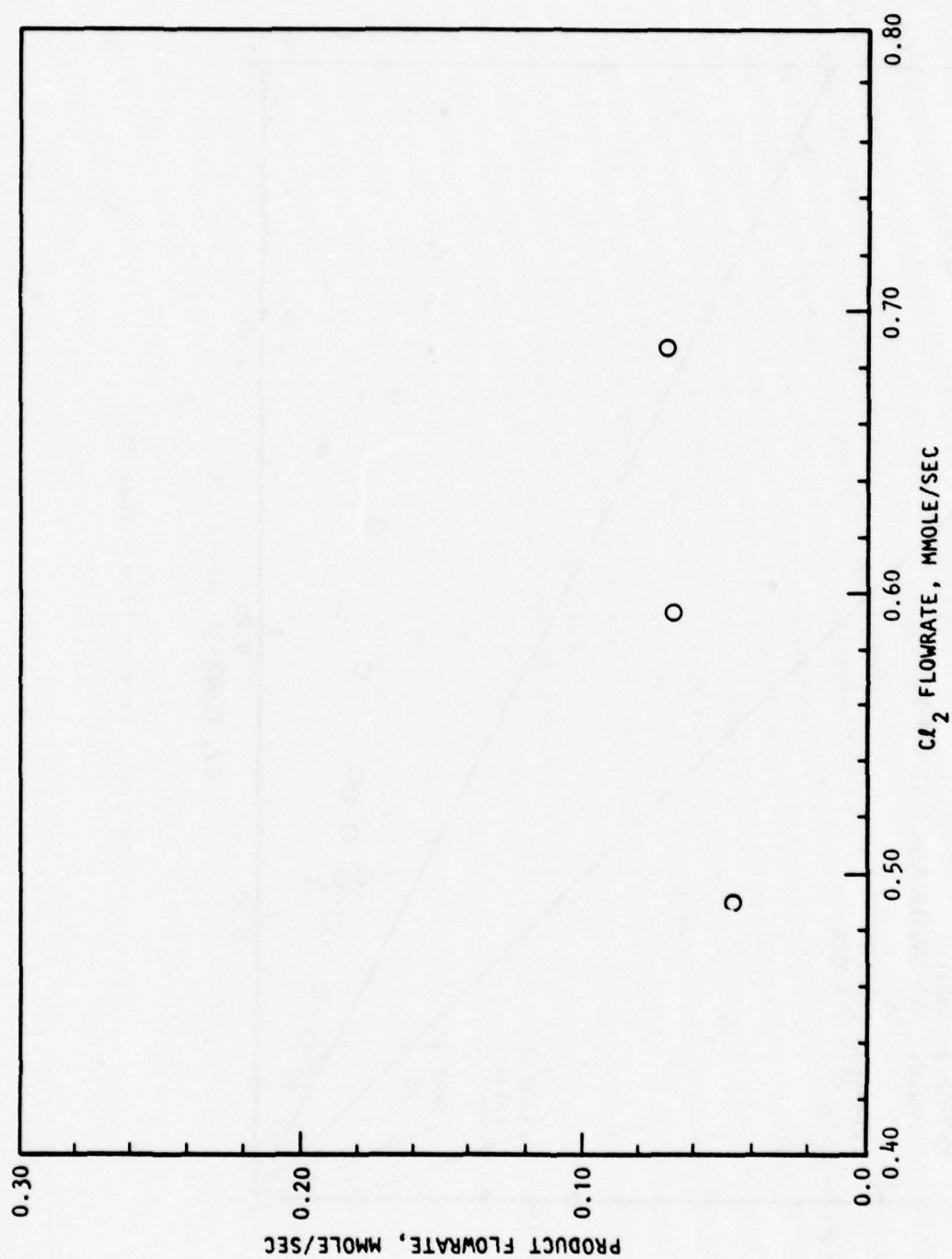


Figure 90. (Concluded)

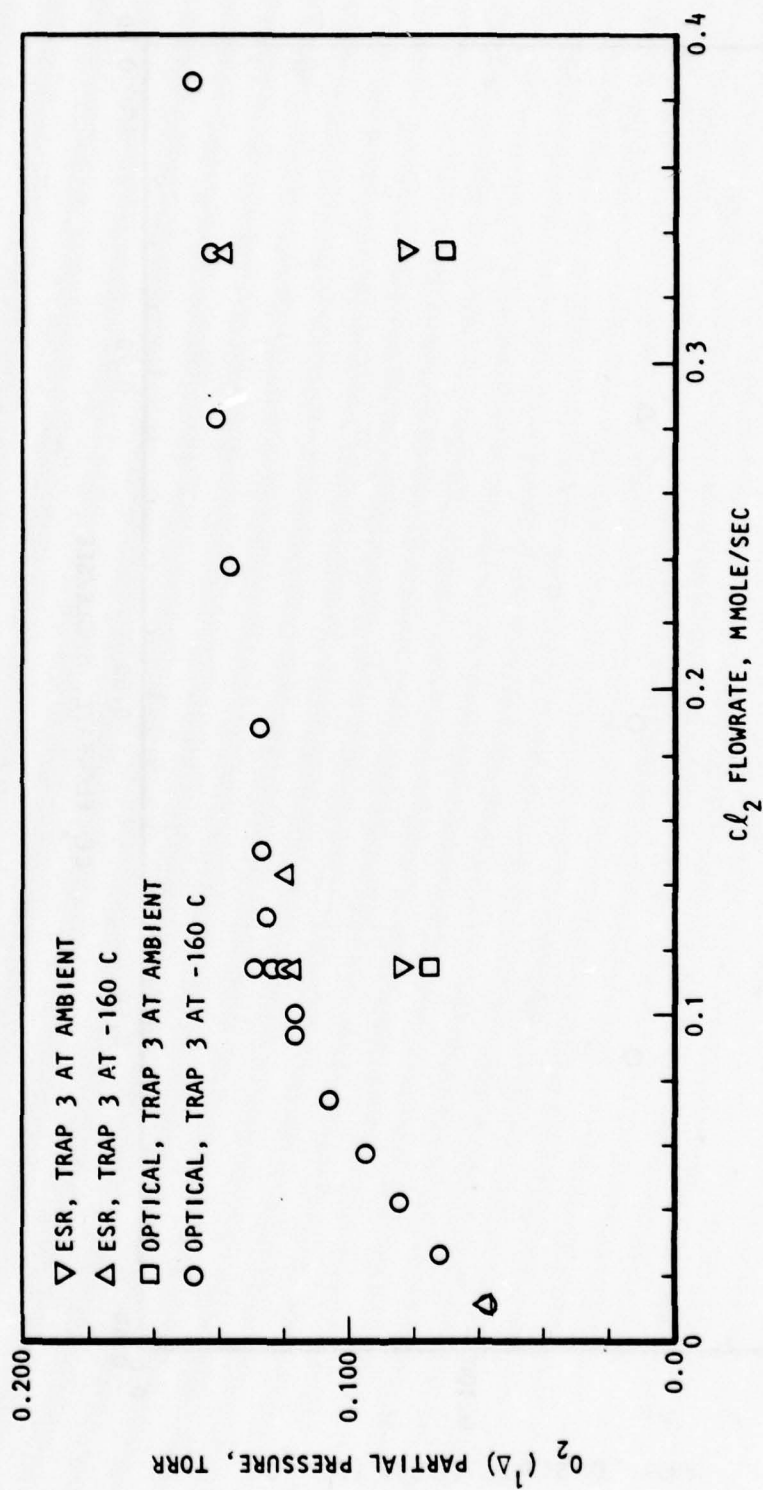


Figure 91. O_2 (Δ) Partial Pressure at P_1 -Test 037

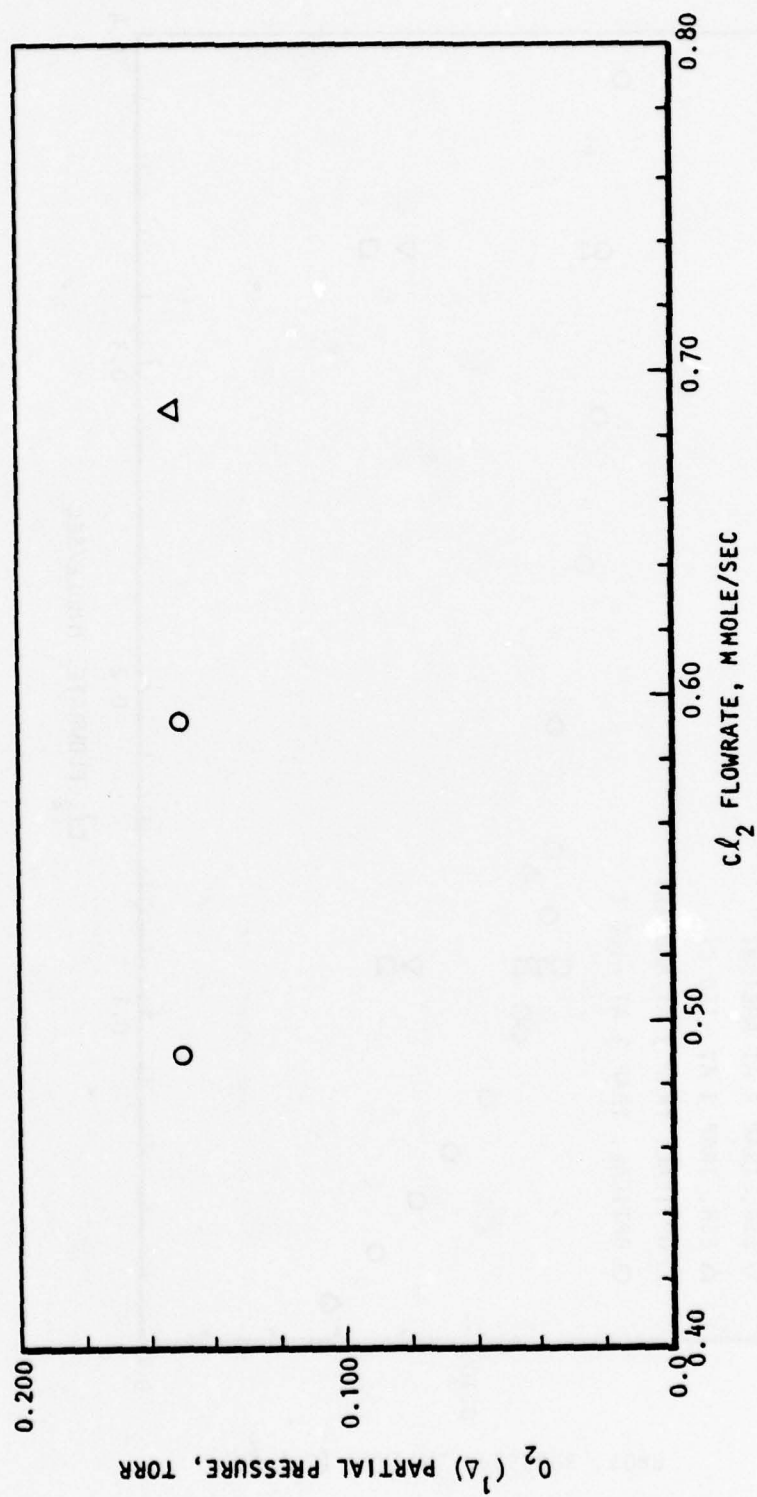


Figure 91. (Concluded)

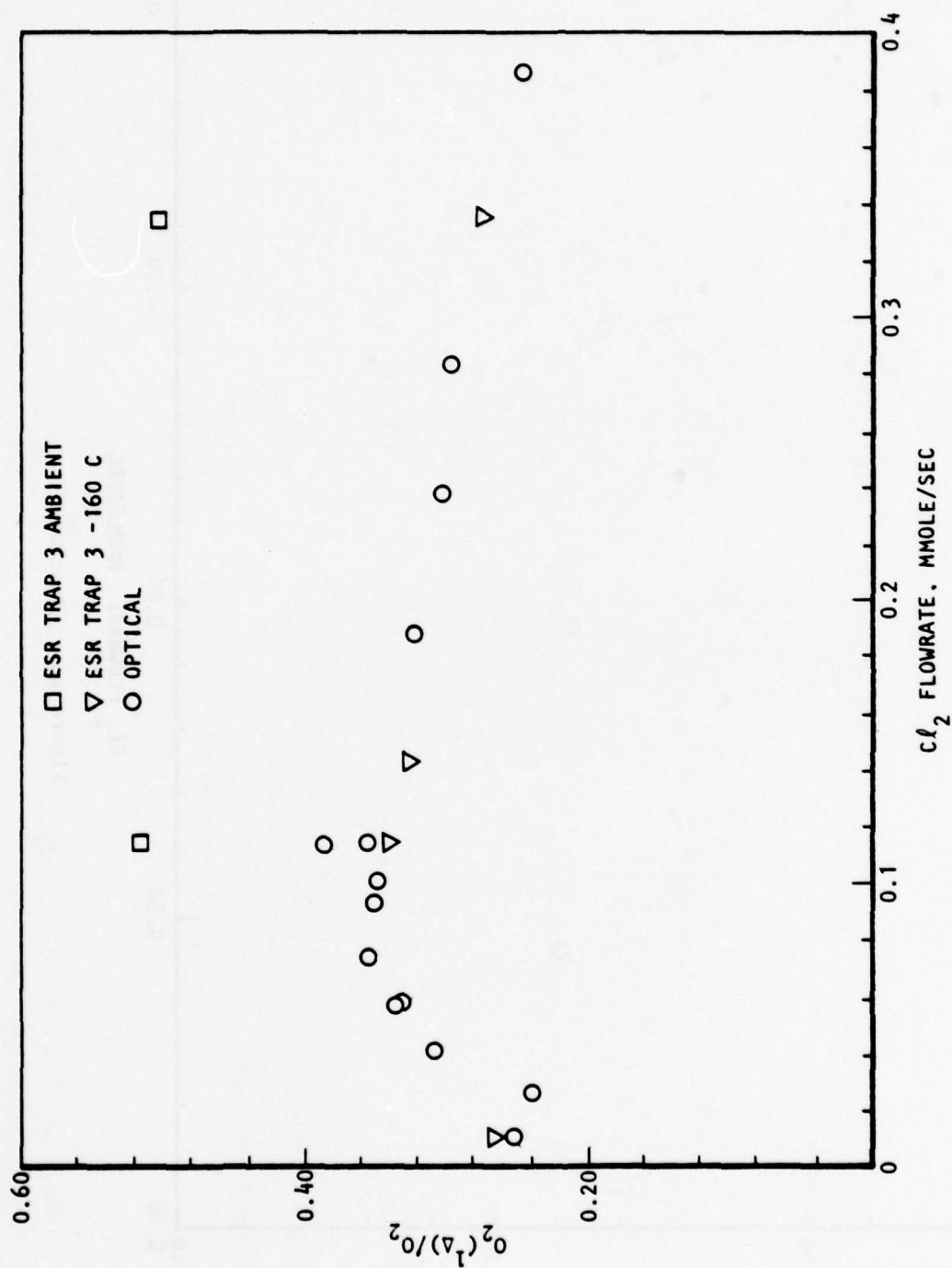


Figure 92. O₂(¹Δ) Yield - Test 038

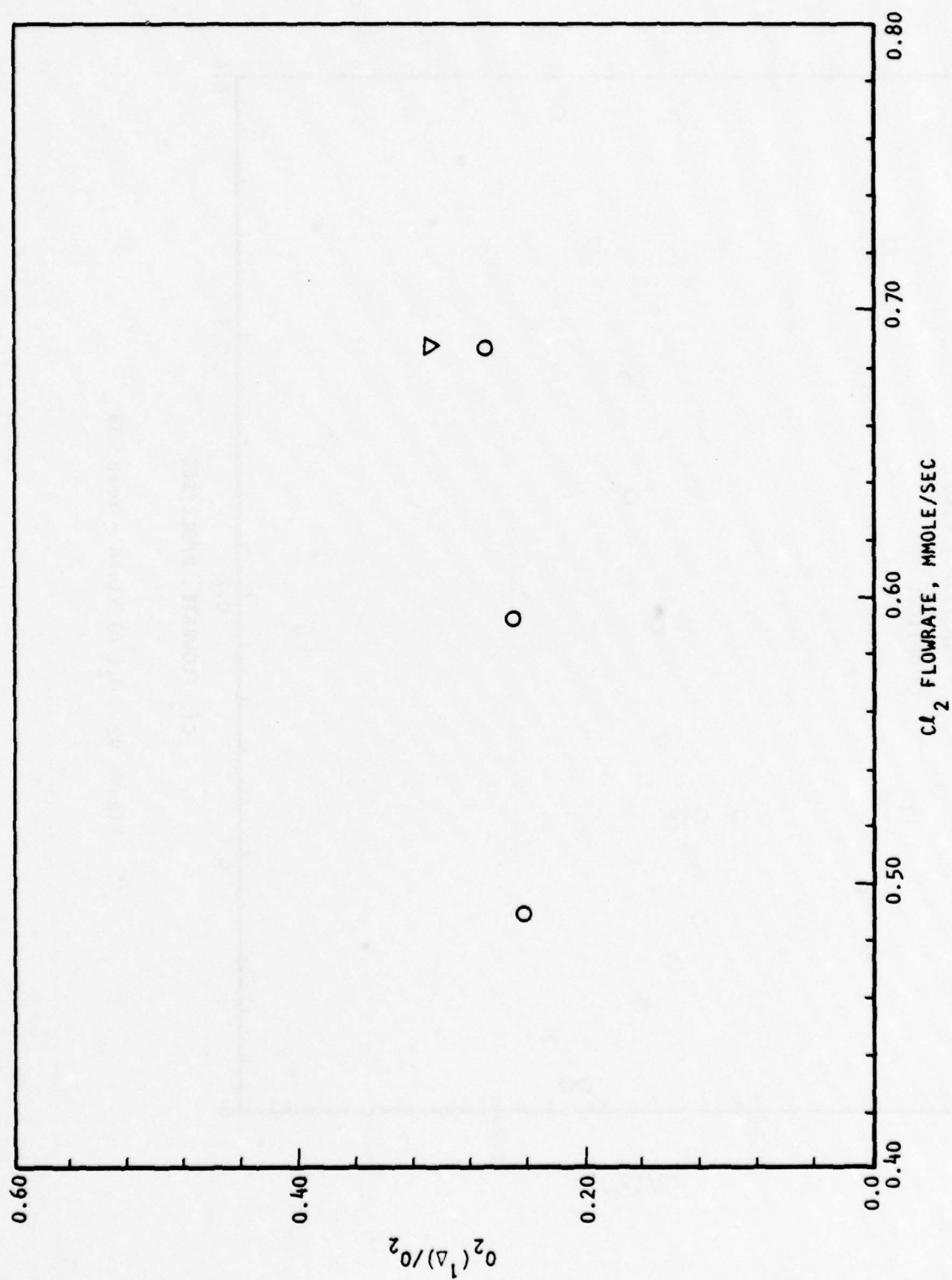


Figure 92. (Concluded)

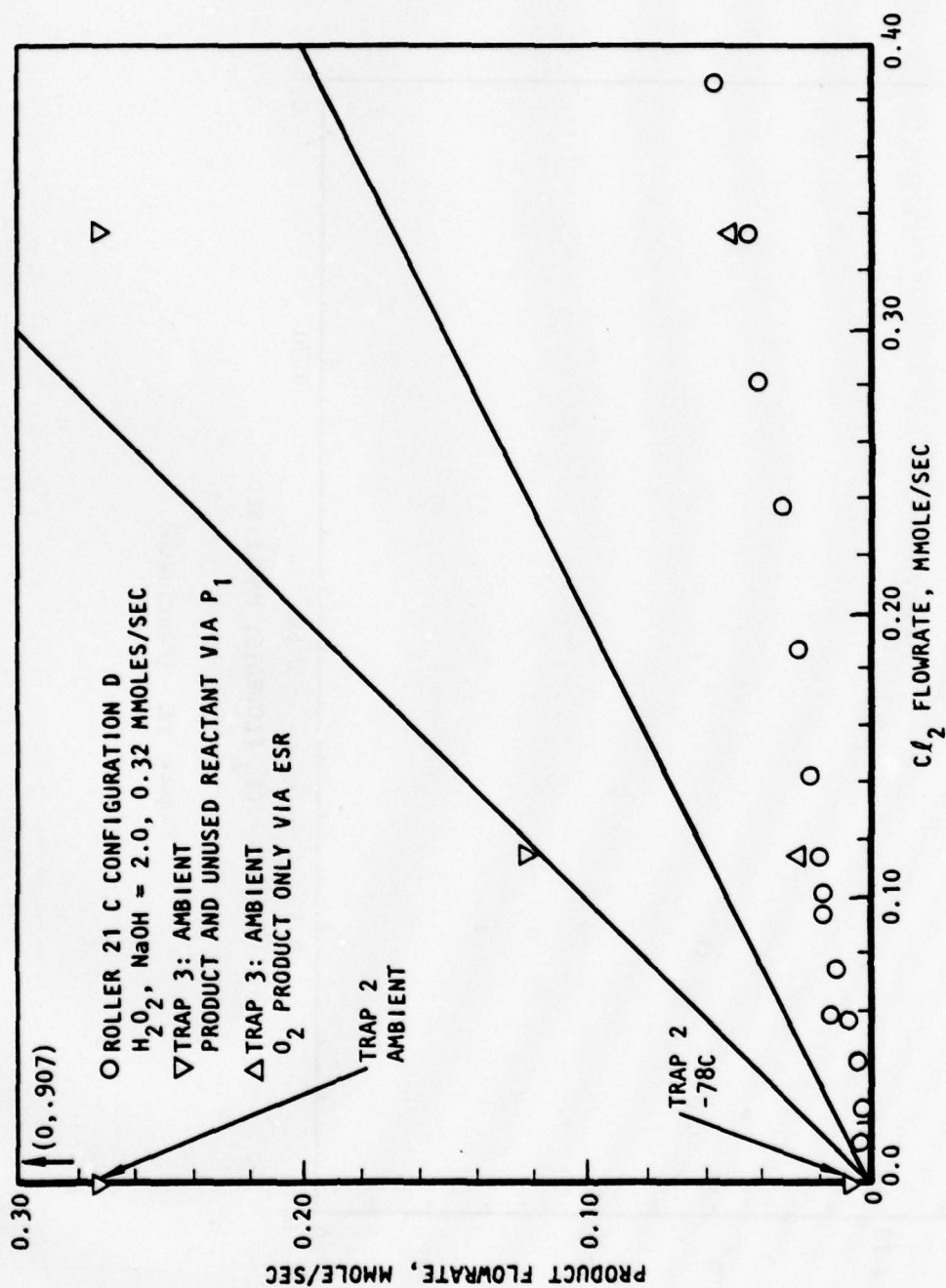


Figure 93. Product Flow - Test 038

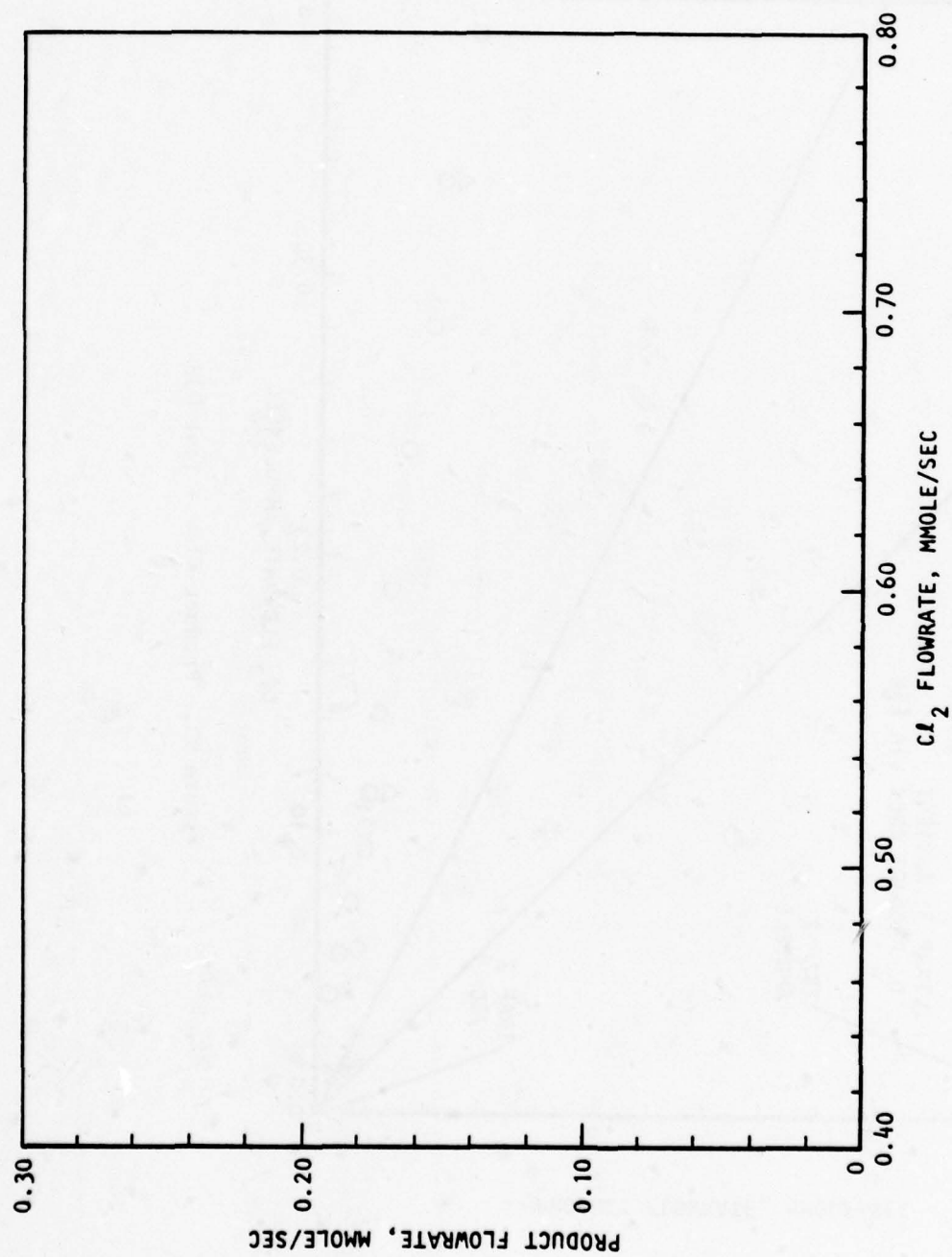


Figure 93. (Concluded)

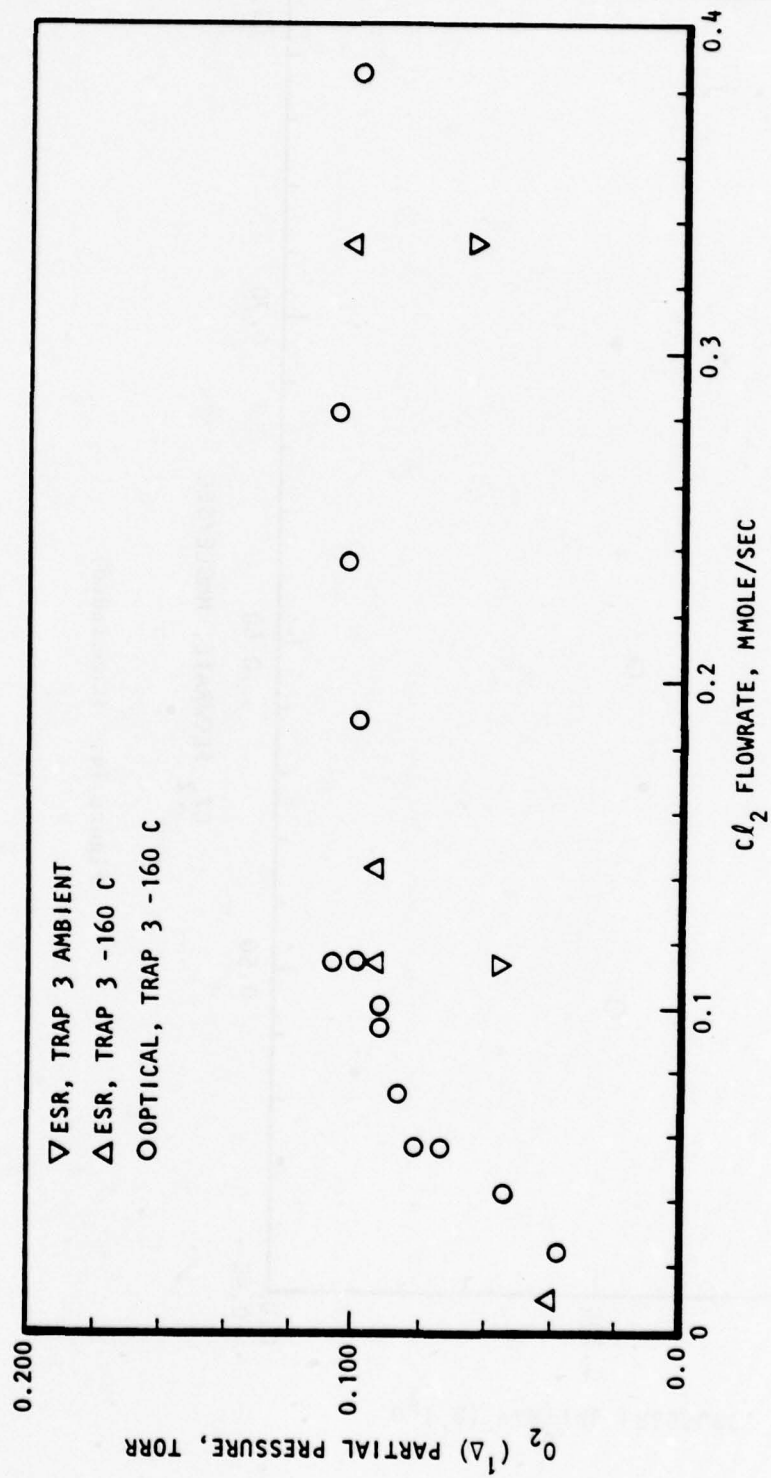


Figure 94. $O_2(^1\Delta)$ Partial Pressure at P_1 -Test 038

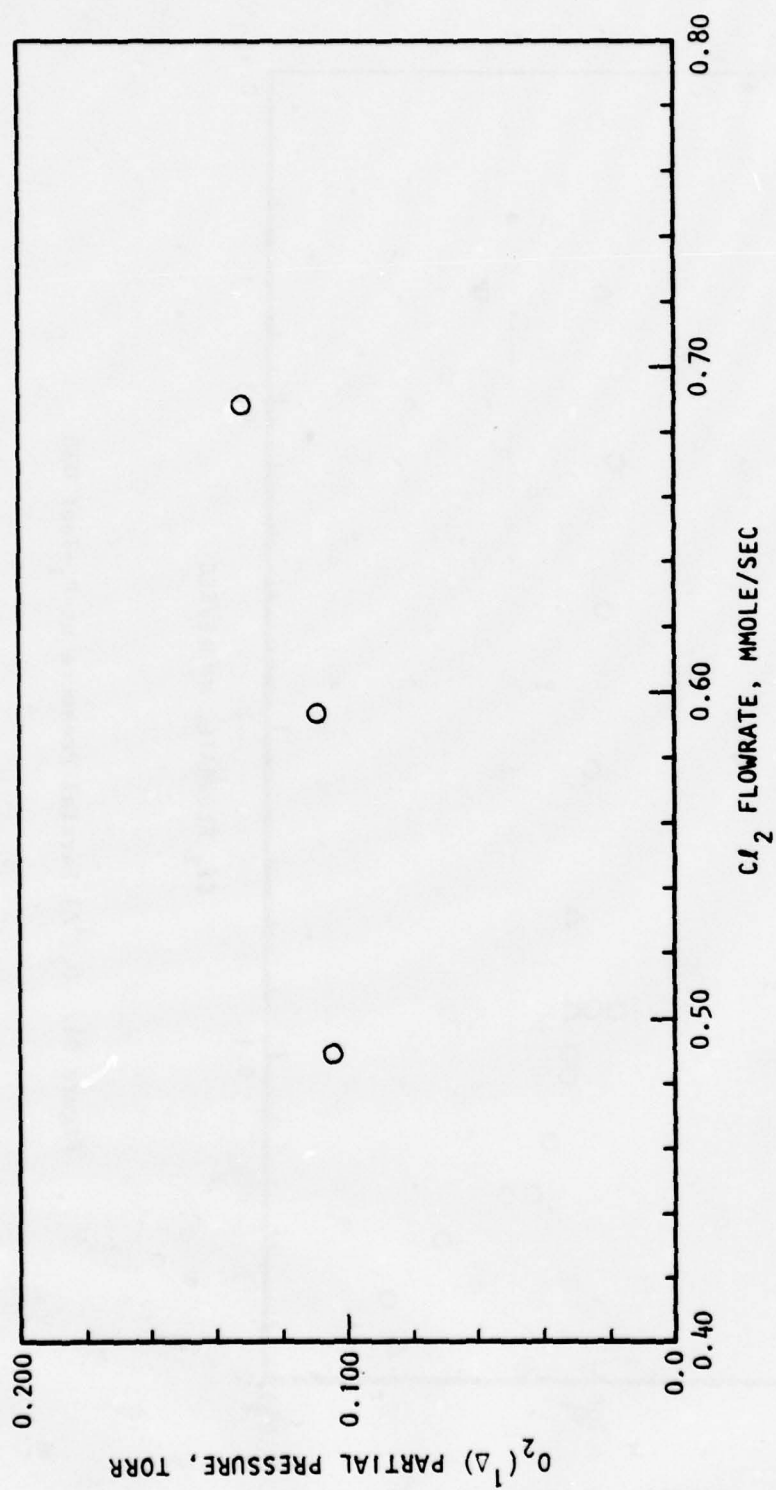
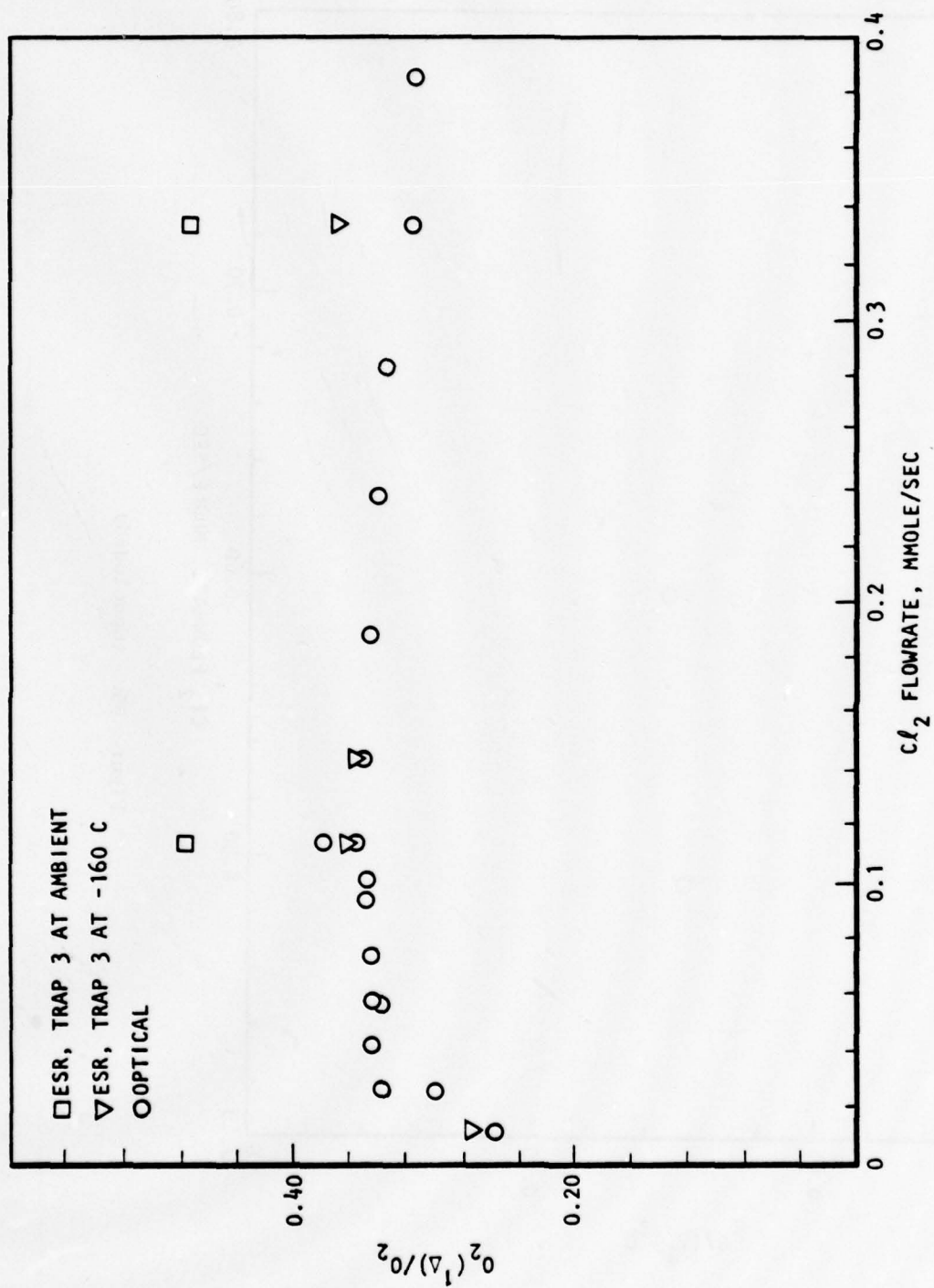


Figure 94. (Concluded)



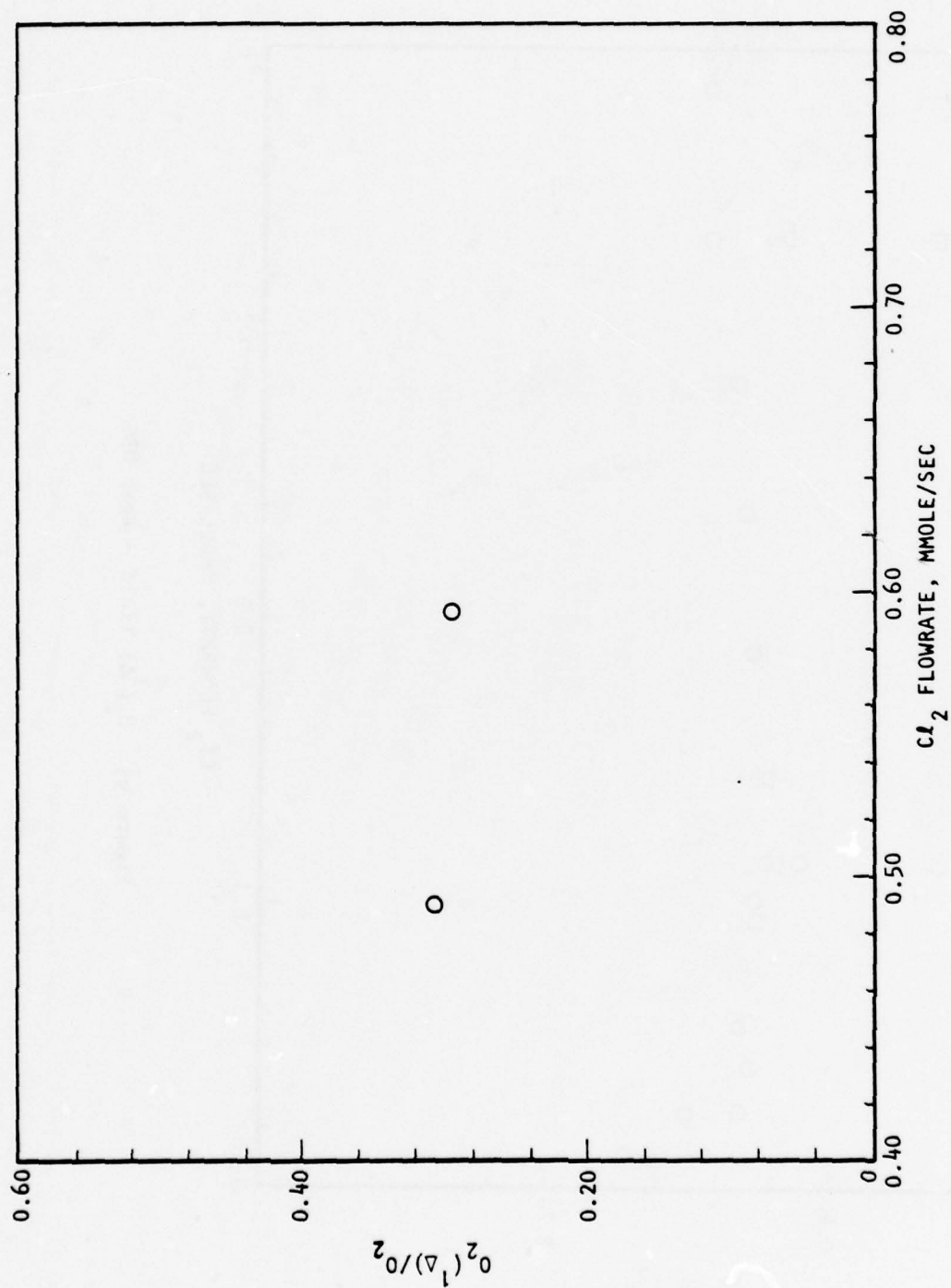


Figure 95. (Concluded)

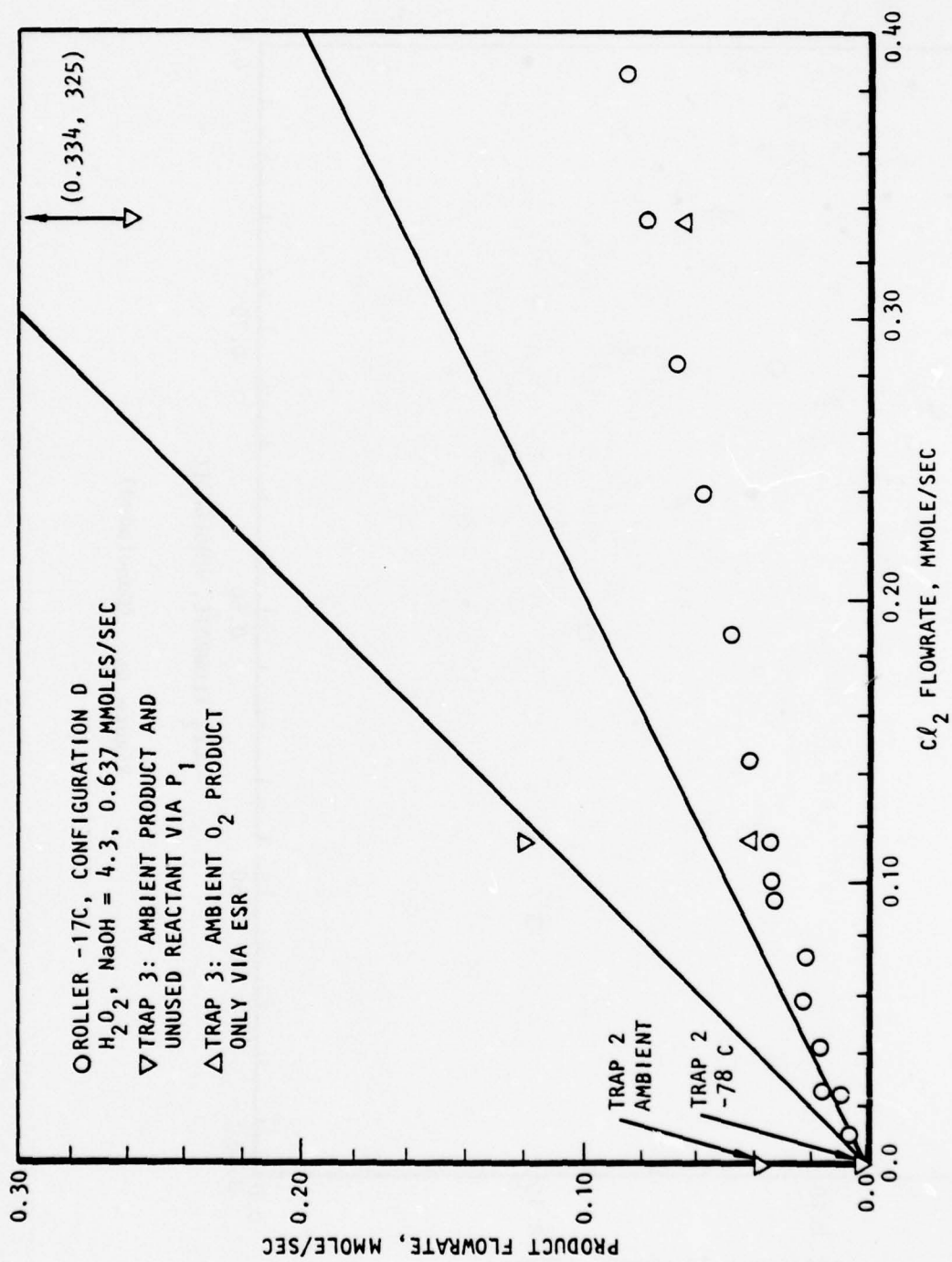


Figure 96. Product Flow-Test 039

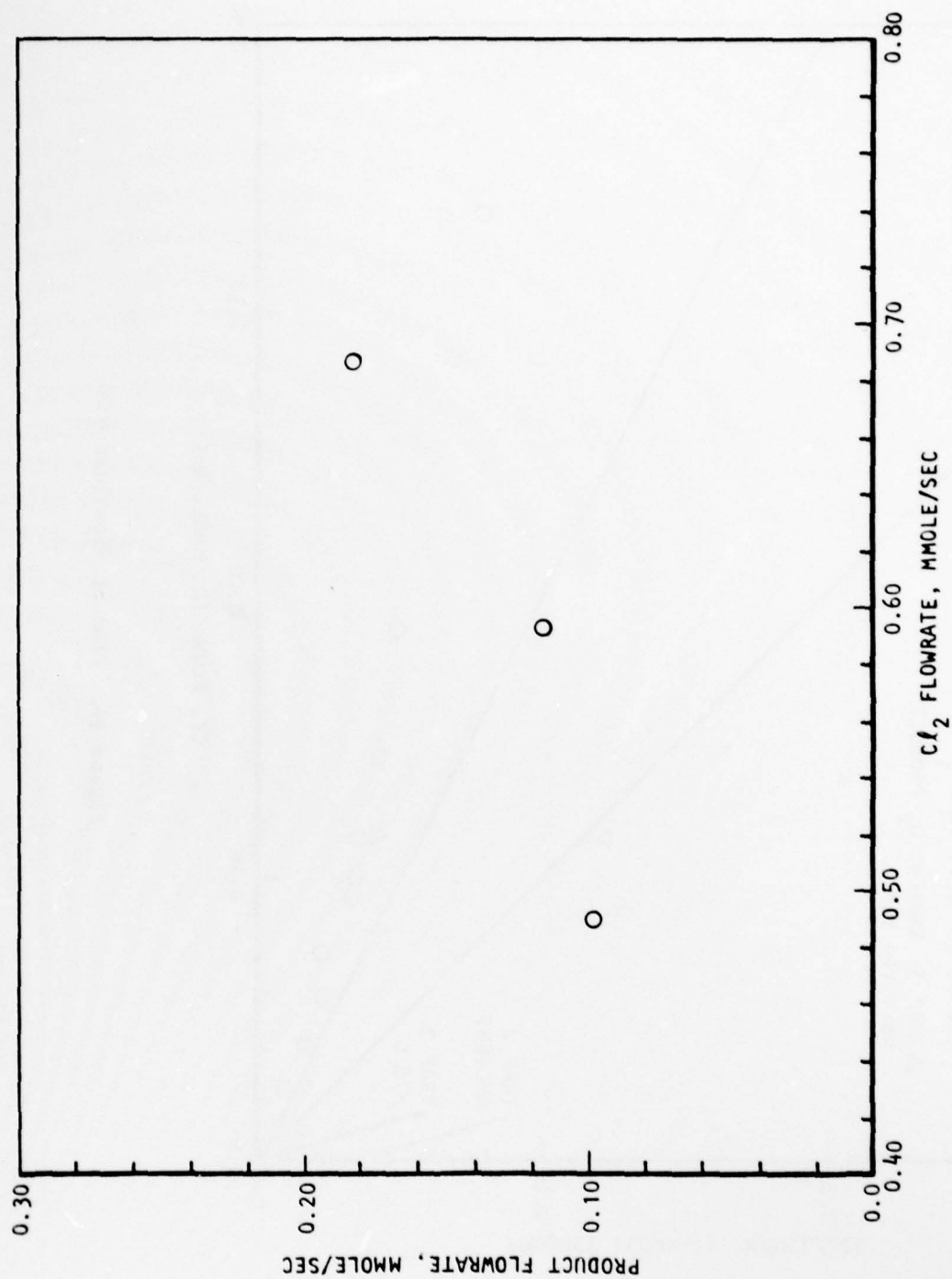


Figure 96. (Concluded)

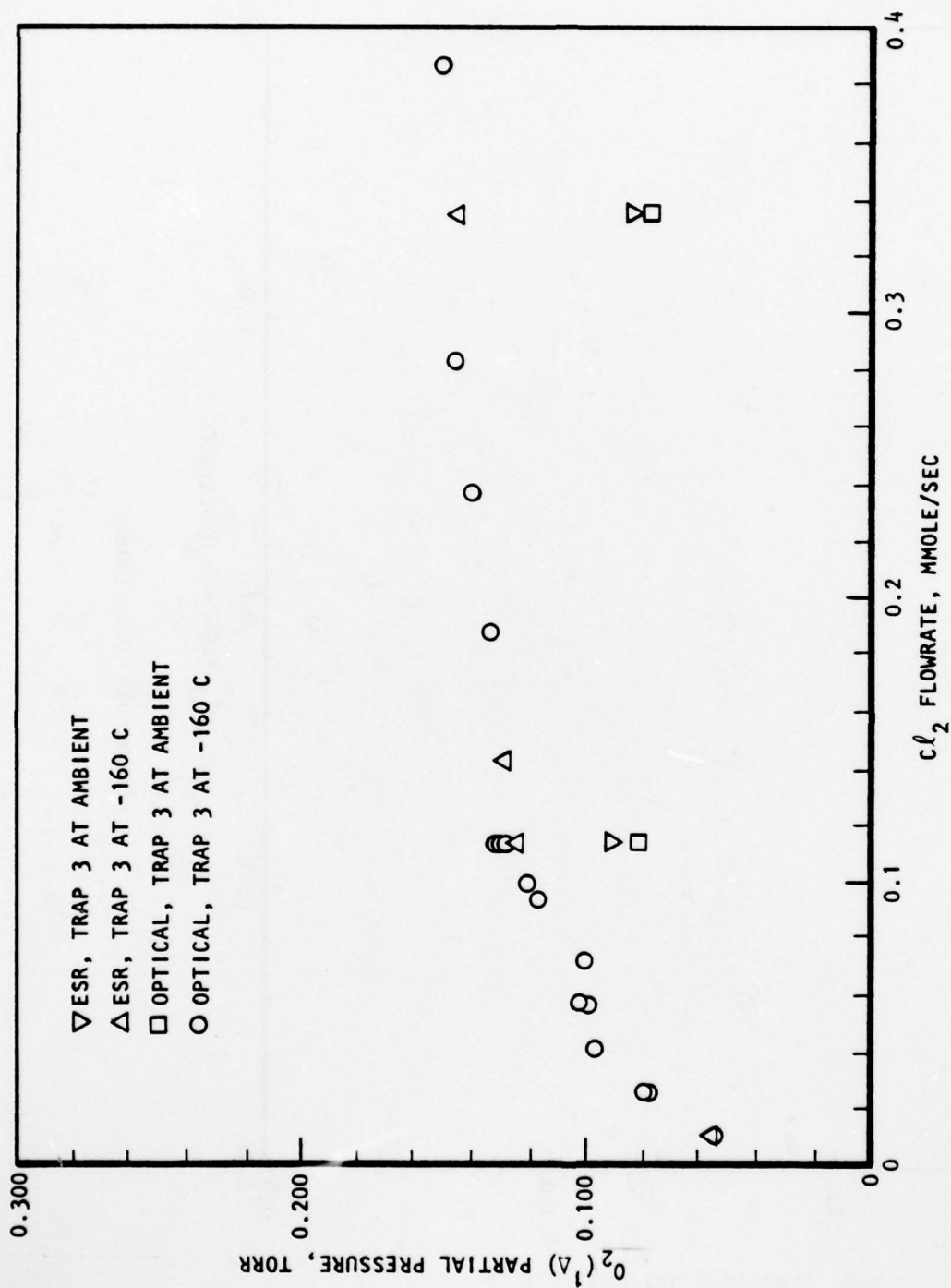


Figure 97. $O_2(^1\Delta)$ Partial Pressure at P_1 - Test 039

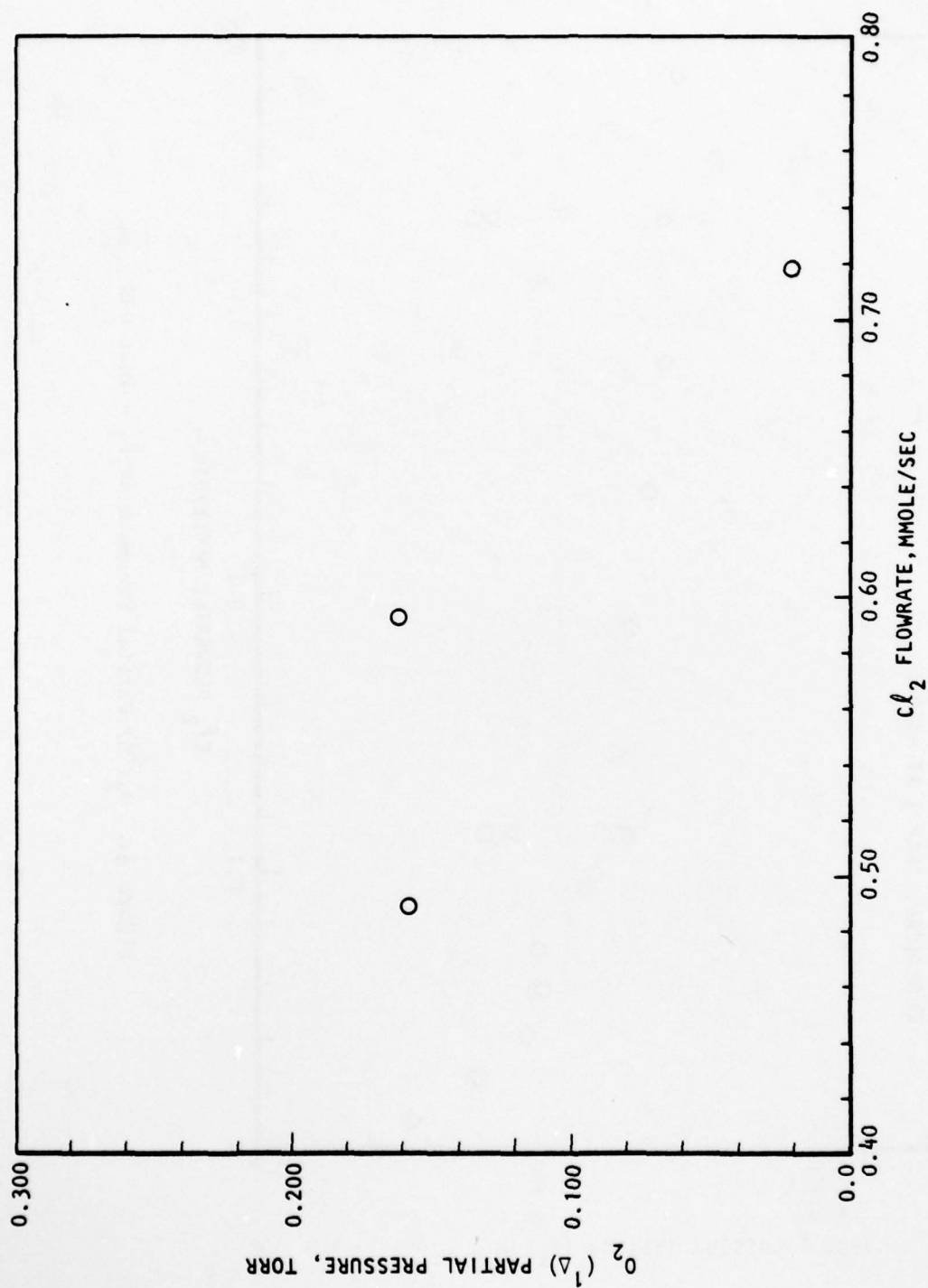


Figure 97. (Concluded)

ROLLER-DRUM REACTOR RESULTS WITH CHLORINE

As mentioned above, the early tests with CFS and basic peroxide were disappointing in $O_2(^1\Delta)$ yield. Gas phase and wall quenching of $O_2(^1\Delta)$ were suspected and experiments and experimental modifications were planned to confirm this hypothesis and to maximize $O_2(^1\Delta)$ yielding by minimizing quenching in the CFS system. It was important to know the effects of the configurational and operational changes on the production and delivery of O_2 and $O_2(^1\Delta)$ in the absence of serious quenching and to have a baseline for comparison of the CFS results. Thus, it was decided to conduct experiments in which data from both the $Cl_2 + H_2O_2/NaOH$ and CFS + $H_2O_2/NaOH$ systems were collected.

A total of 16 tests was conducted in which Cl_2 was used. In 8 of these, Cl_2 was used either before or after CFS. In the other 8, only Cl_2 was used (see Table 8). The Cl_2 -only tests provided somewhat better data both because CFS tended to contaminate the reactor and flow system with undesirable byproducts and because the Cl_2 -only tests were more complete in terms of flow range coverage rather than a few check points. In this section, data for the Cl_2 tests will be discussed in terms of correlation, trends, and interpretations.

Total Oxygen Production

To produce $O_2(^1\Delta)$ in yields compatible with efficient iodine laser operation, a generator must produce good yields of total oxygen, of which a large fraction is in the $^1\Delta$ state. The production of O_2 from Cl_2 and basic peroxide appears to yield initially only the $^1\Delta$ state, which is subsequently quenched to ground state oxygen by other processes in the reactor. Thus, to a first approximation, O_2 production and $O_2(^1\Delta)$ yield may be considered separately in evaluating generator performance. In this section, total oxygen production is considered and, in the following section, $O_2(^1\Delta)$ is considered.

The data presented above on O_2 production are in the form of plots of product flow in mmoles/sec versus Cl_2 flow in mmoles/sec. A $y = x$ line would represent stoichiometric production of O_2 or $O_2/Cl_2 = 1$. This stoichiometric yield was never achieved. The O_2/Cl_2 ratio typically was highest at low Cl_2 flows and dropped significantly at higher flows. Values as high as 0.7 at low flows under certain conditions and as low as 0.10 at high flows under other conditions were observed. The general trend of higher O_2 production at lower Cl_2 flows is consistent with the residence time in the reaction zone. In Section III, total system residence time was plotted versus molar flowrate. The residence time just in the reaction zone may be estimated from:

$$T = \left(\frac{P_o}{T_o} \times \dot{m} \times 27.421 \times 10^3 \right)^{-1} \frac{1_i A_i P_4}{T_i}$$

The pressure, P_4 , in the reaction zone is approximately $1.6 P_1$ for all flows (see Fig. 36) and P_1 is determined by \dot{m} , as in Fig. 35. The reaction zone is 10 by 0.66 by 2.54 cm for a roller-shield gap of 0.66 cm:

$$T = \left(\frac{P_o}{T_o} \times \dot{m} \times 27.421 \times 10^3 \right)^{-1} \times (10 \text{ cm}) \times (0.66 \times 2.54) \\ \times 1.6 P_1 / 290$$

The resulting residence time is plotted against \dot{m} in Fig. 98.

This residence time may be compared with the time for the molar quantity to collide with the wall in an equilibrium situation. The rate of collision of molecules with the reactive surface is given (Ref. 19) by:

$$\phi_o = \frac{P}{\sqrt{2\pi m k T}}$$

19. Reif, F. Fundamentals of Statistical and Thermal Physics, McGraw-Hill Book Company, 1965.

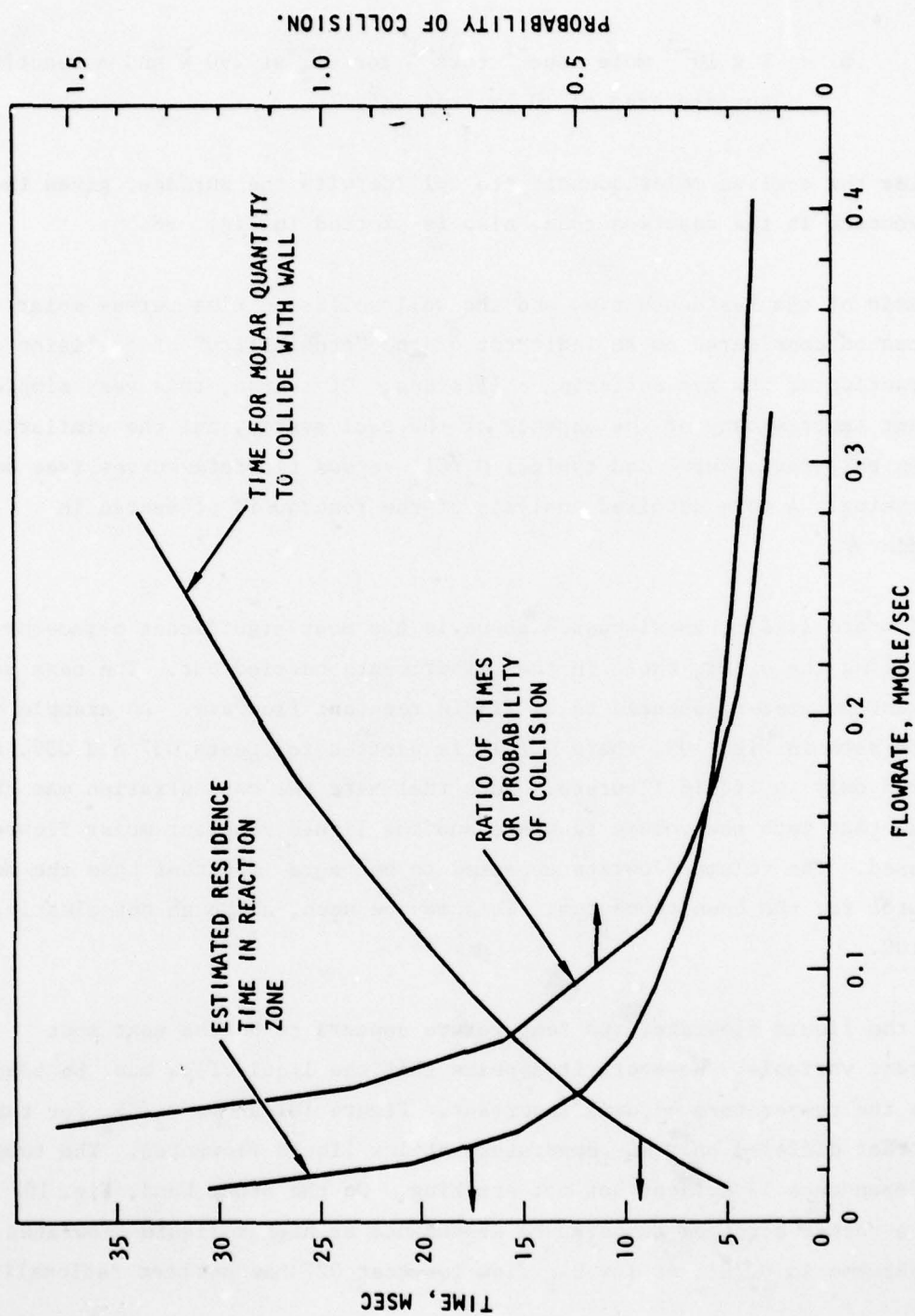


Figure 98. Simple Analysis of Reactor Collisions

$$\phi = 1 \times 10^{-2} \text{ mole sec}^{-1} \text{ torr}^{-1} \text{ for Cl}_2 \text{ at 290 K and a reactive surface area of 10 by 2.54 cm}^2.$$

The time for a given molar quantity to collide with the surface, given the \dot{m} , P dependence in the reaction zone, also is plotted in Fig. 98.

The ratio of the residence time and the wall collision time versus molar flowrate can be considered as an indicator of the "probability" of collision or the fraction of the gas suffering collisions. Of course, this very simple argument ignores many of the aspects of the real system, but the similarity between this ratio curve and typical O_2/Cl_2 versus flowrate curves (see below) is striking. A more detailed analysis of the reactor is presented in Appendix A.

Cl_2 flowrate itself, as discussed above, is the most significant parameter in controlling the O_2/Cl_2 ratio in the experiments carried out. The next most important parameter appeared to be liquid reactant flowrate. An example of this is seen in Fig. 99, where O_2/Cl_2 is plotted for tests 037 and 039, which differed only in liquid flowrate. Note that here the concentration was the same so that both the volume flowrate and the liquid reactant molar flowrate increased. The volume flowrate appeared to be more important than the molar flowrates for the conditions run. This may be seen, although not clearly, in Fig. 100.

After the liquid flowrate, the temperature appears to be the next most important variable. However, it appears that the liquid flow must be adequate before the temperature becomes important. Figure 101 shows O_2/Cl_2 for three tests that differed only in temperature at low liquid flowrates. The temperature dependence is evident but not striking. On the other hand, Fig. 102 shows a rather stronger temperature dependence at higher liquid flowrates. The decrease in O_2/Cl_2 at low Cl_2 flow for test 027 has not been rationalized.

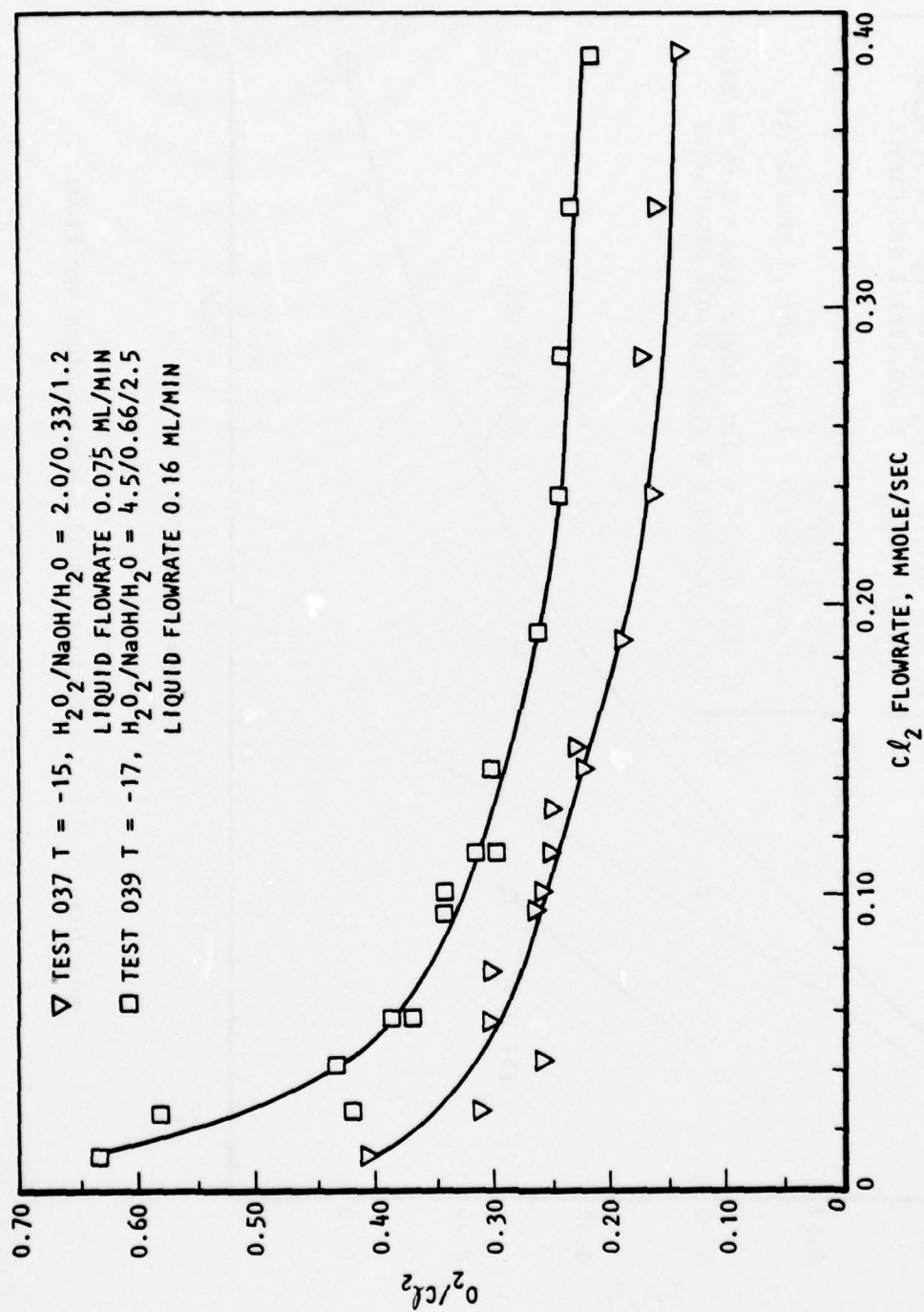


Figure 99. Effect of Liquid Flowrate on Total O_2 Production at Constant Concentration and Temperature, Configuration D.

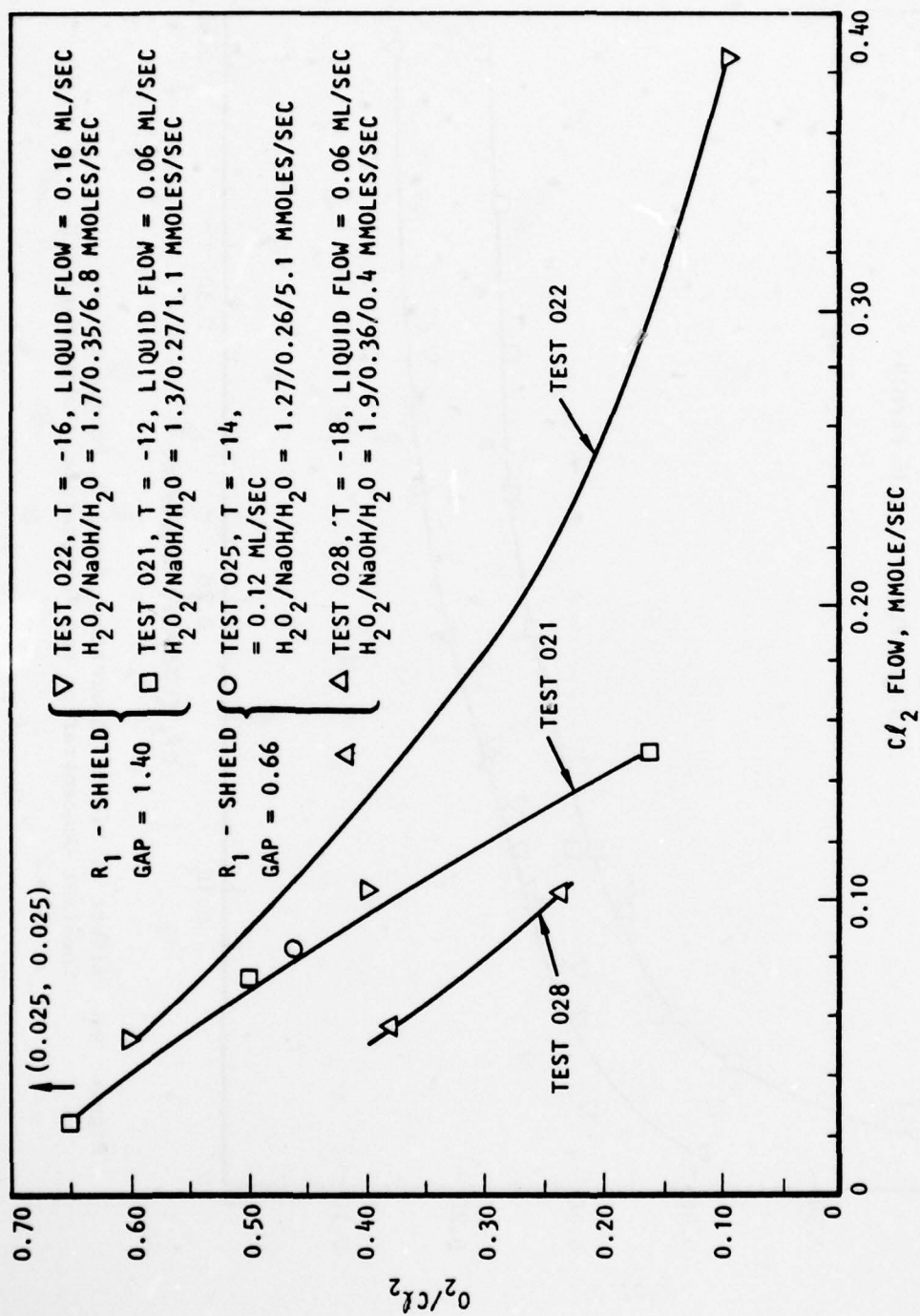


Figure 100. O_2/Cl_2 for Various Liquid Concentrations and Flows

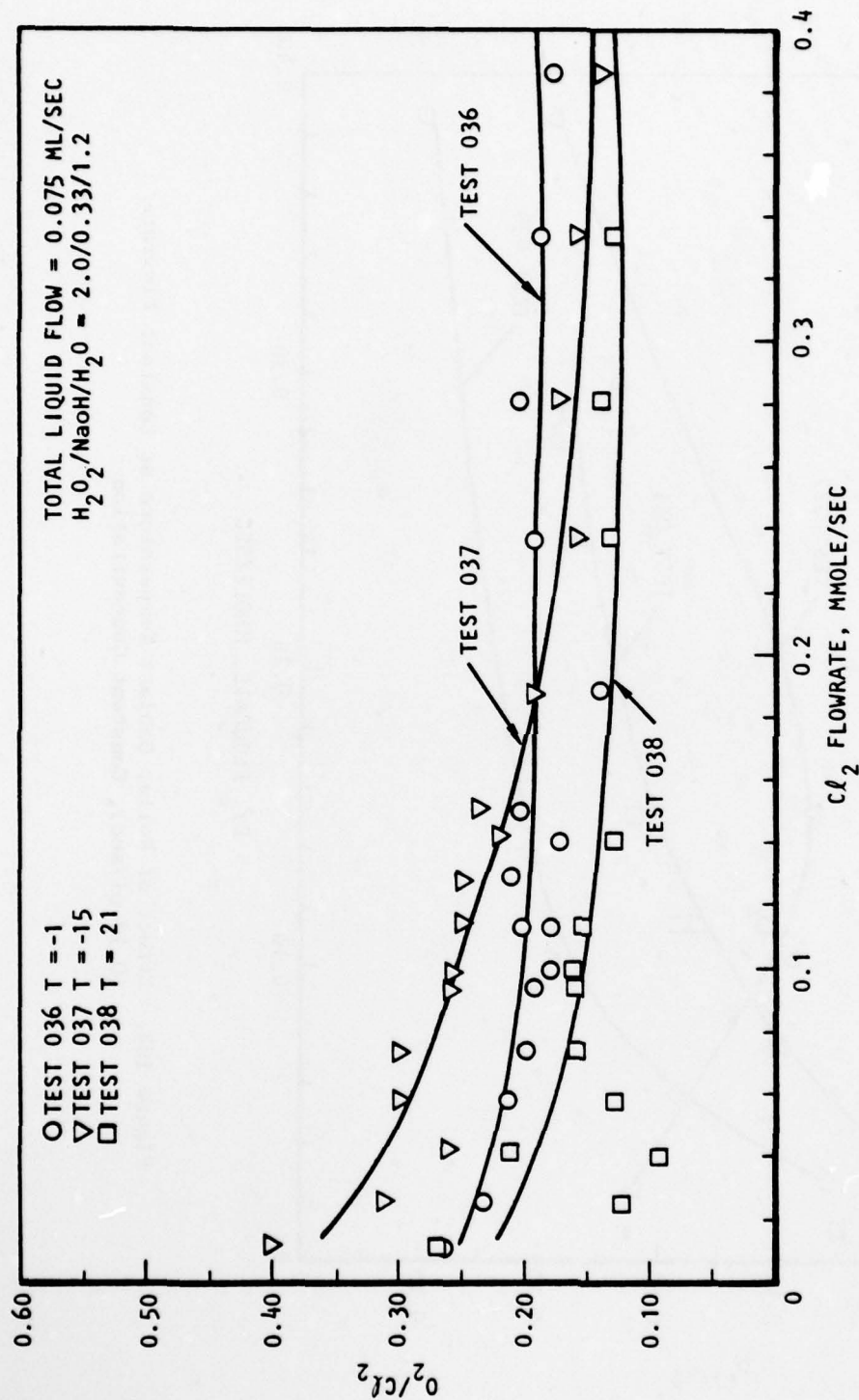


Figure 101. Effect of Roller Coolant Temperature on Total O₂ Production - Configuration D

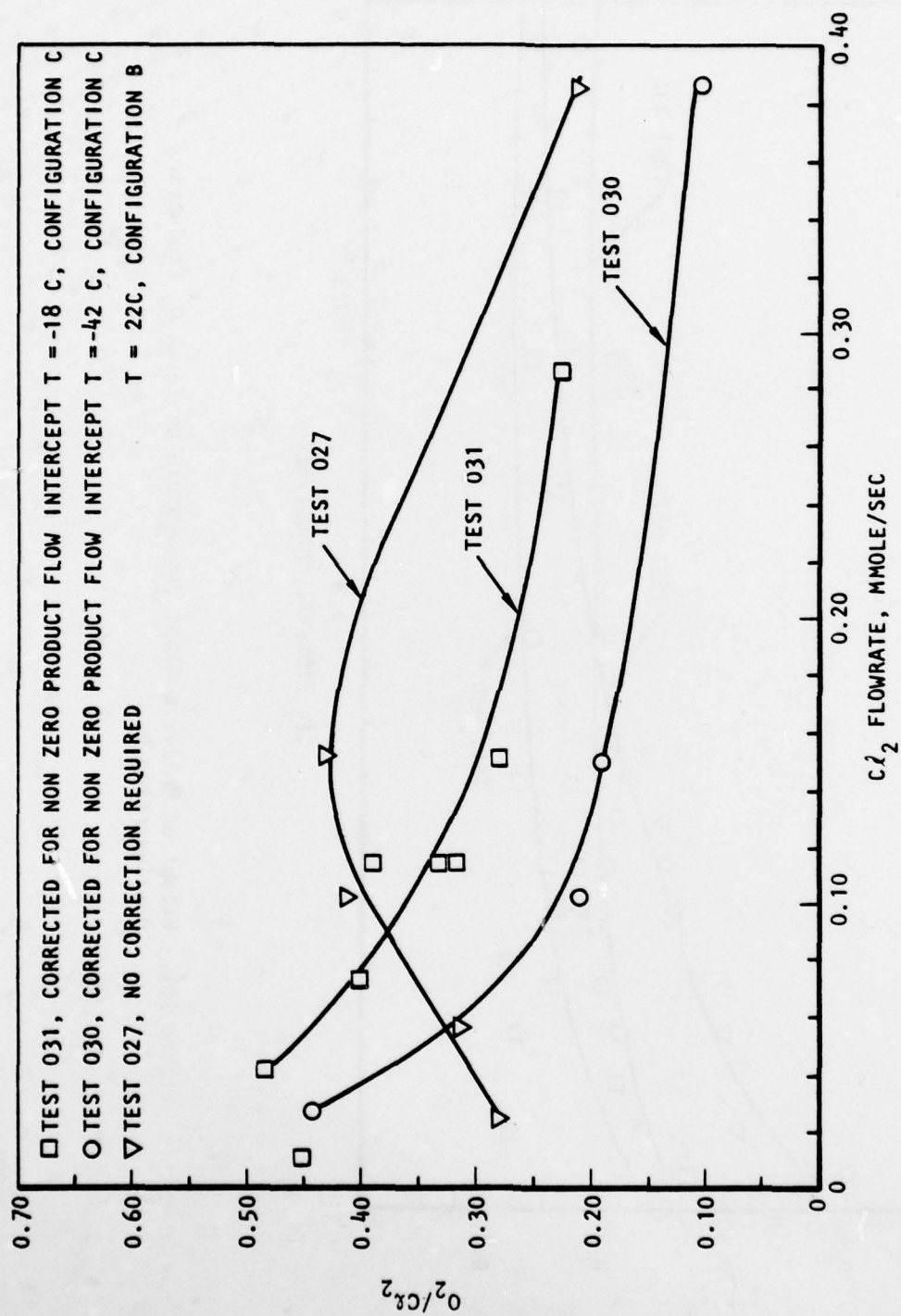


Figure 102. Effect of Roller Coolant Temperature at Constant Flowrate (0.12 ml/sec), Constant Concentration

O₂(¹Δ) Yield With Chlorine

The O₂(¹Δ) yield is taken here as the fraction of the oxygen that is in the ¹Δ state at the location of the diagnostics. The partial pressure of the excited oxygen also is discussed. These quantities are determined using the ESR spectrometer, the germanium detector optical monitor, and the P₁ manometer as described in Section III. Plots of O₂(¹Δ)/O₂ and of the partial pressure of O₂(¹Δ) for all of the tests were presented.

If the oxygen is initially all in the ¹Δ state, ground state oxygen is produced by quenching in the liquid, at the liquid surface, in the gas, or on the walls. Ground state oxygen also is produced directly by peroxide decomposition.

The operational parameter that had the most significant influence on O₂(¹Δ) yield was the Cl₂ flow at low temperatures. This may be rationalized by considering the simple analysis in the preceding paragraphs, which showed a long residence time in the reactor at these low flowrates. This long residence time allows collision of the excited O₂ with the reaction surface from which it was evolved. These collisions are a fairly strong quencher of O₂(¹Δ). This deactivation was reduced during the later chlorine-only tests because no more quenching on the reactor walls by CFS byproducts occurred. In all of the Cl₂-only tests, more or less strong peaks in O₂(¹Δ)/O₂ are observed in the vicinity of 0.1 mmole/sec Cl₂ flow. This may be a result of the tradeoff between quenching by the liquid surface at the low flows and quenching by excess Cl₂ at high flows. Best O₂(¹Δ)/O₂ values in the range 0.32 to 0.40 were typical and the absolute O₂(¹Δ) was then determined by the stronger dependences seen in O₂/Cl₂.

ROLLER-DRUM REACTOR RESULTS WITH CHLORINE FLUOROSULFATE

The major objective of this effort was to obtain good yields of O₂(¹Δ) by reacting chlorine fluorosulfate (CFS) with peroxide in the presence of base. This section describes the results of the experiments in which O₂ and O₂(¹Δ)

were produced and measured. As with Cl_2 , one can consider the production of total O_2 and the delivery of the $\text{O}_2(^1\Delta)/\text{O}_2$ separately.

Total Oxygen Production With Chlorine Fluorosulfate

CFS is a very reactive substance in comparison with Cl_2 as demonstrated, for example, in the basic chemistry experiments in which CFS was reacted with beads coated with H_2O_2 and Cl_2 was evolved and passed through the packed bed without reacting. It was this high reactivity that led to the suggestion that CFS, in spite of its relatively high molecular weight (134.5), might perform well from a system point of view. In terms of total oxygen production, the CFS performed in a way very similar to that described above for Cl_2 . In essentially all cases, the O_2/CFS was equal to or greater than the O_2/Cl_2 produced under the same conditions. The fact that CFS did not perform significantly better than Cl_2 in this regard indicates that the rate-determining steps and/or transport rates may be similar (or identical) in the two systems. All of the dependences discussed above for O_2/Cl_2 apply for O_2/CFS as well.

$\text{O}_2(^1\Delta)$ Yield With Chlorine Fluorosulfate

In contrast with the favorable comparison between CFS and Cl_2 as far as total O_2 production is concerned, good $\text{O}_2(^1\Delta)$ yield was never achieved using the CFS and basic peroxide system. Examination of the $\text{O}_2(^1\Delta)/\text{O}_2$ graphs presented earlier shows that best values in the 0.12 to 0.16 range were typical and that the yield reached its peak and fell off much more quickly with CFS flow than was the case with Cl_2 . This significant difference in behavior suggested quenching by material associated with the CFS flow. As discussed below, CFS itself, as well as its hydrolysis products, fluorosulfuric acid (FSA), sulfuric acid and, presumably, hydrofluoric acid (not tested separately for quenching, in this study), were extremely serious quenchers of $\text{O}_2(^1\Delta)$. As discussed earlier in this section, system modifications were made to transport the flow more quickly to traps for removal of quenchers. Also, reactor temperatures were reduced to lower the production and vapor pressures of the quenchers.

These changes made significant improvements in the $O_2 (^1\Delta)$ yield, compared with the initial experiments, but it remained low in an absolute sense. The poor performance is attributed to the following quenching mechanisms.

1. $O_2(a^1\Delta) + CFS \rightarrow O_2 + CFS$ vapor
2. $H_2O + CFS \rightarrow FSA + HOCl$ vapor, wall, and aerosol
3. $O_2(a^1\Delta) + HOCl \rightarrow O_2 + HOCl$ vapor
4. $FSA + H_2O \rightarrow H_2SO_4 + HF$ vapor, wall, and aerosol
5. $O_2(a^1\Delta) + HF \rightarrow O_2 + HF$ vapor
6. $O_2(a^1\Delta) + H_2SO_4 \rightarrow O_2 + H_2SO_4$ vapor, wall and aerosol

The relative importance of the quenching reactions 1, 3, 5, 6 was not established.

$O_2 (^1\Delta)$ QUENCHING EXPERIMENTS

In the course of the experimental work conducted on the contract, some experiments were carried out to evaluate the effectiveness of various gases, liquids, and solids as $O_2 (^1\Delta)$ quenchers. The experiments were all carried out on various configurations of the flow system described in Section III. Typically, microwaved oxygen was admitted to the system and a signal was established using ESR or optical detector. Then, the quenching species was admitted and the signal measured again.

The experiments were intended only to provide qualitative indication of quenching strength or comparison of relative quenching by various materials, configurations, or path lengths. Figure 103 provides a summary of the results of these experiments.

AD-A078 919

ROCKWELL INTENATIONAL CANOGA PARK CA ROCKETDYNE DIV
CHEMICALLY PUMPED IODINE LASER.(U)

F/6 20/5

SEP 79 S HURLOCK , H LAEGER , R WAGNER

F29601-78-C-0023

UNCLASSIFIED

AFWL-TR-79-52

NI

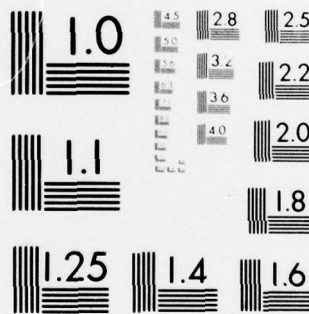
3 OF 3

AD
A078919



END
DATE
FILMED
1-80

DDC



MICROCOPY RESOLUTION TEST CHART
NATIONAL BUREAU OF STANDARDS-1963-A

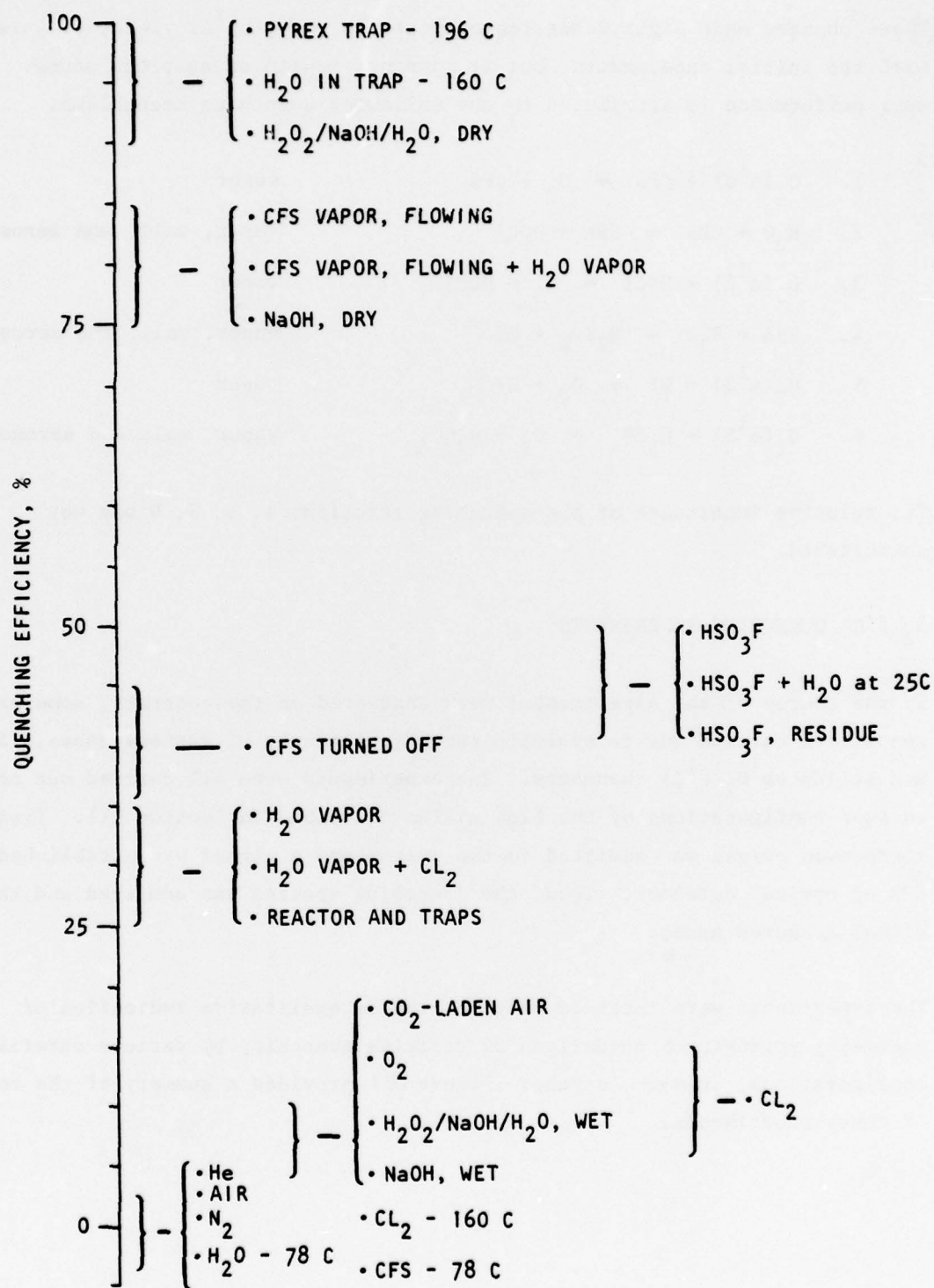


Figure 103. Qualitative Quenching Efficiencies

SECTION V

CONCLUSIONS

In the production of $O_2 (^1\Delta)$ from the reaction of chlorine fluorosulfate with 90% H_2O_2 followed by addition of base (NaOH), it appears that the active species carried from the first stage to the second stage is chlorine. The chlorine then reacts with the base and peroxide to produce $O_2 (^1\Delta)$. When CFS is reacted directly with basic peroxide, $HOOC\dot{C}l$ is the postulated intermediate and all of the oxygen may be generated in the $^1\Delta$ stage. The quenching of the excited oxygen in this system is severe and is attributed to CFS, FSA, HF, H_2SO_4 , and $HOCl$ in vapor or aerosol form. Thus, it appears that CFS is not a viable competitor to Cl_2 for $O_2 (^1\Delta)$ production.

SECTION VI - REFERENCES

1. Pritt, A. T. et al., A Chemical Singlet Molecular Oxygen Generator, Final Report, Contract No. F29601-76-0070, Rockwell International Science Center, May 1978 (AFWL-TR-77-265).
2. McDermott, W. E., N. R. Pchelkin, D. J. Benard, and R. R. Bousek, "An Electronic Transition Chemical Laser," Appl. Phys. Lett. **32** (8), 469-470 (1978).
3. Makarov, S. Z. and N. K. Grigor'eva, Bull. Acad. Sci., U.S.S.R., Div. Chem. Sci., 1955, 15.
4. Operation Instructions - Flowmeters, Manostat Bulletin 0577.
5. Goldberg, I. B. and A. J. Bard, "Analytical Applications of Electron Spin Resonance," I. M. Kolthoff, P. J. Elveng and M. M. Bursey editors, Treatise on Analytical Chemistry; Magnetic Measurements, Vol. 6, 2nd Ed., John Wiley, New York.
6. Westenberg, A. A., "Use of ESR for Quantitative Determination of Gas Phase Atom and Radical Concentrations by ESR," Prog. React. Kinetics, **7**, 23 (1973).
7. Westenberg, A. A. and N. DeHaas, "Quantitative Measurements of Gas Phase O and N Atom Concentrations by ESR," J. Chem. Phys., **40**, 3087 (1964).
8. Westenberg, A. A., "Intensity Relations for Determining Gas Phase OH, Cl, Br, I, and Free Electron Concentrations by Quantitative ESR," J. Chem. Phys., **43**, 1544 (1965).
9. Evenson, K. M. and D. S. Burch, "Use of O₂ for ESR Calibration for Quantitative Measurement of Gas Concentrations," J. Chem. Phys., **44**, 1715 (1965).
10. Goldberg, I. B., "Improving the Analytical Accuracy of Electron Spin Resonance Spectrometry," submitted to Analytical Chemistry.
11. Falick, A. M., B. H. Mahan, and R. J. Myers, "Paramagnetic Resonance of the ¹Δ_g Oxygen Molecule," J. Chem. Phys., **42**, 1837 (1965).
12. Miller, T. A., "Rotational Moment, Rotational g-Factor, Electronic Orbital g-Factors, and Anisotropy of the Magnetic Susceptibility of ¹Δ O₂," J. Chem. Phys., **53**, 909 (1971).

13. Tinkham, M. and M. W. P. Strandberg, "Theory of the Fine Structure of the Molecular Oxygen Ground State," Phys. Rev., 97, 937 (1955).
14. Tinkham, M. and M. W. P. Strandberg, "Interaction of Molecular Oxygen With a Magnetic Field," Phys. Rev., 97, 951 (1955).
15. Bowers, K. D., R. A. Kamper, and C. D. Lustig, "Paramagnetic Resonance Absorption in Molecular Oxygen," Proc. Roy. Soc. (London) A251, 565 (1959).
16. Tischer, R., "On the ESR Spectrum of Molecular Oxygen," Z. Naturforschg, A22, 1711 (1967).
17. Hendrie, J. M. and P. Kusch, "Radio-Frequency Zeeman Effect in O_2 ," Phys. Rev., 107 (1957).
18. McDermott, W. E., N. R. Pchelkin, D. J. Benard, and R. R. Bousek, "An Electronic Transition Chemical Laser," Appl. Phys. Lett. 32 (8), 469-470 (1978).
19. Reif, F., Fundamentals of Statistical and Thermal Physics, McGraw-Hill Book Company, 1965.

APPENDIX A

O_2 CONCENTRATION IN IODINE LASER REACTOR

General Discussion

The iodine laser reactor serves to generate O_2 molecules by chemical reaction of CFS gas with (liquid) basic hydrogen peroxide. The geometric configuration of the reactor can be idealized by a rectangular box as schematically illustrated below.

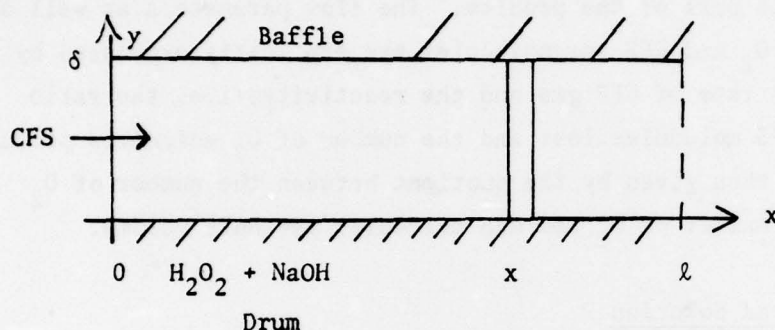


Figure A-1. Schematic of Reactor

CFS molecules enter the reactor at $x = 0$ and react with the basic peroxide that occupies a thin layer at the bottom ($y = 0$). In the course of this chemical reaction a certain percentage of all CFS molecules entering the reactor will combine with other molecules to form liquid side products and at the same time produce a certain number of O_2 molecules. These free O_2 molecules will diffuse into the main stream of CFS gas. It might be reasonable to assume that most of the free O_2 molecules can be found close to the bottom of the reactor where they have been produced. If the reaction is highly violent, however, an "orderly" diffusion process will not take place and the O_2 concentration will be approximately the same at larger distances from the bottom. It appears reasonable, therefore, to consider a mean constant number density of O_2 molecules across the reactor (in y -direction). The stoichiometric part of the problem is then reduced to determining the mean number densities of O_2 and CFS molecules at each distance x from the reactor entrance. Another problem concerns the gas flow itself, i.e., the flow of the gas mixture. Since a certain percentage of CFS gas is lost (converted into the liquid phase), and this amount of lost mass is only partially replaced by O_2 gas, the result will be a change of the flow

characteristics in terms of total pressure, density, gas speed, temperature, and the like.

The present model is based on the assumption that the number density of both O_2 and CFS molecules is only a function of the distance, x , from the reactor entrance, and that the volume occupied by liquid side products is negligibly small compared with the total reactor volume. It accounts for the fluid dynamics as well as stoichiometric part of the problem. The flow parameters as well as the number densities of O_2 and CFS gas molecules are explicitly expressed by two quantities, the loss rate of CFS gas and the reactivity, i.e., the ratio between the number of CFS molecules lost and the number of O_2 molecules produced. The O_2 concentration is then given by the quotient between the number of O_2 molecules and the total number of O_2 and CFS molecules per unit volume.

Analytical Formulation and Solution

The gas flow in the reactor is governed by the steady fluid dynamics equations relating the mean values of pressure, \bar{p} , density, $\bar{\rho}$, and gas speed, \bar{u} , as follows:

$$\frac{\partial \bar{\rho} \bar{u}}{\partial x} = 0 \quad \text{continuity} \quad (A-1a)$$

$$\bar{\rho} \bar{u} \frac{\partial \bar{u}}{\partial x} + \frac{\partial \bar{p}}{\partial x} = 0 \quad \text{momentum} \quad (A-1b)$$

$$\frac{\partial}{\partial x} \left[\frac{1}{2} \bar{u}^2 - \frac{\gamma}{\gamma-1} \frac{\bar{p}}{\bar{\rho}} \right] = 0 \quad \text{energy} \quad A-1c)$$

γ is the adiabatic exponent of the gas mixture; it may vary with x due to the varying concentrations of the constituents.

The total pressure, \bar{p} , is the sum of the partial pressure, p , of the CFS gas,

and the partial pressure, p^* , of O_2 gas. If $n(x)$ and $n^*(x)$ denote respectively the number densities of CFS and O_2 molecules at location x , the total pressure is given by

$$\bar{p}(x) = p(x) + p^*(x) = \left[n(x) + n^*(x) \right] \frac{R \cdot T(x)}{L} \quad (\text{dyn/cm}^2) \quad (\text{A-2a})$$

where $T(x)$ is the temperature prevailing at location x , R is the universal gas constant, and L is the Loschmidt number, i.e. the number of molecules per cm^3 .

$$R = 8.3143 \times 10^7 \quad (\text{erg/mole } ^\circ\text{K})$$

$$L = 6.023 \times 10^{23} \quad (\text{mole}^{-1})$$

The mean density, $\bar{\rho}$, is given by

$$\bar{\rho}(x) = \mu \cdot n(x) + \mu^* \cdot n^*(x) \quad (\text{gr/cm}^3) \quad (\text{A-2b})$$

where μ and μ^* denote respectively the mass of one CFS molecule and one O_2 molecule:

$$\mu = \frac{134.5}{L} \quad (\text{gr})$$

$$\mu^* = \frac{32.0}{L} \quad (\text{gr})$$

Integration of the fluid dynamics equations (1a) - (1c) yields:

$$\bar{\rho} \bar{u} = \bar{\rho}_0 \bar{u}_0 = \text{constant} \quad (\text{A-3a})$$

$$\bar{\rho} \bar{u}^2 + \bar{p} = \bar{\rho}_0 u_0^2 + \bar{p}_0 = \text{constant} \quad (\text{A-3b})$$

$$\frac{1}{2} u^2 + \frac{\gamma}{\gamma-1} \cdot \frac{\bar{p}}{\bar{\rho}} = \frac{1}{2} u_0^2 + \frac{\gamma}{\gamma-1} \cdot \frac{\bar{p}_0}{\bar{\rho}_0} = \text{constant} \quad (\text{A-3c})$$

Here, the subscript o denotes the initial values of the particular variable at the reactor entrance $x = 0$. It is assumed that the O_2 concentration at the reactor entrance vanishes, i.e., that

$$n^*(0) = 0 \quad (A-4)$$

From equations (A-2a) and (A-2b) one obtains then

$$\bar{p}_o = p_o = n_o \cdot \frac{R}{L} \cdot T_o \quad (A-5a)$$

$$\bar{\rho}_o = \rho_o = \mu \cdot n_o \quad (A-5b)$$

with T_o being the entrance temperature.

It is convenient to use the following dimensionless quantities:

$$N(x) = \frac{n(x)}{n_o}$$

$$N^*(x) = \frac{n^*(x)}{n_o} \quad (A-6)$$

$$\tau(x) = \frac{T(x)}{T_o}$$

With the dimensionless constants

$$\lambda = \frac{\mu^*}{\mu}, \quad \sigma = \frac{\rho_o u_o^2}{p_o} \quad (A-7)$$

one obtains from equations (A-2a), (A-2b) and (A-3a) the following relations:

$$\bar{p}(x) = p_o \left[N(x) + N^*(x) \right] \cdot \tau(x) \quad (A-8a)$$

$$\bar{p}(x) = p_0 \left[N(x) + \lambda \cdot N^*(x) \right] \quad (A-8b)$$

$$\bar{u}(x) = u_0 \cdot \frac{1}{N(x) + \lambda N^*(x)} \quad (A-8c)$$

Inserting these expressions into equation (A3-b), it follows that N , N^* , and τ are restricted by the algebraic condition

$$\left[N(x) + \lambda N^*(x) \right] \{ (1 + \sigma) - \left[N(x) + N^*(x) \right] \tau(x) \} = \sigma \quad (A-8d)$$

Equation (A-3c) yields

$$\frac{\gamma(x)}{\gamma(x)-1} = \frac{N(x) + \lambda N^*(x)}{\left[N(x) + N^*(x) \right] \tau(x)} \left\{ \frac{\sigma}{2} \left[1 - \left(\frac{1}{N(x) + \lambda N^*(x)} \right)^2 \right] + \frac{\gamma_0}{\gamma_0 - 1} \right\} \quad (A-8e)$$

where γ_0 is the adiabatic constant of the pure CFS gas. The O_2 concentration, $c(x)$, is by definition

$$c(x) = \frac{n^*(x)}{n(x) + n^*(x)} = \frac{N^*(x)}{N(x) + N^*(x)} \quad (A-8f)$$

Equations (A-8a) - (A-8f) constitute the solution to the overall problem. The variables \bar{p} , $\bar{\rho}$, \bar{u} , γ and c are expressed in terms of the three thermodynamic variables N , N^* , and τ . They are subject to only one constraint expressed in equation (A-8d). The initial conditions follow from equations (A-4) and (A-6):

$$N(0) = 1, \quad N^*(0) = 0, \quad \tau(0) = 1 \quad (A-9)$$

Two additional equations are required to specify the three quantities $N(x)$, $N^*(x)$, and $\tau(x)$ as functions of x . These equations should describe the stoichiometric part of the reaction problem, i.e., the loss of CFS molecules and the gain of O_2 molecules at different locations x . Let it be assumed

that at the location x on the average α CFS molecules per cm^3 are lost and β O_2 molecules per cm^3 are generated. Hence, within the interval x and $x + dx$, the number densities of CFS and O_2 molecules are respectively:

$$n(x + dx) - n(x) = -\alpha(x)dx = \frac{dn(x)}{dx} dx$$

$$n^*(x+dx) - n^*(x) = \beta(x)dx = \frac{dn^*(x)}{dx} dx$$

It follows from equation (A-6) that

$$\frac{dN(x)}{dx} = -n_0 \cdot \alpha(x) \quad (\text{A-10})$$

$$\frac{dN^*(x)}{dx} = n_0 \cdot \beta(x)$$

Equation (A-10) yields

$$\frac{dN(x)}{dx} + r(x) \cdot \frac{dN^*}{dx} = 0 \quad (\text{A-11})$$

where $r(x) = \alpha(x)/\beta(x)$ is the reactivity of CFS and $\text{H}_2\text{O}_2 + \text{NaOH}$, i.e., the ratio between the number of CFS molecules lost and the number of O_2 molecules produced. If the reactivity as a function of x is known, equation (A-11) serves as a second equation for determining the three functions N , N^* , and τ . As a third equation one of the two equations (A-10) could be used if the rates $\alpha(x)$ or $\beta(x)$ were known. It should be pointed out that if one of the flow variables \bar{p} , $\bar{\rho}$, or \bar{u} remains constant - which would constitute a third

condition on N , N^* , and τ - the flow is entirely constant and the O_2 concentration is undetermined. This fact can be shown as follows:

assume that \bar{p} is constant, i.e. according to equation (A-8a)

$$\left[N(x) + N^*(x) \right] \cdot \tau(x) = \text{constant} = 1$$

Inserting this condition into equation (8d) yields

$$N(x) + \lambda N^*(x) = 1$$

Differentiating with respect to x gives

$$\frac{dN}{dx} + \lambda \frac{dN^*}{dx} = 0$$

Comparing this equation with condition (A-11) yields $r = \lambda = u^*/u$, i.e. the reactivity is equal to the ratio between the molecular weights of O_2 and CFS. In other words, to produce $\cdot L = 134.5$ molecules O_2 requires $u^* \cdot L = 32$ molecules CFS. In reality, however, more CFS molecules are lost than O_2 molecules are generated by this chemical reaction. This means that $r \geq 1$.

Continuing the discussion of constant pressure, we insert the equations $N + \lambda N^* = 1$ and $(N + N^*)\tau = 1$ into equations (A-8b), (A-8c) and (A-8e) and find that the flow variables \bar{O} , \bar{u} , as well as the adiabatic exponent γ remain also constant. Equation (A-8f) for the O_2 concentration assumes the form after replacing N^* by $(1-N)/\lambda$:

$$c(x) = \frac{1-N(x)}{1+(\lambda-1)N(x)}$$

Hence, the O_2 concentration is still undetermined since $N(x)$ is not specified. The same result is obtained if any other variable \bar{p} , \bar{u} , or γ is assumed to remain constant.

In order to derive the third equation in question, we argue as follows: the loss of CFS molecules in the interval between x and $x + dx$ is proportional to the number of CFS molecules in that interval, i.e. the more molecules are present the more will be lost. Hence,

$$\frac{dN(x)}{dx} \sim N(x)$$

This proportionality relation is expressed by the equation

$$\frac{dN(x)}{dx} = -s(x) \cdot N(x) \quad (A-12)$$

where $s(x)$ is the loss rate. The negative sign signifies the loss. Equations (A-11) and (A-12) can now be integrated to yield the two functions $N(x)$ and $N^*(x)$ in terms of $r(x)$ and $s(x)$:

$$N(x) = \exp\left(-\int_0^x s(\xi) d\xi\right) \quad (A-13)$$

$$N^*(x) = \int_0^x \frac{s(\eta)}{r(\eta)} \left[\exp\left(-\int_0^\eta s(\xi) d\xi\right) \right] d\eta$$

Equations (A-8a) - (A-8e) serve to determine the functions \bar{p} , $\bar{\rho}$, \bar{u} , τ , and γ , while equations (A-8f) determines the desired O_2 concentration.

Application

For the application of the precedent theory to the roller drum reactor it might be sufficient to use mean values for the reactivity and the loss rate.

$$\bar{r} = \frac{1}{\ell} \int_0^{\ell} r(\xi) d\xi \quad (\text{A-14})$$

$$\bar{s} = \frac{1}{\ell} \int_0^{\ell} s(\xi) d\xi$$

Here, ℓ is the length of the reactor. Using these constant mean values for r and s in equations (A-13), the relative number densities are obtained as

$$\begin{aligned} N(x) &= \exp(-\bar{s} \cdot x) \\ N^*(x) &= \frac{1}{\bar{r}} \left[1 - \exp(-\bar{s} \cdot x) \right] \end{aligned} \quad (\text{A-15})$$

The constants \bar{r} and \bar{s} can be determined experimentally by measuring the total pressure and the temperature at some location $x = x_1 > 0$. Let

$$\begin{aligned} \bar{p}(x_1) &= p_1, \quad T(x_1) = T_1 = T_o \cdot \tau_1 \\ N(x_1) &= N_1 = \exp(-\bar{s} \cdot x_1) \\ N^*(x_1) &= N_1^* = \frac{1}{\bar{r}} \left[1 - \exp(-\bar{s} \cdot x_1) \right] \end{aligned} \quad (\text{A-16})$$

Equations (A-8a) and (A-8e) yield respectively

$$N_1 + N_1^* = \frac{p_1 \cdot T_o}{p_o \cdot T_1} \quad (\text{A-17})$$

$$N_1 + \lambda N_1^* = \frac{\sigma}{1 + \sigma - \frac{p_1}{p_o}} = \frac{\rho_o u_o^2}{p_o - p_1 + \rho_o u_o^2}$$

Hence:

$$N_1 = \frac{1}{1-\lambda} \left[\frac{\rho_o u_o^2}{p_o - p_1 + \rho_o u_o^2} - \frac{\lambda p_1 T_o}{p_o T_1} \right] = \exp(-\bar{s} x_1) \quad (A-18)$$

$$N_1^* = \frac{1}{1-\lambda} \left[\frac{p_1 T_o}{p_o T_1} - \frac{\rho_o u_o^2}{p_o - p_1 + \rho_o u_o^2} \right] = \frac{1}{\bar{r}} \left[1 - \exp(-\bar{s} x_1) \right]$$

i.e., N_1 and N_1^* are expressed in terms of p_o , ρ_o , u_o , T_o , p_1 , T_1 , and λ .

The mean values \bar{r} and \bar{s} are explicitly obtained as

$$\bar{r} = \frac{1-N_1}{N_1^*}, \quad \bar{s} = - \frac{1}{x_1} \ln N_1 \quad (A-19)$$

The O_2 concentration inside the reactor at any location x is finally given by

$$c(x) = \frac{1 - \exp(-\bar{s}x)}{1 + (\bar{r}-1) \exp(-\bar{s}x)} \quad (A-20)$$

We note that the mean values \bar{r} and \bar{s} are ultimately expressed by the entrance conditions p_o , ρ_o , u_o , and T_o of the CFS gas at $x = 0$, the pressure p_1 and temperature T_1 at some interior location $x - x_1 > 0$, and the ratio of the molecular weights, λ , of O_2 and CFS. As long as no experimental data are available for p_1 and T_1 , it appears reasonable to discuss the O_2 concentration $c(x)$ over a range of pressure variations $\Delta p = p_1 - p_o$ and temperature variations $\Delta T = T_1 - T_o$. The question arises

as to selecting positive or negative increments Δp and ΔT , corresponding to a rise or drop in pressure and temperature in downstream direction. This question can be answered by the following argumentation: the nature of the reacting mechanism implies that the CFS concentration is maximal at the entrance and decreases due to the loss of molecules. Hence, $N(x)$ decreases from 1 to a lower (positive) value. Equation (A-19) shows that for $N_1 < 1$ the mean value \bar{s} is positive. Since r denotes the mean reaction rate, the condition $\bar{r} \geq 1$ means that the number of lost CFS molecules is greater than or equal to the number of produced O_2 molecules. Equation (A-19) yields for $\bar{r} \geq 1$ that

$$N_1 + N_1^* \leq 1$$

Using this condition in equation (A-17) one obtains the first condition on P_1 and T_1 :

$$\frac{P_1 \cdot T_0}{P_0 \cdot T_1} \leq 1, \quad \frac{P_1}{P_0} \leq \frac{T_1}{T_0} \quad (A-21)$$

Since $\lambda = 32/134.5 < 1$, the second equation (A-17) leads to

$$N_1 + \lambda N_1^* \leq N_1 + N_1^* \leq 1$$

$$\text{or } N_1 + N_1^* - (1-\lambda)N_1^* \leq 1$$

$$N_1 + N_1^* = \frac{P_1 T_0}{P_0 T_1} \leq 1 + (1-\lambda)N_1^*$$

Using here the second equation of (A-18) yields

$$\frac{p_1 T_o}{p_o T_1} \leq 1 + \frac{p_1 T_o}{p_o T_1} - \frac{\rho_o u_o^2}{p_o - p_1 + \rho_o u_o^2}$$

or

$$p_o - p_1 + \rho_o u_o^2 \geq \rho_o u_o^2$$

$$p_o - p_1 \geq 0 \quad (A-22)$$

i.e. the total pressure drops from p_o to some terminal value $p_1 < p_o$ inside the reactor. Equations (A-20) and (A-21) answer the question as to the pressure and temperature variations inside the reactor:

$$\Delta p = p_1 - p_o \leq 0$$

$$\Delta T = T_1 - T_o \geq \frac{T_o}{p_o} \cdot \Delta p \quad (A-23)$$

While the pressure always stays below the entrance pressure, the temperature always stays above the lowest value T^* which is given by

$$T^* = T_o \cdot \frac{p_{\min}}{p_o}$$

where p_{\min} denotes the lowest pressure at some interior point of the reactor.

The O_2 concentration can now be determined for a range of parameter values Δp and ΔT . The result depends also on the entrance data which are chosen as follows:

$$T_o = 300 \text{ K}$$

$$p_o = 2 \text{ Torr} = 2.6679 \times 10^3 \text{ dyn/cm}^2$$

$$\dot{w} = 0.5 \text{ cm}^3/\text{min} = \frac{0.5}{60} \text{ cm}^3/\text{sec} \quad \text{volumetric flow of liquid CFS}$$

$$k = 1.7 \text{ gr/cm}^3 \text{ specific weight of liquid CFS}$$

$$m = 134.5 \text{ gr/mole} \quad \text{molecular weight of CFS}$$

$$V_m |_{T_o, p_o} = \frac{2.2414 \times 10^4 \times 760 \times T_o}{273.155 \times p_o} \text{ cm}^3 \quad 1 \text{ mole}$$

$$\rho_o = \frac{m}{V_m |_{T_o, p_o}} = 1.4378 \times 10^{-5} \text{ gr/cm}^3 \quad \text{density of CFS gas}$$

$$A = 2.54 \times \delta \text{ cm}^2 \quad \text{cross section of reactor}$$

$$\delta \text{ cm} \quad \text{height of reactor}$$

$$u_o = \frac{\dot{w} \times k}{\rho_o \times A} = 3.8791 \times 10^2 / \delta \text{ cm/sec} \quad \text{gas flow speed}$$

$$\sigma = \frac{\rho_o u_o^2}{p_o} = 8.1095 \times 10^{-4} / \delta^2$$

$$l = 7.62 \text{ cm} \quad \text{reactor length}$$

Choosing the point $x = x_1$ at the reactor exit, i.e. $x_1 = \ell$, the quantities p_1 and T_1 simply denote the exit pressure and temperature, respectively. Equations (18) yield then the relations between \bar{r} and \bar{s} in terms of the entrance conditions p_0, T_0, u_0 , the exit conditions p_1, T_1 , the ratio of the molecular weights λ , and the reactor length ℓ . It is convenient to use dimensionless quantities as follows:

$$\alpha = \frac{p_1}{p_0}, \quad \beta = \frac{T_1}{T_0}, \quad \sigma = \frac{\rho_0 u_0^2}{p_0} \quad (\text{A-24})$$

Equations (A-18) they yield

$$\bar{r} = \frac{\left| (1-\lambda) \beta + \lambda \alpha \right| (1 + \sigma - \alpha) - \sigma \beta}{\alpha (1 + \sigma - \alpha) - \sigma \beta} \quad (\text{A-25})$$

$$\bar{s} = - \frac{1}{\ell} \ln \left\{ \frac{\sigma \beta - \lambda \alpha (1 + \sigma - \alpha)}{(1-\lambda) (1 + \sigma - \alpha) \beta} \right\}$$

The O_2 concentration at the reactor exit can then as well be expressed in terms of the entrance and exit conditions: it is by definition

$$c_1 = \frac{N_1^*}{N_1 + N_1^*}$$

By virtue of equations (A-18) one obtains

$$c_1 = \left(\frac{1}{1-\lambda} \right) \cdot \frac{\left| \alpha (1 + \sigma - \alpha) - \sigma \beta \right|}{\alpha (1 + \sigma - \alpha)} \quad (\text{A-26})$$

The range of the parameters α and β can be determined from equations (24) and (25) if \bar{r} , \bar{s} and c_1 are restricted to the obvious conditions

$$\bar{r} \geq 1, \quad \bar{s} \geq 0, \quad 0 \leq c_1 \leq 1$$

We obtain in particular:

$$\bar{r} \geq 1: \quad (1 - \lambda) (\beta - \alpha) (1 + \sigma - \alpha) \geq 0$$

$$\bar{s} \geq 0: \quad (1 - \lambda) \beta + \lambda \alpha (1 + \sigma - \alpha) \geq \sigma \beta$$

$$c_1 \geq 0: \quad \alpha(1 + \sigma - \alpha) \geq \sigma \beta$$

$$\alpha (1 + \sigma - \alpha) \geq 0$$

(A-27)

$$c_1 \leq 1: \quad \lambda \alpha (1 + \sigma - \alpha) \leq \sigma \beta$$

Since α , β , λ and σ are all nonnegative, and since $\lambda < 1$, the condition $\bar{r} \geq 1$ yields

$$\beta \geq \alpha, \quad \alpha \leq 1 + \sigma$$

With this the first inequality for $c_1 \geq 0$ can be written as

$$\alpha(1 + \sigma - \alpha) \geq \sigma \beta \geq \sigma \alpha$$

Hence:

$$\alpha(1 + \sigma - \alpha) \geq \sigma \alpha$$

or

$$\alpha \leq 1$$

That is, the exit pressure does not exceed the entrance pressure. The result

$$\frac{p_1}{p_0} = \alpha \leq 1, \quad \frac{T_1}{T_0} = \beta \geq \alpha = \frac{p_1}{p_0} \quad (\text{A-28})$$

is identical with the findings in equations (A-20) and (A-21). The remaining inequalities in equations (A-26) are either satisfied by the results in equation (A-27) or lead to a refinement of the particular ranges for α and β .

In equation (A-25) the O_2 concentration at the reactor exit is explicitly expressed in terms of the entrance and exit conditions as well as the ratio of the molecular weights. In discussing this functional relation it is convenient to consider α and β as Cartesian coordinates and determine the lines of constant concentration, i.e., the isoconcentration lines $c_1 = \text{constant}$. Equation (A-25) when solved for β , yields

$$\beta = \left[\frac{1 - c_1(1 - \lambda)}{\sigma} \right] \cdot \alpha \cdot (1 + \sigma - \alpha) \quad (\text{A-29})$$

The lines $c_1 = \text{constant}$ obviously represent parabolas as displayed in Fig. A-2a - A-2d. These lines continue into the domain of (α, β) where $\beta = T_1/T_0$ is smaller than $\alpha = p_1/p_0$. In this domain, however, the condition that the reactivity \bar{r} is greater than unity would be violated (Eq. A-27). For example, if for a reactor height of $\delta = 1.0$ cm the exit pressure is 99.8% of the entrance pressure, and the exit temperature is 148.2% of the entrance temperature, the O_2 concentration at the exit would be 75% (Fig. A-2c and A-2d). The exit conditions $(\alpha, \beta) = (0.998, 1.482)$ correspond, according to equations (A-24), to a mean reactivity of approx. $\bar{r} = 1.647$ and a mean loss rate of approx. $\bar{s} = 0.2337 \text{ (cm}^{-1}\text{)}$ taken over the total reactor length $\ell = 7.62$ cm.

If the two stoichiometric parameters \bar{r} and \bar{s} were known, the O_2 concentration at the reactor exit could be determined more conveniently from these two quantities. Equation (A-20) yields for $x = \ell$:

$$c(\ell) = c_1 = \frac{1 - \exp(-\bar{s} \cdot \ell)}{1 + (\bar{r} - 1) \exp(-\bar{s} \cdot \ell)} \quad (\text{A-30})$$

The isoconcentration lines are obtained as

$$\bar{r} = \left(\frac{1-c_1}{c_1} \right) \left[\exp(+\bar{s} \cdot \ell) - 1 \right] \quad (\text{A-31})$$

They are simply exponential curves in the \bar{r}, \bar{s} - domain (Fig. A-3). The advantage of this representation is that it does not involve explicitly any initial conditions or any other parameter such as the reactor height, ratio of the molecular weights, and the like. Fig. A-3 displays the lines of constant O_2 concentrations at the reactor exit as functions of \bar{r} and \bar{s} . For example, for a mean loss rate of 0.4 per cm and a mean reactivity of 8.6 the O_2 concentration at the reactor exit is 70%.

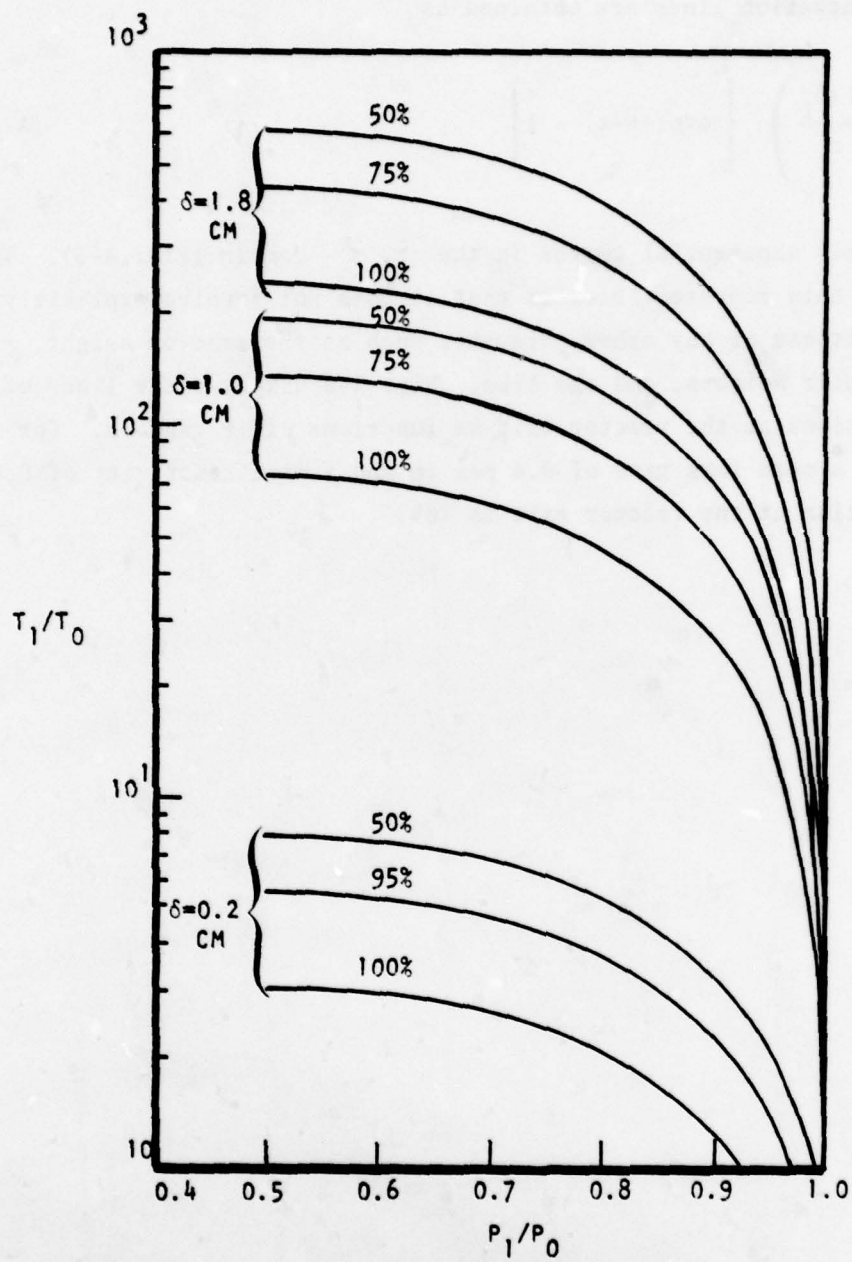


Figure A-2a. Isoconcentration Lines

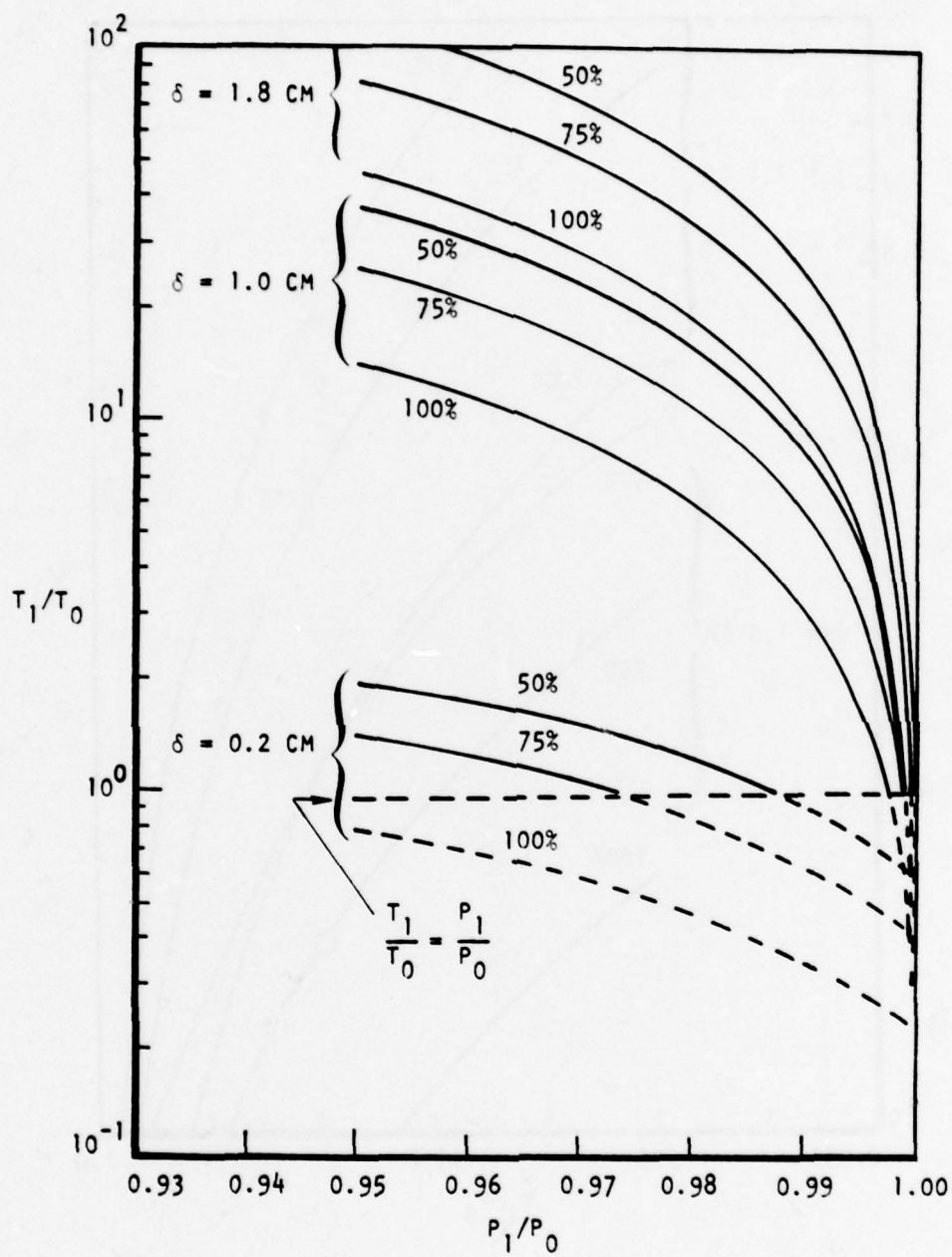


Figure A-2b. Isoconcentration Lines

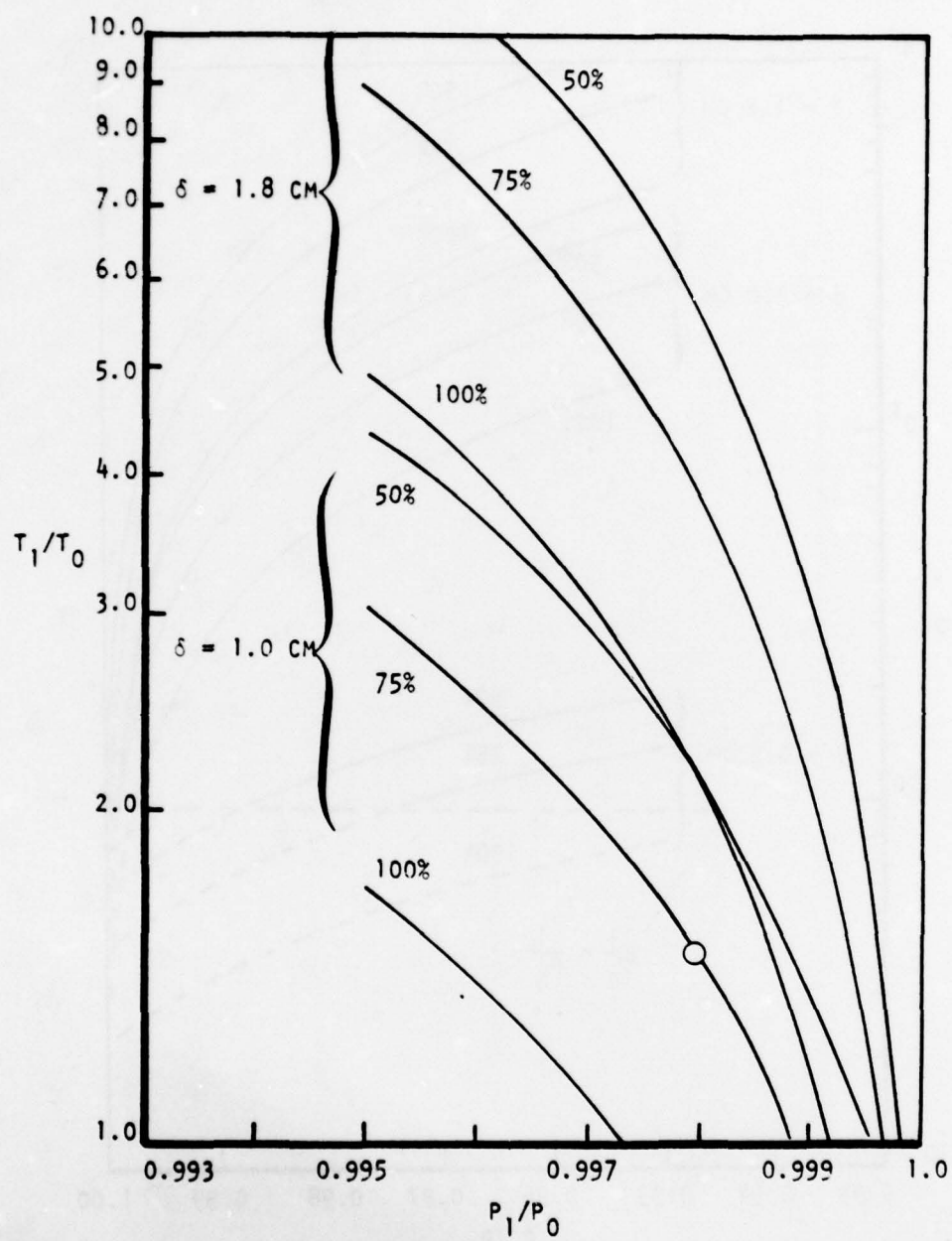


Figure A-2c. Isoconcentration Lines

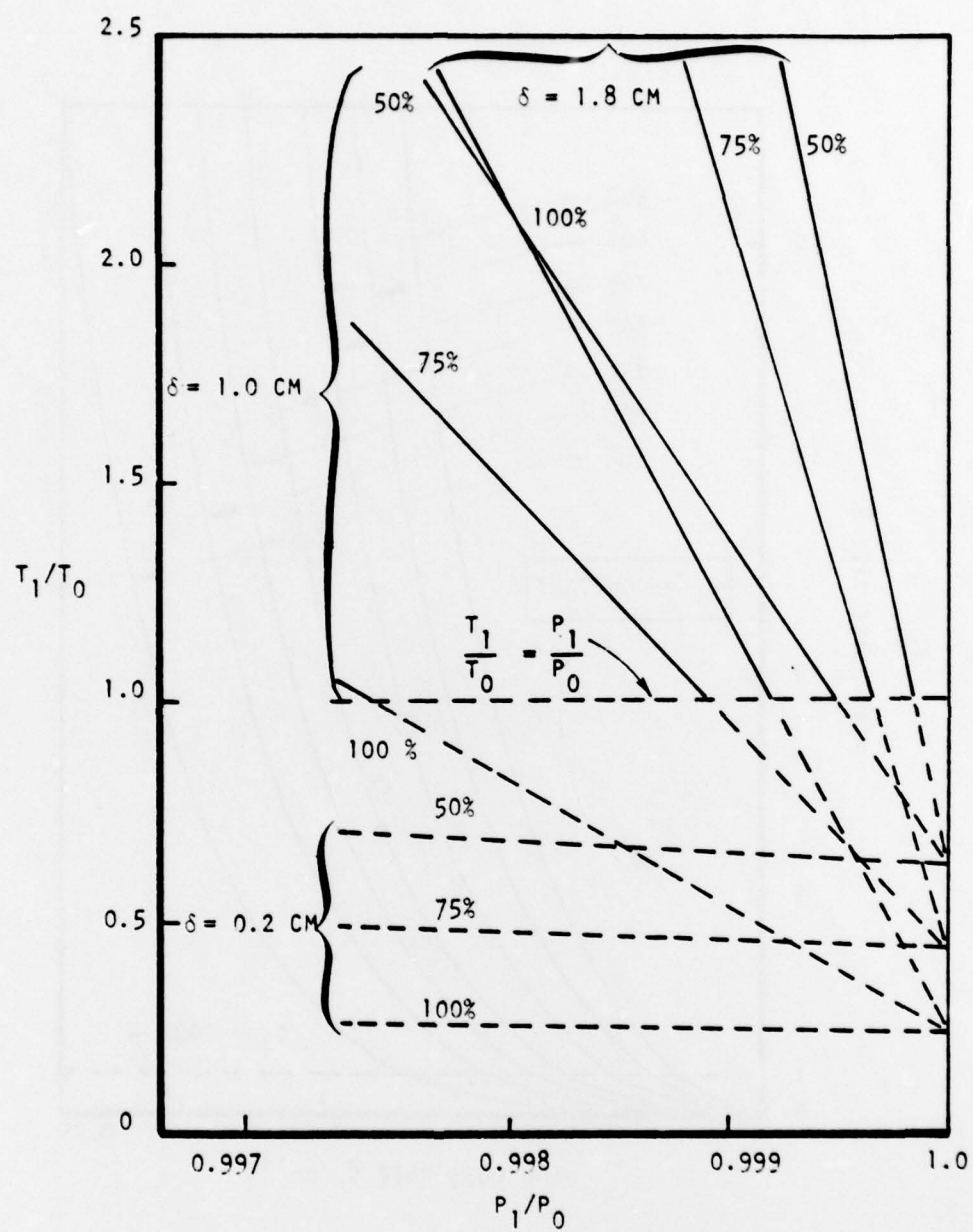


Figure A-2d. Isoconcentration Lines

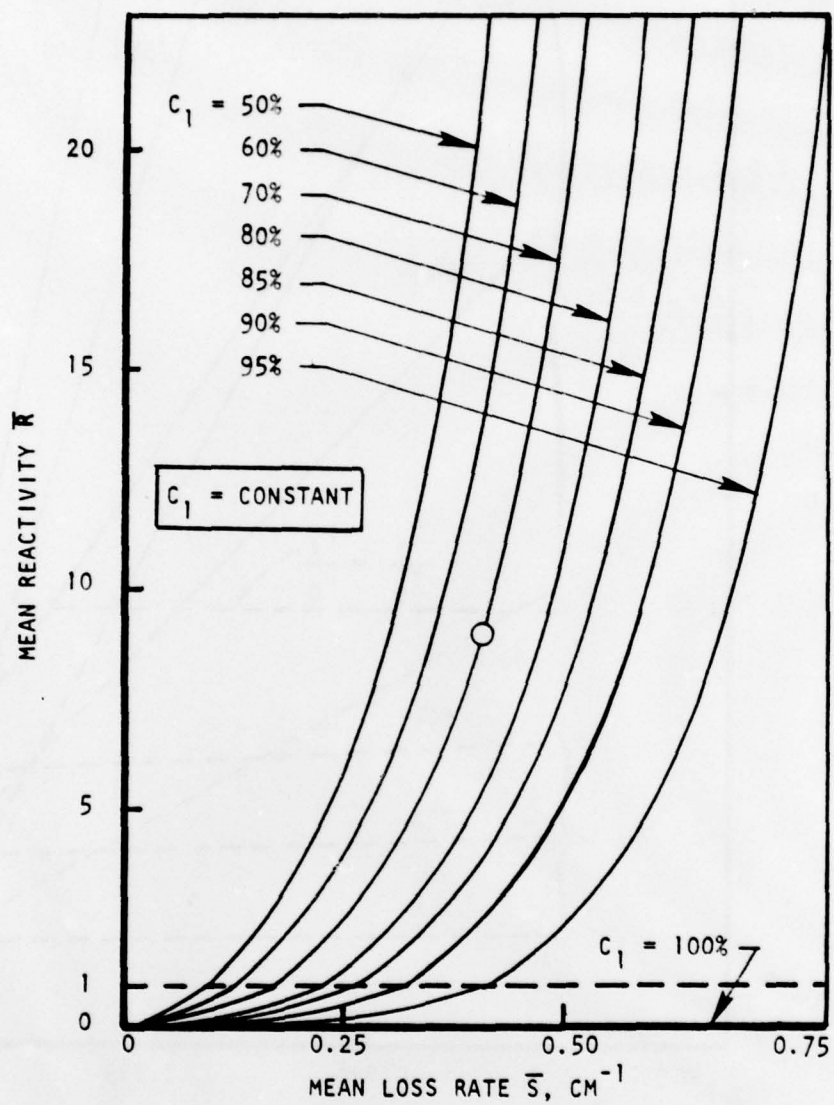
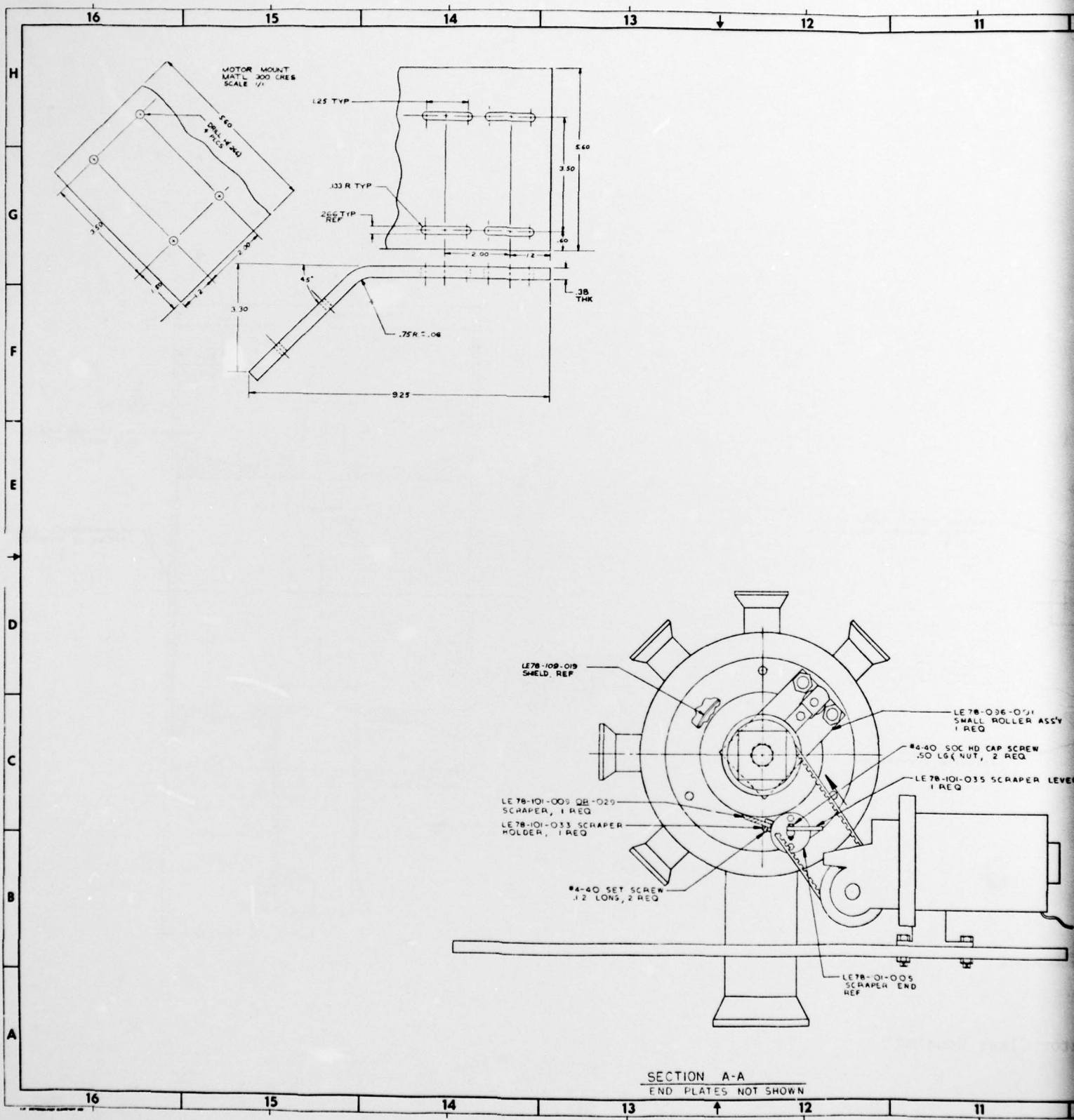
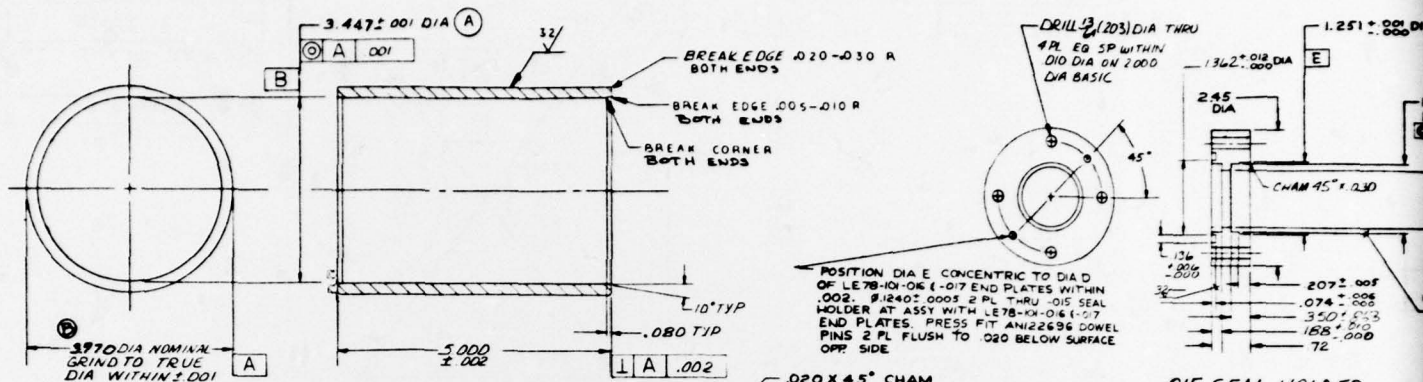


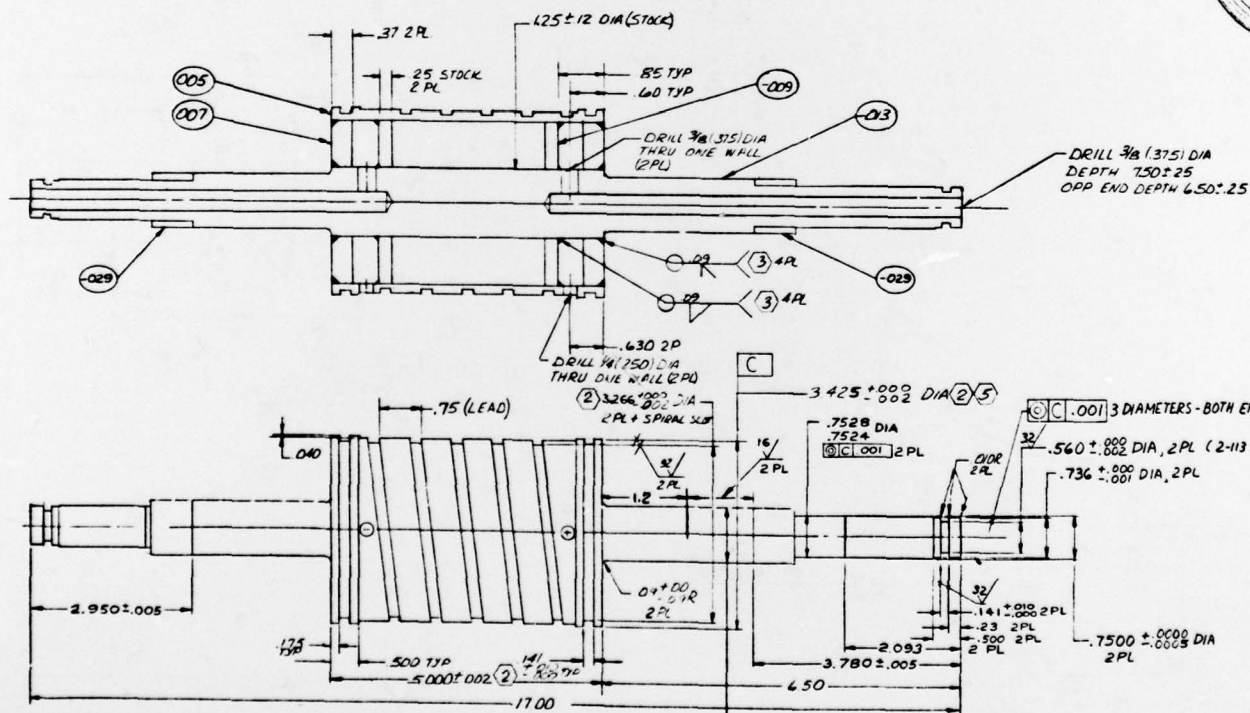
Figure A-3. O_2 Concentrations at Reactor Exit



• MICROFILM OVERLAP AREA •

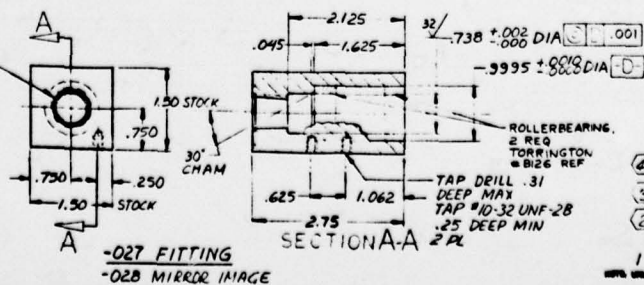


-029 INNER RACE
SCALE 2/1



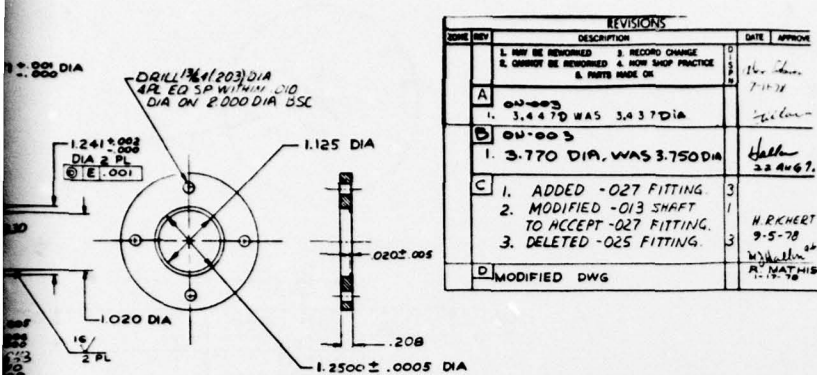
-021 ROTOR ASSY (4)

DRILL 3/8 (.547) THRU CSK 30° X .69 DIA REAM 3/8 PIPE TAPER TAP 3/8 PIPE THREAD PER MIL-P-7103

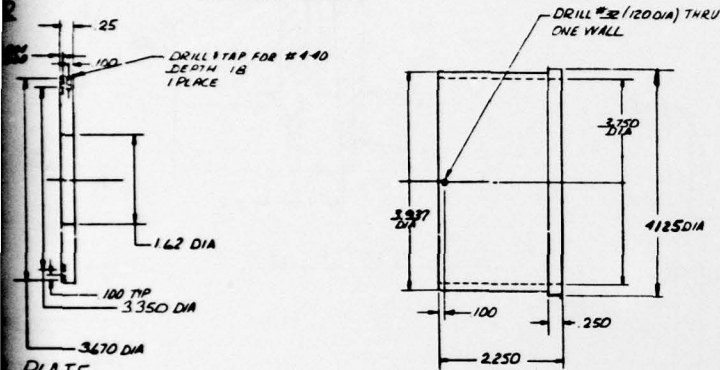


- ④ ANNEAL PER RADIII-DIB AT 1150 ± 25°F
- ③ GTA WELD PER RAD107-D27 CLASS II
- ② FINISH MACHINE AFTER WELDING IS ROUGH MACHINING TO LEAVE ALLOWANCE FOR WARPING
- 1 MACHINE PER RAD105-D16
- UNLESS OTHERWISE SPECIFIED

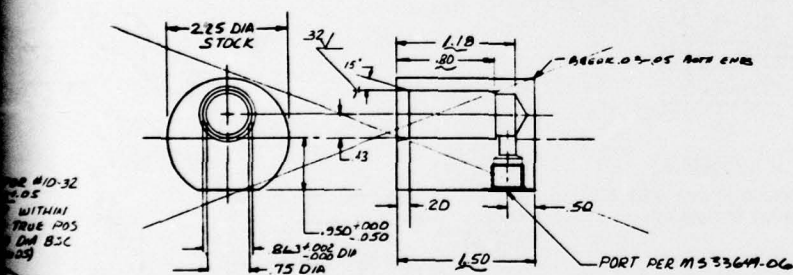




-017 BEARING



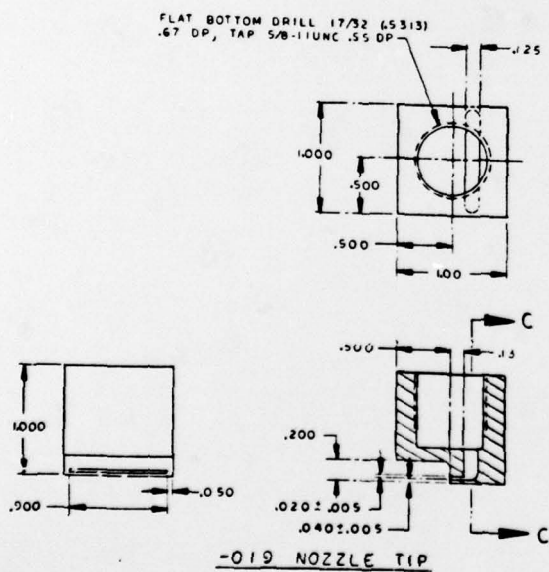
-023 SLEEVE



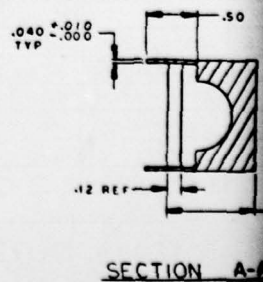
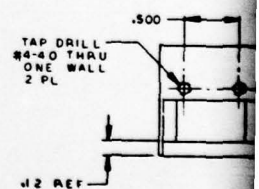
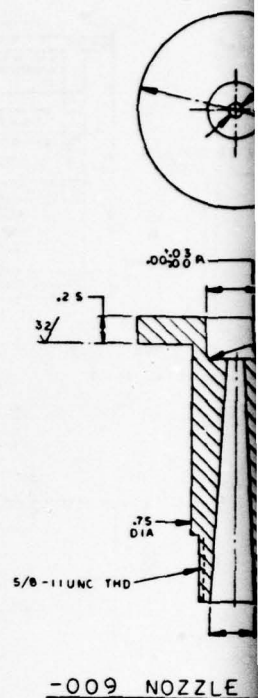
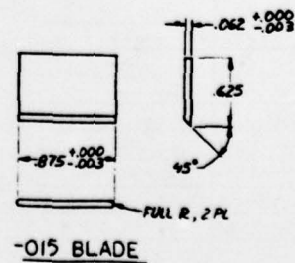
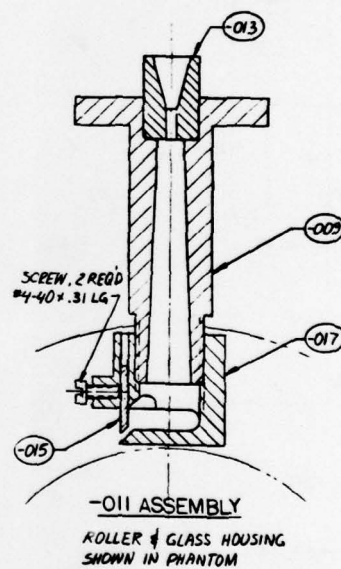
-025 FITTING

	4	STEEL AMS 5132	.125 x .875 PIN	ANI22696
-029	2	17-4 PH CRES		Rc 40-45 (H-900)
-028	1	BRASS	BAR 150X150X2.88 LG	
-027	1	BRASS	BAR 150X150X2.88 LG	
-025	2	BRASS	BAR 22.5 DIA x 1.75	
-023	2	TEFLON	BAR 4.25 DIA x 2.5	
-019	2	300 SERIES CRES	PLATE .25 THK x 3.75 DIA	
-017	2	BRASS	2.5 DIA x .50 BAR	
-015	2	310 SERIES CRES	2.5 DIA x .75 BAR	
-013	021	310 SERIES CRES	BAR 1.25 DIA x 1.75	310 OR 304L PREFERRED
-007	021	310 SERIES CRES	PLATE .25 THK x 3.1 DIA	
-007	021	310 SERIES CRES	PLATE .316 THK x 3.1 DIA	
-005	021	310 SERIES CRES	TUBE 3.50 DIA x 1.75	
-003	-	ALUMINA	3.7500 ± .0005 DIA x 5.03	76% AL ₂ O ₃ MIN
DASH 40	ASST	NO	MATERIAL	SIZE
				SPECIFICATION

Figure 20. Large Roller and Components

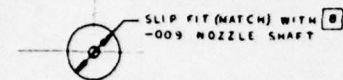
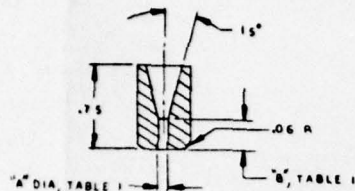


SECTION C-C
Figure 21. CFS, Cl₂ Nozzle

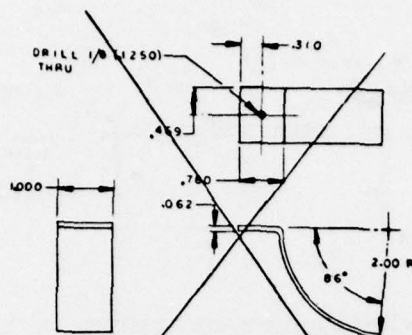


SECTION A-A

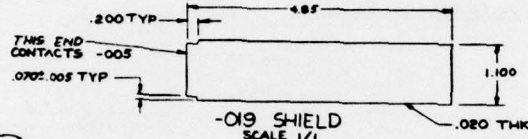
TABLE 1		
NO.	A ±.0010	B ±.010
1	.0938	.281
2	.1160	.348
3	.1336	.534



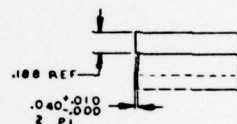
-013 ORIFICE



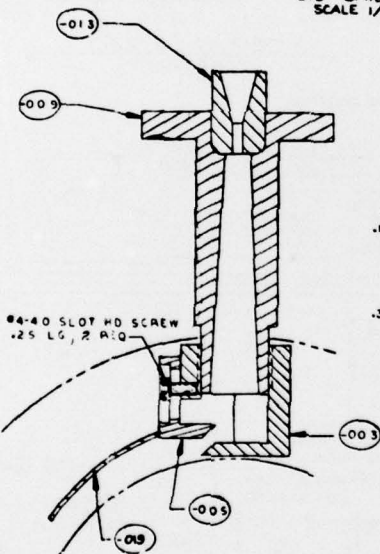
-007 GAS CONFINER
SCALE 1/1



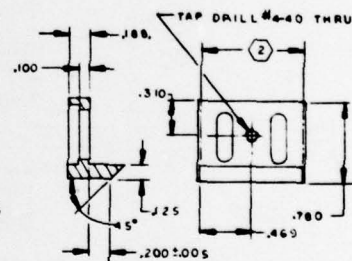
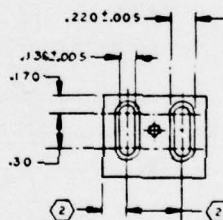
-019 SHIELD
SCALE 1/1



FLAT BOTTOM DRILL
17/32 (.531), .87 DEEP
TAP 5/8-11 UNC, .55 DEEP

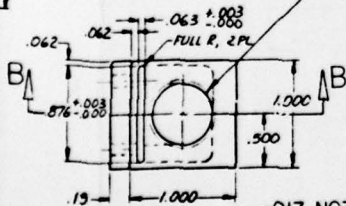


#4-40 SLOT HD SCREW
.25 LG, 2 PL

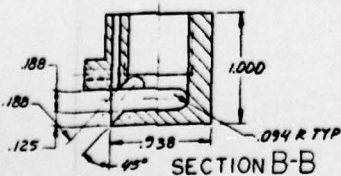


-005 GATE

DRILL 17/32 (.531) TO DEPTH SHOWN
TAP 5/8-11 UNC X .55 DEEP



-017 NOZZLE TIP



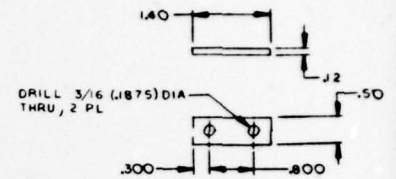
SECTION B-B

-001 ASSEMBLY
ROLLER AND GLASS HOUSING
SHOWN IN PHANTOM

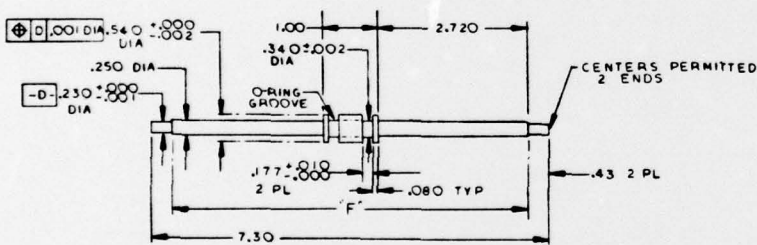
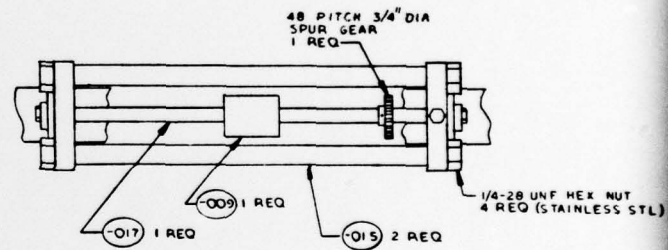
QTY	QTY	NO.	NAME	MATERIAL	SIZE
1	2	-019	SHIELD	PFA TEFLON	4.850 X 1.100 X .020 THK
2			SCREW	TEFLON	#4-40 X .25 LG
1			SCREW		#4-40 X .31 LG
1		-017	TIP		1.25 X 1.00 X 1.00
1		-015	BLADE		1.00 X .75 X .12
1	1	-013	ORIFICE	TEFLON	.75 X .50 DIA
1	1	-005	SH-RT	TEFLON	3 X 1.75 DIA
1		-007	CONFINER	TEFLON	4.850 X 1.100 X .062 THK
1		-005	GATE	TEFLON	1 X 1 X .5
1		-003	TIP	TEFLON	1.00 X 1.00 X 1.00
-011	-001				

REVISIONS			DATE	APPROVED
NO.	REV	DESCRIPTION		
		1. NOT BE RETURNED 2. QUANTITY OF RETURNED 3. PARTS MADE OK		
A	1	ADDED .040 ±.010 TO .005 GATE		
B	1	ADDED -011 ASSY.		
C		DWG MODIFIED		

ATCH WITH -005 NOZZLE TIP WITHIN ±.005.
BEHINE PER RAD103-016

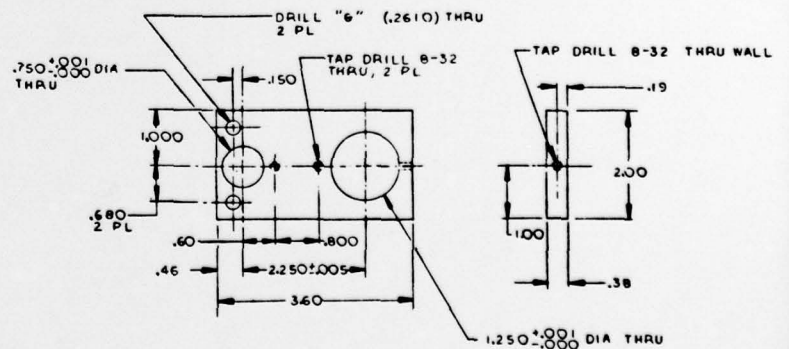


-013

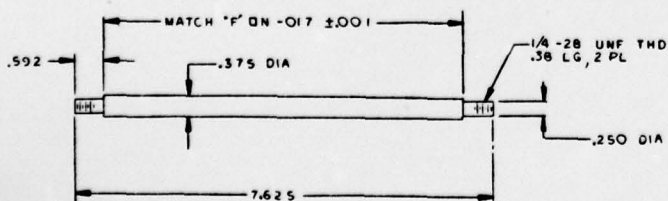


-017

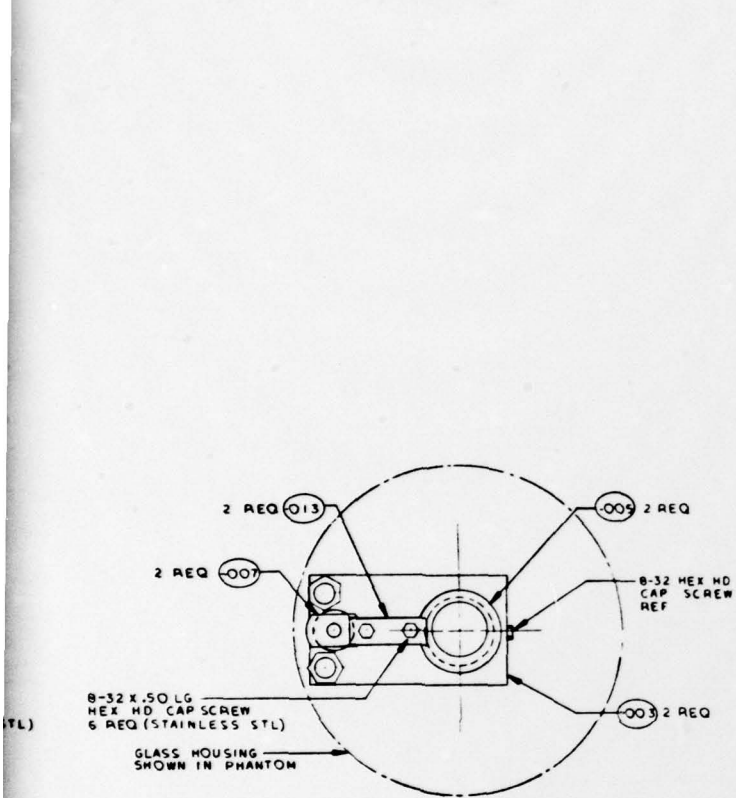
2-203 (PARKER NO) BUNA-N O-RING
NOT SHOWN, 2 REQ



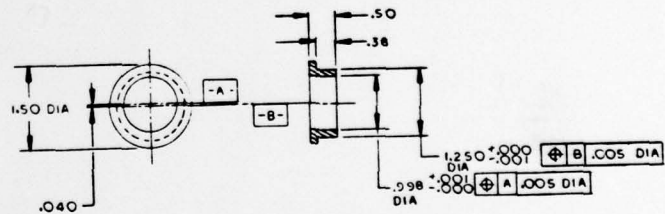
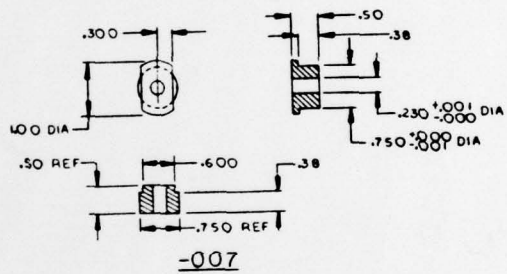
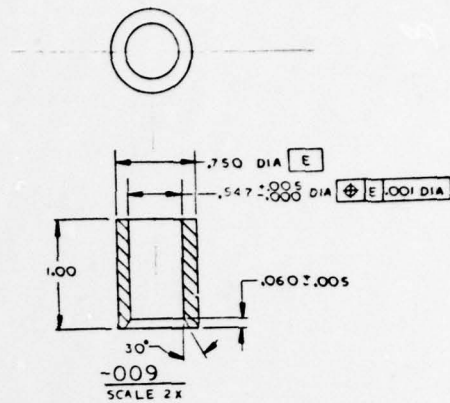
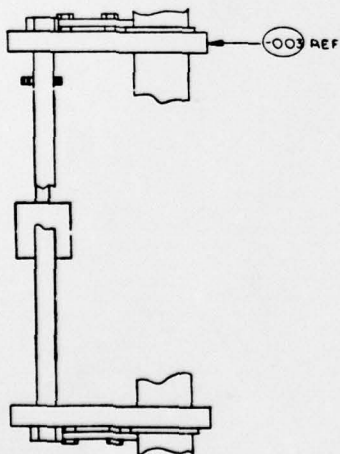
-003



-015



-001 ASSEMBLY



-005

Figure 22. Small Roller Assembly



DISTRIBUTION

AUL/LDE/Maxwell AFB, AL
DDC/TCA/Cameron Sta, Alexandria, VA
AFWL/Kirtland AFB, NM

(SUL)

(HO)

(ALC)

Rocketdyne Div/Rockwell, Canoga Pk, CA

Rockwell Sci Ctr, Thousand Oaks, CA

FJSRL/NC/USAF Academy, CO

AFSC/DLWM/Wash, DC

Official Record Copy/Maj Bousek/ALC